UNIVERSITY OF CALIFORNIA SAN DIEGO

Unbiased Extremum Seeking with Prescribed-Time Convergence and Adaptive Model-Free Control of Continuum Robots

A dissertation submitted in partial satisfaction of the
requirements for the degree Doctor of Philosophy

in

Engineering Sciences (Mechanical Engineering)

by

Cemal Tugrul Yilmaz

Committee in charge:

Professor Miroslav Krstic, Chair
Professor Mamadou Diagne
Professor Tania Morimoto
Professor Jorge Poveda

2024

The Dissertation of Cemal Tugrul Yilmaz is approved, and it is acceptable in quality and form for publication on microfilm and electronically.

University of California San Diego

2024

DEDICATION

To my beloved wife, Elif, for her unwavering support, encouragement, and patience throughout this journey.

TABLE OF CONTENTS

LIST OF FIGURES

LIST OF TABLES

ACKNOWLEDGEMENTS

This thesis is the product of many hands, minds, and hearts working together. I am deeply grateful to all those who have contributed to it.

First and foremost, I am profoundly grateful to my advisor, Prof. Miroslav Krstic, for his unwavering support and insightful guidance. His commitment to producing high-quality research has been a guiding force in shaping my academic growth. His attention to detail, vast knowledge, and ability to critically evaluate and deeply analyze even the most intricate elements of my work have been instrumental in refining my skills as a researcher. His approach has helped me cultivate a deep level of analytical and critical thinking. I have also been consistently inspired by his responsiveness and exceptional time management, which have shown me the value of discipline and dedication, not only in research but in life as a whole.

I extend my heartfelt gratitude to my co-advisor Prof. Mamadou Diagne, who has also been a great mentor over the past two years. I am truly grateful for his insightful conversations, his constant encouragement that lifted my motivation, and for his tremendous support in advancing my development and growth. I also deeply appreciate his unwavering belief in me, his efforts to put me forward, introduce me to remarkable people in the field, and create opportunities for me. These experiences have not only enriched my academic journey but also helped me build valuable connections and grow as a researcher. These invaluable moments will always hold a special place in my heart.

I would also like to thank Prof. Tania Morimoto for her time and effort during our collaboration on the continuum robot project. It was a field I discovered with great enthusiasm and truly enjoyed working in. I am also grateful for her support as a member of my committee.

A milestone in my career was receiving the MAE PhD Outstanding Student of the Year Award, nominated by Prof. Krstic, Prof. Diagne, and Prof. Morimoto. I am deeply grateful for their support and belief in my work.

I extend my sincere gratitude to Prof. Jorge Poveda for his exceptional work on extremum seeking, which has greatly inspired my research, and for dedicating his valuable time to serve on

my committee.

Another valuable person who played a significant role in my career and helped me take my first steps in the field is Dr. Halil Basturk, a former member of the lab and a great advisor during my master's at Bogazici University. I am deeply grateful for his guidance, which helped me develop the skills needed for conducting quality research.

A special thanks goes to my friends, colleagues, lab mates, and collaborators, who have been my companions on this journey: Alan Williams, Bhathiya Rathnayake, Brad Ratto, Cenk Demir, Connor Watson, Drew Steves, Eranda Somathilake, Evelia Zapien Ramos, Imoleayo Abel, Kwang Hak Kim, Luke Bhan, Mohammad Al Suwaidan, Patrick McNamee, Peihan Zhang, Qixu Wang, Shumon Koga, and Velimir Todorovski. I am also grateful to Wenhan Tang, Max Lee, Eric Foss, and Sankalp Kaushik for their tremendous effort and dedication during the experiments.

Last but certainly not least, I wish to express my deepest gratitude to my wife, Elif Sandalci Yilmaz, to whom I dedicate this thesis. Words fall short in capturing my appreciation for her unwavering support, patience, and kindness throughout this journey. My heartfelt thanks also extend to the Yilmaz family—Gulsen, Hudai, Alper, and Firdevs—and to the Sandalci family—Nuray, Cem, Zeynep, and Affan—for their continuous encouragement and support along the way.

This dissertation includes reprints and adaptations of the following papers, which have been published or submitted for publication and are included in Chapters 2 through 6, respectively:

- C. T. Yilmaz and M. Krstic, "Prescribed-Time Extremum Seeking for Delays and PDEs Using Chirpy Probing", *IEEE Transactions on Automatic Control*, 69(11):7710–7725, 2024.

- C. T. Yilmaz, M. Diagne, and M. Krstic, "Exponential and Prescribed-Time Extremum Seeking with Unbiased Convergence", *Automatica*, under review, 2023.

- C. T. Yilmaz, M. Diagne, and M. Krstic, "Unbiased Extremum Seeking for PDEs", *IEEE Conference on Decision and Control (CDC)*, to appear, 2024.
- C. T. Yilmaz, M. Diagne, and M. Krstic, "Asymptotic, Exponential, and Prescribed-Time Unbiasing in Seeking of Time-Varying Extrema", *IEEE Transactions on Automatic Control*, under review, 2024.
- C. T. Yilmaz, C. Watson, T. K. Morimoto, and M. Krstic, "Adaptive Model-Free Disturbance Rejection for Continuum Robots", *Automatica*, vol. 171, p. 111949, 2025.

Chapter 1 includes sections adapted from these publications.

VITA

2015	Bachelor of Science in Mechanical Engineering, Bogazici University, Turkey
2018	Master of Science in Mechanical Engineering, Bogazici University, Turkey
2024	Doctor of Philosophy in Engineering Sciences (Mechanical Engineering), University of California San Diego

PUBLICATIONS

Journal Articles

1. **C. T. Yilmaz**, C. Watson, T. K. Morimoto, M. Krstic, "Adaptive Model-Free Disturbance Rejection for Continuum Robots", *Automatica*, vol. 171, pp. 111949, 2025.

2. **C. T. Yilmaz**, M. Diagne, M. Krstic, "Asymptotic, Exponential, and Prescribed-Time Unbiasing in Seeking of Time-Varying Extrema", *Transactions on Automatic Control*, under review, 2024.

3. **C. T. Yilmaz** and M. Krstic, "Prescribed-Time Extremum Seeking for Delays and PDEs Using Chirpy Probing", *IEEE Transactions on Automatic Control*, 69(11):7710–7725, 2024.

4. **C. T. Yilmaz**, M. Diagne, M. Krstic, "Exponential and Prescribed-Time Extremum Seeking with Unbiased Convergence", *Automatica*, under review, 2023.

5. **C. T. Yilmaz**, H. I. Basturk, "Adaptive Output Regulator for Wave PDEs with Unknown Harmonic Disturbance", *Automatica*, vol. 113, pp. 108808, 2020.

6. **C. T. Yilmaz**, H. I. Basturk, "Output Feedback Control for Unknown LTI Systems Driven by Unknown Periodic Disturbances", *Automatica*, vol. 99, pp. 112–119, 2019.

7. **C. T. Yilmaz**, H. I. Basturk, "Rejection of Sinusoidal Disturbances for Known LTI Systems in the Presence of Output Delay", *Automatica*, vol. 92, pp. 41–48, 2018.

Conference Proceedings

1. **C. T. Yilmaz**, M. Diagne, M. Krstic, "Unbiased Extremum Seeking Based on Lie Bracket Averaging", *submitted to American Control Conference (ACC)*, 2025.

2. **C. T. Yilmaz**, M. Diagne, M. Krstic, "Unbiased Extremum Seeking for PDEs", *Conference on Decision and Control (CDC)*, to appear, 2024.

3. **C. T. Yilmaz**, M. Diagne, M. Krstic, "Perfect Tracking of Time-Varying Optimum by Extremum Seeking", *American Control Conference (ACC)*, pp. 2936–2943, 2024.

4. **C. T. Yilmaz**, M. Diagne, M. Krstic, "Exponential Extremum Seeking with Unbiased Convergence", *Conference on Decision and Control (CDC)*, pp. 6743–6748, 2023.

5. **C. T. Yilmaz**, M. Krstic, "Accelerated Learning and Control of Robots with Uncertain Kinematics and Unknown Disturbances", *American Control Conference (ACC)*, pp. 806–811, 2023.

6. **C. T. Yilmaz**, M. Krstic, "Prescribed-Time Extremum Seeking with Chirpy Probing for PDEs—Part II: Heat PDE", *American Control Conference (ACC)*, pp. 800–805, 2022.

7. **C. T. Yilmaz**, M. Krstic, "Prescribed-Time Extremum Seeking with Chirpy Probing for PDEs—Part I: Delay", *American Control Conference (ACC)*, 1000–1005, 2022.

8. **C. T. Yilmaz**, J. George, A. Chakrabortty, "Observer-Based Extremum Seeking Control of Static Maps with Delays", *American Control Conference (ACC)*, pp. 162–167, 2020.

9. J. George, A. Parayil, **C. T. Yilmaz**, B. Allik, H. Bai, A. Chakrabortty "Multi-Agent Coordination for Distributed Transmit Beamforming", *American Control Conference (ACC)*, pp. 144–149, 2020.

10. J. George, **C. T. Yilmaz**, A. Parayil, A. Chakrabortty "A model-free approach to distributed transmit beamforming", *IEEE International Conference on Acoustics, Speech and Signal Processing (ICASSP)*, pp. 5170–5174, 2020.

11. **C. T. Yilmaz**, H. I. Basturk, "Adaptive Harmonic Disturbance Cancellation for LTI Systems with Heat PDE Actuator Dynamics", *American Control Conference (ACC)*, pp. 1274–1279, 2019.

12. **C. T. Yilmaz**, H. I. Basturk, "Output Feedback Controller Design for LTI Systems with Heat PDE Actuator Dynamics and Periodic Disturbances", *American Control Conference (ACC)*, pp. 1268–1273, 2019.

13. **C. T. Yilmaz**, H. I. Basturk, "Adaptive Backstepping Control Design for Active Suspension Systems with Output Feedback", *American Control Conference (ACC)*, pp. 1712–1717, 2019.

14. **C. T. Yilmaz**, H. I. Basturk, "Adaptive Cancellation of Unmatched Unknown Periodic Disturbances for Unknown LTI Systems by Output Feedback", *American Control Conference (ACC)*, pp. 3026–3031, 2019.

15. **C. T. Yilmaz**, H. I. Basturk, "Compensation of Simultaneous Input/Output Delay and Unknown Sinusoidal Disturbances for Known LTI Systems", *European Control Conference (ECC)*, pp. 2788–2793, 2018.

ABSTRACT OF THE DISSERTATION

Unbiased Extremum Seeking with Prescribed-Time Convergence and Adaptive Model-Free Control of Continuum Robots

by

Cemal Tugrul Yilmaz

Doctor of Philosophy in Engineering Sciences (Mechanical Engineering)

University of California San Diego, 2024

Professor Miroslav Krstic, Chair

This thesis introduces model-free control and optimization strategies for static and dynamic systems with model uncertainties. It comprises two main parts: the first focuses on extremum seeking (ES) control, a model-free, real-time optimization method with a century-old history, while the second develops adaptive control strategies for continuum robots, where kinematic models are complex and variable due to unknown contact forces, and where physiological disturbances, such as respiration and heartbeat, present further challenges.

In the first part, we develop a new form of ES, referred to as prescribed-time ES (PT-ES), which uses time-varying frequencies and gains to achieve convergence to a neighborhood of

the optimum within a user-defined time. Motivated by the optimization challenges in systems governed by partial differential equations (PDEs), we then extend PT-ES to handle delays, wave PDEs, and heat PDEs.

Next, to eliminate the steady-state oscillations inherent in traditional ES and achieve convergence directly to the optimum, we introduce unbiased ES (uES) with a user-defined exponential convergence rate, and unbiased PT-ES (uPT-ES) with user-prescribed convergence time. These approaches gradually shift from exploration to exploitation by employing a perturbation signal with decaying amplitude and a demodulation signal with growing amplitude.

Building on these designs, we introduce PDE-compensated uES strategies as our third ES design. In the fourth design, we extend the uES approach to achieve perfect tracking of time-varying optima, with convergence rates that are asymptotic, exponential, or prescribed-time, depending on the choice of time-varying parameters. We experimentally test the effectiveness of exponential uES on a unicycle seeking a static light source.

The second part of this thesis presents two model-free control strategies for rejecting unknown disturbances in continuum robots. These strategies employ a neural network-based approximation to estimate the uncertain Jacobian matrix using only position measurements. The first strategy is designed for periodic disturbances, integrating an adaptive model-free controller with an adaptive disturbance observer. The second strategy, designed to handle arbitrary disturbances, uses time-varying input gains and adaptation laws that increase monotonically, enabling asymptotic, exponential, or prescribed-time tracking of a reference trajectory. Both strategies are validated experimentally on a concentric tube robot subject to unknown disturbances.

Chapter 1

Introduction

In this thesis, we present two distinct adaptive control strategies: extremum seeking (ES) designs for optimizing unknown cost functions, developed in Chapters 2–5, and adaptive model-free control algorithms for continuum robots, developed in Chapter 6. This chapter begins with a historical background on ES, followed by the motivation, literature survey, and contributions of each ES algorithm developed. These include prescribed-time extremum seeking for partial differential equations (PDEs), unbiased ES for fixed optima, unbiased ES for PDEs, and unbiased ES for tracking time-varying optima, which are presented in Chapters 2, 3, 4, and 5, respectively. Subsequently, we examine the modeling and control challenges in continuum robots, emphasizing the need for model-free control to manage uncertain kinematics and physiological disturbances, and we outline our contributions to this field.

1.1 Extremum Seeking

ES has been an effective optimization technique in real-time optimization for over a century [92], originating from the pioneering work of Maurice LeBlanc, a French industrialist and inventor [63]. The algorithm was studied extensively in the 1950s and 1960s under the names “extremum control” and “self-optimizing control” [15, 72, 84]. After that, ES experienced a period of stagnation. It wasn’t until the development of stability proof in [59] around the year 2000 that the algorithm began to regain momentum. Since then, the field of ES has witnessed

remarkable theoretical advancements [19, 25, 81, 82, 92, 98], and has found practical applications across various domains [26, 93, 126].

This thesis introduces four novel ES designs. In the following subsections, we discuss the motivation, advantages, and contributions of each design, highlighting its unique features and advancements over existing methods.

1.1.1 Prescribed-Time ES for PDE systems

Motivation. Much of the ES literature focuses on optimizing systems modeled by ordinary differential equations (ODEs). However, many physical systems, such as drilling rigs, reactors, batteries, and continuum robots, are more accurately described by partial differential equations (PDEs), presenting unique optimization challenges.

In certain systems like network control systems, and cyber-physical systems, time delays between control action and system response are inevitable. This issue requires a delay-aware ES, as designs that ignore the delay may lead to instability, especially with large delays. In oil drilling systems [1], the input dynamics involve a cascade of wave PDE and ODE, and the objective is to maximize the rate of penetration (ROP) up to a certain threshold known as the foundering point. Beyond this point, ROP starts decreasing, leading to energy wastage and potential cutter damage. In tubular reactors [44], which are defined by coupled hyperbolic PDEs, the goal is to seek a reactor temperature profile maximizing the reactor exit concentration. Another intriguing challenge arises in pool boiling systems [4]. As heat flux increases during boiling, bubbles form and rise to the surface. Beyond a critical heat flux, bubbles cease to rise, and a vapor film covers the heater surface, acting as an insulator. This leads to a significant temperature increase above the heater material's melting point, causing physical burnout of the heater. In such systems, there is a need for an optimizer to stabilize the heat flux at its unknown optimal level.

The ES designs developed in [1, 44] focus on optimization at the steady state and do not fully account for the underlying PDE dynamics. This limits their applicability to PDE systems with slow transient and motivates the development of PDE compensated ES designs.

A notable advancement in recent years is the development of prescribed-time (PT) stabilizing controllers, which feature time-varying gains inspired by classical "proportional navigation" algorithms [41]. These controllers have been attracting extensive interest because they enable the user not only to achieve convergence in some finite time but to achieve it in arbitrary prescribed time, independently of the initial condition and system parameters. This represents an advantage over asymptotic and finite-time stabilization.

The integration of PDE input dynamics compensation and prescribed-time optimization has the potential to greatly enhance system performance by improving stability, responsiveness, and robustness to disturbances. This motivates the development of prescribed-time extremum seeking (PT-ES) with PDE compensators in this thesis.

Literature survey. Recent advancements in ES field have introduced concepts such as finite-time ES [34] and fixed-time ES [86], [87], to accelerate convergence to the optimum's vicinity. The key distinction between these concepts is that in finite-time stability, convergence time depends on initial conditions, while in fixed-time stability, it is determined by the system's parameters regardless of initial conditions. Prescribed-time stability, introduced by [103], strengthens these notions further. It allows users to pre-define a desired terminal time regardless of initial conditions and system's parameters. Incorporating this concept into ES, [110] develops an algorithm for prescribed-time seeking of a repulsive source by a unicycle.

Additionally, ES designs have been developed for functions with input/output delays [82] and for systems with inputs governed by diffusion PDEs [22], wave PDEs [80], and PDE-PDE cascades [79]. For a more comprehensive treatment of the problem, refer to the monograph [81]. However, the PDE-compensating ES designs in [22, 80, 79, 81] are limited to ensuring exponential-in-time convergence to a neighborhood of the optimum.

Contributions. In Chapter 2, we develop PT-ES schemes that incorporate compensation techniques for delay, diffusion, and wave PDEs. We add two new ingredients to the ES toolkit, in order to achieve PT convergence by time-varying feedback: (1) "chirpy" perturbation and demodulation signals (sinusoids whose frequency grows unbounded) and (2) tuning gains which

grow unbounded. In implementation, for noise-robustness and numerical, the gains are "clipped" to some moderately large values, sufficient for the remaining distance to the extremum at the prescribed terminal time T to be imperceptible.

In PT-ES, we replace the conventional probing sinusoid, whose frequency ω is constant, by a sinusoid with the argument $\omega(t_0+(t-t_0)T/(t_0+T-t))$. This argument goes to infinity as the time t approaches the terminal time t_0+T, where T is the prescribed convergence horizon.

To introduce the reader to PT-ES concepts, we start in Section 2.1 with a fundamental result for a static map. We show how the existing theory of infinite-horizon averaging can be employed for a stability study in a finite (prescribed) time setting. In comparison with FxT-ES in [87], which yields a settling time that is user-assignable only with Newton-based algorithms, to make the settling times independent of the unknown Hessian, our use of chirped probing and a time-varying gain achieves a desired settling time T without the estimation of the Hessian's inverse and without the Newton approach.

In Section 2.2, we take the idea of Section 2.1 to delay-compensated PT-ES, which is inspired by maximizing flow through traffic bottlenecks [123], and convert the predictor ideas for infinite-time ES [82] to prescribed time. Already in this section the rather complex relation between the probing and the demodulating chirpy signals becomes evident, as an interesting problem of an open-loop "motion planning" type. For more details on "motion planning" for hyperbolic and parabolic PDEs, refer to [58] and [61].

After giving a not particularly difficult extension from ES under a delay to ES for the wave PDE in Section 2.3, in Section 2.4 we turn our attention to the much harder problem of compensating a diffusion PDE in prescribed time, which is motivated by the melt pool dynamics in additive manufacturing [52]. The "motion planning" design of a chirpy probing signal for the PDEs is far more challenging than for the delay in Section 2.2.

The averaging analysis in Section 2.1 and [110] is quite simple and follows an idea in [53] to employ a time-dilation transformation $\tau(t)=t_0+(t-t_0)T/(t_0+T-t)$ from the finite time horizon $[t_0,t_0+T)$ in the time scale t to the infinite time horizon $[t_0,\infty)$ in the time scale τ. Both

times start at $\tau = t = t_0$. The time τ becomes infinite when $t \to t_0 + T$. The dilation lets us perform design and averaging analysis, done for periodic ODEs, in the infinite time τ, while implementing the algorithm and stating its properties in the finite time $t(\tau) = t_0 + T(\tau - t_0)/(T + \tau - t_0)$.

The averaging for the infinite-dimensional systems in Sections 2.2 and 2.4 is significantly harder. Employing the time dilation results in the transport speed (for the delay) or diffusion (for the heat equation) converging to zero as the dilated time advances to infinity, destroying exponential stability of the time-dilated average system. Therefore, we are forced to develop an averaging method for our infinite-dimensional and not necessarily periodic systems, with not necessarily uniformly bounded right hand sides, over an arbitrarily long subset of the time interval $t \in [t_0, t_0 + T)$. We develop an averaging technique for infinite-dimensional systems, inspired by [16, Theorem 5.16]. In the process, we treat the argument $\mu(t) = T/(t_0 + T - t)$, in chirpy sinusoid $\sin(\omega(t_0 + (t - t_0)\mu(t)))$, as a state of the system rather than as a time-varying signal.

1.1.2 Unbiased ES for seeking fixed optima

Motivation. The fundamental principle of ES is to introduce a small perturbation to the system through an excitation signal, observe the system's response, estimate the gradient by demodulating the output, and adjust the system's inputs towards the vicinity of the optima. Due to the persistent excitation present in the process, achieving exact convergence to the extremum cannot be ensured, and instead, steady-state oscillations around the extremum are commonly observed. While these oscillations ensure robustness against potential drifts in the optima, eliminating them and reducing the convergence error offer significant advantages in various applications, such as maximizing power extraction in solar systems [74], more accurate localization of leakage sources [46], improved tuning of controller parameters [51], and increased efficiency in combustion engines [50]. This motivates the development of a novel ES design that achieves exponential and unbiased convergence directly to the unknown extremum.

As discussed in Section 1.1.1, the PT-ES designs developed in [110] and Chapter 2

guarantee convergence to a neighborhood of the extremum while leading to unbounded control signals, which is impractical for real-world applications. This limitation underscores the need for an unbiased PT-ES (uPT-ES), which converges to the extremum within a user-prescribed time, without bias, and ensures bounded control signals. Furthermore, this fast and precise optimization is critical in specific applications such as particle accelerators with high-frequency electromagnetic fields, where extremely precise control of electric field amplitude and phase is necessary within strict tolerances and short time frames [94].

Literature survey. To address persistent oscillation around the fixed optimum, [109] introduces a method involving a time-varying perturbation amplitude that decays to zero, ensuring practical asymptotic convergence to the global extremum despite local extrema. Another approach in [113] adjusts the perturbation amplitude based on system output. However, the claim of exponential convergence to the optimum in [113] has been theoretically [7] and numerically [33, 38] disputed. Kalman filtering techniques, with feedback to dynamically update the amplitude, are employed in [85] and [8], achieving asymptotic convergence to a neighborhood of the extremum with diminishing oscillation. In [62], the authors established a connection between stochastic approximation and ES by replacing the stochastic perturbations with periodic ones. To minimize convergence bias, [62] employs filtering techniques and reduces learning/update gains while keeping the perturbation amplitude constant. The same work also develops state-dependent probing signals to improve transient performance, but still leads to biased convergence. Regulation of inputs directly to their unknown optimal values is achieved in [32] and [97] using an ES that vanishes at the origin, assuming the optimal value of the cost function is known beforehand. Relaxing this restriction, [2], [33], [38], and [106] present control designs that achieve asymptotic convergence of both inputs and outputs to their unknown optimum values. Specifically, [2] achieves this under certain initial conditions, [38] employs time-varying tuning parameters with decaying frequency and amplitude, [33] reduces the size of the search region by estimating the uncertainty set around the optimizer and updating the amplitude accordingly, and [106] adopts an approach with unboundedly growing update rates and frequencies. In summary, none of the

aforementioned results achieve unbiased convergence directly to the unknown extremum, either exponentially or within a prescribed time.

Contributions. In Chapter 3, we introduce three ES algorithms: (i) exponential uES with vanishing oscillations and unbiased convergence, (ii) robust exponential ES with adjustable oscillations, but less accurate convergence, (iii) unbiased PT-ES (uPT-ES) with vanishing oscillations and unbiased convergence in prescribed time. Our exponential uES is the first to provide exponentially fast convergence directly to the true optimum. The uPT-ES offers the strongest results to date in the field in terms of both rate (arbitrarily fast) and accuracy (zero error). Unlike finite-time ES [34] and fixed-time ES [86, 87] algorithms, which exhibit steady-state oscillations after reaching the terminal time, the developed uPT-ES: (i) eliminates steady-state oscillations, (ii) guarantees unbiased convergence to the extremum, and (iii) achieves this within an arbitrarily defined terminal time, independent of initial conditions and system parameters.

The concept of exponential uES relies on an exponential decay function that reduces the effect of the perturbation signal and the use of its multiplicative inverse, which grows exponentially, to maximize the effect of the demodulation signal multiplied by the high-pass filtered output. Similar to the prescribed-time stabilization concept presented in [103], the convergence of the filtered output occurs at a faster rate than the divergence of the inverse function and the convergence of the perturbation, keeping the controller bounded. For the stability analysis, we transform the system using the exponentially growing function and then apply classical averaging and singular perturbation methods to show the local stability of the transformed system, which in turn implies the local exponential stability of the original system as well as exponential convergence of the output to the extremum with proper choice of gains. We introduce the robust exponential ES, which is our second algorithm, by modifying the exponential decay function so that it converges to a small value arbitrarily defined. Our third and final algorithm, uPT-ES, replaces the exponential decay function with a prescribed-time convergent function and employs chirp signals as perturbation/demodulation signals that grow in frequency over time and ultimately diverge to infinity at the terminal. The prescribed-time

stability of the closed-loop system is achieved by using a time-dilation transformation, a state transformation, a classical averaging method, and a time-contraction transformation.

We evaluate our three ES designs numerically by studying the source seeking problem with a two-dimensional velocity actuated point mass, which has been previously solved with a traditional ES in [126]. *A discovery that stands as a common ground of the proposed unbiased algorithms is a duality between learning and unbiased convergence: learning must occur at a rate that surpasses the rate of decay of the waning oscillations.*

1.1.3 Unbiased ES for PDEs

Motivation. The PDE-compensating ES designs in Chapter 2 and in [22, 79, 80, 81] can only ensure convergence to a neighborhood of the optimum point due to the active perturbing signal in the design, resulting in suboptimal performance.

Contributions. Chapter 4 introduces unbiased ES that compensates for delay and diffusion PDE dynamics while ensuring exponential and unbiased convergence to the optimum. This extends the exponential uES design for maps without PDE dynamics developed in Chapter 3. We present two distinct uES designs: one can handle arbitrarily long and known time delays, while the other compensates for diffusion PDEs. The designs consist of a PDE compensator, a perturbation signal with exponentially decaying amplitude (to eliminate steady-state oscillation), demodulation signals with exponentially growing amplitude and properly selected design parameters (to ensure unbiased convergence).

1.1.4 Unbiased ES for tracking time-varying optima

Motivation. Real-world processes often face changing external conditions, causing the optimal input value to shift over time. It occurs for renewable energy systems operating in fluctuating weather conditions while being subject to varying energy demand, which prompt adjustments of the controller parameters to maximize power generation [57], [74]. In mineral processing, continuously adjusting aeration rates is necessary to maintain optimal air recovery

[119]. In CO_2 heat pump systems, the efficiency, represented by the coefficient of performance, varies due to environmental factors, requiring real-time optimization for maximum efficiency [43]. Therefore, there is a need not only for seeking fixed optima but also for tracking arbitrarily varying ones.

Literature survey. Several ES designs have been developed for plants with periodic steady-state outputs and constant optimizers. A scheme in [112] minimizes the limit cycle size by detecting its amplitude and adjusting a controller parameter to reach a constant optimum value. Another design in [35] uses the system's flatness property to track an optimal orbit of a nonlinear dynamical system. For plants with periodic outputs of known periodicity, an ES controller with a moving-average filter is presented in [39]. However, the reliance on periodic performance functions in these designs limits their applicability to a broad and rich set of engineering applications, such as those investigated in [57, 74, 119, 43] (and the references therein).

The optimization of arbitrary time-varying cost functions using ES is considered in various studies. The groundwork for time-varying optimizers is laid in [55], where a generalized ES scheme is developed to track optimizers with known dynamics but unknown coefficients, employing the internal model principle. For slowly varying optima, [90] introduces a delay-based strategy to extract the gradient signal. This strategy is further extended to handle dynamic systems with input constraints in [120]. In [95], an ES is developed to provide unknown reference tracking and stabilization for a class of unknown nonlinear systems, based on time-varying nonlinear high-gain feedback. To address unstable nonlinear systems with time-varying extrema, [73] presents a model-based adaptive ES algorithm. The results in [31] and [40] establish local and semi-global practical asymptotic stability of the extremum with a dynamic map. While [40] seeks a constant optimizer by ES to optimize time-varying steady-state plant, [31] extends the Lie bracket approximation method to prove convergence toward a neighborhood of a time-varying optimizer. The robustness of Lie bracket-based ES schemes with respect to time-varying parameters is investigated in [60] within the framework of input-to-state stability (ISS). Additionally, [86]

studies ISS-like properties of fixed-time extremum seeking with a time-varying cost function. In contrast to prior results, which utilize high-frequency dither signals, [71] develops a cooperative ES scheme for tracking moving sources without the need for dither signals. Although all these studies achieve convergence to a small neighborhood of the time-varying optimum, they do not ensure perfect tracking.

Contributions. In Chapter 5 of this thesis, we introduce three uES designs that achieve perfect tracking of arbitrarily time-varying optima: asymptotic uES, exponential uES, and prescribed-time uES, which achieve convergence asymptotically, exponentially, and in prescribed time, respectively. Our key contributions are listed below:

- We extend the capabilities of our exponential and PT uES designs from Chapter 3 by (i) broadening the strong convexity assumption to encompass a wider class of convex cost functions, (ii) relaxing the fixed optima assumption to include time-varying optima, and (iii) accommodating $\mathscr{C}^2$ functions (continuously differentiable up to the second order) instead of $\mathscr{C}^4$.

- We establish feasibility conditions for selecting time-varying design parameters and their decay/growth rates in relation to the convexity of the map and the decay/growth rate of the optima. These conditions imply that the use of constant-frequency probing restricts the range of achievable asymptotic unbiasing rates, depending on the "flatness" of the map at the optimum. In contrast, employing chirpy probing enables users to define the unbiasing rate arbitrarily–whether asymptotic, exponential, or in prescribed time–provided that the frequency and adaptation rates grow sufficiently fast.

- Compared to existing designs [2, 33, 38, 106], which achieve asymptotic unbiased convergence, our asymptotic uES design offers convergence at a user-defined asymptotic rate. To the best of our knowledge, perfect tracking of time-varying optima at a desired rate has not been achieved in prior works in the field.

Other contributions are as follows:

- We develop an exponential uES tailored to a unicycle, which requires singular perturbation analysis in addition to averaging.
- We experimentally test the developed design on a light-seeking task by tuning the angular velocity of a unicycle robot based on real-time light sensor data.

Our ES designs are built upon two main methodological advances: state scaling and time scaling. Based on state scaling, the system states are multiplied by an unboundedly growing function, and the original system is converted to a new "transformed system". The stability of the transformed system is equivalent to that of the original system, whether asymptotic, exponential, or within a prescribed time, depending on the growth rate of the scaling function. A crucial aspect of this accelerated control technique is that *the states converge faster than the gains diverge,* which guarantees boundedness of the input signal.

The state scaling technique has its roots in the mid-60s, with work by [91] and [125] on analysis of nonlinear feedback systems, which later became known as the "exponential weighting technique". For systems lacking persistency of excitation (PE), exponentially growing gains is used in [77] to compensate for the PE loss and achieve unbiased parameter identification at a desired exponential rate. A major advancement in stability is introduced in [103] with a scaling function that grows and blows up at a user-defined time. This has spurred significant interest in prescribed-time control [104].

Time scaling provides an alternative approach to achieve faster convergence. By conceptually "dilating" the fixed time interval to infinity, controller design and stability analysis are performed in a virtual infinite time domain. Crucially, stability proven in this dilated time domain translates back to guaranteed stability over the original finite time interval after "contracting" time back. We use this method to dilate time from the domain (not necessarily finite) to a new infinite one, allowing us to handle the arbitrarily varying optimum by slowing its speed in the dilated time domain. This enables tracking of the optimum asymptotically, exponentially, or within a prescribed time.

Throughout this thesis, we refer to these techniques as state transformation and time transformation.

1.2 Adaptive Model-Free Control of Continuum Robots

In this section, we shift focus from extremum seeking to a distinct challenge: adaptive control and disturbance rejection in continuum robots.

Continuum robots, which are characterized by their continuously bending structure, are inherently compliant and can conform to highly curved paths [17]. These features make continuum robots particularly well-suited for minimally invasive surgery, where access to the surgical site is often limited and requires high precision [5]. However, the infinite degrees of freedom and nonlinear properties they possess, result in more complex mathematical models. Moreover, the kinematics of robots operating in constrained environments may differ from those in free space due to unknown contact forces along the body of the robot [121]. Therefore, there is a growing need for more accurate models that account for their nonlinear properties and unknown contact forces, as well as more advanced control strategies that ensure their safe and precise navigation.

Continuum robot modeling. Several models have been developed that describe the kinematics and dynamics of continuum robots. The simplest model is the piecewise constant curvature model, which approximates a multi-segment robot as a finite series of serially connected circular arcs [118]. The pose of the robot's backbone is defined by triplets of arc length, curvature, and orientation angle, but this model neglects the deformations of the robot under external loads. This model is further extended by the variable curvature model, in which each segment is defined by a finite number of serially connected circular arcs, for robots with non-uniform curvature [68]. However, this model has not gained widespread acceptance as it makes the kinematic formulation complex without providing a generalized solution for deformed shapes due to external forces and moments. The Cosserat rod theory has shown promising results in the static modeling of

continuum robots as a set of nonlinear ODEs, as well as in the dynamic modeling of these robots as a set of nonlinear PDEs, for non-constant curvatures deformed by external loading, which cause bending, torsion, shear and extension [89]. The Cosserat rod model, while being a powerful tool, has high computational cost and struggles to capture all nonlinear properties of continuum robots.

Model-based and model-free control of continuum robots. The common approach for model-based control of continuum robots is to compute the kinematic Jacobian matrix, using either an analytical formulation or using numerical methods, and to update the input proportional to the inverse of the Jacobian [24]. Additional approaches have included the development of optimal control techniques [114] and model-predictive control methods [48] based on the Cosserat rod model. Despite their advantages in terms of predictability and reliability, there are still several limitations of these model-based control methods. For example, the analytical solution of the derived model may not be possible, and numerical methods may not produce satisfactory results in terms of accuracy and computation time [28]. Additionally, unstructured external forces on the robot may not be measured or estimated, and sensor feedback may be limited [24]. Without reliable sensor feedback, model-based controllers may cause instability on the robot interacting with unstructured environments [121].

An alternative approach is the use of model-free control techniques, which are appealing due to their adaptability to robot characteristics, changes in the environment, and computational efficiency [24]. One of the widely used model-free control techniques is to estimate the Jacobian matrix online using input-output data and to design a controller using the pseudo-inverse of the Jacobian estimate. Several methods have been developed for Jacobian estimation, including a windowing approach [122], an adaptive Kalman filter [64], an update law that uses the velocity, acceleration information of the end-effector [108, 13] and a technique that uses online image data of robot [111]. Another popular model-free control technique is the use of neural networks [115]. This technique involve training a neural network offline to learn the kinematics of the robot, and then using this pre-trained network to control the robot's movement to a desired

position. Furthermore, by fine-tuning the network online with sensor feedback, the robot can adapt to changes in the environment, making it robust to disturbances.

Physiological disturbance compensation. Continuum robots are designed to be used for surgical operations inside live bodies and interact with dynamic anatomy. However, one of the challenges facing continuum robots in such operations is the presence of physiological disturbances inside the body, such as respiration and heartbeat [27]. These disturbances can cause significant movement of the robot tip, making it difficult to maintain a stable position or to stabilize a camera view with respect to a dynamically disturbed target. Therefore, the compensation of these disturbances is critical for precise and safe surgical operations.

The motion of the heart is a complex and dynamic process that is difficult to model, making it challenging to compensate for the heart motion using traditional control methods. Additionally, the physical limits of most robots, such as the speed of their actuators, can make it difficult to compensate for its fast and unpredictable movement [5]. In contrast, the respiration cycle of a patient under artificial ventilation is often shown to be periodic [27, 83]. This characteristic allows for the design of control algorithms, such as repetitive control [83, 88, 6], model-predictive control [27, 6, 3], and Extended Kalman filter [124, 65, 36], to estimate or compensate for the predictable and repetitive nature of the respiration cycle. However, the breathing frequency may change over time, resulting in a deviation in the estimation of the breathing motion [65]. Overall, there remains a need for disturbance rejection strategies for robots that are subject to both periodic and non-periodic disturbances.

Contributions. In Chapter 6, we introduce a novel model-free adaptive controller that is robust to unknown disturbances and capable of tracking a reference trajectory. We adopt a neural network-based approximation technique, inspired by [66, 76], to estimate the uncertain Jacobian matrix. The neural network weights are estimated online, and a dynamic controller is designed based on the pseudo-inverse of the Jacobian estimate. To reject disturbances, we develop two control strategies. The first strategy is designed for disturbances that are periodic and unknown. The fundamental frequency of the disturbance is determined in an offline mode

while the controller is inactive. Subsequently, an adaptive model-free disturbance rejection algorithm is implemented online, in conjunction with an adaptive disturbance observer, which incorporates the internal model of the disturbance with a finite number of harmonics of the estimated frequency. The adaptation of the neural network and the estimation of the disturbance are performed simultaneously in an online manner. The second control strategy is designed for robustness to any unknown and arbitrary disturbance, which does not necessarily need to be periodic. This strategy utilizes time-varying input and update law gains that grow monotonically and have been shown to be effective in controlling uncertain nonlinear systems for exponential stabilization [105] and for fixed-time stabilization in user-prescribed time [103, 54], herein referred to as prescribed-time stabilization. This speeds up the convergence of the system states and makes the system robust to any arbitrary disturbance. Through the use of these gain functions, we achieve the asymptotic, exponential and prescribed-time convergence of the trajectory tracking error to zero. This stability result is notable compared to the result of the first strategy, which solely guarantees the ultimate boundedness of the tracking error.

Additionally, we present the following contributions:

- The periodic disturbance rejection algorithms presented in [83, 27] compute the fundamental frequency of the disturbance using power spectral density analysis. We introduce an adaptive frequency estimator, presented in Section 6.4, that estimates the fundamental frequency in an adaptive manner. Compared to the adaptive estimators in [69, 12], which employ a cascade of low-pass filters, referred to as prefilters, and additional filters applied to the prefiltered signal to estimate the frequency, our developed estimator employs only low-pass and high-pass filters without any additional filters. This approach results in a reduction in the number of filters used and an improvement in the accuracy of the frequency estimation.

- In contrast to the existing results achieving robustness against disturbances with a sliding-mode term [24], our controllers are continuous, reducing the risk of chattering that may

occur with discontinuous controllers.

- To the best of the our knowledge, this work introduces a novel approach that has not been previously reported in the literature, which utilizes an adaptive observer to estimate a periodic disturbance online and a model-free controller to reject this disturbance, while continuously updating the Jacobian matrix using only position measurements. The accelerated algorithms presented in Section 6.5 are the first results in the literature that achieve rapid convergence to a reference trajectory, as well as robustness against arbitrary disturbances in continuum robots.

Chapter 2

Prescribed-Time Extremum Seeking for Delays and PDEs

In this chapter, we introduce a prescribed-time extremum seeking (PT-ES) approach to reaching the optimum in a user-assignable "prescribed" time (PT), independent of the initial condition of the estimator. Instead of conventional sinusoidal probing signals, we employ "chirpy" perturbations, i.e., sinusoids with growing frequencies. In addition to providing a result for a static input-output map, we provide algorithms for a map in cascade with (1) a delay, (2) a wave PDE, and (3) a heat/diffusion PDE. The designs are based on the time-varying PT backstepping approach, which transforms the PDE-ODE cascade into a suitable PT-stabilized target system, and on averaging-based estimates of the gradient and Hessian of the map. Classical averaging does not apply for the analysis of PT-ES algorithms for four reasons: neither is probing periodic, nor is the 'average system' exponentially stable, nor is the original system finite-dimensional, nor is the interval of operation infinite. We develop an averaging technique needed for this non-periodic finite-time infinite-dimensional problem. Along with PDE Lyapunov analysis, we show that the input converges to the optimizer in prescribed time. We present three numerical examples to illustrate the effectiveness of the proposed technique for delay-free case as well as for compensation of time-delay and diffusion PDE dynamics.

The structure of this chapter is as follows: we introduce the first result in the literature achieving prescribed-time extremum seeking, starting with static maps in Section 2.1 and

extending to maps with delay in Section 2.2. Section 2.3 addresses maps with wave PDE dynamics, while Section 2.4 focuses on those with diffusion PDE dynamics. The paper concludes with Section 2.5, followed by acknowledgments.

Notation. The partial derivatives of a function $u(x,t)$ are denoted by $\partial_x u(x,t) = \partial u(x,t)/\partial x$, $\partial_t u(x,t) = \partial u(x,t)/\partial t$. The spatial $L_2[0,D]$ and $H_1[0,D]$ norm of $u(x,t)$ are denoted by $||u(\cdot,t)||^2_{L_2[0,D]} = \int_0^D u^2(x,t)dx$ and $||u(\cdot,t)||^2_{H_1[0,D]} = ||u(\cdot,t)||^2_{L_2[0,D]} + ||\partial_x u(\cdot,t)||^2_{L_2[0,D]}$, respectively. The real part of a complex number z is denoted by $\mathrm{Re}\{z\}$. $L_k^{(\alpha)}(\cdot), J_m(\cdot)$ and $I_m(\cdot)$ denote the generalized Laguerre polynomial, Bessel function and modified Bessel function of the first kind, respectively, which are defined by the following formulas: $L_k^{(\alpha)}(p) = \sum_{r=0}^{k} \binom{k+\alpha}{k-r} \frac{(-p)^r}{r!}, J_m(p) = \sum_{k=0}^{\infty} \frac{(-1)^k (p/2)^{m+2k}}{k!(k+m)!}, I_m(p) = \sum_{k=0}^{\infty} \frac{(p/2)^{m+2k}}{k!(k+m)!}$.

2.1 Basic PT-ES for Static Map

The main objective of scalar PT-ES is to find the optimum of the unknown static map $Q(\theta)$ in a prescribed-time by employing harmonic excitation to the input $\theta \in \mathbb{R}$, and extracting the gradient information $\hat{G}$ from the output response $y \in \mathbb{R}$. Regarding the structure of the unknown static map, we assume the following:

Assumption 2.1 *The unknown nonlinear static map has the following quadratic form,*

$$Q(\theta) = y^* + \frac{H}{2}(\theta - \theta^*)^2, \tag{2.1}$$

where $y^* \in \mathbb{R}$ and $\theta^* \in \mathbb{R}$ are the unknown optimum output and input value, respectively, $H < 0$ is the unknown Hessian of the static map $Q(\theta)$.

We illustrate the basic procedure of the PT-ES scheme in Fig. 2.1. It is clear from (2.1) and Fig. 2.1 that the output signal $y(t)$ is written as follows

$$y(t) = y^* + \frac{H}{2}(\theta(t) - \theta^*)^2. \tag{2.2}$$

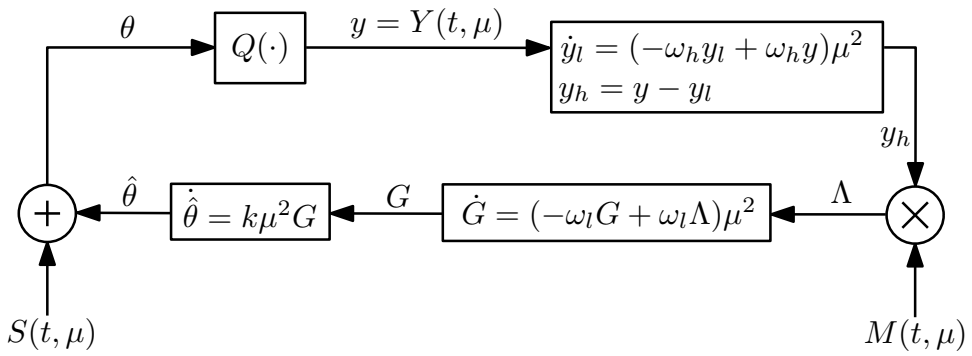

Figure 2.1. Basic PT-ES scheme.

We define the following dilation and contraction transformations

$$\tau = t_0 + (t - t_0)\mu, \tag{2.3}$$

$$t = t_0 + \frac{T(\tau - t_0)}{T + \tau - t_0}, \tag{2.4}$$

with the following smooth function

$$\mu(t) = \frac{T}{T + t_0 - t}, \tag{2.5}$$

for $t \in [t_0, t_0 + T)$, $\tau \in [t_0, \infty)$, where t_0 is the initial time and T is the prescribed-time. The dynamics of the blowing up function (2.5) is given by

$$\dot{\mu} = \frac{1}{T}\mu^2. \tag{2.6}$$

In general, the perturbation signals $S(t)$ and $M(t)$ are chosen as $a\sin(\omega t)$ and $\frac{2}{a}\sin(\omega t)$ in order to ensure the exponential stability of the averaged error-dynamics. To achieve PT convergence to the extremum, we replace the sinusoids with "chirpy" perturbation and demodulation signals whose frequency grows rather than being constant:

$$S(t,\mu) = a\sin\left(\omega(t_0 + (t - t_0)\mu)\right), \tag{2.7}$$

$$M(t,\mu) = \frac{2}{a}\sin\left(\omega(t_0 + (t-t_0)\mu)\right). \tag{2.8}$$

We summarize closed-loop system depicted in Fig. 2.1 as follows

$$\frac{d}{dt}\begin{bmatrix}\tilde{\theta}\\ G\\ \tilde{y}_l\end{bmatrix} = \begin{bmatrix} k\mu^2 G \\ -\omega_l\mu^2 G + \omega_l\mu^2(y - y^* - \tilde{\eta})M(t,\mu) \\ -\omega_h\mu^2\tilde{y}_l + \omega_h\mu^2(y-y^*)\end{bmatrix}, \tag{2.9}$$

in view of the transformations

$$\tilde{\theta} = \hat{\theta} - \theta^*, \tag{2.10}$$

$$\tilde{y}_l = y_l - y^*, \tag{2.11}$$

where $\hat{\theta}$ is the estimate of θ^*, $\tilde{\theta}$ is the estimation error, and y_l is governed by

$$\dot{y}_l = -\omega_h\mu^2 y_l + \omega_h\mu^2 y.$$

Let us note that $\theta = \hat{\theta} + a\sin\left(\omega(t_0 + (t-t_0)\mu)\right)$, which yields $\theta - \theta^* = \tilde{\theta} + a\sin(\omega(t_0 + (t-t_0)$ $\times\mu))$. Then, we can rewrite the output signal (2.2) as follows

$$Y(t,\mu) = y^* + \frac{H}{2}\left(\tilde{\theta} + a\sin(\omega(t_0 + (t-t_0)\mu))\right)^2.$$

Considering (2.3), (2.4) along with

$$\frac{d\tau}{dt} = \mu^2,$$

we can write the system (2.9) in the dilated τ-domain

$$\frac{d}{d\tau}\begin{bmatrix}\tilde{\theta}^{\infty}\\ G^{\infty}\\ \tilde{y}_l^{\infty}\end{bmatrix} = \begin{bmatrix} kG^{\infty} \\ -\omega_l G^{\infty} + \omega_l\left[\frac{H}{2}\left(\tilde{\theta}^{\infty} + a\sin(\omega\tau)\right)^2 - \tilde{\eta}\right]\frac{2}{a}\sin(\omega\tau) \\ -\omega_h\tilde{y}_l^{\infty} + \omega_h\frac{H}{2}\left(\tilde{\theta}^{\infty} + a\sin(\omega\tau)\right)^2\end{bmatrix}, \tag{2.12}$$

where

$$\begin{bmatrix}\tilde{\theta}^{\infty}(\tau)\\ G^{\infty}(\tau)\\ \tilde{y}_l^{\infty}(\tau)\end{bmatrix} = \begin{bmatrix}\tilde{\theta}\left(t_0 + \frac{T(\tau-t_0)}{T+\tau-t_0}\right)\\ G\left(t_0 + \frac{T(\tau-t_0)}{T+\tau-t_0}\right)\\ \tilde{y}_l\left(t_0 + \frac{T(\tau-t_0)}{T+\tau-t_0}\right)\end{bmatrix}.$$

The averaging of (2.12) yields

$$\frac{d}{d\tau}\begin{bmatrix}\tilde{\theta}_{\text{av}}^{\infty}\\ G_{\text{av}}^{\infty}\\ \tilde{y}_{l,\text{av}}^{\infty}\end{bmatrix} = \begin{bmatrix} kG_{\text{av}}^{\infty} \\ -\omega_l G_{\text{av}}^{\infty} + \omega_l H\tilde{\theta}_{\text{av}}^{\infty} \\ -\omega_h\tilde{y}_{l,\text{av}}^{\infty} + \omega_h\frac{H}{2}(\tilde{\theta}_{\text{av}}^{\infty})^2 + \omega_h a^2\frac{H}{4}\end{bmatrix}, \tag{2.13}$$

where $\tilde{\theta}_{\text{av}}^{\infty}, G_{\text{av}}^{\infty}, \tilde{y}_{l,\text{av}}^{\infty}$ denote the average versions of the states $\tilde{\theta}^{\infty}, G^{\infty}, \tilde{y}_l^{\infty}$. We obtain the equilibrium of the average system (2.13) as $\begin{bmatrix}\tilde{\theta}_{\text{av,e}}^{\infty} & G_{\text{av,e}}^{\infty} & \tilde{y}_{l,\text{av,e}}^{\infty}\end{bmatrix} = \begin{bmatrix}0 & 0 & Ha^2/4\end{bmatrix}$. The Jacobian of the average system (2.13) at the equilibrium $\begin{bmatrix}\tilde{\theta}_{\text{av,e}}^{\infty} & G_{\text{av,e}}^{\infty} & \tilde{y}_{l,\text{av,e}}^{\infty}\end{bmatrix}$ is given by

$$J_{\text{av,e}} = \begin{bmatrix} 0 & k & 0 \\ \omega_l H & -\omega_l & 0 \\ 0 & 0 & -\omega_h\end{bmatrix},$$

which is Hurwitz. Then, we deduce the local exponential stability of the average system (2.13) in τ-domain, $\tau \in [t_0, \infty)$ as well as the local stability of the system (2.9) in t-domain, $t \in [t_0, t_0 + T)$. The following theorem concludes the properties of the basic PT-ES scheme depicted in Fig. 2.1.

Theorem 2.1 *Consider the system in Fig. 2.1 and the transformations* (2.3)*,* (2.4) *under Assumption 2.1. There exists* $\omega^* > 0$ *such that* $\forall \omega > \omega^*$*, the feedback system* (2.12) *with states* $\tilde{\theta}^{\infty}(\tau), G^{\infty}(\tau), \tilde{y}_l^{\infty}(\tau)$ *has a unique prescribed-time stable solution in* t*-domain, denoted by* $\tilde{\theta}^{\Pi}(t_0+(t-t_0)\mu)$*,* $G^{\Pi}(t_0+(t-t_0)\mu)$*,* $\tilde{y}_l^{\Pi}(t_0+(t-t_0)\mu)$*, where* $\tilde{\theta}^{\Pi}(\tau), G^{\Pi}(\tau), \tilde{y}_l^{\Pi}(\tau)$ *are the unique exponentially stable periodic solutions in* τ *of period* $\Pi = 2\pi/\omega$ *satisfying* $\forall \tau \geq t_0$*:*

$$\left(\left|\tilde{\theta}^{\Pi}(\tau)\right|^2 + \left|G^{\Pi}(\tau)\right|^2 + \left|\tilde{y}_l^{\Pi}(\tau) - Ha^2/4\right|^2\right)^{1/2} \leq \mathscr{O}(1/\omega). \tag{2.14}$$

Furthermore,

$$\lim_{t \to t_0+T} \sup |\theta(t) - \theta^*| = \mathscr{O}(a + 1/\omega), \tag{2.15}$$

$$\lim_{t \to t_0+T} \sup |y(t) - y^*| = \mathscr{O}(a^2 + 1/\omega^2). \tag{2.16}$$

Proof By the application of the averaging theorem [49] to (2.13), we prove the existence of unique exponentially stable periodic solutions of (2.12), $\tilde{\theta}^{\Pi}(\tau), G^{\Pi}(\tau), \tilde{y}_l^{\Pi}(\tau)$, which satisfy (2.14). Performing the time contraction $\tau \to t$ in (2.14), we deduce the PT stable solution of (2.9). Then, we can write

$$\begin{aligned}
\lim_{\tau \to \infty} \sup |\tilde{\theta}^{\infty}(\tau)|^2 &= \lim_{\tau \to \infty} \sup \left\{ |\tilde{\theta}^{\infty}(\tau) + \tilde{\theta}^{\Pi}(\tau) - \tilde{\theta}^{\Pi}(\tau)|^2 \right\}, \\
&\leq \sqrt{2} \lim_{\tau \to \infty} \sup \left\{ |\tilde{\theta}^{\infty}(\tau) - \tilde{\theta}^{\Pi}(\tau)|^2 + |\tilde{\theta}^{\Pi}(\tau)|^2 \right\}, \\
&= \mathscr{O}(1/\omega),
\end{aligned}$$

by noting (2.14) and recalling that $\tilde{\theta}^{\infty}(\tau) \to \tilde{\theta}^{\Pi}(\tau)$ as $\tau \to \infty$. Considering the property of $\theta^{\infty}(\tau) - \theta^* = \tilde{\theta}^{\infty}(\tau) + a\sin(\omega\tau)$ and performing the time contraction $\tau \to t$, we get (2.15). Considering (2.2) and (2.15), we conclude (2.16). ■

Example 2.1 *[Numerical simulation (delay-free)] We consider the following static quadratic*

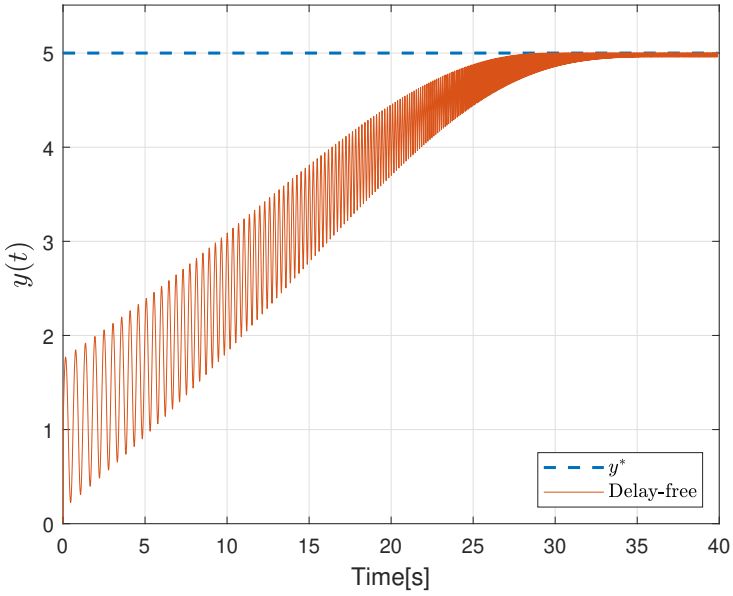

Figure 2.2. The performance of the delay-free PT-ES.

map

$$Q(\Theta) = 5 - (\Theta - 2)^2. \tag{2.17}$$

We assume that the map (2.17) *is measured with no delay. We select the perturbation signal parameters* $a = 0.2$, $\omega = 10$, *the initial time* $t_0 = 0$, *the terminal time* $T = 40$ *and set all initial conditions to zero. The cut-off frequencies of the high-pass and low-pass filters are* $\omega_l = \omega_h = 5$. *We implement the basic delay-free PT-ES algorithm with the gain* $k = 0.01$, *the time step* 10^{-4} *and show the result in Fig. 2.2. It is clear that the output signals oscillate with the frequency, which grows over time and converges to the neighborhood of the extremum in the prescribed-time.*

Remark 2.1 *The utilization of chirpy signals and time-varying gains in the ES loop offers distinct advantages over the use of existing sinusoidal perturbations. In addition to enabling convergence within user-defined time interval, the introduced PT-ES also provides enhanced robustness against dynamic variations of extrema and external disturbances. For an in-depth*

discussion on the performance of classical ES and PT-ES concerning the problem of source seeking by a unicycle in the presence of destabilizing drift, interested readers can refer to [110].

Remark 2.2 *The application of our PT-ES approach to a physical system presents a significant challenge due to the presence of the blow-up gain μ. In order to address this concern, a pragmatic approach involves 'clipping' the function μ to feasible large values that enable convergence to a sufficiently close neighborhood to the extremum. Regarding the numerical implementation of a delay-free PT-ES approach for a unicycle, the incorporation of a saturation function to restrict the growth of μ is detailed in [110].*

2.2 PT-ES with Delays

In this section, we consider the case that the output $y(t)$ has a known and constant delay $D \in \mathbb{R}$, i.e.,

$$y(t) = Q(\theta(t-D)). \tag{2.18}$$

Note that the static map $Q(\theta)$ allows us to write the delay D as $D = D_u + D_y$, where D_u and D_y are the delays in the actuation and measurement path, respectively. Our aim is to design a scalar PT-ES which compensates the delay and stabilizes the output signal $y(t)$ around a small neighborhood of the extremum in the prescribed time $T > D$. In addition to Assumption 2.1, we make the following assumption regarding the bound of the Hessian.

Assumption 2.2 *The lower bound of the unknown Hessian of the static map, $\bar{H} < H$, is known.*

Considering Assumption 2.1, we can write the output of the static map as follows

$$y(t) = y^* + \frac{H}{2}(\theta(t-D) - \theta^*)^2. \tag{2.19}$$

Fig. 2.3 illustrates the closed-loop ES with prescribed-time delay compensation controller, which is to be designed.

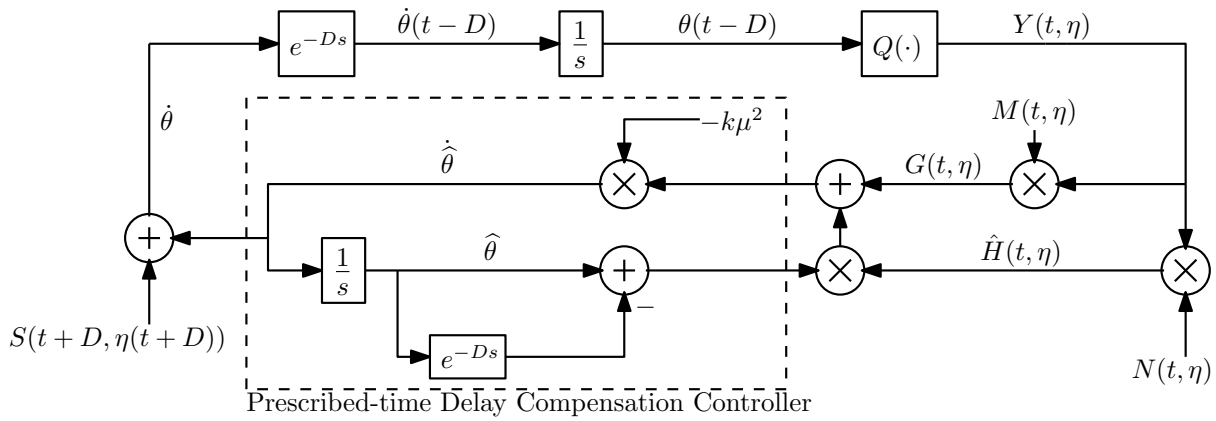

Figure 2.3. PT-ES scheme with delay compensation.

Remark 2.3 *We incorporate modified high-pass and low-pass filters into the delay-free ES scheme depicted in Fig. 2.1. These filters are specifically designed to smooth the estimates of the gradient $G(t)$ and Hessian estimate $\hat{H}(t)$ over a predefined time interval. However, the integration of these filters into the ES loop in Fig. 2.3 and the temporal transformation from $t \in [0,T)$ to $\tau \in [t_0,\infty)$, results in a nonlinear evolution equation, which requires more rigorous analysis as pointed out in [67]. The ES schemes and numerical simulations presented in this section, as well as subsequent sections, do not incorporate these filters.*

2.2.1 Perturbation signals and gradient/Hessian estimates

In this subsection, we define the signals introduced in Fig. 2.3. We introduce the following estimator

$$\hat{\theta}(t) = \theta(t) - a\sin\left(\omega(t_0 + (t+D-t_0)\mu(t+D))\right), \tag{2.20}$$

for $t \in [t_0+D, t_0+T)$ and $\hat{\theta}(t) = \hat{\theta}_0 \in \mathbb{R}$ for $t \in [t_0, t_0+D)$. We define the delayed parameter estimation error as follows

$$\vartheta(t) = \hat{\theta}(t-D) - \theta^*, \tag{2.21}$$

for $t \in [t_0+D, t_0+T+D)$. Considering (2.21) and using the technique in [56], we can write the following transport PDE

$$\vartheta(t) = \bar{u}(0,t), \tag{2.22}$$

$$\partial_t \bar{u}(x,t) = \partial_x \bar{u}(x,t), \tag{2.23}$$

$$\bar{u}(D,t) = \hat{\theta}(t) - \theta^*, \tag{2.24}$$

where the solution of (2.23) and (2.24) is given by $\bar{u}(x,t) = \hat{\theta}(t+x-D) - \theta^*$. Let us define an infinite dimensional state $\eta : \mathscr{X} \to \mathscr{X}$, where $\mathscr{X} := \mathbb{R} \times \mathbb{R} \times L_2[0,D] \times \mathbb{R}$, by

$$\eta(t) = \begin{bmatrix} \vartheta(t), & \mu(t), & \bar{u}(\cdot,t), & \hat{\theta}(t) \end{bmatrix}^T. \tag{2.25}$$

Then, we rewrite the output signal (2.19) using (2.20), (2.21) in the following form

$$Y(t,\eta) = y^* + \frac{H}{2}(\vartheta + a\sin(\omega(t_0 + (t-t_0)\mu)))^2, \tag{2.26}$$

for $t \in [t_0+D, t_0+T+D)$. Moreover, one gets from (2.20) and Fig. 2.3 that

$$\dot{\theta}(t) = \dot{\hat{\theta}}(t) + S(t+D, \eta(t+D)),$$

where the perturbation signal is

$$S(t+D,\eta(t+D)) = a\omega\cos\left(\omega(t_0 + (t+D-t_0)\mu(t+D))\right)\mu^2(t+D),$$

for $t \in [t_0+D, t_0+T)$. The final step before proceeding to the controller design is to generate the estimate of the gradient and Hessian as follows

$$G(t,\eta) = M(t,\eta)Y(t,\eta), \tag{2.27}$$

$$\hat{H}(t,\eta) = N(t,\eta)Y(t,\eta), \tag{2.28}$$

with the following multiplicative excitation signals

$$M(t,\eta) = \frac{2}{a}\sin\left(\omega(t_0+(t-t_0)\mu)\right), \tag{2.29}$$

$$N(t,\eta) = -\frac{8}{a^2}\cos\left(2\omega(t_0+(t-t_0)\mu)\right). \tag{2.30}$$

Lemma 2.1 *The averaged version of the gradient* (2.27) *and Hessian estimate* (2.28) *are given by*

$$G_{\text{av}}(t,\eta) = H\vartheta, \tag{2.31}$$

$$\hat{H}_{\text{av}}(t,\eta) = H. \tag{2.32}$$

Proof Considering (2.4), let us define

$$G^{\infty}(\tau,\eta^{\infty}(\tau)) = G\left(t_0+\frac{T(\tau-t_0)}{T+\tau-t_0}, \eta\left(t_0+\frac{T(\tau-t_0)}{T+\tau-t_0}\right)\right),$$
$$\hat{H}^{\infty}(\tau,\eta^{\infty}(\tau)) = \hat{H}\left(t_0+\frac{T(\tau-t_0)}{T+\tau-t_0}, \eta\left(t_0+\frac{T(\tau-t_0)}{T+\tau-t_0}\right)\right),$$
$$\vartheta^{\infty}(\tau) = \vartheta(t_0+T(\tau-t_0)/(T+\tau-t_0),$$

and compute (2.27), (2.28) along with (2.26), (2.29), (2.30) in τ-domain as follows

$$G^{\infty}(\tau,\eta^{\infty}) = \frac{2}{a}\sin(\omega\tau)\left[y^* + \frac{H}{2}(\vartheta^{\infty}+a\sin(\omega\tau))^2\right],$$
$$\hat{H}^{\infty}(\tau,\eta^{\infty}) = -\frac{8}{a^2}\cos(2\omega\tau)\left[y^* + \frac{H}{2}(\vartheta^{\infty}+a\sin(\omega\tau))^2\right]$$

from which we conclude that their average with respect to τ over the period $2\pi/\omega$ treating ϑ^{∞} as constant are computed as $G^{\infty}_{\text{av}}(\tau,\eta^{\infty}) = H\vartheta^{\infty}$, $\hat{H}^{\infty}_{\text{av}}(\tau,\eta^{\infty}) = H$. Performing the time contraction

$\tau \to t$, we prove (2.31) and (2.32). ■

2.2.2 Controller design

Let us take the derivative of (2.22)–(2.24) as follows

$$\dot{\vartheta}(t) = u(0,t), \tag{2.33}$$

$$\partial_t u(x,t) = \partial_x u(x,t), \tag{2.34}$$

$$u(D,t) = \dot{\hat{\theta}}(t), \tag{2.35}$$

where $u(x,t) = \partial_t \bar{u}(x,t)$. Following the technique discussed in [56], we consider the following backstepping transformation

$$w(x,t) = u(x,t) + \bar{k}\mu^2(t+x-D)\left(\vartheta(t) + \int_0^x u(y,t)dy\right), \tag{2.36}$$

which maps (2.33)–(2.35) into the target system

$$\dot{\vartheta}(t) = -\bar{k}\mu^2(t-D)\vartheta(t) + w(0,t), \tag{2.37}$$

$$\partial_t w(x,t) = \partial_x w(x,t), \tag{2.38}$$

$$w(D,t) = 0, \tag{2.39}$$

where $\bar{k} > 0$. By letting $x = D$ in (2.36), we obtain the controller as follows

$$\dot{\hat{\theta}}(t) = -\bar{k}\mu^2(t)\left(\vartheta(t) + \int_0^D u(y,t)dy\right). \tag{2.40}$$

The implementation of the controller (2.40) is not possible since there is no measurement of $\vartheta(t)$. To achieve this, let us define $\bar{k} = kH$ where $H < 0$ is the unknown Hessian and the gain $k < 0$ is assigned by the user. Considering Lemma (2.1), we can rewrite the controller (2.40) in

terms of (2.27) and (2.28) as follows

$$\dot{\hat{\theta}}(t) = \hat{H}(t,\eta(t))Q(\eta(t)) + G(t,\eta(t))P(\eta(t)), \tag{2.41}$$

where

$$\begin{aligned} Q(\eta(t)) =& -k\mu^2(t)\int_0^D \partial_t \bar{u}(y,t)dy \\ =& -k\mu^2(t)\left(\hat{\theta}(t) - \hat{\theta}(t-D)\right), \end{aligned} \tag{2.42}$$

$$P(\eta) = -k\mu^2. \tag{2.43}$$

In (2.42), we use the fact that $\partial_t \bar{u}(y,t) = u(y,t) = \dot{\hat{\theta}}(t+y-D)$ and $\partial_t \hat{\theta}(t+y-D) = \partial_y \hat{\theta}(t+y-D)$. Let us substitute (2.27) and (2.28) into (2.41). Then, we obtain the following closed-loop error system

$$\vartheta(t) = \bar{u}(0,t), \tag{2.44}$$

$$\partial_t \bar{u}(x,t) = \partial_x \bar{u}(x,t), \tag{2.45}$$

$$\bar{u}(D,t) = \tilde{\theta}(t), \tag{2.46}$$

$$\begin{aligned} \dot{\tilde{\theta}} =& -kH\mu^2\tilde{\theta} + \sin\left(\omega(t_0 + (t-t_0)\mu)\right) f_1(\eta) - \cos\left(2\omega(t_0 + (t-t_0)\mu)\right) f_2(\eta) \\ & - \sin\left(3\omega(t_0 + (t-t_0)\mu)\right) f_3(\eta) + \cos\left(4\omega(t_0 + (t-t_0)\mu)\right) f_4(\eta), \end{aligned} \tag{2.47}$$

where

$$f_1(\eta) = P(\eta)\left[\frac{2y^*}{a} + \frac{H}{a}\vartheta^2 + \frac{3Ha}{4}\right] + Q(\eta)\left[\frac{4H}{a}\vartheta\right], \tag{2.48}$$

$$f_2(\eta) = P(\eta)[H\vartheta] + Q(\eta)\left[2H + \frac{8y^*}{a^2} + \frac{4H}{a^2}\vartheta^2\right], \tag{2.49}$$

$$f_3(\eta) = P(\eta)\left[\frac{Ha}{4}\right] + Q(\eta)\left[\frac{4H}{a}\vartheta\right], \tag{2.50}$$

$$f_4(\eta) = Q(\eta)H. \tag{2.51}$$

2.2.3 Numerical simulation (with delay)

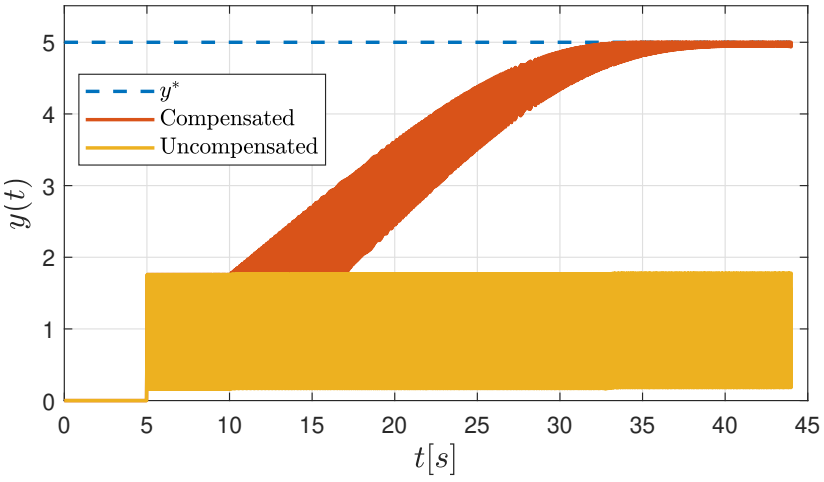

(a)

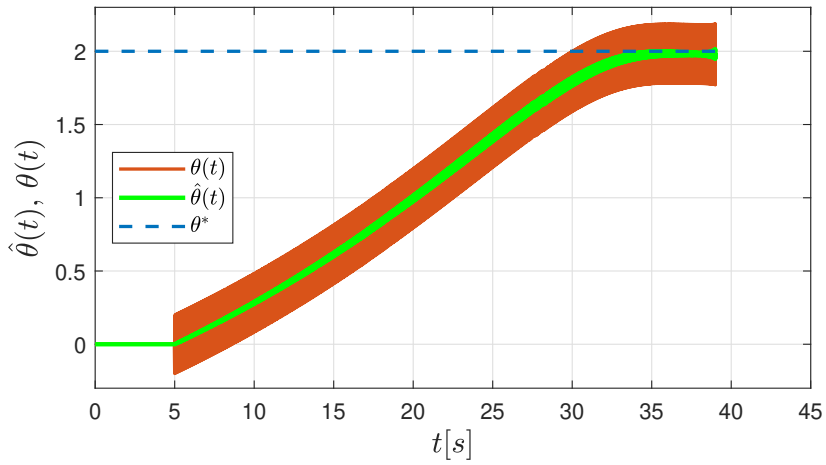

(b)

Figure 2.4. (a) The performance comparison of the delay-free PT-ES and the delay compensated PT-ES in the presence of delay (b) The evolution of the input $\theta(t)$, the estimate $\hat{\theta}(t)$ and the optimum input θ^* under the delay compensated PT-ES.

We return to Example 2.1 and consider the map (2.17). We select the parameters a, the initial time t_0, the terminal time T and the initial conditions as in Example 2.1. We choose $\omega = 80$.

We assume that the measurement $y(t)$ is subject to a known delay $D = 5$. We implement the delay-compensated PT-ES (2.41) with $k = -0.01$. In Fig. 2.4 (a), we compare the performance of the basic delay-free PT-ES and the proposed delay-compensated PT-ES in the presence of delay. One can see that the proposed PT-ES algorithm compensates the delay and ensures convergence of the output towards a vicinity of the extremum point y^*, whereas the basic PT-ES which ignores the delay cannot achieve the convergence. In Fig. 2.4 (b), we present the evolution of relevant variables under the proposed scheme.

2.2.4 Stability analysis

The main theorem is stated as follows.

Theorem 2.2 *For $\bar{T} > D$ arbitrarily close to T, there exists some $\omega^*(\bar{T})$, where $\omega^*(\bar{T}) \to \infty$ as $\bar{T} \to T$, such that $\forall \omega > \omega^*(\bar{T})$, the error system* (2.44)–(2.47) *satisfies*

$$\limsup_{t \to t_0 + \bar{T} + D} \left(|\vartheta(t)| + ||\bar{u}(\cdot, t)||_{L_2[0,D]} \right) = \mathscr{O}(1/\omega), \tag{2.52}$$

and

$$\limsup_{t \to t_0 + \bar{T}} |\hat{\theta}(t) - \theta^*| = \mathscr{O}(1/\omega). \tag{2.53}$$

Furthermore,

$$\limsup_{t \to t_0 + \bar{T}} |\theta(t) - \theta^*| = \mathscr{O}(a + 1/\omega), \tag{2.54}$$

$$\limsup_{t \to t_0 + \bar{T} + D} |y(t) - y^*| = \mathscr{O}(a^2 + 1/\omega^2). \tag{2.55}$$

Proof Let us proceed through the proof step by step.

Step 1: (Averaging operation) Let us define a linear operator $\mathscr{A} : \mathscr{D}(\mathscr{A}) \subset \mathscr{X} \to \mathscr{X}$

by

$$\mathscr{A}\eta(t) = \begin{bmatrix} \frac{d\bar{u}(0,t)}{dx} & 0 & \frac{d\bar{u}(\cdot,t)}{dx} & 0 \end{bmatrix}^T,$$

and the domain

$$\mathscr{D}(\mathscr{A}) = \left\{ [\vartheta(t), \mu(t), \bar{u}(\cdot,t), \hat{\theta}(t)] \in \mathscr{X} : \bar{u}(D,t) = \hat{\theta}(t) - \theta^* \right\}.$$

We can write the derivative of the infinite-dimensional state vector (2.25) as follows

$$\dot{\eta} = \mathscr{A}\eta + J(\omega t, \eta), \tag{2.56}$$

for $t \in [t_0 + D, t_0 + \bar{T}]$ where

$$J(\omega t, \eta) = \begin{bmatrix} 0 & \frac{1}{T}\mu^2 & 0 & -kH\mu^2\tilde{\theta} + \check{f}(\omega t, \eta) \end{bmatrix}^T,$$

with

$$\begin{aligned} \check{f}(\omega t, \eta) = {} & \sin\left(\omega(t_0 + (t - t_0)\mu)\right) f_1(\eta) - \cos\left(2\omega(t_0 + (t - t_0)\mu)\right) f_2(\eta) \\ & - \sin\left(3\omega(t_0 + (t - t_0)\mu)\right) f_3(\eta) + \cos\left(4\omega(t_0 + (t - t_0)\mu)\right) f_4(\eta). \end{aligned} \tag{2.57}$$

Let us define the following averaged system

$$\dot{\eta}_{\text{av}} = \mathscr{A}\eta_{\text{av}} + J_{\text{av}}(\eta_{\text{av}}), \tag{2.58}$$

where

$$J_{\text{av}}(\eta) = \lim_{\omega \to \infty} \frac{1}{\omega(\bar{T} - D)} \int_0^{\omega(\bar{T} - D)} J(s, \eta) ds,$$

$$= \begin{bmatrix} 0 & \frac{1}{T}\mu^2 & 0 & -kH\mu^2\tilde{\theta} \end{bmatrix}^T.$$

Inspired by [16, Theorem 5.16], we write the weak formulation of (2.56) by adding and subtracting the term $\left\langle \int_{t_0+D}^{t} J_{\text{av}}(\eta(s))ds, \varphi \right\rangle$, where $\langle \cdot, \cdot \rangle$ stands for the inner product on $\mathscr{X}$, as follows

$$\begin{aligned} \langle \eta(t), \varphi \rangle = \langle \eta(t_0+D), \varphi \rangle + \int_{t_0+D}^{t} \langle \eta(s), \mathscr{A}^* \varphi \rangle \, ds + \left\langle \int_{t_0+D}^{t} J_{\text{av}}(\eta(s))ds, \varphi \right\rangle \\ + \left\langle \int_{t_0+D}^{t} \left[J(\omega s, \eta(s)) - J_{\text{av}}(\eta(s)) \right] ds, \varphi \right\rangle, \end{aligned} \tag{2.59}$$

with $\eta(t_0+D) \in \mathscr{X}$ for all $\varphi \in \text{dom}(\mathscr{A}^*)$ with $\mathscr{A}^*$, the adjoint operator of $\mathscr{A}$. Let us denote the final term of (2.59) by $R(t)$ and define $\sigma = \omega(s - t_0 - D)$, $\check{\eta}(\sigma) = \eta\left(\sigma/\omega + t_0 + D\right)$. Then, we write

$$R(t) = \left\langle \frac{1}{\omega} \int_0^{\omega(t-t_0-D)} J_e\left(\sigma, \check{\eta}(\sigma)\right) d\sigma, \varphi \right\rangle, \tag{2.60}$$

where

$$\begin{aligned} J_e(\sigma, \check{\eta}) &= J(\bar{\sigma}, \check{\eta}) - J_{\text{av}}(\check{\eta}), \\ &= \begin{bmatrix} 0, & 0, & 0, & 0, & \check{f}(\bar{\sigma}, \check{\eta}) \end{bmatrix}^T, \end{aligned} \tag{2.61}$$

and $\bar{\sigma} = \sigma + \omega(t_0 + D)$. It follows from the second line of (2.42), (2.43), (2.48)–(2.51), (2.57), (2.61), that $J_e(\sigma, \check{\eta})$ is a continuous function of $\check{\eta}$. Let us assume for now that $||\check{\eta}||_{\mathscr{X}} \leq C_f$ for some $C_f > 0$ for all $\sigma \in [0, \omega(\bar{T} - D)]$, where $||\cdot||_{\mathscr{X}}$ denotes the induced norm of $\mathscr{X}$. Let us compute the upper bound of (2.60) as follows

$$||R(t)||_{\mathscr{X}} \leq \frac{1}{\omega} \delta(\bar{T}) ||\varphi||_{\mathscr{X}}, \tag{2.62}$$

where

$$\delta(\bar{T}) = \sup_{||\breve{\eta}||_{\mathscr{X}} \leq C_f t_0 + D \leq t < t_0 + \bar{T}} \sup \left|\left| \int_0^{\omega(t-t_0-D)} J_e(\sigma, \breve{\eta})\, d\sigma \right|\right|_{\mathscr{X}}. \tag{2.63}$$

Consider (2.57), (2.61), (2.63) and note the following fact

$$\left| \int_0^{\omega(t-t_0-D)} \sin\left(k_s(\sigma + \omega(t_0+D))\breve{\mu} + \phi_s\right) d\sigma \right| \leq \frac{2}{k_s \breve{\mu}},$$

for any $k_s \in \mathbb{R}^+, \phi_s \in \mathbb{R}$. Then, from (2.62), we get

$$||R(t)||_{\mathscr{X}} = \mathscr{O}(1/\omega), \qquad \forall t \in [t_0 + D, t_0 + \bar{T}], \tag{2.64}$$

for all $\omega > \omega^*(\bar{T}) \gg \delta(\bar{T})$. Then, we conclude that $\eta(t)$ in (2.59) becomes a weak solution of (2.58) as $\omega \to \infty$ and

$$||\eta(t) - \eta_{\text{av}}(t)||_{\mathscr{X}} = \mathscr{O}(1/\omega), \quad \forall t \in [t_0 + D, t_0 + \bar{T}] \tag{2.65}$$

for all $\omega > \omega^*(\bar{T})$. From (2.58), we obtain the average PDE system

$$\vartheta_{\text{av}}(t) = \bar{u}_{\text{av}}(0,t), \tag{2.66}$$

$$\partial_t \bar{u}_{\text{av}}(x,t) = \partial_x \bar{u}_{\text{av}}(x,t), \tag{2.67}$$

$$\bar{u}_{\text{av}}(D,t) = \tilde{\theta}_{\text{av}}(t), \tag{2.68}$$

$$\dot{\tilde{\theta}}_{\text{av}} = -kH\mu^2 \tilde{\theta}_{\text{av}}. \tag{2.69}$$

Step 2: (Stability analysis) It is obvious from (2.69) and (2.66) that $\tilde{\theta}_{\text{av}}(t) \to 0$ as $t \to t_0 + T$ and $\vartheta_{\text{av}}(t) = \tilde{\theta}_{\text{av}}(t-D) \to 0$ as $t \to t_0 + T + D$, respectively. Let us define the norm

$W(t) := ||\bar{u}_{\text{av}}(\cdot,t)||^2_{L_2[0,D]}$ and take its derivative as follows

$$\begin{aligned}\dot{W}(t) &= \int_0^D -2\mu^2(t+x-D)\bar{u}^2_{\text{av}}(x,t)dx \\ &\leq -2\mu^2(t-D)W(t). \end{aligned} \tag{2.70}$$

It follows from (2.70) that

$$||\bar{u}_{\text{av}}(\cdot,t)||^2_{L_2[0,D]} \leq e^{-2T(\mu(t-D)-1)}||\bar{u}_{\text{av}}(\cdot,t_0)||^2_{L_2[0,D]},$$

from which we can conclude that $||\bar{u}_{\text{av}}(\cdot,t)||_{L_2[0,D]} \to 0$ as $t \to t_0+T+D$.

Step 3: (Convergence to a small neighborhood of the extremum) Recalling $\vartheta^2_{\text{av}}(t) + ||\bar{u}_{\text{av}}(\cdot,t)||^2_{L_2[0,D]} \to 0$ as $t \to t_0+T$, we prove (2.52) from (2.65). In view of the fact that $\tilde{\theta}_{\text{av}}(t) \to 0$ as $t \to t_0+T$, we show (2.53) from (2.65). Considering (2.10) and (2.20), we get the relation $\theta(t) - \theta^* = \tilde{\theta}(t) + a\sin(\omega(t_0 + (t+D-t_0)\mu(t+D)))$ and prove (2.54). Finally, from (2.26) and (2.52), we prove (2.55). ■

2.3 PT-ES for Wave PDEs

In this section, we consider the following cascade of a wave PDE and ODE (integrator) with Neumann interconnection

$$\dot{\Theta}(t) = \partial_x\alpha(0,t), \tag{2.71}$$

$$\partial_{tt}\alpha(x,t) = \partial_{xx}\alpha(x,t), \tag{2.72}$$

$$\alpha(0,t) = 0, \tag{2.73}$$

$$\partial_x\alpha(D,t) = \dot{\theta}(t), \tag{2.74}$$

where $(x,t) \in [0,D]\times[t_0,t_0+T)$. The reason why we deal with this particular case of wave PDE dynamics is that we can reformulate this wave PDE compensation problem as the compensation

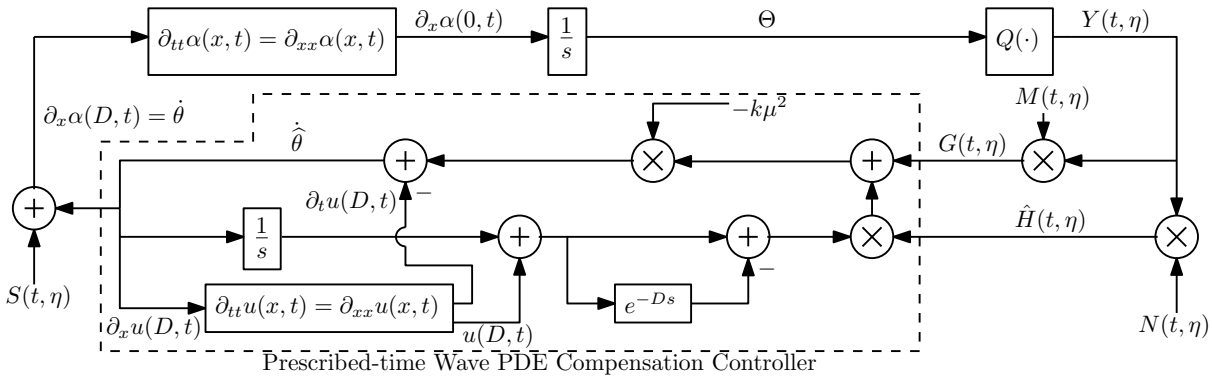

Figure 2.5. ES algorithm that compensates the wave PDE actuation dynamics in prescribed time.

of the cascade of two transport PDEs and an ODE using a set of transformations, which allows us to use the procedure presented in Section 2.2 for the reformulated cascade system. Fig. 2.5 illustrates the closed-loop ES with actuation dynamics and prescribed-time wave PDE compensation controller, which is to be designed. The integrator at the output of the PDE is leveraged to generate an estimate of the optimal input, Θ^*, of the unknown static map $Q(\Theta)$. The output of the static map is given by

$$y = y^* + \frac{H}{2}(\Theta - \Theta^*)^2. \tag{2.75}$$

This problem is motivated by an optimization challenge encountered in oil drilling systems. In these systems, the goal is to maximize the rate of penetration until a specific threshold, referred to as the 'foundering point', is reached. Beyond this threshold, the rate of penetration decreases, resulting in cutter damage and energy wastage, as discussed in [1]. Furthermore, it's demonstrated that a convex static mapping exists between the input (weight on bit) and the output (rate of penetration) with input dynamics represented by the wave PDE-ODE cascade. The task of optimization within a specified time frame could be one of the potential challenges in these systems.

Let us define the following estimators in order to find the optimal unknown actuator Θ^*

$$\widehat{\Theta} = \Theta - a\sin\left(\omega(t_0 + (t-t_0)\mu)\right), \tag{2.76}$$

$$\hat{\theta}(t) = \theta(t) - \int_{t_0}^{t} S(\sigma, \eta(\sigma))d\sigma. \tag{2.77}$$

In [80], the dither signal $S(t,\eta)$ is designed such that $S(t)$ at the input of the wave PDE produces $a\sin(\omega t)$ at the output. Similar to this idea, since we want to achieve the prescribed-time stabilization, we design the following PDE system to obtain the "chirpy" probing signal $a\sin\left(\omega(t_0 + (t-t_0)\mu)\right)$ after the integration of the output of the wave PDE,

$$S(t,\eta(t)) = \partial_x \beta(D,t), \tag{2.78}$$

$$\partial_{tt}\beta(x,t) = \partial_{xx}\beta(x,t), \tag{2.79}$$

$$\beta(0,t) = 0, \tag{2.80}$$

$$\partial_x \beta(0,t) = a\omega\cos\left(\omega(t_0 + (t-t_0)\mu(t))\right)\mu^2(t), \tag{2.81}$$

where

$$\eta(t) = \left[\vartheta(t), \quad \mu(t), \quad \bar{u}(\cdot,t), \quad \hat{\theta}(t)\right]^T, \tag{2.82}$$

and $\bar{u}(\cdot,t)$ is to be defined. The estimation errors at the input and output of the actuator dynamics can be defined as follows

$$\tilde{\theta} = \hat{\theta} - \Theta^*, \tag{2.83}$$

$$\vartheta = \widehat{\Theta} - \Theta^*. \tag{2.84}$$

Let us define the following error system

$$\vartheta(t) = \partial_x \bar{u}(0,t), \tag{2.85}$$

$$\partial_{tt}\bar{u}(x,t) = \partial_{xx}\bar{u}(x,t), \tag{2.86}$$

$$\bar{u}(0,t) = 0, \tag{2.87}$$

$$\partial_x \bar{u}(D,t) = \hat{\theta}(t) - \Theta^*, \tag{2.88}$$

in which the time derivative is given by

$$\dot{\vartheta}(t) = \partial_x u(0,t), \tag{2.89}$$

$$\partial_{tt} u(x,t) = \partial_{xx} u(x,t), \tag{2.90}$$

$$u(0,t) = 0, \tag{2.91}$$

$$\partial_x u(D,t) = \dot{\hat{\theta}}(t), \tag{2.92}$$

by noting that $u(x,t) = \partial_t \bar{u}(x,t) = \alpha(x,t) - \beta(x,t)$ for $(x,t) \in [0,D] \times [t_0, t_0+T)$. Considering (2.76), (2.82) and (2.84), we can rewrite the output as follows

$$Y(t,\eta) = y^* + \frac{H}{2}\left(\vartheta + a\sin(\omega(t_0 + (t-t_0)\mu))\right). \tag{2.93}$$

Note that $G(t,\eta), \hat{H}(t,\eta), M(t,\eta), N(t,\eta)$ in Fig. 2.5 have the same form as in (2.27), (2.28), (2.29) and (2.30) respectively.

Lemma 2.2 *The solution for $S(t,\eta(t))$ in* (2.78) *is given by*

$$S(t,\eta) = \mathrm{Re}\left\{ \sum_{k=0}^{\infty} a\omega \frac{1}{T^{2k}} \mu^{2k+2} (2k)! e^{j\omega(t_0+(t-t_0)\mu)} L_{2k}^{(1)}\left(-(Tj\omega)\mu\right) \frac{D^{2k}}{(2k)!} \right\}, \tag{2.94}$$

for $t \in [t_0, t_0+T)$.

Proof We can consider (2.78)–(2.81) as a trajectory generation problem. Following the approach

in [58, Ch. 12], we search for the solution in the following form:

$$\beta(x,t) = \sum_{k=0}^{\infty} a_k(t)\frac{x^k}{k!}, \tag{2.95}$$

where the time-varying coefficients $a_k(t)$ are determined from (2.79)–(2.81). From (2.80) and (2.81), we obtain

$$a_0(t) = 0 \tag{2.96}$$

$$\begin{aligned} a_1(t) &= a\omega\cos\left(\omega(t_0+(t-t_0)\mu(t))\right)\mu^2(t) \\ &= \mathrm{Re}\left\{a\omega e^{j\omega(t_0+(t-t_0)\mu(t))}\mu^2(t)\right\}. \end{aligned} \tag{2.97}$$

By substituting (2.95) into (2.79), we get the following recursive relationship

$$a_{k+2}(t) = \ddot{a}_k(t), \tag{2.98}$$

which implies that $a_{2k}(t) = 0$ from (2.96). Considering (2.98) in view of (2.6), we can compute a_{2k+1} for $k = 1,2$ as follows

$$\begin{aligned} a_3(t) &= \mathrm{Re}\Big\{a\omega\frac{1}{T^2}\mu^4(t)\Big((Tj\omega)^2\mu^2(t)+6(Tj\omega)\mu(t)+6\Big)e^{j\omega(t_0+(t-t_0)\mu(t))}\Big\}, \\ a_5(t) &= \mathrm{Re}\Big\{a\omega\frac{1}{T^4}\mu^6(t)\Big((Tj\omega)^4\mu^4(t)+20(Tj\omega)^3\mu^3(t)+120(Tj\omega)^2\mu^2(t) \\ &\qquad +240(Tj\omega)\mu(t)+120\Big)e^{j\omega(t_0+(t-t_0)\mu(t))}\Big\}. \end{aligned}$$

The iterative computations lead to the following recursive pattern

$$a_{2k+1}(t) = \mathrm{Re}\left\{a\omega\frac{1}{T^{2k}}\mu^{2k+2}(t)(2k)!e^{j\omega(t_0+(t-t_0)\mu(t))}L_{2k}^{(1)}\left(-(Tj\omega)\mu(t)\right)\right\}. \tag{2.99}$$

Substituting (2.99) into (2.95), we get

$$\beta(x,t) = \mathrm{Re}\Bigg\{ \sum_{k=0}^{\infty} a\omega \frac{1}{T^{2k}} \mu^{2k+2}(t)(2k)! e^{j\omega(t_0+(t-t_0)\mu(t))} L_{2k}^{(1)}\left(-(Tj\omega)\mu(t)\right) \frac{x^{2k+1}}{(2k+1)!} \Bigg\}, \tag{2.100}$$

which blows up at $t = t_0 + T$. By taking the partial derivative of (2.100) with respect to x and evaluating at $x = D$, we get (2.94). ■

Next step is to convert the wave PDE-ODE cascade (2.89)–(2.92) to a cascade of two first-order transport PDEs convecting in opposite directions by performing the following Riemann transformations

$$\bar{\zeta}(x,t) = \partial_t u(x,t) + \partial_x u(x,t),$$
$$\bar{\omega}(x,t) = \partial_t u(x,t) - \partial_x u(x,t).$$

Then, system (2.89)–(2.92) is reformulated as

$$\dot{\vartheta}(t) = \bar{\zeta}(0,t), \tag{2.101}$$
$$\partial_t \bar{\omega}(x,t) = -\partial_x \bar{\omega}(x,t), \tag{2.102}$$
$$\bar{\omega}(0,t) = -\bar{\zeta}(0,t), \tag{2.103}$$
$$\partial_t \bar{\zeta}(x,t) = \partial_x \bar{\zeta}(x,t), \tag{2.104}$$
$$\bar{\zeta}(D,t) = \dot{\hat{\theta}}(t) + \partial_t u(D,t). \tag{2.105}$$

Let us employ the following backstepping transformations

$$z(x,t) = \bar{\zeta}(x,t) + \bar{k}\mu^2(t+x-D)\left[\vartheta(t) + \int_0^x \bar{\zeta}(y,t)dy\right], \tag{2.106}$$
$$p(x,t) = \bar{\omega}(x,t) - \bar{k}\mu^2(t-x-D)\left[\vartheta(t) + \int_0^x \bar{\omega}(y,t)dy\right],$$

which map (2.101)–(2.105) into the following target system

$$\dot{\vartheta}(t) = -\bar{k}\mu^2(t-D)\vartheta(t) + z(0,t), \tag{2.107}$$

$$\partial_t z(x,t) = \partial_x z(x,t), \tag{2.108}$$

$$z(D,t) = 0, \tag{2.109}$$

$$z(0,t) = -p(0,t), \tag{2.110}$$

$$\partial_t p(x,t) = -\partial_x p(x,t). \tag{2.111}$$

Let us set $x = D$ in (2.106) and derive the controller as

$$\dot{\hat{\theta}}(t) = -\bar{k}\mu^2(t)\left[\vartheta(t) + \int_0^D \bar{\zeta}(y,t)dy\right] - \partial_t u(D,t). \tag{2.112}$$

For the implementation of the controller, we replace (2.112) by

$$\dot{\hat{\theta}}(t) = -k\mu^2(t)\left[G(t,\mu(t)) + \hat{H}(t,\mu(t))\left(\hat{\theta}(t) + u(D,t) - \hat{\theta}(t-D) - u(D,t-D)\right)\right] - \partial_t u(D,t), \tag{2.113}$$

for $k < 0$, where we use the solution $\bar{\zeta}(x,t) = \dot{\hat{\theta}}(t+x-D) + \partial_t u(D,t+x-D)$ from (2.104)–(2.105) and apply the integration by parts. We limit our attention only to the derivation of the controller $\dot{\hat{\theta}}(t)$ for this problem. A detailed stability analysis is omitted since it can be performed similarly to the proof of Theorem 2.2.

2.4 PT-ES for Diffusion PDEs

We consider actuation dynamics governed by a diffusion PDE with an integral at its output,

$$\dot{\Theta}(t) = \partial_x \alpha(0,t), \tag{2.114}$$

$$\partial_t \alpha(x,t) = \partial_{xx}\alpha(x,t), \tag{2.115}$$

$$\alpha(0,t) = 0, \tag{2.116}$$

$$\partial_x \alpha(D,t) = \dot{\theta}(t), \tag{2.117}$$

where $(x,t) \in [0,D] \times [t_0, t_0+T)$. This ODE-PDE cascade with Neumann interconnection arises in Stefan models of thermal phase change [52] though in this chapter we limit our attention to a linearized version on a fixed spatial interval. The compensation of Stefan PDE by ES has been recently considered in [23] without any time constraint. The diffusion PDE with Neumann actuation is also applicable to tubular reactors (see [101, 58], and references therein). ES has also been shown to be a useful tool for optimizing the reactor exit components at steady state [44]. The compensation of input dynamics and optimization within a specified time frame could contribute to enhanced reactor performance.

2.4.1 Perturbation signal

We need to redesign the perturbation signal $S(t,\eta)$, which can compensate the diffusion process as well as the integrator. Let us define this trajectory generation problem as follows

$$S(t,\eta(t)) = \partial_x \beta(D,t), \tag{2.118}$$

$$\partial_t \beta(x,t) = \partial_{xx}\beta(x,t), \tag{2.119}$$

$$\beta(0,t) = 0, \tag{2.120}$$

$$\partial_x \beta(0,t) = a\omega \cos\left(\omega(t_0 + (t-t_0)\mu(t))\right) \mu^2(t), \tag{2.121}$$

for $(x,t) \in [0,D] \times [t_0, t_0+T)$, where $\eta : \mathscr{X} \to \mathscr{X}$, $\mathscr{X} := \mathbb{R} \times \mathbb{R} \times H_1[0,D] \times \mathbb{R}$, is defined by

$$\eta(t) = \left[\vartheta(t), \quad \mu(t), \quad \bar{u}(\cdot,t), \quad \tilde{\theta}(t)\right]^T, \tag{2.122}$$

and $\bar{u}(\cdot,t)$ is to be defined. Similarly to the proof of Lemma 2.2, the explicit solution for $S(t,\eta)$ in (2.118) is obtained by

$$S(t,\eta) = \mathrm{Re}\left\{ \sum_{k=0}^{\infty} \frac{a\omega}{T^k} \mu^{k+2} k! e^{j\omega(t_0+(t-t_0)\mu} L_k^{(1)}\left(-(Tj\omega)\mu\right) \frac{D^{2k}}{(2k)!} \right\},$$

which diverges to infinity as $t \to t_0 + T$. Let us define the following error system

$$\vartheta(t) = \partial_x \bar{u}(0,t) \tag{2.123}$$

$$\partial_t \bar{u}(x,t) = \partial_{xx} \bar{u}(x,t), \tag{2.124}$$

$$\bar{u}(0,t) = 0, \tag{2.125}$$

$$\partial_x \bar{u}(D,t) = \hat{\theta}(t) - \Theta^*, \tag{2.126}$$

in which the time derivative is given by

$$\dot{\vartheta}(t) = \partial_x u(0,t), \tag{2.127}$$

$$\partial_t u(x,t) = \partial_{xx} u(x,t), \tag{2.128}$$

$$u(0,t) = 0, \tag{2.129}$$

$$\partial_x u(D,t) = \dot{\hat{\theta}}(t), \tag{2.130}$$

by noting that $u(x,t) = \partial_t \bar{u}(x,t) = \alpha(x,t) - \beta(x,t)$ for $(x,t) \in [0,D] \times [t_0, t_0+T)$.

2.4.2 Controller design and error dynamics

Consider the PDE–ODE cascade (2.127)–(2.130) and use the backstepping transformation

$$w(x,t) = u(x,t) - \int_0^x q(x,y,t)u(y,t)dy - \gamma(x,t)\vartheta(t), \tag{2.131}$$

for $(x,t) \in [0,D] \times [t_0, t_0+T)$ with the kernels

$$\partial_t q(x,y,t) = \partial_{xx} q(x,y,t) - \partial_{yy} q(x,y,t) - \mu_0 \mu^2(t) q(x,y,t), \tag{2.132}$$

$$q(x,0,t) = \gamma(x,t), \tag{2.133}$$

$$q(x,x,t) = -\frac{x}{2} \mu_0 \mu^2(t), \tag{2.134}$$

for $t \in [t_0, t_0+T)$, $(x,y) \in \mathscr{T} = \{(x,y) \in \mathbb{R}^2 \,|\, 0 \le y \le x \le D\}$ and

$$\partial_t \gamma(x,t) = \partial_{xx} \gamma(x,t) - \mu_0 \mu^2(t) \gamma(x,t), \tag{2.135}$$

$$\gamma(0,t) = 0, \tag{2.136}$$

$$\partial_x \gamma(0,t) = -\bar{k} \mu^2(t), \tag{2.137}$$

for $(x,t) \in [0,D] \times [t_0, t_0+T)$ which transforms (2.127)–(2.130) into the target system

$$\dot{\vartheta}(t) = -\bar{k} \mu^2(t) \vartheta(t) + \partial_x w(0,t), \tag{2.138}$$

$$\partial_t w(x,t) = \partial_{xx} w(x,t) - \mu_0 \mu^2(t) w(x,t), \tag{2.139}$$

$$w(0,t) = 0, \tag{2.140}$$

$$\partial_x w(D,t) = 0, \tag{2.141}$$

with $\bar{k}, \mu_0 > 0$. By taking the partial derivative of the backstepping transformation (2.131) with respect to x, and evaluating at $x = D$, we get the controller as follows

$$\dot{\hat{\theta}}(t) = q(D,D,t) u(D,t) + \int_0^D \partial_x q(D,y,t) u(y,t) dy + \partial_x \gamma(D,t) \vartheta(t). \tag{2.142}$$

Note that we impose the time–varying damping, which blows up at $t = t_0 + T$, to (2.139) and recover the prescribed time-stabilization rather than exponential stabilization, which is to be proved in Section 2.4.5. However, the controller (2.142) is not implementable because $\vartheta(t)$ is

not directly measured. Considering the averaging-based estimates (2.31) and (2.32) and noting $\partial_t \bar{u}(x,t) = u(x,t)$, we can redesign the controller (2.142) as follows

$$\dot{\hat{\theta}} = \hat{H}(t,\eta)Q(\eta) + G(t,\eta)P(\eta) + R(\eta), \tag{2.143}$$

where

$$Q(\eta) = \int_0^D \partial_x q_c(D,y,t)\partial_t \bar{u}(y,t)dy, \tag{2.144}$$

$$P(\eta) = \partial_x \gamma_c(D,t), \tag{2.145}$$

$$R(\eta) = q_r(D,D,t)\partial_t \bar{u}(D,t) + \int_0^D \partial_x q_r(D,y,t)\partial_t \bar{u}(y,t)dy,$$

and $G(t,\eta), \hat{H}(t,\eta)$ have the same form as in (2.27), (2.28), respectively, with

$$\partial_t q_c(x,y,t) = \partial_{xx} q_c(x,y,t) - \partial_{yy} q_c(x,y,t) - \mu_0 \mu^2(t) q_c(x,y,t), \tag{2.146}$$

$$q_c(x,0,t) = \gamma_c(x,t), \tag{2.147}$$

$$q_c(x,x,t) = 0, \tag{2.148}$$

and

$$\partial_t q_r(x,y,t) = \partial_{xx} q_r(x,y,t) - \partial_{yy} q_r(x,y,t) - \mu_0 \mu^2(t) q_r(x,y,t), \tag{2.149}$$

$$q_r(x,0,t) = 0, \tag{2.150}$$

$$q_r(x,x,t) = -\frac{x}{2}\mu_0 \mu^2(t), \tag{2.151}$$

and

$$\partial_t \gamma_c(x,t) = \partial_{xx} \gamma_c(x,t) - \mu_0 \mu^2(t)\gamma_c(x,t), \tag{2.152}$$

$$\gamma_c(0,t) = 0, \tag{2.153}$$

$$\partial_x \gamma_c(0,t) = -k\mu^2(t), \tag{2.154}$$

by choosing $\bar{k} = kH$, where $H < 0$ is the unknown Hessian and the gain $k < 0$ is assigned by the user. Let us substitute (2.27) and (2.28) into (2.143) and substitute the resulting expression into (2.130). Then, we obtain the following closed-loop error system

$$\vartheta(t) = \partial_x \bar{u}(0,t), \tag{2.155}$$

$$\partial_t \bar{u}(x,t) = \partial_{xx} \bar{u}(x,t), \tag{2.156}$$

$$\bar{u}(0,t) = 0, \tag{2.157}$$

$$\partial_x \bar{u}(D,t) = \tilde{\theta}(t), \tag{2.158}$$

$$\dot{\tilde{\theta}} = q(D,D,t)\partial_t \bar{u}(D,t) + \int_0^D \partial_x q(D,y,t)\partial_t \bar{u}(y,t)dy + \partial_x \gamma(D,t)\vartheta + \check{f}(\omega t, \eta), \tag{2.159}$$

for $(x,t) \in [0,D] \times [t_0, t_0+T)$, where $\check{f}(\omega t, \eta)$ has the same form as in (2.57), f_1, f_2, f_3, f_4 are as in (2.48), (2.49), (2.50) and (2.51), respectively, except that $Q(\eta), P(\eta)$ are defined in (2.144) and (2.145), respectively.

It is worth noting that the solution to kernels with time-varying diffusion coefficients is addressed in [102]. These results are then extended to a more general setting in [70], in which the diffusion coefficient varies with both time and space. However, the solution of our kernel PDEs require a significantly different treatment due to the blow-up characteristics of the diffusion coefficient, as well as boundary conditions that differ from those in the aforementioned papers. The solutions of the kernel PDEs (2.146)–(2.148), (2.149)–(2.151) and (2.152)–(2.154) are given in Appendix A.1.

2.4.3 Inverse transformation

The invertibility of the transformation (2.131) needs to be shown to analyze the stability of the original system (2.127)–(2.130). It is given by

$$u(x,t) = w(x,t) + \int_0^x p(x,y,t)w(y,t)dy + \Gamma(x,t)\vartheta(t),$$

for $(x,t) \in [0,D] \times [t_0, t_0+T)$ with the kernels

$$\partial_t p(x,y,t) = \partial_{xx} p(x,y,t) - \partial_{yy} p(x,y,t) + \mu_0 \mu^2(t) p(x,y,t), \tag{2.160}$$

$$p(x,0,t) = \Gamma(x,t), \tag{2.161}$$

$$p(x,x,t) = -\frac{x}{2}\mu_0 \mu^2(t), \tag{2.162}$$

for $t \in [t_0, t_0+T)$, $(x,y) \in \mathscr{T}$ and

$$\partial_t \Gamma(x,t) = \partial_{xx}\Gamma(x,t) + kH\mu^2(t)\Gamma(x,t), \tag{2.163}$$

$$\Gamma(0,t) = 0, \tag{2.164}$$

$$\partial_x \Gamma(0,t) = -kH\mu^2(t), \tag{2.165}$$

for $(x,t) \in [0,D] \times [t_0, t_0+T)$, which transforms the target system (2.138)–(2.141) into the original system (2.127)–(2.130). The solutions of the inverse kernel PDEs (2.160)–(2.162) and (2.163)–(2.165) are given in Appendix A.

2.4.4 Numerical simulation

We again return to Example 2.1 and consider the map (2.17) with same parameters (except ω) and initial conditions and consider the coupled diffusion PDE-ODE dynamics (2.114)–(2.117) with the domain length $D = 1$. We choose $\omega = 100, k = -0.01, \mu_0 = 0.01$. The simulation of the diffusion PDE (2.115)–(2.117) is carried out by the Crank-Nicholson method, where we use

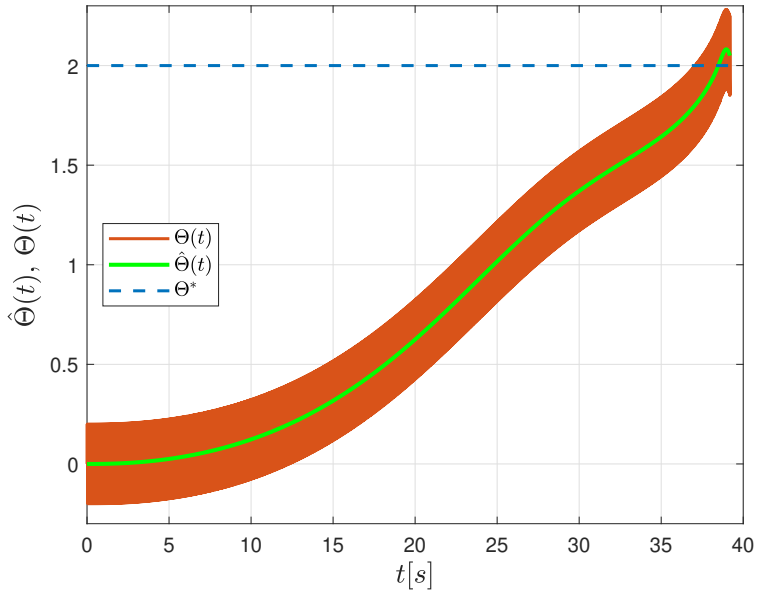

Figure 2.6. The evolution of the input $\Theta(t)$, the estimate $\hat{\Theta}(t)$ and the optimum input θ^* under the diffusion PDE compensated PT-ES.

grid size $N = 50$ in space and time step $\Delta t = 10^{-4}$. The kernel (2.146)–(2.148) is numerically computed by the proposed successive approximation formulas, where the time derivative of the kernels are computed numerically. In Fig. 2.6, we depict the evolution of the input signal $\Theta(t)$ and estimate $\hat{\Theta}(t)$ with respect to time under the effect of the diffusion PDE compensated PT-ES.

2.4.5 Stability analysis

The main theorem is stated as follows.

Theorem 2.3 *For $\bar{T} > 0$ arbitrarily close to T, there exists some $\omega^*(\bar{T})$, where $\omega^*(\bar{T}) \to \infty$ as $\bar{T} \to T$, such that $\forall \omega > \omega^*(\bar{T})$, the error system* (2.155)–(2.159) *satisfies*

$$\limsup_{t \to t_0 + \bar{T}} \left(|\vartheta(t)| + ||\bar{u}(\cdot,t)||_{L_2[0,D]} + ||\partial_x \bar{u}(\cdot,t)||_{L_2[0,D]} + |\hat{\theta}(t) - \Theta^*| \right) = \mathcal{O}(1/\omega) \tag{2.166}$$

provided that the gains k, μ_0, which both tune the convergence rate, are selected such that

$\min\{kH, \mu_0\} > 3D^2/T^2$. *Furthermore,*

$$\limsup_{t \to t_0 + \bar{T}} |\Theta(t) - \Theta^*| = \mathscr{O}(a + 1/\omega), \tag{2.167}$$

$$\limsup_{t \to t_0 + \bar{T}} |y(t) - y^*| = \mathscr{O}(a^2 + 1/\omega^2). \tag{2.168}$$

Proof Let us proceed through the proof step by step.

Step 1: (Averaging operation) Define a linear operator $\mathscr{A} : \mathscr{D}(\mathscr{A}) \subset \mathscr{X} \to \mathscr{X}$ by

$$\mathscr{A}\eta(t) = \begin{bmatrix} \frac{d^3\bar{u}(0,t)}{dx^3} & 0 & \frac{d^2\bar{u}(\cdot,t)}{dx^2} & 0 \end{bmatrix}^T \tag{2.169}$$

and the domain

$$D(\mathscr{A}) = \left\{ [\vartheta(t), \mu(t), \bar{u}(\cdot,t), \hat{\theta}(t)] \in \mathscr{X} : \frac{d\bar{u}(D,t)}{dx} = \hat{\theta}(t) - \Theta^*, \bar{u}(0,t) = 0 \right\}. \tag{2.170}$$

We can write the derivative of the infinite-dimensional state vector (2.122) with the help of (2.155)–(2.159) as follows

$$\dot{\eta} = \mathscr{A}\eta + J(\omega t, \eta), \tag{2.171}$$

for $t \in [t_0, t_0 + \bar{T}]$ where

$$J(\omega t, \eta) = \begin{bmatrix} 0 & \frac{1}{T}\mu^2 & 0 & \breve{g}(\eta) + \breve{f}(\omega t, \eta) \end{bmatrix}^T, \tag{2.172}$$

with

$$\breve{g}(\eta(t)) = q(D,D,t)\partial_t \bar{u}(D,t) + \int_0^D \partial_x q(D,y,t)\partial_t \bar{u}(y,t)dy + \partial_x \gamma(D,t)\vartheta(t). \tag{2.173}$$

Let us define the following averaged system

$$\dot{\eta}_{\text{av}} = \mathscr{A}\eta_{\text{av}} + J_{\text{av}}(\eta_{\text{av}}), \tag{2.174}$$

where

$$\begin{aligned} J_{\text{av}}(\eta) &= \lim_{\omega\to\infty} \frac{1}{\omega\bar{T}} \int_0^{\omega\bar{T}} J(s,\eta)ds \\ &= \begin{bmatrix} 0 & \frac{1}{T}\mu^2 & 0 & \breve{g}(\eta) \end{bmatrix}^T. \end{aligned} \tag{2.175}$$

Following the similar steps done through (2.59)–(2.65), we conclude that

$$||\eta(t) - \eta_{\text{av}}(t)||_{\mathscr{X}} = \mathscr{O}(1/\omega), \qquad \forall t \in [t_0, t_0 + \bar{T}], \tag{2.176}$$

for all $\omega > \omega^*(\bar{T})$. Recall that $||\cdot||_{\mathscr{X}}$ denotes the induced norm of $\mathscr{X}$. By noting $\partial_t \bar{u}(x,t) = \partial_{xx}\bar{u}(x,t) = u(x,t)$, we write the following average PDE system from (2.174)

$$\dot{\vartheta}_{\text{av}}(t) = \partial_x u_{\text{av}}(0,t), \tag{2.177}$$

$$\partial_t u_{\text{av}}(x,t) = \partial_{xx} u_{\text{av}}(x,t), \tag{2.178}$$

$$u_{\text{av}}(0,t) = 0, \tag{2.179}$$

$$\partial_x u_{\text{av}}(D,t) = q(D,D,t)u_{\text{av}}(D,t) + \int_0^D \partial_x q(D,y,t)u_{\text{av}}(y,t)dy + \partial_x \gamma(D,t)\vartheta_{\text{av}}(t) \tag{2.180}$$

for $(x,t) \in \mathscr{T}_2$.

Step 2: (Backstepping transformation) The backstepping transformation

$$w(x,t) = u_{\text{av}}(x,t) - \int_0^x q(x,y,t)u_{\text{av}}(y,t)dy - \gamma(x,t)\vartheta_{\text{av}}(t) \tag{2.181}$$

with the gain kernels (2.132)–(2.134) and (2.135)–(2.137) transforms (2.177)–(2.180) into the

target system

$$\dot{\vartheta}_{\text{av}}(t) = -kH\mu^2(t)\vartheta_{\text{av}}(t) + \partial_x w(0,t), \tag{2.182}$$

$$\partial_t w(x,t) = \partial_{xx} w(x,t) - \mu_0 \mu^2(t) w(x,t), \tag{2.183}$$

$$w(0,t) = 0, \tag{2.184}$$

$$\partial_x w(D,t) = 0. \tag{2.185}$$

Step 3: (Stability of the target system) Let us consider the following Lyapunov functional

$$\Upsilon(t) = \frac{\vartheta_{\text{av}}^2(t)}{2} + \frac{1}{2}||w(\cdot,t)||^2_{L_2[0,D]} + \frac{c_w}{2}||\partial_x w(\cdot,t)||^2_{L_2[0,D]} \tag{2.186}$$

with $c_w = \sqrt{1/(2\mu_0 kH)}$. Taking the time derivative of $\Upsilon(t)$ along with (2.182)–(2.185) and applying the integration by parts, we obtain

$$\begin{aligned}\dot{\Upsilon}(t) =& -kH\mu^2(t)\vartheta_{\text{av}}^2(t) + \partial_x w(0,t)\vartheta_{\text{av}}(t) - \mu_0\mu^2(t)\Big(||w(t)||^2_{L_2[0,D]} + c_w||\partial_x w(t)||^2_{L_2[0,D]}\Big) \\ &- \Big(||\partial_x w(t)||^2_{L_2[0,D]} + c_w||\partial_{xx} w(t)||^2_{L_2[0,D]}\Big).\end{aligned} \tag{2.187}$$

Let us apply Young's and Agmon's inequalities on the cross term $\partial_x w(0,t)\vartheta_{\text{av}}(t)$

$$\begin{aligned}\partial_x w(0,t)\vartheta_{\text{av}}(t) &\leq \frac{kH}{2}\vartheta_{av}^2(t) + \frac{1}{2kH}(\partial_x w(0,t))^2 \\ &\leq \frac{kH}{2}\vartheta_{av}^2(t) + \frac{c_w\mu_0}{2}||\partial_x w(\cdot,t)||^2_{L_2[0,D]} + \frac{1}{2c_w\mu_0(kH)^2}||\partial_{xx} w(\cdot,t)||^2_{L_2[0,D]}.\end{aligned} \tag{2.188}$$

Then, noting this inequality as well as $c_w = \sqrt{1/(2\mu_0(kH)^2)}$, we rewrite (2.187) as follows

$$\dot{\Upsilon}(t) \leq -\frac{kH}{2}\mu^2(t)\vartheta_{\text{av}}^2(t) - \mu_0\mu^2(t)||w(\cdot,t)||^2_{L_2[0,D]} - \frac{c_w\mu_0}{2}\mu^2(t)||\partial_x w(\cdot,t)||^2_{L_2[0,D]}. \tag{2.189}$$

We obtain for $c_0 = \min\{kH, \mu_0\}$ that $\dot{\Upsilon}(t) \leq -c_0\mu^2(t)\Upsilon(t)$. Hence, we get

$$\Upsilon(t) \leq e^{-c_0T(\mu(t)-1)}\Upsilon(t_0). \tag{2.190}$$

Step 4: (Stability of the original system) Let us consider the inverse transformation

$$u_{\text{av}}(x,t) = w(x,t) + \int_0^x p(x,y,t)w(y,t)dy + \Gamma(x,t)\vartheta_{\text{av}}(t), \tag{2.191}$$

where the kernels $p(x,y,t)$ and $\Gamma(x,t)$ satisfy (2.160)–(2.162) and (2.163)–(2.165), respectively. From the inverse transformation (2.191), we obtain the following inequalities

$$\begin{aligned}||u_{\text{av}}(\cdot,t)||^2_{H_1[0,D]} \leq& \left[4 + D^2\mu_0^2\mu^4(t) + 3D^2|p(\cdot,\cdot,t)|^2 + 4D^2|\partial_x p(\cdot,\cdot,t)|^2\right]||w(\cdot,t)||^2_{H_1[0,D]} \\ &+ \left(3D|\Gamma(\cdot,t)|^2 + 4D|\partial_x\Gamma(\cdot,t)|^2\right)\vartheta^2_{\text{av}}(t), \qquad (2.192)\\ (\partial_x u_{\text{av}}(D,t))^2 \leq& 4(\partial_x w(D,t))^2 + \left[4D^3\mu_0^2\mu^4(t) + 4D|\partial_x p(\cdot,\cdot,t)|^2\right]||w(\cdot,t)||^2_{H_1[0,D]} \\ &+ 4(\partial_x\Gamma(\cdot,t))^2\vartheta^2_{\text{av}}(t). \qquad (2.193)\end{aligned}$$

Let us compute the bound of the following terms from (A.27), (A.28), (A.29) and (A.30)

$$\left(|\Gamma(\cdot,t)|^2 + |\partial_x\Gamma(\cdot,t)|^2\right)\vartheta^2_{\text{av}}(t) \leq C_{14}\mu^4(t)e^{\mu(t)\left(\frac{2D^2}{T} - c_0T\right)}\vartheta^2_{av}(t_0), \tag{2.194}$$

$$\left(|p(\cdot,\cdot,t)|^2 + |\partial_x p(\cdot,\cdot,t)|^2\right)||w(\cdot,t)||^2_{H_1[0,D]} \leq C_{15}\mu^6(t)e^{\mu(t)\left(\frac{3D^2}{T} - c_0T\right)}||w(\cdot,t_0)||^2_{H_1[0,D]}, \tag{2.195}$$

where $C_{14} = (C_7^2 + (kH)^2)e^{c_0T}$, $C_{15} = (C_{12}^2 + C_{13}^2)e^{c_0T}$, from which we prove that (2.194) and (2.195) converge to zero as $t \to t_0 + T$ provided that $c_0 > 3D^2/T^2$. In view of this fact, we obtain from (2.192) and (2.193) that $||u_{\text{av}}(\cdot,t)||_{H_1[0,D]}$ and $\partial_x u_{\text{av}}(D,t) \to 0$ as $t \to t_0 + T$. Applying Poincare's inequality twice and noting $\partial_t\bar{u}_{\text{av}}(x,t) = \partial_{xx}\bar{u}_{\text{av}}(x,t) = u_{\text{av}}(x,t)$, we get

$$||\bar{u}_{\text{av}}(\cdot,t)||^2_{H_1[0,D]} \leq (2 + 8D^2)\vartheta^2_{\text{av}}(t) + (4D^2 + 16D^4)||u_{\text{av}}(\cdot,t)||^2, \tag{2.196}$$

from which we conclude $||\bar{u}_{\text{av}}(\cdot,t)||^2_{H_1[0,D]} \to 0$ as $t \to t_0 + T$.

Step 4: (Convergence to a small neighborhood of the extremum) Considering the PT stability results in Step 3, we prove (2.166) from (2.176). In view of (2.76) and (2.84), we can write $\Theta(t) - \Theta^* = \vartheta(t) + a\sin(\omega(t_0 + (t-t_0)\mu(t)))$. Then, we prove (2.167). Recalling (2.93) and (2.166), we prove (2.168). ■

2.5 Conclusion

The heavily-studied problems of (finite- and infinite-dimensional) PT stabilization and the exponential convergence of PDE-compensated ES algorithms are seemingly disparate. We combine them to achieve PT convergence to extrema of unknown maps with PDE input dynamics. We employ the tools of time dilation, chirpy signals, finite-time PDE motion planning, PDE backstepping, averaging, and Lyapunov analysis to design PT-convergent PDE-compensated ES algorithms. The numerical simulations illustrate the PT convergence of the system output to a small neighborhood of the extremum.

2.6 Acknowledgments

Chapter 2 is a reprint of the material as it appears in:

- C. T. Yilmaz and M. Krstic, "Prescribed-Time Extremum Seeking for Delays and PDEs Using Chirpy Probing", *IEEE Transactions on Automatic Control*, 69(11):7710–7725, 2024.

The dissertation author was the primary investigator and author of this paper.

Chapter 3

Exponential and Prescribed-Time Extremum Seeking with Unbiased Convergence

In this chapter, we present multivariable extremum seeking (ES) designs that achieve unbiased convergence of the inputs to their corresponding optima, eliminating steady-state oscillations. Two designs are introduced: one with exponential unbiased convergence (unbiased extremum seeker, uES) and the other with user-assignable prescribed-time unbiased convergence (unbiased PT extremum seeker, uPT-ES). In contrast to the conventional ES, which uses persistent sinusoids and results in steady-state oscillations around the optimum, the exponential uES employs an exponentially decaying amplitude in the perturbation signal (for achieving convergence) and an exponentially growing demodulation signal (for making the convergence unbiased). The achievement of unbiased convergence also entails employing an adaptation gain that is sufficiently large in relation to the decay rate of the perturbation amplitude. Stated concisely, the bias is eliminated by having the learning process outpace the waning of the perturbation. The other algorithm, uPT-ES, employs prescribed-time convergent/blow-up functions in place of constant amplitudes of sinusoids, and it also replaces constant-frequency sinusoids with chirp signals whose frequency grows over time. Among the convergence results in the ES literature, uPT-ES may be the strongest yet in terms of the convergence rate (prescribed-time) and accuracy (unbiased). To enhance the robustness of uES to a time-varying optimum, exponential functions

are modified to keep oscillations at steady state. Stability analysis of the designs is based on a state transformation, averaging, local exponential/PT stability of the averaged system, local stability of the transformed system, and local exponential/PT stability of the original system. For numerical implementation of the developed ES schemes and comparison with previous ES designs, the problem of source seeking by a two-dimensional velocity-actuated point mass is considered.

The structure of this chapter is as follows: Section 3.1 presents the exponential ES scheme for static maps, followed by an extension to dynamic systems in Section 3.3. Section 3.2 introduces the concept of uPT-ES, while Section 3.4 covers the robust exponential ES. Our approaches to the source-seeking problem are discussed in Section 3.5. Numerical results and their analysis are provided in Section 3.6, and the chapter concludes with Section 3.7.

3.1 Exponential Unbiased Extremum Seeker for Static Maps

We consider the following optimization problem

$$\max_{\theta \in \mathbb{R}^n} h(\theta), \tag{3.1}$$

where $\theta \in \mathbb{R}^n$ is the input and $h \in \mathbb{R}^n \to \mathbb{R}$ is an unknown smooth function. We make the following assumption regarding the unknown static map $h(\cdot)$:

Assumption 3.1 *The function h is $\mathscr{C}^4$, and there exists $\theta^* \in \mathbb{R}^n$ such that*

$$\frac{\partial}{\partial \theta} h(\theta^*) = 0, \tag{3.2}$$

$$\frac{\partial^2}{\partial \theta^2} h(\theta^*) = H < 0, \quad H = H^T. \tag{3.3}$$

Assumption 3.1 requires the function $h(\cdot)$ to be four times continuously differentiable. Compared to the $\mathscr{C}^2$ assumption made in the classical design [59], the $\mathscr{C}^4$ assumption is necessary for

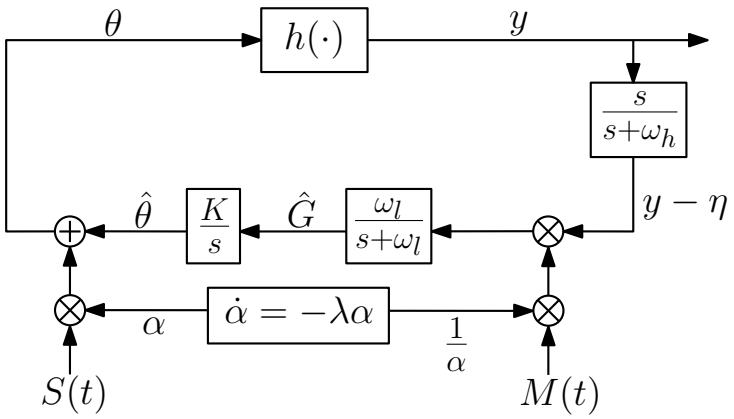

Figure 3.1. Exponential uES scheme. The design uses an exponential decay function α to gradually reduce the effect of the perturbation signal $S(t)$ and its multiplicative inverse $\frac{1}{\alpha}$ to gradually increase the effect of the demodulation signal $M(t)$.

the application of the classical averaging theorem, as the perturbation and demodulation signal amplitudes in our closed-loop system are time-varying and treated as part of the system state. A detailed discussion on this is to be given. The conditions (3.2) and (3.3) ensure the existence and uniqueness of a maximum of the function $h(\theta)$ at $\theta = \theta^*$. The negative definite Hessian matrix H in (3.3) implies strong concavity at θ^* (or strong convexity if H were positive definite).

We measure the unknown function $h(\theta)$ in real time as follows

$$y(t) = h(\theta(t)), \qquad t \in [t_0, \infty), \tag{3.4}$$

in which $y \in \mathbb{R}$ is the output. Our aim is to design an ES algorithm using output feedback $y(t)$ in order to achieve exponential convergence of θ to θ^* while simultaneously maximizing the steady state value of y, without requiring prior knowledge of either θ^* or the function $h(\cdot)$. Our exponential uES design for static maps is schematically illustrated in Fig. 3.1, where K is an $n \times n$ positive diagonal matrix, the filter coefficients ω_h and ω_l are positive real numbers, the perturbation and demodulation signals are defined as

$$S(t) = \begin{bmatrix} a_1 \sin(\omega_1 t) & \cdots & a_n \sin(\omega_n t) \end{bmatrix}^T, \tag{3.5}$$

$$M(t) = \begin{bmatrix} \frac{2}{a_1}\sin(\omega_1 t) & \cdots & \frac{2}{a_n}\sin(\omega_n t) \end{bmatrix}^T, \tag{3.6}$$

respectively and the exponential decay function α is governed by

$$\dot{\alpha}(t) = -\lambda\,\alpha(t), \qquad \alpha(t_0) = \alpha_0. \tag{3.7}$$

The parameters α_0, λ are positive real numbers, the amplitudes a_i are real numbers, ω_i/ω_j are rational and the frequencies are chosen such that $\omega_i \neq \omega_j$ and $\omega_i + \omega_j \neq \omega_k$ for distinct i, j and k. Note that the magnitude of α_0 determines the initial perturbation amplitude; a larger α_0 leads to larger-amplitude oscillations at the beginning. We select the probing frequencies ω_i's as follows

$$\omega_i = \omega\omega_i', \qquad i \in \{1, 2, \ldots, n\}, \tag{3.8}$$

where ω is a positive constant and and ω_i' is a rational number. In addition, the parameters should satisfy the following conditions:

$$\lambda < \frac{\omega_l}{2}, \frac{\omega_h}{2}, \tag{3.9}$$

$$K > (\omega_l - \lambda)\frac{\lambda}{\omega_l}\left(\frac{1}{-H}\right) > 0, \tag{3.10}$$

where division by the matrix $-H$ denotes multiplication by its inverse, $-H^{-1}$. Note that if $K > \frac{\lambda}{-H}$, stability is achieved for all admissible λ (not exceeding $\omega_l/2$). The algorithm can be used without the low-pass filter, in which case these conditions become, taking the limit $\omega_l \to \infty$,

$$\lambda < \frac{\omega_h}{2}, \tag{3.11}$$

$$K > \frac{\lambda}{-H} > 0. \tag{3.12}$$

The interpretation of the conditions is that perturbation amplitude α and the demodulation

amplitude $1/\alpha$ can decay and grow, respectively, but not too fast, while the estimate $\hat{\theta}$ needs to be updated fast enough, for the given rate of decay/growth of the amplitudes. In essence, learning needs to outpace the waning of the perturbation. Additionally, to satisfy the condition in (3.10) or (3.12), the gain K should be chosen sufficiently large as the Hessian matrix H is unknown. However, a large gain K may adversely affect transient performance, leading to significant overshoot. To make the conditions independent of H, a potential solution is to employ a Newton-based approach, as developed in [25].

We summarize closed-loop system depicted in Fig. 3.1 as follows

$$\frac{d}{dt}\begin{bmatrix}\tilde{\theta}\\ \hat{G}\\ \tilde{\eta}\\ \alpha\end{bmatrix} = \begin{bmatrix}K\hat{G}\\ -\omega_l\hat{G}+\omega_l(y-h(\theta^*)-\tilde{\eta})\frac{1}{\alpha}M(t)\\ -\omega_h\tilde{\eta}+\omega_h(y-h(\theta^*))\\ -\lambda\alpha\end{bmatrix}, \tag{3.13}$$

in view of the transformations

$$\tilde{\theta} = \hat{\theta} - \theta^*, \tag{3.14}$$

$$\tilde{\eta} = \eta - h(\theta^*), \tag{3.15}$$

where η is governed by

$$\dot{\eta} = -\omega_h\eta + \omega_h y. \tag{3.16}$$

The convergence result is stated in the following theorem.

Theorem 3.1 *Consider the feedback system* (3.13) *with the parameters that satisfy* (3.9)*,* (3.10) *under Assumption 3.1. There exists* $\bar{\omega}$ *and for any* $\omega > \bar{\omega}$ *there exists an open ball* $\mathscr{B}$ *centered at the point* $(\hat{\theta},\hat{G},\eta,\alpha) = (\theta^*,0,h(\theta^*),0) =: \Upsilon$ *such that for any initial condition starting in the ball* $\mathscr{B}$*, the system* (3.13) *has a unique solution and the solution converges exponentially to*

Υ. *Furthermore, $y(t)$ exponentially converges to $h(\theta^*)$.*

Before presenting the proof, we need to emphasize that the system (3.13) does not exhibit an equilibrium point in the conventional sense. Theorem 3.1 establishes the convergence of the system to a point Υ within the state space. This point, Υ, is not an asymptotically or exponentially stable equilibrium; rather, it represents a specific point in the state space towards which the system converges.

Proof Let us proceed through the proof step by step.

Step 1: State transformation. Consider the following transformations

$$\tilde{\theta}_f = \frac{1}{\alpha}\tilde{\theta}, \qquad \hat{G}_f = \frac{1}{\alpha}\hat{G}, \qquad \tilde{\eta}_f = \frac{1}{\alpha^2}\tilde{\eta}, \tag{3.17}$$

which transform (3.13) to the following system

$$\frac{d}{dt}\begin{bmatrix} \tilde{\theta}_f \\ \hat{G}_f \\ \tilde{\eta}_f \\ \alpha \end{bmatrix} = \begin{bmatrix} \lambda\tilde{\theta}_f + K\hat{G}_f \\ (\lambda-\omega_l)\hat{G}_f + \omega_l\left[\nu(\tilde{\theta}_f\alpha + S(t)\alpha) - \tilde{\eta}_f\alpha^2\right]\frac{M(t)}{\alpha^2} \\ (2\lambda-\omega_h)\tilde{\eta}_f + \omega_h\frac{1}{\alpha^2}\nu(\tilde{\theta}_f\alpha + S(t)\alpha) \\ -\lambda\alpha \end{bmatrix}, \tag{3.18}$$

where

$$\nu(z) = h(\theta^* + z) - h(\theta^*) \tag{3.19}$$

with $z = \tilde{\theta}_f\alpha + S(t)\alpha$ in view of $\theta = \hat{\theta} + S(t)\alpha$ and (3.14). From Assumption 3.1, we get

$$\nu(0) = 0, \quad \frac{\partial}{\partial z}\nu(0) = 0, \quad \frac{\partial^2}{\partial z^2}\nu(0) = H < 0. \tag{3.20}$$

Step 2: Verification of the feasibility of (3.18) **for averaging.** We rewrite the system

(3.18) in the time scale $\tau = \omega t$ as follows

$$\frac{d}{d\tau}\begin{bmatrix}\tilde{\theta}_f\\ \hat{G}_f\\ \tilde{\eta}_f\\ \alpha\end{bmatrix} = \frac{1}{\omega}\begin{bmatrix}\lambda\tilde{\theta}_f + K\hat{G}_f\\ (\lambda-\omega_l)\hat{G}_f + \omega_l\left[\nu(\tilde{\theta}_f\alpha + \bar{S}(\tau)\alpha) - \tilde{\eta}_f\alpha^2\right]\frac{\bar{M}(\tau)}{\alpha^2}\\ (2\lambda-\omega_h)\tilde{\eta}_f + \omega_h\frac{1}{\alpha^2}\nu(\tilde{\theta}_f\alpha + \bar{S}(\tau)\alpha)\\ -\lambda\alpha\end{bmatrix}, \tag{3.21}$$

where $\bar{S}(\tau) = S(\tau/\omega), \bar{M}(\tau) = M(\tau/\omega)$. Let us write the system (3.21) in compact form as

$$\frac{d\zeta_f}{d\tau} = (1/\omega)\mathscr{F}(\tau, \zeta_f), \tag{3.22}$$

where $\zeta_f = \begin{bmatrix}\tilde{\theta}_f & \hat{G}_f & \tilde{\eta}_f & \alpha\end{bmatrix}^T$, and $\mathscr{F}(\tau, \zeta_f)$ represents the vector on the right-hand side of (3.21). For the application of the averaging theorem in [49], we need to show that $\mathscr{F}(\tau, \zeta_f)$ and its partial derivatives with respect to ζ_f up to the second order on compact sets of ζ_f for all $\tau \geq \omega t_0$ are continuous and bounded. The proof is trivial for $\mathscr{F}(\tau, \zeta_f)$ excluding the term $\nu(\alpha\tilde{\theta}_f + \alpha\bar{S}(\tau))\frac{1}{\alpha^2}$. To complete the proof, we utilize Taylor's theorem to write

$$\nu(z) = \sum_{i=1}^{n}\sum_{j=1}^{n} z_i z_j \int_0^1 (1-s)\frac{\partial^2\nu}{\partial z_i \partial z_j}(sz)ds \tag{3.23}$$

in view of (3.20). By substituting $z = \alpha\tilde{\theta}_f + \alpha\bar{S}(\tau)$ into (3.23) and multiplying both sides by $\frac{1}{\alpha^2}$, we obtain

$$\begin{aligned}\frac{1}{\alpha^2}\nu(\tilde{\theta}_f\alpha + \bar{S}(\tau)\alpha) = &\sum_{i=1}^{n}\sum_{j=1}^{n}(\tilde{\theta}_{f_i} + a_i\sin(\omega_i'\tau))(\tilde{\theta}_{f_j} + a_j\sin(\omega_j'\tau))\\ &\times\int_0^1 (1-s)\frac{\partial^2\nu}{\partial z_i\partial z_j}\left(s\tilde{\theta}_f\alpha + s\bar{S}(\tau)\alpha\right)ds.\end{aligned} \tag{3.24}$$

Next, we apply the mean value theorem to obtain

$$\frac{1}{\alpha^2}\nu(\tilde{\theta}_f\alpha+\bar{S}(\tau)\alpha)=\frac{1}{2}\sum_{i=1}^{n}\sum_{j=1}^{n}(\tilde{\theta}_{f_i}+a_i\sin(\omega_i'\tau))(\tilde{\theta}_{f_j}+a_j\sin(\omega_j'\tau))\frac{\partial^2\nu}{\partial z_i\partial z_j}\left(\mathfrak{s}\tilde{\theta}_f\alpha+\mathfrak{s}\bar{S}(\tau)\alpha\right) \tag{3.25}$$

for some $\mathfrak{s}\in[0,1]$. By Assumption 3.1, (3.25) is continuous and bounded on compact sets of $\tilde{\theta}_f$ and α. Considering the $\mathscr{C}^4$ property of ν and using the mean value theorem, we prove the continuity and boundedness of the partial derivatives of (3.24) with respect to $\tilde{\theta}_f$ and α up to the second order on compact sets of $\tilde{\theta}_f$ and α. Therefore, $\mathscr{F}(\tau,\zeta_f)$ satisfies the continuity and boundedness assumptions of the averaging theorem in [49].

Step 3: Averaging operation. Let us define the common period of the probing frequencies as follows

$$\Pi=2\pi\times\text{LCM}\left\{\frac{1}{\omega_i}\right\},\qquad i\in\{1,2\ldots,n\}, \tag{3.26}$$

where LCM stands for the least common multiple. The average of the system (3.21) over the period Π is given by

$$\frac{d}{d\tau}\begin{bmatrix}\tilde{\theta}_f^a\\ \hat{G}_f^a\\ \tilde{\eta}_f^a\\ \alpha^a\end{bmatrix}^T=\frac{1}{\omega}\begin{bmatrix}\lambda\tilde{\theta}_f^a+K\hat{G}_f^a\\ (\lambda-\omega_l)\hat{G}_f^a\\ (2\lambda-\omega_h)\tilde{\eta}_f^a\\ -\lambda\alpha^a\end{bmatrix}+\frac{1}{\omega}\begin{bmatrix}0\\ \omega_l\frac{1}{\Pi}\int_0^{\Pi}\nu(\tilde{\theta}_f^a\alpha^a+\bar{S}(\sigma)\alpha^a)\frac{\bar{M}(\sigma)}{(\alpha^a)^2}d\sigma\\ \omega_h\frac{1}{\Pi}\int_0^{\Pi}\nu(\tilde{\theta}_f^a\alpha^a+\bar{S}(\sigma)\alpha^a)\frac{1}{(\alpha^a)^2}d\sigma\\ 0\end{bmatrix}, \tag{3.27}$$

where $\tilde{\theta}_f^a,\hat{G}_f^a,\tilde{\eta}_f^a$ and α^a denote the average versions of the states $\tilde{\theta}_f,\hat{G}_f,\tilde{\eta}_f$ and α, respectively. It follows from (3.27) that the average equilibrium denoted as $\begin{bmatrix}\tilde{\theta}_f^{a,e} & \hat{G}_f^{a,e} & \tilde{\eta}_f^{a,e} & \alpha^{a,e}\end{bmatrix}^T$ satisfies

$$\lambda\tilde{\theta}_f^{a,e}=-K\hat{G}_f^{a,e},$$

$$
\begin{aligned}
\alpha^{a,e} &= 0, \\
(\omega_l - \lambda)\hat{G}_f^{a,e} &= \lim_{\alpha^{a,e}\to 0}\left[\frac{\omega_l}{\Pi}\int_0^{\Pi} \nu(\tilde{\theta}_f^{a,e}\alpha^{a,e} + \bar{S}(\sigma)\alpha^{a,e})\frac{\bar{M}(\sigma)}{(\alpha^{a,e})^2}d\sigma\right], \\
(\omega_h - 2\lambda)\tilde{\eta}_f^{a,e} &= \lim_{\alpha^{a,e}\to 0}\left[\frac{\omega_h}{\Pi}\int_0^{\Pi} \nu(\tilde{\theta}_f^{a,e}\alpha^{a,e} + \bar{S}(\sigma)\alpha^{a,e})\frac{1}{(\alpha^{a,e})^2}d\sigma\right].
\end{aligned} \tag{3.28}
$$

By performing a Taylor series approximation of ν in view of (3.20) as follows

$$
\nu(z) = \frac{1}{2}\sum_{i=1}^{n}\sum_{j=1}^{n}\frac{\partial^2\nu}{\partial z_i \partial z_j}(0)z_i z_j + \frac{1}{3!}\sum_{i=1}^{n}\sum_{j=1}^{n}\sum_{k=1}^{n}\frac{\partial^3\nu}{\partial z_i \partial z_j \partial z_k}(0)z_i z_j z_k + \mathscr{O}(|z|^4) \tag{3.29}
$$

with $z = \tilde{\theta}_f^{a,e}\alpha^{a,e} + \bar{S}(\sigma)\alpha^{a,e}$, we compute

$$
\begin{aligned}
&\lim_{\alpha^{a,e}\to 0}\left[\frac{1}{\Pi}\int_0^{\Pi} \nu(\tilde{\theta}_f^{a,e}\alpha^{a,e} + \bar{S}(\sigma)\alpha^{a,e})\frac{\bar{M}(\sigma)}{(\alpha^{a,e})^2}d\sigma\right] \\
&\qquad = \lim_{\alpha^{a,e}\to 0}\left[\frac{1}{\Pi}\int_0^{\Pi}\frac{1}{2}\sum_{i=1}^{n}\sum_{j=1}^{n}\frac{\partial^2\nu}{\partial z_i \partial z_j}(0)(\tilde{\theta}_{f_i}^{a,e} + a_i\sin(\omega_i'\sigma))\right. \\
&\qquad\qquad \left.\times(\tilde{\theta}_{f_j}^{a,e} + a_j\sin(\omega_j'\sigma))(\alpha^{a,e})^2\frac{\bar{M}(\sigma)}{(\alpha^{a,e})^2}d\sigma + \frac{(\alpha^{a,e})^3}{(\alpha^{a,e})^2}\mathscr{O}(|a|^2)\right], \\
&\qquad = H\tilde{\theta}_f^{a,e},
\end{aligned} \tag{3.30}
$$

and

$$
\lim_{\alpha^{a,e}\to 0}\left[\frac{1}{\Pi}\int_0^{\Pi} \nu(\tilde{\theta}_f^{a,e}\alpha^{a,e} + \bar{S}(\sigma)\alpha^{a,e})\frac{1}{(\alpha^{a,e})^2}d\sigma\right] = \frac{1}{2}\sum_{i=1}^{n}\sum_{j=1}^{n}H_{i,j}\tilde{\theta}_{f_i}^{a,e}\tilde{\theta}_{f_j}^{a,e} + \frac{1}{4}\sum_{i=1}^{n}H_{i,i}a_i^2, \tag{3.31}
$$

by L'Hospital's rule, where $H_{i,j} = \frac{\partial^2\nu}{\partial z_i \partial z_j}(0)$ and $\tilde{\theta}_{f_i}^{a,e}$ is the ith element of $\tilde{\theta}_f^{a,e}$. Then, we obtain

the equilibrium of the average system (3.27) as

$$\begin{bmatrix} \tilde{\theta}_f^{a,e} \\ \hat{G}_f^{a,e} \\ \tilde{\eta}_f^{a,e} \\ \alpha^{a,e} \end{bmatrix} = \begin{bmatrix} 0_{1\times n} \\ 0_{1\times n} \\ \frac{\omega_h}{4(\omega_h-2\lambda)} \sum_{i=1}^{n} H_{i,i} a_i^2 \\ 0 \end{bmatrix}, \tag{3.32}$$

provided that $\omega_l \neq \lambda, \omega_h \neq 2\lambda$ and $K \neq \lambda(\lambda-\omega_l)\omega_l^{-1}H^{-1}$.

Step 4: Stability analysis. The Jacobian of the average system (3.27) at the equilibrium (3.32) is given by

$$J_f^a = \frac{1}{\omega} \begin{bmatrix} \lambda I_{n\times n} & K & 0_{n\times 1} & 0_{n\times 1} \\ \omega_l H & (\lambda-\omega_l) I_{n\times n} & 0_{n\times 1} & \frac{\omega_l}{\Pi}\int_0^{\Pi} \frac{\partial\left(\frac{\nu\bar{M}}{(\alpha^a)^2}\right)}{\partial \alpha^a} d\sigma \\ 0_{1\times n} & 0_{1\times n} & (2\lambda-\omega_h) & \frac{\omega_h}{\Pi}\int_0^{\Pi} \frac{\partial\left(\frac{\nu}{(\alpha^a)^2}\right)}{\partial \alpha^a} d\sigma \\ 0_{1\times n} & 0_{1\times n} & 0 & -\lambda \end{bmatrix}. \tag{3.33}$$

Note that J_f^a is block-upper-triangular and Hurwitz provided that (3.9) and (3.10) are satisfied. This proves the local exponential stability of the average system (3.27). Then, based on the averaging theorem [49], we show that there exists $\bar{\omega}$ and for any $\omega > \bar{\omega}$, the system (3.21) has a unique exponentially stable periodic solution $(\tilde{\theta}_f^{\Pi}(\tau), \hat{G}_f^{\Pi}(\tau), \tilde{\eta}_f^{\Pi}(\tau), \alpha^{\Pi}(\tau))$ of period Π and this solution satisfies

$$\left\| \begin{bmatrix} \tilde{\theta}_f^{\Pi}(\tau) \\ \hat{G}_f^{\Pi}(\tau) \\ \tilde{\eta}_f^{\Pi}(\tau) - \frac{\omega_h}{4(\omega_h-2\lambda)} \sum_{i=1}^{n} H_{i,i} a_i^2 \\ \alpha^{\Pi}(\tau) \end{bmatrix} \right\| \leq \mathscr{O}\left(\frac{1}{\omega}\right). \tag{3.34}$$

In other words, all solutions $(\tilde{\theta}_f(\tau), \hat{G}_f(\tau), \tilde{\eta}_f(\tau), \alpha(\tau))$ exponentially converge to an $\mathscr{O}(1/\omega)$-

neighborhood of the equilibrium point in (3.32). The signal $\alpha(\tau)$, in particular, exponentially converges to zero. Noting this fact and recalling the transformations (3.17), we can deduce that the system (3.13) with states $\tilde{\theta}(t), \hat{G}(t), \tilde{\eta}(t)$ has a unique solution and is exponentially stable at the origin. In particular, based on (3.17), both $\tilde{\theta}(t)$ and $\hat{G}(t)$ exhibit exponential convergence to zero at a rate of λ, while $\tilde{\eta}(t)$ converges to zero exponentially with a rate of 2λ.

Step 5: Convergence to extremum. Considering the results in Step 4 and recalling from (3.17) and Fig. 3.1 that

$$\theta(t) = \alpha(t)\tilde{\theta}_f(t) + \theta^* + \alpha(t)S(t), \tag{3.35}$$

we conclude the exponential convergence of $\theta(t)$ to θ^* at the rate of λ. Taking into account the boundedness of $\tilde{\theta}_f(t)$ for all $t \geq t_0$, we deduce from (3.19) and (3.25) the exponential convergence of $y(t) = h(\theta(t))$ to $h(\theta^*)$ at the rate of 2λ. This completes the proof of Theorem 3.1. ■

According to Theorem 3.1, the initial value of the decaying function $\alpha(t)$ should be sufficiently close to zero, which limits the range of possible values for α_0 in (3.7). This can also be interpreted as the requirement for the amplitudes to be small enough in traditional extremum seeking approaches.

3.2 Unbiased Prescribed-Time Extremum Seeker for Static Maps

In this section, our aim is to design an ES algorithm for static maps, which guarantees the unbiased convergence of θ to θ^* within a terminal time T, where the time T is prescribed by user a priori. Our uPT-ES design is schematically illustrated in Fig. 3.2. Different from the exponentially convergent α-dynamics (3.7), we define a prescribed-time convergent α-dynamics

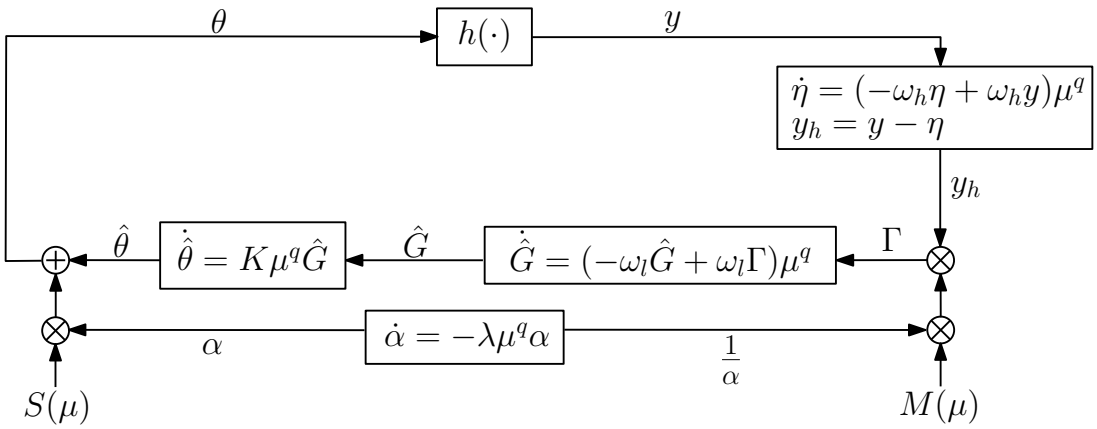

Figure 3.2. uPT-ES scheme. The design modifies the exponential uES in Fig. 3.1 by incorporating μ^q, with $q \geq 1$, into all system dynamics and using hyperbolic chirps in the perturbation and demodulation signals.

as follows

$$\dot{\alpha}(t) = -\lambda \mu^q (t - t_0)\alpha(t), \qquad \alpha(t_0) = \alpha_0 \tag{3.36}$$

with $q \geq 1$ and the following smooth function

$$\mu(t - t_0) = \frac{T}{T + t_0 - t}, \quad t \in [t_0, t_0 + T). \tag{3.37}$$

The solution of (3.36) is given by

$$\begin{aligned} \alpha(t) &= \alpha(t_0) e^{-\lambda \int_{t_0}^{t} \mu^q(\sigma - t_0) d\sigma} \\ &= \begin{cases} \alpha_0 \mu^{-\lambda T}(t - t_0), & \text{if } q = 1, \\ \alpha_0 e^{-\frac{\lambda T}{q-1}\left(\mu^{q-1}(t-t_0)-1\right)}, & \text{if } q > 1 \end{cases} \end{aligned} \tag{3.38}$$

with the property that $\alpha(t_0 + T) = 0$. Note that the growth of the μ-signal in the second condition of (3.38) increases as q is increased beyond 1, resulting in a faster decay of the α-signal.

We summarize closed-loop system depicted in Fig. 3.2 as follows

$$\frac{d}{dt}\begin{bmatrix}\tilde{\theta}\\ \hat{G}\\ \tilde{\eta}\\ \alpha\end{bmatrix}=\begin{bmatrix}K\mu^q\hat{G}\\ -\omega_l\mu^q\hat{G}+\omega_l\mu^q(y-h(\theta^*)-\tilde{\eta})\frac{1}{\alpha}M(\mu)\\ -\omega_h\mu^q\tilde{\eta}+\omega_h\mu^q(y-h(\theta^*))\\ -\lambda\mu^q\alpha\end{bmatrix}, \tag{3.39}$$

in view of the transformations (3.14), (3.15) where η is governed by

$$\dot{\eta}=(-\omega_h\eta+\omega_h y)\mu^q. \tag{3.40}$$

We define the following dilation and contraction transformations

$$\breve{\tau}=\begin{cases}t_0+T\ln(\mu), & \text{if } q=1,\\ t_0+T\left(\frac{\mu^{q-1}-1}{q-1}\right), & \text{if } q>1,\end{cases} \tag{3.41}$$

$$t=\begin{cases}t_0+T\left(1-e^{-\frac{\breve{\tau}-t_0}{T}}\right), & \text{if } q=1,\\ t_0+T\left(1-\left(\frac{T}{T+(q-1)(\breve{\tau}-t_0)}\right)^{\frac{1}{q-1}}\right), & \text{if } q>1,\end{cases} \tag{3.42}$$

for $\breve{\tau}\in[t_0,\infty)$, $t\in[t_0,t_0+T)$. To achieve PT convergence to the extremum, we replace the sinusoids with "chirpy" perturbation and demodulation signals whose frequency grows rather than being constant:

$$S(\mu)=\begin{cases}\left[a_1\sin(\omega_1(t_0+T\ln(\mu)) \quad \cdots \quad a_n\sin(\omega_n(t_0+T\ln(\mu))\right]^T, & \text{if } q=1,\\ \left[a_1\sin\left(\omega_1\left(t_0+T\frac{\mu^{q-1}-1}{q-1}\right)\right) \quad \cdots \quad a_n\sin\left(\omega_n\left(t_0+T\frac{\mu^{q-1}-1}{q-1}\right)\right)\right]^T, & \text{if } q>1,\end{cases} \tag{3.43}$$

$$M(\mu)=\begin{cases}\left[\frac{2}{a_1}\sin(\omega_1(t_0+T\ln(\mu)) \quad \cdots \quad \frac{2}{a_n}\sin(\omega_n(t_0+T\ln(\mu))\right]^T, & \text{if } q=1,\\ \left[\frac{2}{a_1}\sin\left(\omega_1\left(t_0+T\frac{\mu^{q-1}-1}{q-1}\right)\right) \quad \cdots \quad \frac{2}{a_n}\sin\left(\omega_n\left(t_0+T\frac{\mu^{q-1}-1}{q-1}\right)\right)\right]^T, & \text{if } q>1.\end{cases} \tag{3.44}$$

PT convergence is achieved at the expense of unboundedly growing excitation frequencies. In practice, the instantaneous frequencies (i.e., the first derivatives of the arguments of the sinusoids in (3.43) and (3.44)) can be limited to suitably large values that enable convergence to a sufficiently close neighborhood of the extremum.

The convergence result is stated in the following theorem.

Theorem 3.2 *Consider the feedback system* (3.39) *with the parameters that satisfy* (3.9), (3.10) *under Assumption 3.1. There exists* $\bar{\omega}$ *and for any* $\omega > \bar{\omega}$ *there exists an open ball* $\mathscr{B}$ *centered at the point* $(\hat{\theta},\hat{G},\eta,\alpha)=(\theta^*,0,h(\theta^*),0)=:\Upsilon$ *such that for any initial condition starting in the ball* $\mathscr{B}$*, the system* (3.39) *has a unique solution and the solution converges to* Υ *in prescribed time* T*. Furthermore,* $y(t)$ *converges to* $h(\theta^*)$ *in prescribed time* T*.*

Proof

Step 0: Time dilation from t to $\check{\tau}$. Considering (3.41), (3.42) along with

$$\frac{d\check{\tau}}{dt}=\mu^q(t-t_0), \tag{3.45}$$

we can write the system (3.39) in the dilated $\check{\tau}$-domain

$$\frac{d}{d\check{\tau}}\begin{bmatrix}\tilde{\theta}\\ \hat{G}\\ \tilde{\eta}\\ \alpha\end{bmatrix}=\begin{bmatrix}K\hat{G}\\ -\omega_l\hat{G}+\omega_l(y-h(\theta^*)-\tilde{\eta})\frac{1}{\alpha}\mathscr{M}(\check{\tau})\\ -\omega_h\tilde{\eta}+\omega_h(y-h(\theta^*))\\ -\lambda\alpha\end{bmatrix}, \tag{3.46}$$

with the following perturbation/demodulation signals

$$\mathscr{S}(\check{\tau}) = \begin{bmatrix} a_1 \sin(\omega_1 \check{\tau}) & \cdots & a_n \sin(\omega_n \check{\tau}) \end{bmatrix}^T, \tag{3.47}$$

$$\mathscr{M}(\check{\tau}) = \begin{bmatrix} \frac{2}{a_1} \sin(\omega_1 \check{\tau}) & \cdots & \frac{2}{a_n} \sin(\omega_n \check{\tau}) \end{bmatrix}^T. \tag{3.48}$$

Note that the system (3.46) with (3.47), (3.48) is in the similar form to (3.13) with (3.5), (3.6), except that the dilated time $\check{\tau}$ is used instead of t. The utilization of this temporal transformation technique facilitates the application of the averaging theorem because the frequency of perturbation/demodulation signals becomes constant in $\check{\tau}$-domain. The remainder of the proof can be completed similarly to the proof of Theorem 3.1 by following steps from 1 to 5 and performing time contraction from $\check{\tau}$ to t. ■

3.3 Exponential Unbiased Extremum Seeker for Dynamic Systems

In this section, we extend our results in Section 3.1 to dynamic systems. For this, we consider a general multi-input single-output nonlinear model

$$\dot{x} = f(x,u), \tag{3.49}$$

$$y = h(x), \tag{3.50}$$

where $x \in \mathbb{R}^m$ is the state, $u \in \mathbb{R}^n$ is the input, $y \in \mathbb{R}$ is the output and the unknown functions $f : \mathbb{R}^m \times \mathbb{R}^n \to \mathbb{R}^m$ and $h : \mathbb{R}^m \to \mathbb{R}$ are smooth. Suppose there is a smooth control law

$$u = \phi(x,\theta) \tag{3.51}$$

parametrized by a vector parameter $\theta \in \mathbb{R}^n$. The closed-loop system

$$\dot{x} = f(x, \phi(x, \theta)) \tag{3.52}$$

then has equilibria parameterized by θ. We make the following assumptions about the closed-loop system:

Assumption 3.2 *There exists a smooth function $l : \mathbb{R}^n \to \mathbb{R}^m$ such that $f(x, \phi(x, \theta)) = 0$ if and only if $x = l(\theta)$.*

Assumption 3.3 *For each $\theta \in \mathbb{R}^n$, the equilibrium $x = l(\theta)$ of the system* (3.52) *is locally exponentially stable uniformly in θ.*

Assumption 3.4 *The function $h \circ l$ is $\mathscr{C}^4$, and there exists $\theta^* \in \mathbb{R}^n$ such that*

$$\frac{\partial}{\partial \theta}(h \circ l)(\theta^*) = 0, \tag{3.53}$$

$$\frac{\partial^2}{\partial \theta^2}(h \circ l)(\theta^*) = H < 0, \quad H = H^T. \tag{3.54}$$

Assumptions 3.2–3.4, standard in the literature (e.g., [59, 25, 109]), ensure the existence and local exponential stability of the equilibrium $x = l(\theta)$ for the closed-loop system (3.52). Assumption 3.4 states that the steady-state output, $y = (h \circ l)(\theta)$, exhibits a unique global maximum at θ^*, is four times continuously differentiable, and strongly concave in the vicinity of θ^*, similar to the static map case in Assumption 3.1. For a visual representation of the implications of Assumptions 3.2-3.4, please see [92].

We aim to design a controller u to drive the output y directly to its optimum $h \circ l(\theta^*)$ exponentially without any steady-state oscillation and without the need for knowledge of θ^*, h, or l.

The perturbation and demodulation signals are defined by (3.5) and (3.6), respectively, and α is governed by (3.7). The probing frequencies ω_i's, the filter coefficients ω_h and ω_l, the

gain K, and the parameter λ are selected as follows

$$\omega_i = \omega\omega_i' = \mathscr{O}(\omega), \qquad i \in \{1,2,\ldots,n\}, \tag{3.55}$$

$$\omega_h = \omega\omega_H = \omega\delta\omega_H' = \mathscr{O}(\omega\delta), \tag{3.56}$$

$$\omega_l = \omega\omega_L = \omega\delta\omega_L' = \mathscr{O}(\omega\delta), \tag{3.57}$$

$$K = \omega K' = \omega\delta K'' = \mathscr{O}(\omega\delta), \tag{3.58}$$

$$\lambda = \omega\lambda' = \omega\delta\lambda'' = \mathscr{O}(\omega\delta), \tag{3.59}$$

where ω and δ are small positive constants, ω_i' is a rational number, ω_H', ω_L' and λ'' are $\mathscr{O}(1)$ positive constants, K'' is a $n \times n$ diagonal matrix with $\mathscr{O}(1)$ positive elements. In addition, the parameters should satisfy (3.9) and (3.10). Note that the selection of the parameters according to (3.55)–(3.59) implies that the frequencies ω_i need to be large in relation to the parameters $\omega_h, \omega_l, K, \lambda$.

We summarize the closed-loop system as follows

$$\frac{d}{dt}\begin{bmatrix} x \\ \tilde{\theta} \\ \hat{G} \\ \tilde{\eta} \\ \alpha \end{bmatrix} = \begin{bmatrix} f(x, \phi(x, \theta^* + \tilde{\theta} + S(t)\alpha)) \\ K\hat{G} \\ -\omega_l\hat{G} + \omega_l(y - h\circ l(\theta^*) - \tilde{\eta})\frac{1}{\alpha}M(t) \\ -\omega_h\tilde{\eta} + \omega_h(y - h\circ l(\theta^*)) \\ -\lambda\alpha \end{bmatrix}. \tag{3.60}$$

The convergence result is stated in the following theorem.

Theorem 3.3 *Consider the feedback system* (3.60) *with the parameters* (3.55)–(3.59) *that satisfy* (3.9), (3.10) *under Assumptions 3.2–3.4. There exists* $\bar{\omega} > 0$ *and for any* $\omega \in (0, \bar{\omega})$ *there exists* $\bar{\delta} > 0$ *such that for the given* ω *and* $\delta \in (0, \bar{\delta})$ *there exists an open ball* $\mathscr{B}$ *centered at the point* $(x, \hat{\theta}, \hat{G}, \eta) = (l(\theta^*), \theta^*, 0, h\circ l(\theta^*)) =: \Upsilon$ *such that for any initial condition starting in the ball* $\mathscr{B}$*, the system* (3.60) *has a unique solution and the solution converges exponentially to*

Υ. *Furthermore, $y(t)$ exponentially converges to $h \circ l(\theta^*)$.*

Proof Let us proceed through the proof step by step.

Step 1: Time-scale separation. We rewrite the system (3.60) in the time scale $\tau = \omega t$ as

$$\omega \frac{\mathrm{d}x}{\mathrm{d}\tau} = f(x, \phi(x, \theta^* + \tilde{\theta} + \bar{S}(\tau)\alpha)), \tag{3.61}$$

$$\frac{d}{d\tau}\begin{bmatrix} \tilde{\theta} \\ \hat{G} \\ \tilde{\eta} \\ \alpha \end{bmatrix} = \delta \begin{bmatrix} K''\hat{G} \\ -\omega_L'\hat{G} + \omega_L'(y - h \circ l(\theta^*) - \tilde{\eta})\frac{1}{\alpha}\bar{M}(\tau) \\ -\omega_H'\tilde{\eta} + \omega_H'(y - h \circ l(\theta^*)) \\ -\lambda''\alpha \end{bmatrix}, \tag{3.62}$$

where $\bar{S}(\tau) = S(\tau/\omega), \bar{M}(\tau) = M(\tau/\omega)$.

Step 2: State transformation. Consider the following transformations

$$\tilde{\theta}_f = \frac{1}{\alpha}\tilde{\theta}, \qquad \hat{G}_f = \frac{1}{\alpha}\hat{G}, \qquad \tilde{\eta}_f = \frac{1}{\alpha^2}\tilde{\eta}, \tag{3.63}$$

which transform (3.61), (3.62) to the following system

$$\omega \frac{\mathrm{d}x}{\mathrm{d}\tau} = f(x, \phi(x, \theta^* + \tilde{\theta}_f\alpha + \bar{S}(\tau)\alpha)), \tag{3.64}$$

$$\frac{d\zeta_f}{d\tau} = \delta E(\tau, x, \zeta_f), \tag{3.65}$$

where $\zeta_f = \begin{bmatrix} \tilde{\theta}_f & \hat{G}_f & \tilde{\eta}_f & \alpha \end{bmatrix}^T$ and

$$E(\tau, x, \zeta_f) = \begin{bmatrix} \lambda''\tilde{\theta}_f + K''\hat{G}_f \\ (\lambda'' - \omega_L')\hat{G}_f + \omega_L'(y - h \circ l(\theta^*) - \tilde{\eta}_f\alpha^2)\frac{1}{\alpha^2}\bar{M}(\tau) \\ (2\lambda'' - \omega_H')\tilde{\eta}_f + \omega_H'\frac{1}{\alpha^2}(y - h \circ l(\theta^*)) \\ -\lambda''\alpha \end{bmatrix}. \tag{3.66}$$

Step 3: Averaging analysis for reduced system. We first freeze x in (3.64) at its equilibrium value $x = L(\tau, \zeta_f) = l(\theta^* + \tilde{\theta}_f \alpha + \bar{S}(\tau)\alpha)$, substitute it into (3.65) and then get the reduced system

$$\frac{d\zeta_{f,r}}{d\tau} = \delta E(\tau, L(\tau, \zeta_{f,r}), \zeta_{f,r}), \tag{3.67}$$

where $\zeta_{f,r} = \begin{bmatrix} \tilde{\theta}_{f,r} & \hat{G}_{f,r} & \tilde{\eta}_{f,r} & \alpha \end{bmatrix}^T$,

$$E(\tau, L(\tau, \zeta_{f,r}), \zeta_{f,r}) = \begin{bmatrix} \lambda'' \tilde{\theta}_{f,r} + K'' \hat{G}_{f,r} \\ (\lambda'' - \omega_L') \hat{G}_{f,r} + \omega_L' (\nu(\tilde{\theta}_{f,r}\alpha + \bar{S}(\tau)\alpha) - \tilde{\eta}_{f,r}\alpha^2) \frac{\bar{M}(\tau)}{\alpha^2} \\ (2\lambda'' - \omega_H') \tilde{\eta}_{f,r} + \omega_H' \frac{1}{\alpha^2} \nu(\tilde{\theta}_{f,r}\alpha + \bar{S}(\tau)\alpha) \\ -\lambda'' \alpha \end{bmatrix} \tag{3.68}$$

and

$$\nu(z) = h \circ l(z + \theta^*) - h \circ l(\theta^*) \tag{3.69}$$

with $z = \tilde{\theta}_{f,r}\alpha + \bar{S}(\tau)\alpha$. From Assumption 3.4, we get

$$\nu(0) = 0, \quad \frac{\partial}{\partial z}\nu(0) = 0, \quad \frac{\partial^2}{\partial z^2}\nu(0) = H < 0. \tag{3.70}$$

Note that the reduced system (3.67) has the same structure as (3.21) except the different constant parameters. Therefore, we can perform averaging analysis and stability analysis in Step 3 and 4 of the proof of Theorem 1, respectively, for the reduced system (3.67). Then, we conclude that there exists δ such that for all $\delta \in (0, \bar{\delta})$, the system (3.67) has a unique exponentially stable

periodic solution $\zeta^{\Pi}_{f,r}(\tau) = \begin{bmatrix} \tilde{\theta}^{\Pi}_{f,r}(\tau) & \hat{G}^{\Pi}_{f,r}(\tau) & \tilde{\eta}^{\Pi}_{f,r}(\tau) & \alpha^{\Pi}(\tau) \end{bmatrix}^T$ such that

$$\frac{d\zeta^{\Pi}_{f,r}(\tau)}{d\tau} = \delta E(\tau, L(\tau, \zeta^{\Pi}_{f,r}(\tau)), \zeta^{\Pi}_{f,r}(\tau)). \tag{3.71}$$

Step 4: Singular perturbation analysis. To convert the system (3.64) and (3.65) into the standard singular perturbation form, we shift the states ζ_f and x using the transformations $\tilde{\zeta}_f = \zeta_f - \zeta^{\Pi}_{f,r}(\tau)$ and $\tilde{x} = x - L(\tau, \zeta_f)$ such that

$$\frac{d\tilde{\zeta}_f}{d\tau} = \delta \tilde{E}(\tau, \tilde{x}, \tilde{\zeta}_f), \tag{3.72}$$

$$\omega \frac{d\tilde{x}}{d\tau} = \tilde{F}(\tau, \tilde{x}, \tilde{\zeta}_f), \tag{3.73}$$

where

$$\tilde{E}(\tau, \tilde{x}, \tilde{\zeta}_f) = E(\tau, \tilde{x} + L(\tau, \tilde{\zeta}_f + \zeta^{\Pi}_{f,r}(\tau)), \tilde{\zeta}_f + \zeta^{\Pi}_{f,r}(\tau)) - E(\tau, L(\tau, \zeta^{\Pi}_{f,r}(\tau)), \zeta^{\Pi}_{f,r}(\tau)), \tag{3.74}$$

$$\tilde{F}(\tau, \tilde{x}, \tilde{\zeta}_f) = f\Big(\tilde{x} + L(\tau, \tilde{\zeta}_f + \zeta^{\Pi}_{f,r}(\tau)), \phi\left(\tilde{x} + L(\tau, \tilde{\zeta}_f + \zeta^{\Pi}_{f,r}(\tau)), \theta^* + \tilde{\zeta}_{f_1}\alpha + \zeta^{\Pi}_{f_1,r}(\tau)\alpha + \bar{S}(\tau)\alpha\right)\Big), \tag{3.75}$$

where $\tilde{\zeta}_{f_1} = \tilde{\theta}_f - \tilde{\theta}^{\Pi}_{f,r}(\tau)$ and $\zeta^{\Pi}_{f_1,r}(\tau) = \tilde{\theta}^{\Pi}_{f,r}(\tau)$. Note that $\tilde{x} = 0$ is the quasi-steady state. By substituting the quasi-steady state into (3.72), we obtain the following reduced model

$$\frac{d\tilde{\zeta}_{f,r}}{d\tau} = \delta \tilde{E}(\tau, 0, \tilde{\zeta}_{f,r}), \tag{3.76}$$

which has an equilibrium at the origin $\tilde{\zeta}_{f,r} = 0$. We prove in Step 3 that this equilibrium is exponentially stable.

The next step in the singular perturbation analysis is to examine the boundary layer model

in the time scale $t = \tau/\omega$ as follows

$$\begin{aligned}\frac{\mathrm{d}x_{\mathrm{b}}}{\mathrm{d}t} &= \tilde{F}(\tau, x_b, \tilde{\zeta}_f),\\ &= f(x_{\mathrm{b}} + l(\theta), \phi(x_{\mathrm{b}} + l(\theta), \theta)).\end{aligned} \tag{3.77}$$

Recalling $f(l(\theta), \phi(l(\theta), \theta)) \equiv 0$, we deduce that $x_{\mathrm{b}} \equiv 0$ is an equilibrium of (3.77). According to Assumption 2, this equilibrium is locally exponentially stable uniformly in θ.

By combining exponential stability of the reduced model (3.76) with the exponential stability of the boundary layer model (3.77), and noting that $\tilde{E}(\tau, 0, 0) = 0, \tilde{F}(\tau, 0, 0) = 0$, we conclude from Theorem 11.4 of [49] that $\tilde{\zeta}_f \to 0$ and $\tilde{x} \to 0$, i.e., $\zeta_f \to \zeta_{f,r}^{\Pi}$ and $x \to l(\theta) = L(\tau, \zeta_f)$ exponentially as $\tau \to \infty$.

Step 5: Convergence to extremum. Note that $\tilde{\theta}_f(\tau) \to \tilde{\theta}_f^{\Pi}(\tau)$ and $\alpha \to 0$ exponentially. It follows then that $\theta(\tau) = \theta^* + \tilde{\theta}_f(\tau)\alpha + \bar{S}(\tau)\alpha \to \theta^*$ exponentially and $l(\theta) = l(\theta^* + \tilde{\theta}_f\alpha + \bar{S}(\tau)\alpha) \to l(\theta^*)$ exponentially. Consequently, $y = h(x)$ exponentially converges to $h \circ l(\theta^*)$. ■

Remark 3.1 *The concept of time scale separation in stability analysis requires further discussion. The plant dynamics in* (3.61) *operate on a fast time scale, while the dither signal with a small* ω *varies more slowly. The ES scheme in* (3.62) *has the slowest dynamics, characterized by a small* δ*. In Section 3.2, a similar principle is applied for static maps, where the dither signal must vary faster than the ES dynamics, necessitating a high* ω*. In dynamic maps, however, a small* ω *is needed to ensure that the plant dynamics in* (3.61) *remain fast, while a small* δ *ensures that the ES dynamics* (3.62) *with small parameters* (3.56)–(3.59) *are much slower than the probing signal.*

3.4 Robust Exponential Extremum Seeker

An important aspect of our design depicted in Fig. 3.1 is that the multiplicative inverse of the function α experiences exponential growth, while the high-pass filtered signal $y - \eta$ decays to

zero at a much faster rate, resulting in a bounded signal. However, in practical implementations, the boundedness of the resulting signal may not be guaranteed due to various factors such as measurement noise which prevents the complete convergence of $y-\eta$ to zero, and numerical inaccuracies that may arise from the multiplication of large and small values. The aforementioned limitation is not specific to our design but applies to any given prescribed-time stabilization scheme available in the literature [103], [104]. Furthermore, there may be instances where the extremum point changes over time, rather than being stationary, in which case the traditional extremum seeking design is capable of tracking it. To overcome these challenges and enhance the robustness of our design, we propose a modified α-signal that exponentially converges to an arbitrarily defined small positive number β rather than exponential decay function (3.7). In this case, our design offers a convergence to the neighborhood of the extremum with adjustable steady state oscillations. The new α-signal is governed by the following dynamics

$$\dot{\alpha}(t) = -\lambda\alpha(t) + \lambda\beta, \qquad \alpha(t_0) = \alpha_0. \tag{3.78}$$

Remark 3.2 *Our new design may seem to boil down to the traditional ES in [59]. However, a classical ES design that employs a constant, small perturbation amplitude $\alpha(t) \equiv \beta$ for all $t \geq t_0$ in Figure 3.1 may lead to a large overshoot due to a high demodulation amplitude $1/\beta$ (i.e., a high gain in the update of the gradient estimate), while converging to a much smaller neighborhood of the optimum. Our design, with an amplitude starting large initially and gradually decaying, addresses this issue. A further discussion is provided in Section 3.6.*

By relaxing the $\mathscr{C}^4$ condition in Assumption 3.1, we make the following assumption:

Assumption 3.5 *The function h is $\mathscr{C}^2$, and there exists $\theta^* \in \mathbb{R}^n$ such that*

$$\frac{\partial}{\partial\theta}h(\theta^*) = 0, \tag{3.79}$$

$$\frac{\partial^2}{\partial\theta^2}h(\theta^*) = H < 0, \quad H = H^T. \tag{3.80}$$

We summarize the closed-loop system depicted in Fig. 3.1 with the modified α-dynamics (3.78) as follows

$$\frac{d}{dt}\begin{bmatrix}\tilde{\theta}\\ \hat{G}\\ \tilde{\eta}\\ \alpha\end{bmatrix} = \begin{bmatrix} K\hat{G} \\ -\omega_l\hat{G}+\omega_l(y-h(\theta^*)-\tilde{\eta})\frac{1}{\alpha}M(t) \\ -\omega_h\tilde{\eta}+\omega_h(y-h(\theta^*)) \\ -\lambda\alpha+\lambda\beta \end{bmatrix}. \tag{3.81}$$

We present the following result for static maps, which can be easily extended to dynamic systems.

Theorem 3.4 *Consider the feedback system* (3.81) *under Assumption 3.5. There exist* $\bar{\omega},\bar{a}>0$ *such that for all* $\omega>\bar{\omega}$ *and* $\beta|a|\in(0,\bar{a})$ *there exists an open ball* $\mathscr{B}$ *centered at the point* $(\hat{\theta},\hat{G},\eta,\alpha)=(\theta^*,0,h(\theta^*),\beta)=:\Upsilon$ *such that for any initial condition starting in the ball* $\mathscr{B}$*, the system* (3.81) *has a unique solution and the solution converges exponentially to an* $\mathscr{O}(\beta/\omega+\beta|a|)$*-neighborhood of* Υ*. Furthermore,* $y(t)$ *exponentially converges to an* $\mathscr{O}(\beta^2/\omega^2+\beta^2|a|^2)$*-neighborhood of* $h(\theta^*)$*.*

The proof of this result is given in Appendix B.

From Theorem 3.4, we conclude that the estimate $\hat{\theta}$ converges to a neighborhood of the optimum θ^*, characterized by β, a, and ω. Its average converges to a point biased from the optimum due to higher-order terms in (B.11), which do not appear in quadratic maps. As a result, the robust ES with non-zero β introduces a bias in both the system states and their averages. As β approaches 0, this bias vanishes, aligning the robust ES with the exponential uES.

3.5 Source Seeking by a Velocity-Actuated Point Mass

In this section, we investigate the problem of source localization using an autonomous vehicle modeled as a point mass in a two-dimensional plane

$$\dot{x}_1 = v_{x_1}, \qquad \dot{x}_2 = v_{x_2}, \tag{3.82}$$

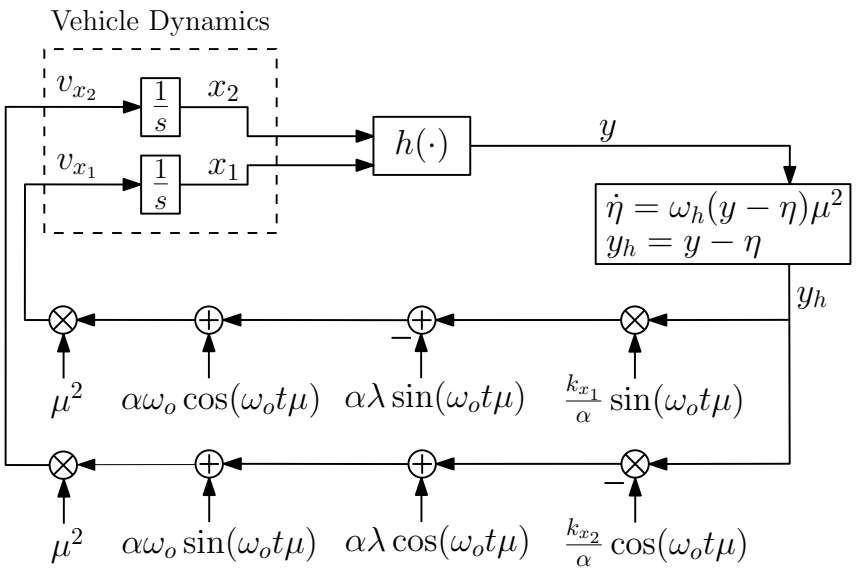

Figure 3.3. The developed ES scheme for a velocity-actuated point mass. For exponential convergence, choose $\mu \equiv 1, \alpha = \alpha_0 e^{-\lambda t}\ \forall t \in [0,\infty)$ and for prescribed-time convergence, choose $\mu = \frac{T}{T-t}, \alpha = \alpha_0 e^{\lambda T\left(1-\frac{T}{T-t}\right)}\ \forall t \in [0,T)$ with $\alpha_0, \lambda > 0$.

in which the vehicle's position is represented by the vector $\begin{bmatrix} x_1 & x_2 \end{bmatrix}^T$, and its velocity is controlled by the inputs v_{x_1} and v_{x_2}. The objective of this problem is to guide the vehicle towards the static source of a scalar signal in an environment where the vehicle's position data is not available. The only information provided to the vehicle at its current location is the strength of the signal, which is assumed to decrease as the distance from the source increases. Our specific goal is to detect the source while continuously measuring the source signal, ultimately bringing the vehicle to a complete stop at the exact location of the source. We give a block diagram in Fig. 3.3, in which we can apply our exponential uES and uPT-ES designs by using their corresponding μ and α functions.

For simplicity, but without loss of generality, we assume that the nonlinear map is quadratic with diagonal Hessian matrix, i.e.,

$$h(x_1,x_2) = h^* - q_{x_1}(x_1 - x_1^*)^2 - q_{x_2}(x_2 - x_2^*)^2, \tag{3.83}$$

where (x_1^*, x_2^*) is the unknown maximizer, $h^* = h(x_1^*, x_2^*)$ is the unknown maximum, and q_{x_1}, q_{x_2}

are some unknown positive constants.

Before presenting our results, let us first introduce the new coordinates

$$\tilde{x}_1 = x_1 - x_1^* - \alpha \sin(\omega_o t \mu), \tag{3.84}$$

$$\tilde{x}_2 = x_2 - x_2^* + \alpha \cos(\omega_o t \mu), \tag{3.85}$$

$$\tilde{\eta} = \eta - h(x_1^*, x_2^*), \tag{3.86}$$

where the signal η is defined in (3.16). For exponential stability, we can choose $\mu \equiv 1$ and α as in (3.7) for all $t \in [0, \infty)$. For prescribed-time stability, we can choose μ and α as in (3.37), (3.38), respectively, for all $t \in [0, T)$. Then, we summarize the system in Fig. 3.3 as follows

$$\frac{d}{dt}\begin{bmatrix} \tilde{x}_1 \\ \tilde{x}_2 \\ \tilde{\eta} \\ \alpha \end{bmatrix} = \begin{bmatrix} +k_{x_1}\mu^2 \sin(\omega_o t \mu)(y - h^* - \tilde{\eta})(1/\alpha) \\ -k_{x_2}\mu^2 \cos(\omega_o t \mu)(y - h^* - \tilde{\eta})(1/\alpha) \\ -\omega_h \mu^2 \tilde{\eta} + \omega_h \mu^2 (y - h^*) \\ -\lambda \mu^2 \alpha \end{bmatrix} \tag{3.87}$$

with the parameters chosen as

$$\omega_h > 2\lambda, \qquad k_{x_i} > \lambda / q_{x_i}, \qquad i = 1, 2. \tag{3.88}$$

An extension of the exponential uES result in Theorem 3.1 as well as the uPT-ES result in Theorem 3.2 to the system (3.87) can be easily done. For convenience, we give the uPT-ES result for this source seeking problem below without a proof.

Theorem 3.5 *Consider the feedback system* (3.87) *with the parameters that satisfy* (3.88) *and with the nonlinear map of the form* (3.83)*. There exists* $\bar{\omega}_o$ *and for any* $\omega_o > \bar{\omega}_o$*, there exists an open ball* $\mathscr{B}$ *centered at the point* $(x_1, x_2, \eta, \alpha) = (x_1^*, x_2^*, h^*, 0) =: \Upsilon$ *such that for any initial condition starting in the ball* $\mathscr{B}$*, the system* (3.87) *has a unique solution and the solution converges to* Υ *in prescribed time* T*. Hence,* $y(t)$ *converges to* $h(x_1^*, x_2^*)$ *in prescribed time* T*.*

Furthermore, the velocity inputs remain bounded over $[0,T)$.

The main contribution of the developed uPT-ES technique in Fig. 3.3 is that we achieve to drive the vehicle directly to the source h^* by keeping the velocities v_{x_1}, v_{x_2} bounded whereas the PT-ES technique in Chapter 2 (which can be suitably modified to fit the structure shown in Figure 3.3 with $\lambda = 0$, $\alpha \equiv \alpha_0$ and μ-function (3.37)) achieves the convergence of the vehicle to a small neighborhood the source with the velocities growing unbounded. The boundedness of the velocities v_{x_1}, v_{x_2} in our design follows from the fact that the signal $y - \eta$ converges to zero in prescribed time proportionally to α as well as the fact that the square of the blow-up function μ is multiplied by the function α which decays to zero faster, resulting in the boundedness and convergence of the velocities to zero, i.e.,

$$\lim_{t\to T}\left(\alpha(t)\mu(t)^2\right) = \lim_{t\to T}\left(\alpha_0 \frac{T^2}{(T-t)^2} e^{\lambda T\left(1-\frac{T}{T-t}\right)}\right) = 0. \tag{3.89}$$

3.6 Application to Source Seeking Problem

We consider the application of the developed ES techniques to the problem of source seeking by a velocity-actuated point mass as defined in Section 3.5. The velocity of the vehicle in Fig. 3.3 is controlled by the following ES controllers with appropriate μ and α functions:

- **Controller 1.** Nominal ES with $\mu \equiv 1$, $\alpha \equiv \alpha_0$, (i.e., $\lambda = 0$). This design boils down to Fig. 1 in [126], in which the vehicle asymptotically converges to a neighborhood of the source and shows steady-state oscillations around it.

- **Controller 2.** Exponential uES with $\mu \equiv 1$, α-function dynamics (3.7). This design is a modified version of Fig. 3.1.

- **Controller 3.** Robust Exponential ES with $\mu \equiv 1$, α-function dynamics (3.78) and additional terms $\lambda\beta\sin(\omega_o t)$ in v_{x_1} as well as $-\lambda\beta\cos(\omega_o t)$ in v_{x_2}. This design is a modified version of Fig. 3.1 with α-dynamics (3.78).

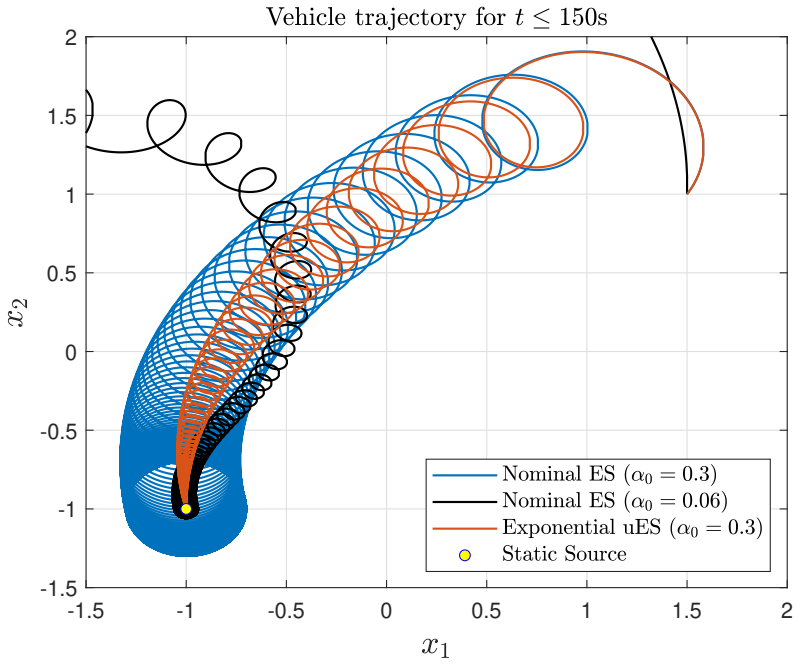

Figure 3.4. Static source seeking by an autonomous vehicle (3.82). The nominal ES with low amplitude α_0 approaches the source more closely but requires high initial velocity, leading to an initial deviation from the source. The exponential uES (3.13), with its exponentially decaying amplitude, avoids this issue.

- **Controller 4.** uPT-ES with μ-function (3.37), α-function (3.38). This design is a modified version of Fig. 3.2 with $q = 2$.

We now present the results of four numerical simulations to demonstrate the performance of Controllers 1-4 for the source-seeking problem. The real-time measurement is defined as $y(t) = h(x_1(t), x_2(t))$, where the function $h(\cdot)$ is described in (3.83) and its parameters are chosen as $(x_1^*, x_2^*) = (-1,-1), h^* = 1, q_{x_1} = 1, q_{x_2} = 0.5$.

Controller 1 and 2. The first simulation compares the performance of the nominal ES and exponential uES for a static source. The parameters in Fig. 3.3 are selected as $\omega_h = 1$, $k_{x_1} = k_{x_2} = 0.1, \lambda = 0.045$ and $\omega_o = 5$. The comparison between the nominal ES and exponential uES is shown in Fig. 3.4. The exponential uES exhibits exponential convergence to the source at $(-1,-1)$ with circular trajectories and exponentially decaying amplitude. On the other hand, the nominal ES with constant amplitude asymptotically converges to the vicinity of the source and

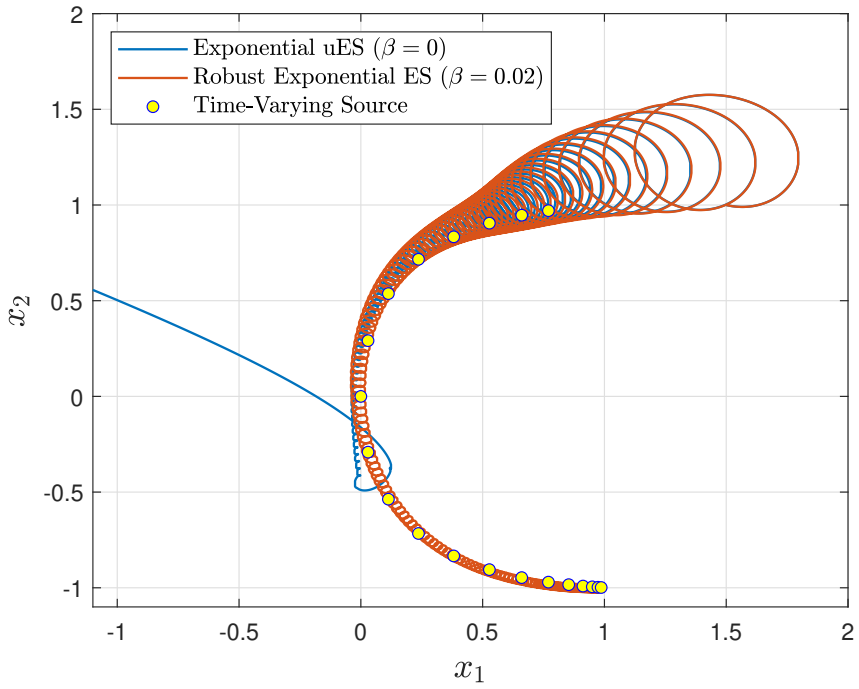

Figure 3.5. Time-varying source seeking by an autonomous vehicle (3.82). The trajectory of the source is illustrated by yellow circles at 10 second intervals. The robust exponential design (3.81) successfully tracks the source, owing to its amplitude that decays but does not vanish, while exponential design (3.13) fails to track.

shows steady-state oscillation around it. The nominal design with $\alpha_0 = 0.06$ converges closer to the source than the one with $\alpha_0 = 0.3$, but it initially moves away from the source due to its high initial velocity. Low initial velocity and perfect convergence are achieved through our design.

Controller 2 and 3. The second simulation examines the case of a time-varying source. The source is modeled as

$$x_1^*(t) = 1 - e^{-0.0003(t-70)^2}, \tag{3.90}$$

$$x_2^*(t) = -\tanh(0.03(t-70)). \tag{3.91}$$

Note that the Gaussian function in (3.90) and the hyperbolic tangent function in (3.91) can be referred to as saturating activation functions. The performance of the exponential uES and the robust exponential ES for tracking the time-varying source is shown in Fig. 3.5. The parameters

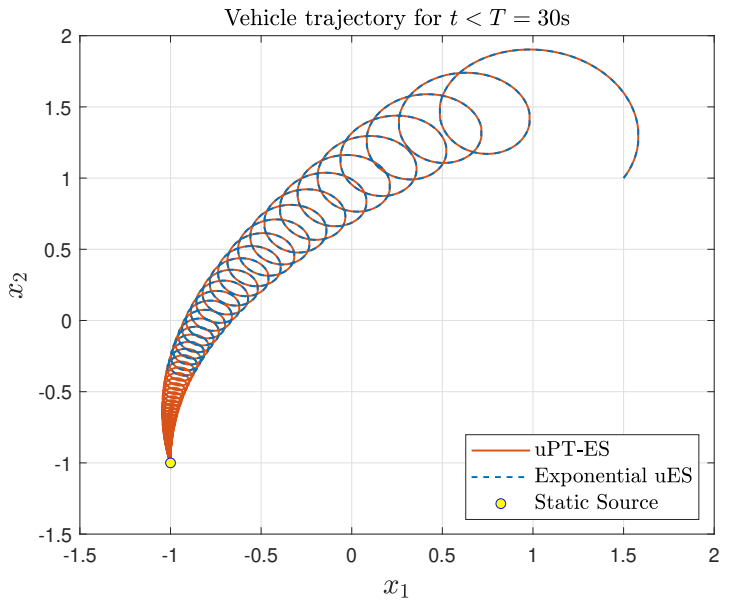

(a)

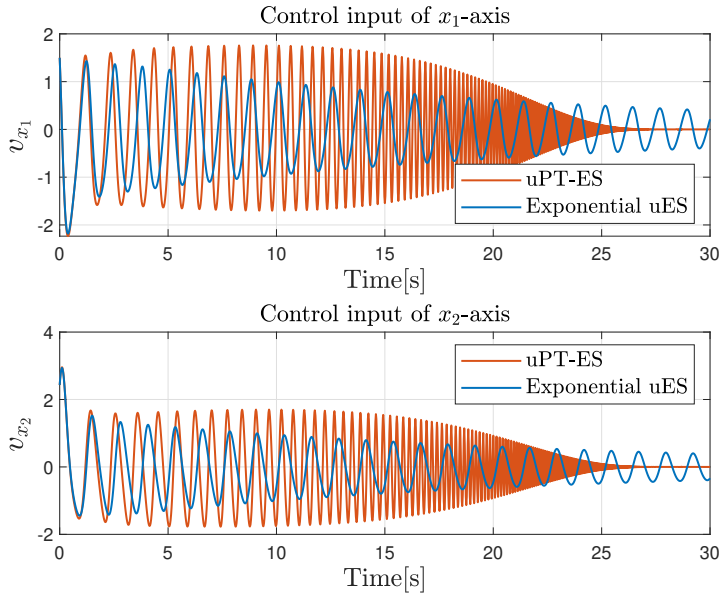

(b)

Figure 3.6. Static source seeking for $t \in [0, 30)$ in seconds. (a) Both designs follow the same trajectory, but the exponential uES (3.13) falls behind the uPT-ES (3.39). (b) The velocity inputs of the uPT-ES (3.39) exhibit more rapid changes compared to those of the exponential uES (3.13).

are set as $\beta = 0.02, k_{x_1} = 0.2, k_{x_2} = 0.3$ with $\alpha_0, \omega_h, \omega_o$ being the same as the first simulation.

The robust design demonstrates robustness to non-stationary sources with adjustable amplitude,

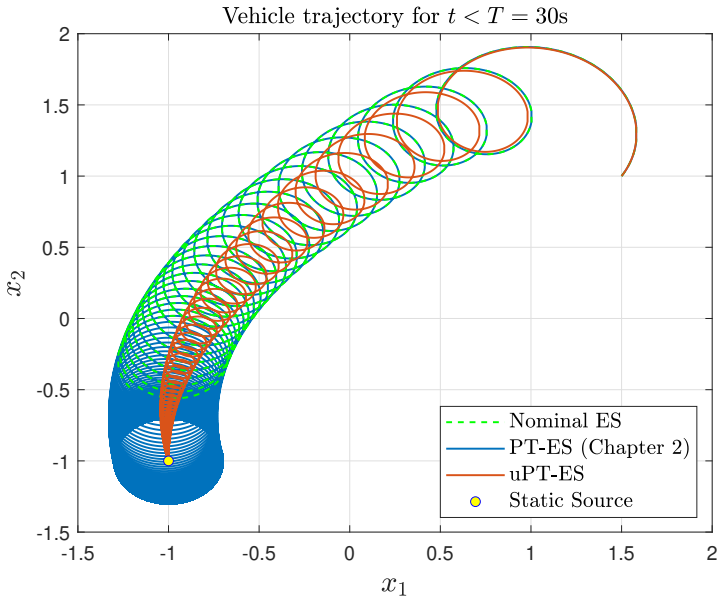

(a)

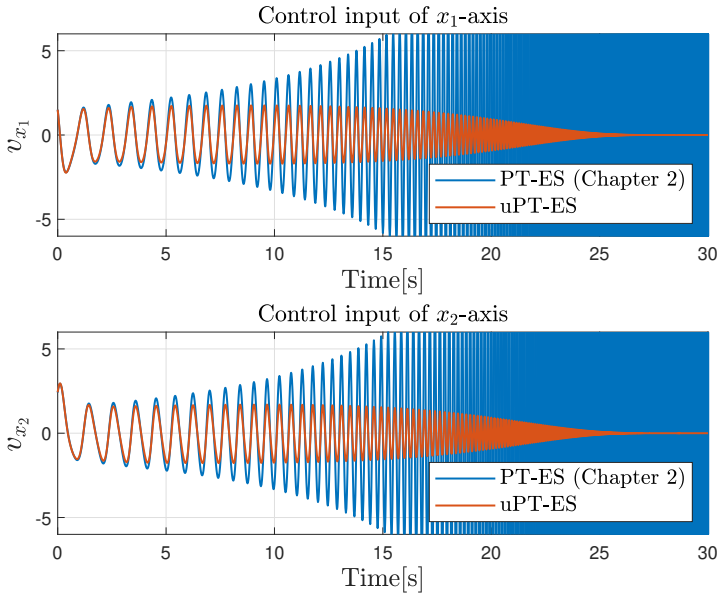

(b)

Figure 3.7. Static source seeking for $t \in [0, 30)$ in seconds. (a) The convergence of our uPT-ES (3.39) is compared with the one of delay-free PT-ES in Chapter 2, which is implemented on the 2D vehicle illustrated in Fig. 3.3 by choosing $\lambda = 0$, $\alpha \equiv \alpha_0$, and μ as in (3.37). (b) The velocity inputs in our design are kept bounded, while the inputs in Chapter 2 grow unbounded.

while the exponential uES fails to achieve convergence.

Controller 2 and 4. The third simulation considers the static source problem and

implements both the exponential uES design and uPT-ES design for comparison. The final time is set to $T = 30s$, and the rest of the parameters are chosen as in the first simulation. As shown in Fig. 3.6a, both designs track the same trajectory, but the exponential uES cannot reach the source in prescribed time. This is because the uPT-ES design performs more rapid velocity changes, resulting in bounded but high acceleration in the vehicle, as seen in Fig. 3.6b.

Controller 4 and the Delay-Free PT-ES in Chapter 2. In our fourth and final simulation, we illustrate the difference between these two different prescribed-time ES designs. The delay-free design in Chapter 2 can be implemented into Fig. 3.3 by choosing $\lambda = 0, \alpha \equiv \alpha_0$, and μ as in (3.37). The final time is set to $T = 30s$, and the rest of the parameters are the same as in the first simulation. The PT-ES in Chapter 2 basically improves the convergence of the nominal ES as demonstrated in Fig. 3.7a. However, we can see in Fig. 3.7b that this comes with the cost of velocities growing unbounded. Our design, on the other hand, achieves unbiased convergence in prescribed time with bounded velocities.

Remark 3.3 *The capabilities of the developed designs extend beyond closed-loop systems assumed to be stable under Assumption 3.3. By selecting a Lyapunov function as the cost function to optimize, as demonstrated in [98], we can achieve model-free stabilization of unstable dynamic systems. Consider the open-loop unstable scalar system*

$$\dot{x} = cx + bu, \qquad c > 0, \tag{3.92}$$

where the control direction b is unknown and non-zero. The classical ES controller is given by

$$u = a\omega\cos(\omega t) - \frac{k}{a}\sin(\omega t)V(x), \tag{3.93}$$

where the Lyapunov function $V(x) = x^2$. Performing the change of variables $\tilde{x} = x - ab\sin(\omega t)$, we obtain $\dot{\tilde{x}} = c\tilde{x} + cab\sin(\omega t) - b\frac{k}{a}\sin(\omega t)(\tilde{x} + ab\sin(\omega t))^2$. The average system is $\dot{\tilde{x}}^a = (c - kb^2)\tilde{x}^a$, which is exponentially stable for $k > c/b^2$. This implies local stability of the x-

system for sufficiently large ω, according to the averaging theorem [49, Theorem 10.4]. For exponential and prescribed-time stabilization at the origin, the controller can be updated as follows

$$u = \mu^2 \left(\alpha\omega \cos(\omega t \mu) - \alpha\lambda \sin(\omega t \mu) - \frac{k}{\alpha} \sin(\omega t \mu) V(x) \right), \tag{3.94}$$

where $k > c/b^2 + \lambda$ and the signals μ and α are defined as described in the caption of Fig. 3.3. This approach can be extended to multi-input systems, following the methodology in [98].

3.7 Conclusion

In this chapter, we address the issue of steady-state oscillations in classical ES. We develop accelerated ES algorithms that not only eliminate the steady-state oscillations, but also achieves unbiased convergence to the extremum exponentially and in prescribed time by employing proper time-varying functions in the perturbation and demodulation stage of the ES loop. For tracking non-stationary optima, we introduce a robust ES scheme with user-adjustable oscillations that gradually decrease but remains non-zero. We evaluate the performance of our ES algorithms on a source-seeking problem. With bounded velocity inputs, our uPT-ES design accurately locates the source, while the delay-free PT-ES algorithm in Chapter 2 converges to a neighborhood of the source with unbounded input growth.

3.8 Acknowledgments

Chapter 3 is a reprint of the material as it appears in:

- C. T. Yilmaz, M. Diagne, and M. Krstic, "Exponential and Prescribed-Time Extremum Seeking with Unbiased Convergence", *Automatica*, under review, 2023.

The dissertation author was the primary investigator and author of this paper.

Chapter 4

Unbiased Extremum Seeking for PDEs

In this chapter, we present two distinct unbiased extremum seeking (uES) designs: one can handle arbitrarily long and known time delays, while the other compensates for diffusion PDEs. The designs consist of a PDE compensator, a perturbation signal with exponentially decaying amplitude (to eliminate steady-state oscillation), demodulation signals with exponentially growing amplitude and properly selected design parameters (to ensure unbiased convergence). Unlike previous PDE-compensating ES designs in the literature, which only guarantee local stability around the extremum, our uES designs not only compensate for PDE dynamics but also ensure exponential, unbiased convergence to the optimum. Our method leverages exponentially decaying/growing signals within the modulation/demodulation stages and carefully selected design parameters. The stability analysis of our designs relies on a state transformation, infinite-dimensional averaging, local exponential stability of the averaged system, local stability of the transformed system, and local exponential stability of the original system. Numerical simulations are presented to demonstrate the efficacy of the developed designs.

This chapter is structured as follows. Section 4.1 presents problem formulation. Section 4.2 and Section 4.3 introduce unbiased ES with delay compensator and unbiased ES with diffusion PDE compensator, respectively, along with formal stability analysis. Numerical results are presented in Section 4.4, followed by the conclusion in Section 4.5 and acknowledgments.

Notation. We denote the Euclidean norm by $|\cdot|$. The partial derivatives of a function

$u(x,t)$ are denoted by $\partial_x u(x,t) = \partial u(x,t)/\partial x$, $\partial_t u(x,t) = \partial u(x,t)/\partial t$. The spatial $L_2[0,D]$ norm of $u(x,t)$ is denoted by $||u(\cdot,t)||^2 = \int_0^D u^2(x,t)dx$.

4.1 Problem Statement

We consider the optimization problem given by

$$\min_{\theta \in \mathbb{R}} Q(\theta), \tag{4.1}$$

where $\theta \in \mathbb{R}$ represents the input, $Q \in \mathbb{R} \to \mathbb{R}$ is an unknown smooth function. We introduce the following assumption regarding the unknown static map $Q(\cdot)$.

Assumption 4.1 *The unknown static map is characterized by the following quadratic form*

$$Q(\theta) = y^* + \frac{H}{2}(\theta - \theta^*)^2, \tag{4.2}$$

where $y^* \in \mathbb{R}$ and $\theta^* \in \mathbb{R}$ denote the unknown optimal output and input values, respectively, and $H > 0$ represents the unknown Hessian of the static map $Q(\theta)$.

In Chapter 3, we design a multivariable ES that achieves unbiased and exponential convergence to the optimum, assuming the absence of actuator dynamics. This work addresses a more challenging and application-relevant optimization problem by considering the same objective function (4.1) but incorporating actuator dynamics modeled by a delay and diffusion PDE. Our current objective is to develop a scalar unbiased ES that effectively compensates for PDE dynamics and exponentially guides the input $\theta(t)$ towards the optimum θ^*.

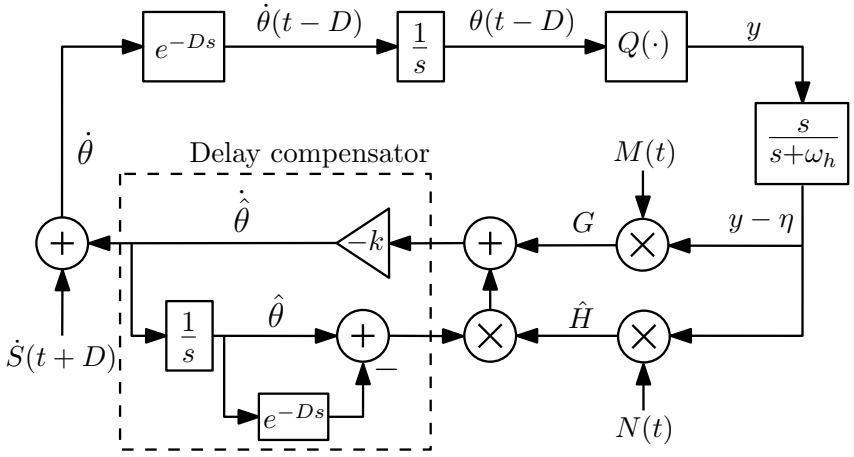

Figure 4.1. Unbiased ES with delay compensator. The design employs exponentially growing multiplicative signals, $M(t) = \frac{2}{a}e^{\lambda t}\sin(\omega t)$, and $N(t) = -\frac{8}{a^2}e^{2\lambda t}\cos(2\omega t)$, as well as exponentially decaying dither signal $\dot{S}(t+D) = \frac{d}{dt}\left(e^{-\lambda(t+D)}a\sin(\omega(t+D))\right)$ to achieve exponential and unbiased convergence to the optimum θ^* at the rate of the user-defined $\lambda > 0$.

4.2 Unbiased ES with Delay

In this section, we consider the scenario where the output $y(t)$ is subject to a known and constant delay $D \geq 0$, expressed as

$$y(t) = Q(\theta(t-D)), \quad t \in [0,\infty). \tag{4.3}$$

Note that the static map $Q(\theta)$ enables the representation of the overall delay D as the sum of individual components, denoted as D_u and D_y, corresponding to the delays in the actuation and measurement paths, respectively. Fig. 4.1 illustrates the closed-loop unbiased ES with delay compensator. Before delving into the estimator design, we introduce the signals presented in Fig. 4.1 in the following subsection.

4.2.1 Excitation signals and gradient/Hessian estimates

Let us define the following parameter estimate

$$\hat{\theta}(t) = \theta(t) - S(t+D), \tag{4.4}$$

with the perturbation signal

$$S(t+D) = e^{-\lambda(t+D)} a \sin(\omega(t+D)), \tag{4.5}$$

where $\lambda > 0$ is the decay rate of the perturbation signal, $a \in \mathbb{R}$ is the perturbation amplitude, $\omega > 0$ is the probing frequency. Let us define the delay-free and delayed parameter estimation error variables

$$\tilde{\theta}(t) = \hat{\theta}(t) - \theta^*, \quad \tilde{\theta}(t-D) = \hat{\theta}(t-D) - \theta^*. \tag{4.6}$$

Applying the technique in [56], we represent the signals (4.6) through the transport PDE as

$$\tilde{\theta}(t-D) = \bar{u}(0,t), \tag{4.7}$$

$$\partial_t \bar{u}(x,t) = \partial_x \bar{u}(x,t), \tag{4.8}$$

$$\bar{u}(D,t) = \tilde{\theta}(t) \tag{4.9}$$

for $x \in (0,D)$. The solution of this PDE is given by

$$\bar{u}(x,t) = \tilde{\theta}(t+x-D). \tag{4.10}$$

We compute the estimate of the gradient and Hessian as follows

$$G(t) = M(t)(y(t) - \eta(t)), \tag{4.11}$$

$$\hat{H}(t) = N(t)(y(t) - \eta(t)), \tag{4.12}$$

where the multiplicative excitation signals are given by

$$M(t) = \frac{2}{a} e^{\lambda t} \sin(\omega t), \quad N(t) = -\frac{8}{a^2} e^{2\lambda t} \cos(2\omega t) \tag{4.13}$$

and $\eta(t)$ is governed by

$$\dot{\eta}(t) = -\omega_h \eta(t) + \omega_h y(t). \tag{4.14}$$

We use exponentially decaying signals in the modulation stage, as defined in (4.5), and exponentially growing signals in the demodulation stage, as defined in (4.11) and (4.12). The important aspect of our design lies in the fact that the high-pass filtered state $y - \eta$ exhibits exponential decay to zero at the rate of 2λ. This crucial feature ensures that despite the growing amplitudes in (4.13), the estimates in (4.11) and (4.12) remain bounded.

4.2.2 Parameter estimator design and error dynamics

The time derivative of (4.7)–(4.9) is given by

$$\dot{\hat{\theta}}(t-D) = u(0,t), \tag{4.15}$$

$$\partial_t u(x,t) = \partial_x u(x,t), \tag{4.16}$$

$$u(D,t) = \dot{\hat{\theta}}(t), \tag{4.17}$$

by noting $\dot{\tilde{\theta}}(t) = \dot{\hat{\theta}}(t)$ from (4.6). Following the methodology presented in [56], we consider the following backstepping transformation

$$w(x,t) = u(x,t) + \bar{k}\left(\tilde{\theta}(t-D) + \int_0^x u(\sigma,t)d\sigma\right) \tag{4.18}$$

to convert the system (4.15)–(4.17) into the target system

$$\dot{\tilde{\theta}}(t-D) = -\bar{k}\tilde{\theta}(t-D) + w(0,t), \tag{4.19}$$

$$\partial_t w(x,t) = \partial_x w(x,t), \tag{4.20}$$

$$w(D,t) = 0, \tag{4.21}$$

with the gain $\bar{k} > 0$. By substituting $x = D$ into (4.18) and considering (4.17) and (4.21), we obtain the update law

$$\begin{aligned}\dot{\hat{\theta}}(t) = & -\bar{k}\left(\tilde{\theta}(t-D) + \int_0^D u(\sigma,t)d\sigma\right), \\ = & -\bar{k}\tilde{\theta}(t-D) - \bar{k}\left(\hat{\theta}(t) - \hat{\theta}(t-D)\right),\end{aligned} \tag{4.22}$$

where we use the property $u(\sigma,t) = \partial_t \bar{u}(\sigma,t) = \partial_x \bar{u}(\sigma,t)$, use the solution (4.10), and recall (4.6). We obviously cannot use (4.22) since the error $\tilde{\theta}(t-D)$ is not measured. To overcome this limitation, we define $\bar{k} = kH$, where $H > 0$ represents the unknown Hessian, and the user specifies the positive gain k. Then, we replace the signals $H\tilde{\theta}(t-D)$ and H with their respective estimates, $G(t)$ from (4.11) and $\hat{H}(t)$ from (4.12). This leads to the following implementable version of (4.22)

$$\dot{\hat{\theta}}(t) = -kG(t) - k\hat{H}(t)\left(\hat{\theta}(t) - \hat{\theta}(t-D)\right). \tag{4.23}$$

The design parameters should satisfy the following conditions

$$\lambda < \frac{\omega_h}{2}, \qquad k > \frac{\lambda}{H}. \tag{4.24}$$

The essence of these conditions is that the adaptation (learning) rate should surpass the decay rate of the perturbation (exploration) signal.

In view of the transformation,

$$\tilde{\eta}(t) = \eta(t) - y^*, \tag{4.25}$$

we write the closed-loop system in the form

$$\tilde{\theta}(t-D) = \bar{u}(0,t), \tag{4.26}$$

$$\partial_t \bar{u}(x,t) = \partial_x \bar{u}(x,t), \tag{4.27}$$

$$\bar{u}(D,t) = \tilde{\theta}(t), \tag{4.28}$$

$$\dot{\tilde{\theta}}(t) = -kG(t) - k\hat{H}(t)(\tilde{\theta}(t) - \tilde{\theta}(t-D)), \tag{4.29}$$

$$\dot{\tilde{\eta}}(t) = -\omega_h \tilde{\eta}(t) + \omega_h (y(t) - y^*), \tag{4.30}$$

where (4.11) and (4.12) are rewritten as

$$G(t) = \frac{2}{a} e^{\lambda t} \sin(\omega t) (y(t) - y^* - \tilde{\eta}(t)), \tag{4.31}$$

$$\hat{H}(t) = -\frac{8}{a^2} e^{2\lambda t} \cos(2\omega t) (y(t) - y^* - \tilde{\eta}(t)). \tag{4.32}$$

Recalling (4.2)–(4.6), the output (4.3) is rewritten as

$$y(t) = y^* + \frac{H}{2} \left(\tilde{\theta}(t-D) + e^{-\lambda t} a \sin(\omega t) \right)^2. \tag{4.33}$$

4.2.3 Stability analysis

The main theorem is stated as follows.

Theorem 4.1 *Let Assumption 4.1 hold and the parameters satisfy* (4.24)*. Then, there exists* $\bar{\omega}$ *and for any* $\omega > \bar{\omega}$*, the closed-loop system* (4.26)–(4.30) *is exponentially stable at the origin in the sense of the norm*

$$\left(||\bar{u}(\cdot,t)||^2 + |\tilde{\theta}(t)|^2 + |\tilde{\eta}(t)|^2 \right)^{1/2}. \tag{4.34}$$

Furthermore, the input $\theta(t)$ *and output* $y(t)$ *exponentially converge to* θ^* *and* y^**, respectively.*

Proof Let us proceed through the proof step by step.

Step 1: State transformation. Let us consider the following transformations

$$\tilde{\theta}_f(t-D) = e^{\lambda(t-D)}\bar{u}(0,t), \tag{4.35}$$

$$\bar{u}_f(x,t) = e^{\lambda(t+x-D)}\bar{u}(x,t), \tag{4.36}$$

$$\tilde{\theta}_f(t) = e^{\lambda t}\tilde{\theta}(t), \tag{4.37}$$

$$\tilde{\eta}_f(t) = e^{2\lambda t}\tilde{\eta}(t), \tag{4.38}$$

which transform (4.26)–(4.30) to the following system

$$\tilde{\theta}_f(t-D) = \bar{u}_f(0,t), \tag{4.39}$$

$$\partial_t \bar{u}_f(x,t) = \partial_x \bar{u}_f(x,t), \tag{4.40}$$

$$\bar{u}_f(D,t) = \tilde{\theta}_f(t), \tag{4.41}$$

$$\begin{aligned}\dot{\tilde{\theta}}_f(t) = {} & \lambda\,\tilde{\theta}_f(t) - k\frac{2}{a}\sin(\omega t)\frac{H}{2}\left[\left(e^{\lambda D}\tilde{\theta}_f(t-D) + a\sin(\omega t)\right)^2 - \tilde{\eta}_f(t)\right] \\ & - k\left(-\frac{8}{a^2}\cos(2\omega t)\right)\frac{H}{2}\left[\left(e^{\lambda D}\tilde{\theta}_f(t-D) + a\sin(\omega t)\right)^2 - \tilde{\eta}_f(t)\right] \\ & \times\left(\tilde{\theta}_f(t) - e^{\lambda D}\tilde{\theta}_f(t-D)\right),\end{aligned} \tag{4.42}$$

$$\dot{\tilde{\eta}}_f(t) = -(\omega_h - 2\lambda)\tilde{\eta}_f(t) + \omega_h\frac{H}{2}\left(e^{\lambda D}\tilde{\theta}_f(t-D) + a\sin(\omega t)\right)^2, \tag{4.43}$$

in view of (4.31)–(4.33).

Step 2: Averaging operation. The average of the transformed system (4.39)–(4.43) over the period $\Pi = 2\pi/\omega$ is given by

$$\tilde{\theta}_f^{\mathrm{av}}(t-D) = \bar{u}_f^{\mathrm{av}}(0,t), \tag{4.44}$$

$$\partial_t \bar{u}_f^{\mathrm{av}}(x,t) = \partial_x \bar{u}_f^{\mathrm{av}}(x,t), \tag{4.45}$$

$$\bar{u}_f^{\mathrm{av}}(D,t) = \tilde{\theta}_f^{\mathrm{av}}(t), \tag{4.46}$$

$$\dot{\tilde{\theta}}_f^{\mathrm{av}}(t) = -(kH - \lambda)\tilde{\theta}_f^{\mathrm{av}}(t), \tag{4.47}$$

$$\dot{\tilde{\eta}}_f^{\text{av}}(t) = -(\omega_h - 2\lambda)\tilde{\eta}_f^{\text{av}}(t) + \omega_h \frac{H}{2}\left(e^{2\lambda D}(\tilde{\theta}_f^{\text{av}}(t-D))^2 + a^2/2\right), \tag{4.48}$$

where $\tilde{\theta}_f^{\text{av}}(t)$, $\bar{u}_f^{\text{av}}(\cdot,t)$, and $\tilde{\eta}_f^{\text{av}}(t)$ denote the average versions of the states $\tilde{\theta}_f(t)$, $\bar{u}_f(\cdot,t)$, and $\tilde{\eta}_f(t)$, respectively.

Step 3: Stability of average system. The solution to (4.47) is given by $\tilde{\theta}_f^{\text{av}}(t) = \tilde{\theta}_f^{\text{av}}(0)e^{-(kH-\lambda)t}$. Then, we write the solution to the PDE (4.45) as

$$\bar{u}_f^{\text{av}}(x,t) = \tilde{\theta}_f^{\text{av}}(0)e^{-(kH-\lambda)(t+x-D)}. \tag{4.49}$$

Thus, the $(\tilde{\theta}_f^{\text{av}}, \bar{u}_f^{\text{av}})$-system is exponentially stable at the origin for $kH > \lambda$. Using this fact, it is trivial to show that $\tilde{\eta}_f^{\text{av}}(t)$ of (4.48) exponentially converges to $\frac{\omega_h H a^2}{4(\omega_h - 2\lambda)}$ for $\omega_h > 2\lambda$.

Step 4: Invoking averaging theorem. Applying the averaging theorem for infinite-dimensional systems [37], we establish that there exists $\bar{\omega}$ and for any $\omega > \bar{\omega}$, the transformed system (4.39)–(4.43) with states $(\bar{u}_f(\cdot,t), \tilde{\theta}_f(t), \tilde{\eta}_f(t))$ has a unique exponentially stable periodic solution $(\bar{u}_f^{\Pi}(\cdot,t), \tilde{\theta}_f^{\Pi}(t), \tilde{\eta}_f^{\Pi}(t))$ of period $\Pi = 2\pi/\omega$ and this solution satisfies

$$\left(||\bar{u}_f^{\Pi}(\cdot,t)||^2 + |\tilde{\theta}_f^{\Pi}(t)|^2 + \left|\tilde{\eta}_f^{\Pi}(t) - \frac{\omega_h H a^2}{4(\omega_h - 2\lambda)}\right|^2\right)^{\frac{1}{2}} \leq \mathscr{O}\left(\frac{1}{\omega}\right) \tag{4.50}$$

for all $t \geq 0$. Considering (4.50) and recalling the transformations (4.35)–(4.38), we deduce that the original error system (4.26)–(4.30) with states $\bar{u}(\cdot,t), \tilde{\theta}(t), \tilde{\eta}(t)$ has a unique solution and is exponentially stable at the origin in the sense of the norm (4.34).

Step 5: Convergence to extremum. Taking into account the results in Step 4 and recalling from (4.4)–(4.6), (4.37) that

$$\theta(t) = e^{-\lambda t}\tilde{\theta}_f(t) + \theta^* + e^{-\lambda(t+D)} a \sin(\omega(t+D)), \tag{4.51}$$

we conclude the exponential convergence of $\theta(t)$ to θ^*. We establish the convergence of the

output $y(t)$ to y^* from (4.33) and complete the proof of Theorem 4.1. ■

4.3 Unbiased ES with Diffusion PDE

In this section, we consider the following cascade of a diffusion PDE and ODE (integrator) with Neumann interconnection

$$\dot{\theta}(t) = \partial_x \alpha(0,t), \tag{4.52}$$

$$\partial_t \alpha(x,t) = \partial_{xx} \alpha(x,t), \tag{4.53}$$

$$\alpha(0,t) = 0, \tag{4.54}$$

$$\partial_x \alpha(D,t) = \dot{\Theta}(t) \tag{4.55}$$

for $(x,t) \in (0,D) \times [0,\infty)$. The output of the static map is

$$y(t) = y^* + \frac{H}{2}(\theta(t) - \theta^*)^2. \tag{4.56}$$

The diffusion PDE with Neumann actuation arises in thermal systems, such as Stefan models of thermal phase change [52], tubular reactors [9], and batteries [75], where the control input is the heat flux. Our methodology can be extended to systems with Dirichlet actuation. The unbiased ES with diffusion PDE compensator is schematically illustrated in Fig. 4.2.

4.3.1 Perturbation signal

Let us define the following parameter estimates to determine the optimal unknown actuator θ^*

$$\hat{\theta}(t) = \theta(t) - e^{-\lambda t} a \sin(\omega t), \tag{4.57}$$

$$\hat{\Theta}(t) = \Theta(t) - S(t). \tag{4.58}$$

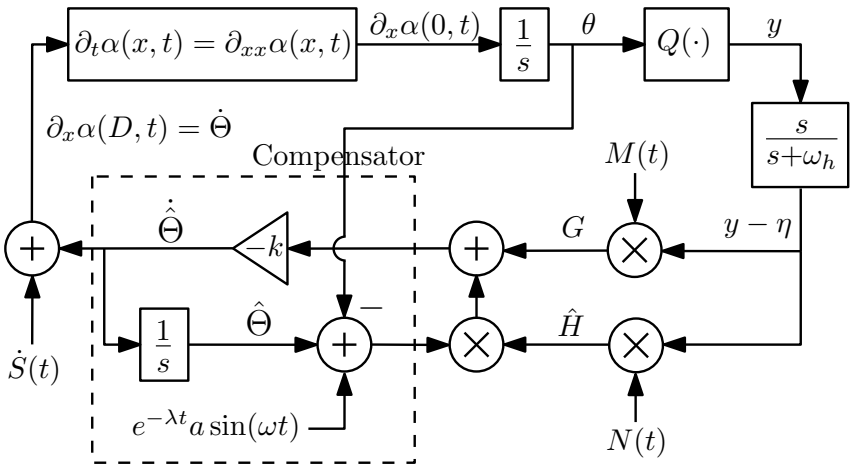

Figure 4.2. Unbiased ES with diffusion PDE compensator. The design requires feedback of θ, uses the same excitation signals, $M(t)$ and $N(t)$ as in Fig. 4.1, and employs a properly designed perturbation signal, $\dot{S}(t)$.

We need to redesign the perturbation signal, $S(t)$, such that when applied as input to the diffusion PDE it produces the desired output, $e^{-\lambda t}a\sin(\omega t)$. We formulate this trajectory generation problem as follows

$$S(t)=\partial_x\beta(D,t), \tag{4.59}$$

$$\partial_t\beta(x,t)=\partial_{xx}\beta(x,t), \tag{4.60}$$

$$\beta(0,t)=0, \tag{4.61}$$

$$\partial_x\beta(0,t)=e^{-\lambda t}a\sin(\omega t) \tag{4.62}$$

for $(x,t)\in(0,D)\times[0,\infty)$. We present the solution to $S(t)$ in the following lemma.

Lemma 4.1 *The explicit solution to $S(t)$ in* (4.59) *is*

$$S(t)=\frac{a}{2}e^{-\lambda t}\left(\sin(\omega t+qD)e^{pD}+\sin(\omega t-qD)e^{-pD}\right), \tag{4.63}$$

where $p=\sqrt{\frac{\sqrt{\lambda^2+\omega^2}-\lambda}{2}}$ and $q=\sqrt{\frac{\sqrt{\lambda^2+\omega^2}+\lambda}{2}}$.

Proof Following the PDE-based motion planning technique presented in [58, Ch. 12], we seek the solution in the following form

$$\beta(x,t) = \sum_{k=0}^{\infty} c_k(t)\frac{x^k}{k!}, \tag{4.64}$$

where $c_k(t)$ are the time-varying coefficients. To determine these coefficients, we first use the boundary conditions (4.61) and (4.62), and obtain

$$c_0(t) = 0, \tag{4.65}$$

$$c_1(t) = e^{-\lambda t} a \sin(\omega t) = \mathrm{Im}\left\{ a e^{(-\lambda + j\omega)t} \right\}. \tag{4.66}$$

Next, we substitute (4.64) into (4.60), resulting in the recursive relationship $c_{k+2}(t) = \dot{c}_k(t)$. From (4.65) and (4.66), we get

$$c_{2k}(t) = 0, \tag{4.67}$$

$$c_{2k+1}(t) = \mathrm{Im}\left\{ a(-\lambda + j\omega)^k e^{(-\lambda + j\omega)t} \right\}. \tag{4.68}$$

Substituting (4.68) into (4.64), we get

$$\begin{aligned}
\beta(x,t) &= \mathrm{Im}\left\{ \sum_{k=0}^{\infty} a(-\lambda + j\omega)^k \frac{x^{2k+1}}{(2k+1)!} e^{(-\lambda + j\omega)t} \right\}, \\
&= \mathrm{Im}\left\{ \sum_{k=0}^{\infty} \frac{a\left(\sqrt{(-\lambda + j\omega)}x\right)^{2k+1}}{\sqrt{(-\lambda + j\omega)}(2k+1)!} e^{(-\lambda + j\omega)t} \right\}, \\
&= \mathrm{Im}\left\{ \frac{a}{\sqrt{-\lambda + j\omega}} \sinh(\sqrt{(-\lambda + j\omega)}x) e^{(-\lambda + j\omega)t} \right\}, \\
&= \mathrm{Im}\left\{ \left(e^{px - \lambda t + j(qx + \omega t)} - e^{-px - \lambda t + j(-qx + \omega t)} \right) + a(p - jq)/(2p^2 + 2q^2) \right\},
\end{aligned} \tag{4.69}$$

where $p+jq=\sqrt{(-\lambda+j\omega)}$ and p and q are defined after (4.63). Finally, we arrive at

$$\begin{aligned}\beta(x,t)=\big[&(p\sin(\omega t+qx)-q\cos(\omega t+qx))\,e^{px-\lambda t}\\&-(p\sin(\omega t-qx)-q\cos(\omega t-qx))\,e^{-px-\lambda t}\big]a/(2p^2+2q^2).\end{aligned}\tag{4.70}$$

Differentiating (4.70) with respect to x and setting $x=D$, we derive (4.63). ■

Defining the error variables

$$\tilde{\theta}(t)=\hat{\theta}(t)-\theta^*,\qquad \tilde{\Theta}(t)=\hat{\Theta}(t)-\theta^*,\tag{4.71}$$

we write the following error system

$$\tilde{\theta}(t)=\partial_x\bar{u}(0,t),\tag{4.72}$$

$$\partial_t\bar{u}(x,t)=\partial_{xx}\bar{u}(x,t),\tag{4.73}$$

$$\bar{u}(0,t)=0,\tag{4.74}$$

$$\partial_x\bar{u}(D,t)=\tilde{\Theta}(t),\tag{4.75}$$

where the time derivative is given by

$$\dot{\hat{\theta}}(t)=\partial_x u(0,t),\tag{4.76}$$

$$\partial_t u(x,t)=\partial_{xx}u(x,t),\tag{4.77}$$

$$u(0,t)=0,\tag{4.78}$$

$$\partial_x u(D,t)=\dot{\hat{\Theta}}(t),\tag{4.79}$$

by noting that $u(x,t)=\partial_t\bar{u}(x,t)=\alpha(x,t)-\partial_t\beta(x,t)$ for $(x,t)\in(0,D)\times[0,\infty)$ and recalling the cascades (4.52)–(4.55), (4.59)–(4.62) and the solution of $\beta(x,t)$ in (4.70).

4.3.2 Parameter estimator design and error dynamics

We consider the following backstepping transformation

$$w(x,t) = u(x,t) + \int_0^x q(x,r)u(r,t)dr + \gamma(x)\tilde{\theta}(t), \tag{4.80}$$

with the gain kernels $q(x,r) = \bar{k}(x-r)$ and $\gamma(x) = \bar{k}x$, $\bar{k} < 0$, which transform the cascade (4.76)–(4.79) into the target system

$$\dot{\tilde{\theta}}(t) = -\bar{k}\tilde{\theta}(t) + \partial_x w(0,t), \tag{4.81}$$

$$\partial_t w(x,t) = \partial_{xx} w(x,t), \quad x \in (0,D), \tag{4.82}$$

$$w(0,t) = 0, \tag{4.83}$$

$$\partial_x w(D,t) = 0, \tag{4.84}$$

by noting $\dot{\tilde{\theta}}(t) = \dot{\hat{\theta}}(t)$ from (4.71). Taking the derivative of (4.80) with respect to x, setting $x = D$ in the resulting expression, and recalling (4.84), we derive the update law as

$$\begin{aligned}\dot{\hat{\Theta}}(t) &= -\bar{k}\tilde{\theta}(t) - \bar{k}\int_0^D u(r,t)dr, \\ &= -\bar{k}\tilde{\theta}(t) - \bar{k}\big(\hat{\Theta}(t) - \hat{\theta}(t)\big).\end{aligned} \tag{4.85}$$

In (4.85), we apply the property that $u(x,t) = \partial_t \bar{u}(x,t) = \partial_{xx}\bar{u}(x,t)$, and use (4.71), (4.72), and (4.75). However, (4.85) requires direct measurement of $\tilde{\theta}(t)$. As discussed in the text following (4.22), we can redesign (4.85) as follows

$$\dot{\hat{\Theta}}(t) = -kG(t) - k\hat{H}(t)\Big(\hat{\Theta}(t) - \theta(t) + e^{-\lambda t}a\sin(\omega t)\Big) \tag{4.86}$$

by recalling (4.57), using the feedback of $\theta(t)$, and choosing $\bar{k} = kH$ where $H > 0$ represents the unknown Hessian and $k > 0$ is the user-defined gain. The estimates $G(t)$, $\hat{H}(t)$, and η-dynamics

have the same form as in (4.11), (4.12) and (4.14), respectively. Additionally, the parameters should satisfy the following conditions

$$\lambda < \min\left\{\frac{\omega_h}{2}, \frac{\pi^2}{4D^2}\right\}, \qquad k > \frac{\lambda}{H}. \tag{4.87}$$

Using (4.14), (4.25), (4.57), (4.71)–(4.75), and (4.86), we write the following closed-loop error system

$$\tilde{\theta}(t) = \partial_x \bar{u}(0,t), \tag{4.88}$$

$$\partial_t \bar{u}(x,t) = \partial_{xx} \bar{u}(x,t), \tag{4.89}$$

$$\bar{u}(0,t) = 0, \tag{4.90}$$

$$\partial_x \bar{u}(D,t) = \tilde{\Theta}(t), \tag{4.91}$$

$$\dot{\tilde{\Theta}}(t) = -kG(t) - k\hat{H}(t)\big(\tilde{\Theta}(t) - \tilde{\theta}(t)\big), \tag{4.92}$$

$$\dot{\tilde{\eta}}(t) = -\omega_h \tilde{\eta}(t) + \omega_h \left(y(t) - y^*\right), \tag{4.93}$$

where $G(t)$ and $\hat{H}(t)$ are rewritten in the same form as (4.31) and (4.32), respectively. Using (4.57), (4.71), the output (4.56) is rewritten as

$$y(t) = y^* + \frac{H}{2}(\tilde{\theta}(t) + a\sin(\omega t))^2. \tag{4.94}$$

4.3.3 Stability analysis

The main theorem is stated as follows:

Theorem 4.2 *Let Assumption 1 hold and parameters satisfy* (4.87)*. Then, there exists* $\bar{\omega}$ *and for any* $\omega > \bar{\omega}$*, the closed-loop system* (4.88)–(4.93) *exponentially stable at the origin in the sense of the norm*

$$\left(||\bar{u}(\cdot,t)||^2 + |\tilde{\Theta}(t)|^2 + |\tilde{\eta}(t)|^2\right)^{1/2}. \tag{4.95}$$

Furthermore, the input $\theta(t)$ and output $y(t)$ exponentially converge to θ^* and y^*, respectively.

Proof Let us proceed through the proof step by step.

Step 1: State transformation. Let us consider the following transformations

$$\tilde{\theta}_f(t) = e^{\lambda t}\partial_x \bar{u}(0,t), \tag{4.96}$$

$$u_f(x,t) = e^{\lambda t}\bar{u}(x,t), \tag{4.97}$$

$$\tilde{\Theta}_f(t) = e^{\lambda t}\tilde{\Theta}(t), \tag{4.98}$$

$$\tilde{\eta}_f(t) = e^{2\lambda t}\tilde{\eta}(t), \tag{4.99}$$

which transform (4.88)–(4.93) to the following system

$$\tilde{\theta}_f(t) = \partial_x \bar{u}_f(0,t), \tag{4.100}$$

$$\partial_t \bar{u}_f(x,t) = \partial_{xx}\bar{u}_f(x,t) + \lambda u_f(x,t), \tag{4.101}$$

$$\bar{u}_f(0,t) = 0, \tag{4.102}$$

$$\partial_x \bar{u}_f(D,t) = \tilde{\Theta}_f(t), \tag{4.103}$$

$$\begin{aligned}\dot{\tilde{\Theta}}_f(t) = {} & \lambda\tilde{\theta}_f(t) - k\frac{2}{a}\sin(\omega t)\frac{H}{2}\left[\left(\tilde{\theta}_f(t) + a\sin(\omega t)\right)^2 - \tilde{\eta}_f(t)\right] - k\left(-\frac{8}{a^2}\cos(2\omega t)\right) \\ & \times \frac{H}{2}\left[\left(\tilde{\theta}_f(t) + a\sin(\omega t)\right)^2 - \tilde{\eta}_f(t)\right]\left(\tilde{\Theta}_f(t) - \tilde{\theta}_f(t)\right),\end{aligned} \tag{4.104}$$

$$\dot{\tilde{\eta}}_f(t) = -(\omega_h - 2\lambda)\tilde{\eta}_f(t) + \omega_h\frac{H}{2}\left[\tilde{\theta}_f(t) + a\sin(\omega t)\right]^2. \tag{4.105}$$

Step 2: Averaging operation. The average of the transformed system (4.100)–(4.105) over the period $\Pi = 2\pi/\omega$ is given by

$$\tilde{\theta}_f^{\mathrm{av}}(t) = \partial_x \bar{u}_f^{\mathrm{av}}(0,t), \tag{4.106}$$

$$\partial_t \bar{u}_f^{\mathrm{av}}(x,t) = \partial_{xx}\bar{u}_f^{\mathrm{av}}(x,t) + \lambda u_f^{\mathrm{av}}(x,t), \tag{4.107}$$

$$\bar{u}_f^{\mathrm{av}}(0,t) = 0, \tag{4.108}$$

$$\partial_x \bar{u}_f^{\text{av}}(D,t) = \tilde{\Theta}_f^{\text{av}}(t), \tag{4.109}$$

$$\dot{\tilde{\Theta}}_f^{\text{av}}(t) = -(kH-\lambda)\tilde{\Theta}_f^{\text{av}}(t), \tag{4.110}$$

$$\dot{\tilde{\eta}}_f^{\text{av}}(t) = -(\omega_h - 2\lambda)\tilde{\eta}_f^{\text{av}}(t) + \omega_h \frac{H}{2}\left((\tilde{\theta}_f^{\text{av}}(t))^2 + \frac{a^2}{2}\right), \tag{4.111}$$

where $\tilde{\theta}_f^{\text{av}}(t)$, $\bar{u}_f^{\text{av}}(\cdot,t)$, $\tilde{\Theta}_f^{\text{av}}(t)$, and $\tilde{\eta}_f^{\text{av}}(t)$ denote the average versions of the states $\tilde{\theta}_f(t)$, $\bar{u}_f(\cdot,t)$, $\tilde{\Theta}_f(t)$, and $\tilde{\eta}_f(t)$, respectively.

Step 3: Stability of average system. The solution to (4.110) is given by $\tilde{\Theta}_f^{\text{av}}(t) = \tilde{\Theta}_f^{\text{av}}(0)e^{-(kH-\lambda)t}$. Then, using the method of separation of variables, we obtain the exact solution to the reaction-diffusion equation (4.107)–(4.109) as

$$\begin{aligned}\bar{u}_f^{\text{av}}(x,t) = &\left(\frac{\tilde{\Theta}_f^{\text{av}}(0)}{\sqrt{kH}\cos(\sqrt{kH}D)}\right)\sin\left(\sqrt{kH}x\right)e^{-(kH-\lambda)t} + \sum_{n=1}^{\infty} e^{\left(\lambda - \frac{\pi^2(2n-1)^2}{4D^2}\right)t} \\ &\times \sin\left(\frac{\pi(2n-1)x}{2D}\right)M_n,\end{aligned} \tag{4.112}$$

where

$$M_n = \frac{1}{D}\int_0^{2D} \bar{u}_f^{\text{av}}(x,0)\sin\left(\frac{\pi(2n-1)x}{2D}\right)dx. \tag{4.113}$$

Thus, the $(\tilde{\Theta}_f^{\text{av}}, \bar{u}_f^{\text{av}})$-system is exponentially stable at the origin for $kH > \lambda$ and $\lambda < \frac{\pi^2}{4D^2}$. We establish the exponential convergence of $\tilde{\theta}_f^{\text{av}}(t)$ to zero recalling (4.106) and using (4.112). Using this fact, it is trivial to show that $\tilde{\eta}_f^{\text{av}}(t)$ of (4.111) exponentially converges to $\frac{\omega_h H a^2}{4(\omega_h - 2\lambda)}$ for $\omega_h > 2\lambda$.

Step 4: Invoking averaging theorem. Applying the averaging theorem [37], we establish that there exists $\bar{\omega}$ and for any $\omega > \bar{\omega}$, the transformed system (4.100)–(4.105) with states $(\bar{u}_f(\cdot,t), \tilde{\Theta}_f(t), \tilde{\eta}_f(t))$ has a unique exponentially stable periodic solution $(\bar{u}_f^{\Pi}(\cdot,t), \tilde{\Theta}_f^{\Pi}(t), \tilde{\eta}_f^{\Pi}(t))$

of period $\Pi = 2\pi/\omega$ and this solution satisfies

$$\left(||\bar{u}_f^{\Pi}(\cdot,t)||^2 + |\tilde{\Theta}_f^{\Pi}(t)|^2 + \left| \tilde{\eta}_f^{\Pi}(t) - \frac{\omega_h H a^2}{4(\omega_h - 2\lambda)} \right|^2 \right)^{\frac{1}{2}} \leq \mathscr{O}\left(\frac{1}{\omega}\right) \tag{4.114}$$

for all $t \geq 0$. Considering (4.114) and recalling the transformations (4.96)–(4.99), we deduce that the original error system (4.88)–(4.93) with states $\bar{u}(\cdot,t), \tilde{\Theta}(t), \tilde{\eta}(t)$ has a unique solution and is exponentially stable at the origin in the sense of the norm (4.95). In addition, $\tilde{\theta}(t) = \partial_x \bar{u}(0,t)$ exponentially converges to zero.

Step 5: Convergence to extremum. Taking into account the results in Step 4 and recalling from (4.57), (4.71) that

$$\theta(t) = e^{-\lambda t}\tilde{\theta}_f(t) + \theta^* + e^{-\lambda t} a \sin(\omega t), \tag{4.115}$$

we conclude the exponential convergence of $\theta(t)$ to θ^*. Then, we establish the convergence of the output $y(t)$ to y^* from (4.56) and complete the proof of Theorem 4.2. ■

4.4 Numerical Simulation

In this section, we perform a numerical simulation to evaluate the performance of the developed ES algorithms. We consider the following static quadratic map

$$Q(\theta) = 1 + (\theta - 2)^2. \tag{4.116}$$

In the first scenario, we examine a case where the map (4.116) is measured with a known delay of $D = 5$. We implement the delay-compensated uES (4.23) with parameters $k = 0.03, a = 0.8, \omega = 5, \omega_h = 1, \lambda = 0.04$. All initial conditions are set to zero. As illustrated in Fig. 4.3, the delay-compensated uES algorithm effectively compensates for the delay and ensures unbiased convergence of the input θ to its optimum value $\theta^* = 2$ exponentially at a rate

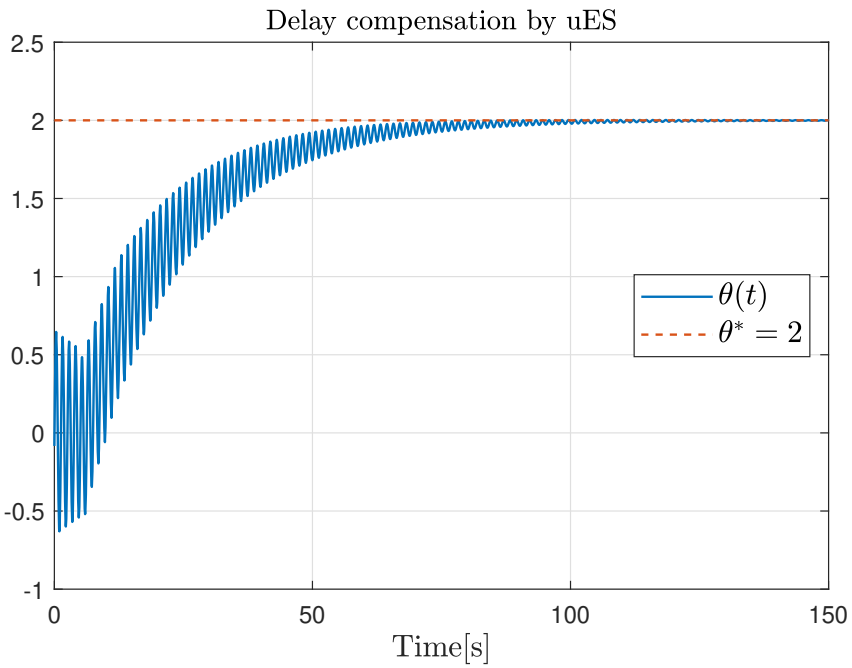

Figure 4.3. The trajectory of input θ resulting from the application of the delay-compensated uES (4.23) in the presence of a delay of $D = 5$ seconds.

of λ.

In the second scenario, we examine a case where the map (4.116) is coupled with a diffusion PDE (4.52)–(4.55), with $D = 1$. We employ the diffusion PDE-compensated uES (4.86) with parameters identical to those used in the delay-compensated design, and depict the result in Figure 4.4. Our approach effectively compensates for the diffusion PDE dynamics and achieves exponential convergence to the optimum $\theta^* = 2$.

4.5 Conclusion

Motivated by the need to address optimization challenges in complex physical systems described by PDEs, we introduce two distinct uES algorithms designed to handle PDE dynamics. One algorithm addresses arbitrarily long input-output delays, while the other deals with diffusion PDE input dynamics. Unlike existing designs that use constant amplitude dither signals, we use additive and multiplicative dither signals with exponentially decaying and growing amplitudes, respectively. By carefully adjusting the design parameters, we achieve unbiased convergence at

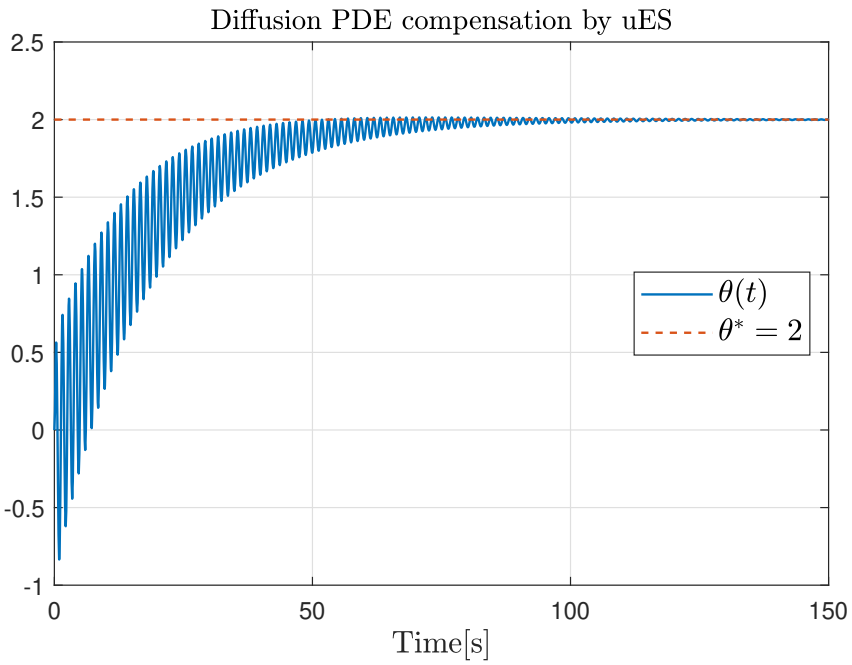

Figure 4.4. The trajectory of input θ resulting from the application of the diffusion PDE-compensated uES (4.86).

a user-defined exponential rate. A promising direction for future research would be to explore the application of this approach for seeking the critical heat flux in pool boiling systems.

4.6 Acknowledgment

Chapter 4 is a reprint of the material as it appears in:

- C. T. Yilmaz, M. Diagne, and M. Krstic, "Unbiased Extremum Seeking for PDEs", *IEEE Conference on Decision and Control (CDC)*, to appear, 2024.

The dissertation author was the primary investigator and author of this paper.

Chapter 5

Asymptotic, Exponential, and Prescribed-Time Unbiasing in Seeking of Time-Varying Extrema

Our "unbiased" extremum seeking (uES) algorithms developed in Chapter 3 ensure perfect convergence to the optimum at a user-assigned exponential rate, in spite of not using the Newton approach, or, more powerfully, within a user-prescribed time. Unlike classical approach, these algorithms use time-varying adaptation and controller gains, along with constant or time-varying probing frequencies (chirp signals). This chapter advances our earlier uES designs from strongly convex maps with static optima to a broader class of convex cost functions with time-varying optima diverging at arbitrary rates, even in finite time. This advancement first motivates the use of Lie bracket averaging instead of classical averaging due to the average system system, which doesn't necessarily need to be exponentially convergent, and the existence of non-periodic time-varying parameters; second, it necessitates the formulation of non-trivial and key feasibility conditions for the choice of time-varying design parameters and their decay/growth rates in relation to the convexity of the map and the divergence rate of optima. These conditions indicate that, for constant-frequency probing, the user-defined asymptotic rate of unbiasing is limited by the convexity of the map. However, this rate can be made arbitrarily fast (including asymptotic, exponential, and prescribed time) using chirpy probing, which requires sufficiently rapid frequency and adaptation growth to enable tracking of faster-diverging optima.

Furthermore, our uES methodology leverages state and time scaling techniques. State scaling involves scaling the state by an unboundedly growing function, while time scaling involves time dilation/contraction transformations. The practical stability of the state-scaled system in the dilated time domain is established through Lie bracket averaging, which provides unbiased and accelerated convergence of states to the optimum in the original time domain. In addition to numerical simulations of the designs, we experimentally test the feasibility of exponential uES for tuning the angular velocity of a unicycle to seek a static light source.

The structure of this chapter is as follows. Section 5.1 introduces fundamental stability concepts, which serve as references throughout the chapter. Section 5.2 outlines the problem formulation. Sections 5.3, 5.4, and 5.5 introduce designs for asymptotic, exponential and prescribed-time uES, along with formal stability analysis. Section 5.6 considers the problem of source seeking and presents the experimental results obtained. Finally, Section 5.7 concludes the chapter.

Notation. We denote the Euclidean norm by $|\cdot|$. The δ-neighborhood of a set $\mathscr{S} \subset \mathbb{R}^n$ is denoted by $U_\delta^{\mathscr{S}} = \{x \in \mathbb{R}^n : \inf_{e\in\mathscr{S}} |x-e| < \delta\}$. The Lie bracket of two vector fields $f, g : \mathbb{R}^n \times \mathbb{R} \to \mathbb{R}^n$ with $f(\cdot,t), g(\cdot,t)$ being continuously differentiable is defined by $[f,g](x,t) := \frac{\partial g(x,t)}{\partial x} f(x,t) - \frac{\partial f(x,t)}{\partial x} g(x,t)$. The notation e_i corresponds to the ith unit vector in $\mathbb{R}^n$. $\mathbb{R}^+$ denotes the set of non-negative real numbers. We denote the gradient of a function $h : \mathbb{R}^n \to \mathbb{R}$ by $\nabla h(x)$.

5.1 Preliminaries

5.1.1 Lie bracket averaging

Consider a control-affine system

$$\dot{x} = f_0(x,t) + \sum_{i=1}^{m} f_i(x,t)\sqrt{\omega}u_i(\omega t), \tag{5.1}$$

where $x(t_0) = x_0 \in \mathbb{R}^n$, $t_0 \in \mathbb{R}^+$, $\omega > 0$, $f_j \in \mathscr{C}^2 : \mathbb{R}^n \times \mathbb{R}^+ \to \mathbb{R}^n$ for $j = 0,\ldots,m$, and $u_i \in \mathscr{C}^1 : \mathbb{R}^+ \to \mathbb{R}$ for $i = 1,\ldots,m$. The functions u_i are T-periodic with some $T > 0$, and $\int_0^T u_i(\sigma)d\sigma = 0$

for $i = 1, \ldots, m$. We compute the Lie bracket system corresponding to (5.1) as follows

$$\dot{\bar{x}} = f_0(\bar{x}, t) + \frac{1}{T} \sum_{\substack{i=1 \\ j=i+1}}^{m} [f_i, f_j](\bar{x}, t) \int_0^T \int_0^{\vartheta} u_j(\vartheta) u_i(\sigma) \, d\sigma \, d\vartheta, \tag{5.2}$$

where $\bar{x}(t_0) = x(t_0)$. We make the following assumption regarding the boundedness of vector fields and their partial derivatives:

Assumption 5.1 *For every compact set $\mathscr{X} \subset \mathbb{R}^n$, $|f_i(x,t)|$, $\left|\frac{\partial f_i(x,t)}{\partial t}\right|$, $\left|\frac{\partial f_i(x,t)}{\partial x}\right|$, $\left|\frac{\partial^2 f_j(x,t)}{\partial t \partial x}\right|$, $\left|\frac{\partial [f_j, f_k](x,t)}{\partial t}\right|$, $\left|\frac{\partial [f_j, f_k](x,t)}{\partial x}\right|$ are bounded for all $x \in \mathscr{X}$, $t \geq t_0$, $i = 0, \ldots, m$, $j = 1, \ldots, m$, $k = j, \ldots, m$.*

To understand the relationship between the stability of (5.1) and (5.2), we revisit a theorem presented in [19]. Refer to Definition C.1 in Appendix C.2 for the formal definition of practical stability.

Theorem 5.1 ([19]) *Consider the system* (5.1) *under Assumption 5.1. If a compact set $\mathscr{S} \subset \mathbb{R}^n$ is locally (globally) uniformly asymptotically stable for* (5.2)*, then $\mathscr{S}$ is locally (semi-globally) practically uniformly asymptotically stable for* (5.1)*.*

5.1.2 Singularly perturbed Lie bracket averaging

Consider the system of the form

$$\dot{x} = \varepsilon f_0(x, z, \varepsilon t) + \varepsilon \sqrt{\omega} \sum_{i=1}^{m} f_i(x, z, \varepsilon t) u_i(\omega \varepsilon t), \tag{5.3}$$

$$\dot{z} = g(x, z), \tag{5.4}$$

with $x(t_0) = x_0 \in \mathbb{R}^n$, $z(t_0) = z_0 \in \mathbb{R}^m$, $t_0 \in \mathbb{R}^+$, $\varepsilon, \omega > 0$, $f_j \in \mathscr{C}^2 : \mathbb{R}^n \times \mathbb{R}^m \times \mathbb{R}^+ \to \mathbb{R}^n$ for $j = 0, \ldots, m$, and $u_i \in \mathscr{C}^1 : \mathbb{R}^+ \to \mathbb{R}$ for $i = 1, \ldots, m$. The functions u_i are T-periodic with some $T > 0$, and $\int_0^T u_i(\sigma) d\sigma = 0$ for $i = 1, \ldots, m$. To analyze stability, we first find the quasi-steady-state, denoted by $l(x)$, which satisfies $g(x, l(x)) = 0$. Performing the change of variables

$z_b = z - l(x)$, we get the boundary layer model as

$$\dot{z}_b = g(x, z_b + l(x)). \tag{5.5}$$

Then, by substituting the quasi-steady state into (5.3), we obtain a reduced model as

$$\dot{x}_r = \varepsilon f_0(x_r, l(x_r), \varepsilon t) + \varepsilon\sqrt{\omega}\sum_{i=1}^{m} f_i(x_r, l(x_r), \varepsilon t)u_i(\omega\varepsilon t), \tag{5.6}$$

in which the corresponding Lie bracket average, for $\varepsilon = 1$, is given by

$$\dot{\bar{x}}_r = f_0(\bar{x}_r, l(\bar{x}_r), t) + \frac{1}{T}\sum_{i=1}^{m}\sum_{j=i+1}^{m}[f_i, f_j](\bar{x}_r, l(\bar{x}_r), t)\int_0^T\int_0^{\vartheta} u_j(\vartheta)u_i(\sigma)d\sigma d\vartheta. \tag{5.7}$$

We make the following assumption, similar to Assumption 5.1:

Assumption 5.2 *For every compact sets $\mathscr{X} \subset \mathbb{R}^n$ and $\mathscr{Z} \subset \mathbb{R}^m$, $|f_i(x,z,t)|$, $\left|\frac{\partial f_i(x,z,t)}{\partial t}\right|$, $\left|\frac{\partial f_i(x,z,t)}{\partial x}\right|$, $\left|\frac{\partial f_i(x,z,t)}{\partial z}\right|$, $\left|\frac{\partial^2 f_j(x,z,t)}{\partial t \partial x}\right|$, $\left|\frac{\partial^2 f_j(x,z,t)}{\partial t \partial z}\right|$, $\left|\frac{\partial [f_j,f_k](x,z,t)}{\partial t}\right|$, $\left|\frac{\partial [f_j,f_k](x,z,t)}{\partial x}\right|$, $\left|\frac{\partial [f_j,f_k](x,z,t)}{\partial z}\right|$ are bounded for all $x \in \mathscr{X}$, $z \in \mathscr{Z}$, $t \geq t_0$, $i = 0, \ldots, m$, $j = 1, \ldots, m$, $k = j, \ldots, m$.*

We present the following theorem from [18] and provide the corresponding stability definition in Definition C.2 in Appendix C.2.

Theorem 5.2 ([18]) *Consider the system* (5.3) *and* (5.4) *under Assumption 5.2. Suppose that a compact set $\mathscr{S} \subset \mathbb{R}^n$ is globally uniformly asymptotically stable for the average of the reduced system* (5.7) *and the origin of the boundary layer model* (5.5) *is globally exponentially stable. Then, the set $\mathscr{S}$ is singularly semi-globally practically uniformly asymptotically stable for* (5.3).

5.2 Problem Statement

We consider the following optimization problem

$$\min_{\theta \in \mathbb{R}^n} J(\theta), \tag{5.8}$$

where $\theta \in \mathbb{R}^n$ is the input, $J \in \mathscr{C}^2 : \mathbb{R}^n \to \mathbb{R}$ is an unknown cost function. We make the following assumptions regarding the unknown static map $J(\cdot)$.

Assumption 5.3 *The cost function $J(\cdot)$ has a unique minimum at $\theta^*(t) \in \mathbb{R}^n$, i.e., $J(\theta^*(t)) < J(\theta)$ for $\forall \theta \neq \theta^*(t)$ with $\nabla J(\theta^*(t)) = 0$.*

Assumption 5.4 *There exist constants ρ_1, ρ_2, ρ_3, $\rho_4 > 0$ and $\kappa \in \mathbb{N}$ such that*

$$\rho_1 |\theta - \theta^*(t)|^{2\kappa} \leq J(\theta) - J(\theta^*(t)) \leq \rho_2 |\theta - \theta^*(t)|^{2\kappa}, \tag{5.9}$$

$$(\theta - \theta^*(t))^T \nabla J(\theta) \leq \rho_3 |\theta - \theta^*(t)|^{2\kappa}, \tag{5.10}$$

$$\left| \frac{\partial^2 J(\theta)}{\partial \theta^2} \right| \leq \rho_4 |\theta - \theta^*(t)|^{2\kappa - 2} \tag{5.11}$$

for all $\theta, \theta^*(t) \in \mathbb{R}^n$.

Assumption 5.5 *The derivatives of the time-varying optimizer $\theta^*(t)$ and the time-varying optimum $J(\theta^*(t))$ up to the second order obey the following bounds:*

$$|\dot{\theta}^*(t)| + |\ddot{\theta}^*(t)| \leq M_\theta \phi^c(t), \quad t \in [t_0, \infty), \tag{5.12}$$

$$\left|\dot{J}(\theta^*(t))\right| + \left|\ddot{J}(\theta^*(t))\right| \leq M_J \phi^d(t), \quad t \in [t_0, \infty), \tag{5.13}$$

with unknown constants $M_\theta, M_J \geq 0$, $c, d \in \mathbb{R}$, and a continuous strictly increasing function $\phi(t) : \mathbb{R}^+ \to \mathbb{R}$.

Assumption 5.3 guarantees the existence of a minimum of the function $J(\theta)$ at $\theta = \theta^*(t)$. Assumption 5.4 establishes bounds on the cost function $J(\theta)$, its gradient, and its Hessian. These bounds exhibit specific growth rates governed by power functions, similar to those exploited in [32] and [110]. For $\kappa = 1$, this simplifies to a more conservative assumption of strong convexity, which is considered in Chapter 3. For $\kappa > 1$, the assumption requires a specific class of convexity for $J(\theta)$. Assumption 5.5 imposes bounds on the growth or decay of the time-varying optimizer

and optimum, based on the parameters c and d. Note that this assumption encompasses scenarios where the optimum diverges asymptotically, exponentially, or even in finite time.

Using the first order condition of convexity [10, pp. 69], we obtain from (5.9) that

$$(\theta - \theta^*(t))^T \nabla J(\theta) \geq \rho_1 |\theta - \theta^*(t)|^{2\kappa}. \tag{5.14}$$

We measure the unknown function $J(\theta)$ in real time as

$$y(t) = J(\theta(t)), \qquad t \in [t_0, \infty), \tag{5.15}$$

in which $y \in \mathbb{R}$ is the output. Our aim is to design ES algorithms using output feedback $y(t)$ in order to achieve the unbiased convergence of θ to $\theta^*(t)$ while simultaneously minimizing the steady state value of y, without requiring prior knowledge of either the optimum input $\theta^*(t)$ or the function $J(\cdot)$.

In the subsequent sections, we present three types of unbiased ES algorithms: asymptotic uES, exponential uES, and prescribed-time uES. These algorithms aim to achieve the aforementioned objective asymptotically, exponentially, and in user-prescribed time. For visualization, Figures 5.1 and 5.2 depict the uES designs schematically. These figures illustrate constant-frequency probing and chirpy probing approaches, which can handle both convergent and divergent optimums. Further details on amplitude and gain functions can be found in Tables 5.1 and 5.2. It is important to note that our uES design modifies the alternative ES design [96], which can only ensure practical stability around the fixed optimum, by incorporating time-varying design parameters.

Remark 5.1 *In the unbiased ES designs depicted in Fig. 5.1, the gain $k_i\phi^r(t)$ experiences either asymptotic or exponential growth based on the chosen ES type, while the update rate $\phi^p(t)\sqrt{\alpha_i\omega_i}$ experiences asymptotic or exponential decay corresponding to the specific ES type. The crucial aspect of our designs is that the high-pass filtered state $y - \eta$ decays to zero at least as fast as*

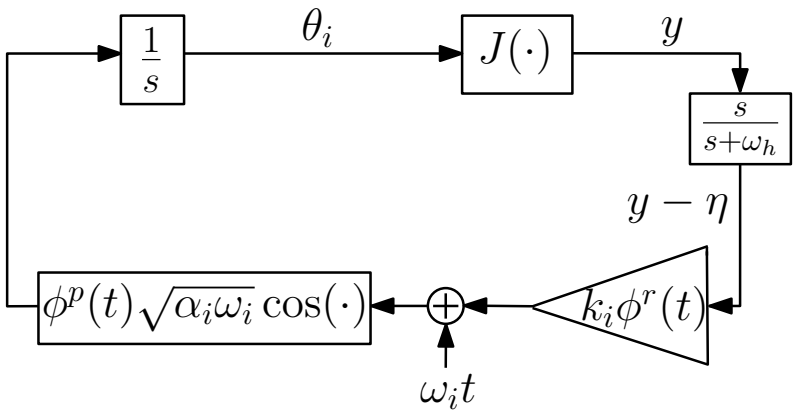

Figure 5.1. Unbiased ES scheme with constant-frequency probing for the ith element θ_i of θ, which guarantees $\theta \to \theta^*(t)$ at the rate that $1/\phi(t)$ converges to zero. Refer to Table 5.1 for the function and parameters.

Table 5.1. Time-varying functions used in Figure 5.1.

	$\phi(t)$	p	Conditions
Asymptotic uES	$(1+\beta\ (t-t_0))^{\frac{1}{v}}$	-1	$\kappa \geq 1$ $v > 2\kappa - r \geq 0$ $k_i, \alpha_i, \beta > 0$ $c < -1-2\kappa+r$ $d < -2\kappa$
Exponential uES	$e^{\lambda(t-t_0)}$	-1	$\kappa = 1$ $r = 2$ $k_i\alpha_i > 2\lambda/\rho_1$ $0 < \lambda < \omega_h/2$ $c < -1$ $d < -2$

the gain $k_i\phi^r(t)$ grows, ensuring the boundedness of the resulting signal. For a more detailed analysis, refer to Theorem 5.3 and 5.5.

Remark 5.2 *Another point that requires discussion is how parameters r and v influence the performance of asymptotic uES with constant-frequency probing in Fig. 5.1. The constraint on r is $r \leq 2\kappa$, as provided in Table 5.1. When κ is known, one can choose $r = 2\kappa$ and satisfy the condition $v > 2\kappa - r \geq 0$ with any arbitrarily small v. This makes the rate of growth of $\phi(t)$ faster, which in turn accelerates convergence. For a κ-blind user, the "safe" choice of r and v would be 2 and a sufficiently large value, respectively, compromising the rate of convergence.*

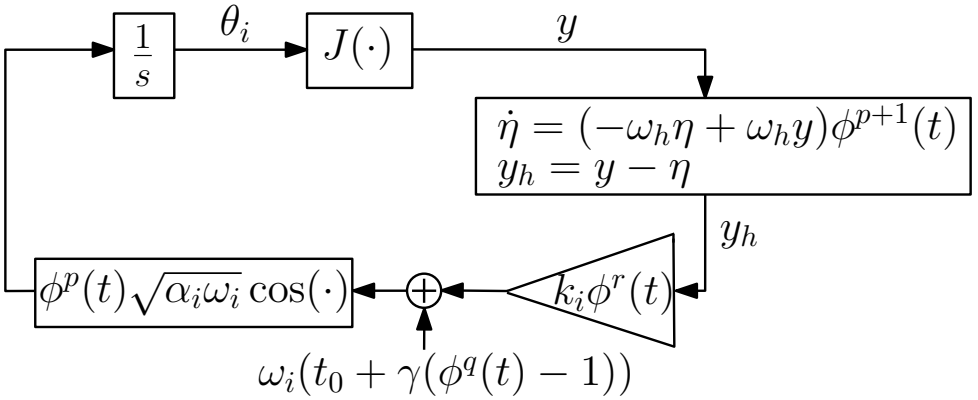

Figure 5.2. Unbiased ES scheme with chirpy probing for the ith element θ_i of θ, which guarantees $\theta \to \theta^*(t)$ at the rate that $1/\phi(t)$ converges to zero. Refer to Table 5.2 for the function and parameters.

Table 5.2. Time-varying functions used in Figure 5.2 with any $\beta, \lambda, v, \rho, k_i, \alpha_i > 0$ for $i = 1, \ldots, n$.

	$\phi(t)$	p	Conditions
Asymptotic uES	$(1+\beta\ (t-t_0))^{\frac{1}{v}}$	$q-v-1$	$\kappa \geq 1$ $q > 2\kappa - r \geq 0$ $\gamma = v/(\beta q)$ $c < p - 2\kappa + r$ $d < p - 2\kappa + 1$
Exponential uES	$e^{\lambda(t-t_0)}$	$q-1$	$\kappa \geq 1$ $q > 2\kappa - r \geq 0$ $\gamma = 1/(\lambda q)$ $c < p - 2\kappa + r$ $d < p - 2\kappa + 1$
Prescribed-time uES	$\left(\frac{T}{T+t_0-t}\right)^{\frac{1}{\rho}}$	$q+\rho-1$	$\kappa \geq 1$ $q > 2\kappa - r \geq 0$ $\gamma = \rho T/q$ $c < p - 2\kappa + r$ $d < p - 2\kappa + 1$

Remark 5.3 *The uES designs with chirpy probing in Table 5.2 relax the conditions on c and d in* (5.12) *and* (5.13)*, which characterize the rate of growth of optima. A divergent optimum with any growth rate can be tracked perfectly with a sufficiently large p, which determines the growth rate of the adaptation and frequency. In addition, compared to the exponential uES in Table 5.1, the exponential uES with chirp probing in Table 5.2 achieves convergence for any* $\kappa \geq 1$.

Remark 5.4 *In practical scenarios, the implementation of the developed algorithms might*

be limited by various factors. To mitigate this, the time-varying signal $\phi(t)$ along with the instantaneous frequency $\omega_i \gamma d\phi^q/dt$ in the case of chirped probing, can be constrained to moderately large values that are sufficient for close tracking of the extremum.

5.3 Asymptotic uES

5.3.1 Asymptotic uES with constant-frequency probing

We introduce an ES with asymptotic and unbiased convergence in the following theorem.

Theorem 5.3 *Consider the following asymptotic uES design*

$$\begin{cases} \dot{\theta} = \xi^{-1}(t) \sum_{i=1}^{n} \sqrt{\alpha_i \omega_i} e_i \cos\Big(\omega_i t + k_i \xi^r(t)(J(\theta) - \eta)\Big), \\ \dot{\eta} = -\omega_h \eta + \omega_h J(\theta), \end{cases} \tag{5.16}$$

with the asymptotically growing function

$$\xi(t) = (1 + \beta(t - t_0))^{\frac{1}{v}}, \qquad t \in [t_0, \infty). \tag{5.17}$$

Let $\omega_i = \omega\hat{\omega}_i$ such that $\hat{\omega}_i \neq \hat{\omega}_j \ \forall i \neq j$, $t_0 \geq 0$, $\alpha_i, k_i, \beta, \omega_h > 0 \ \forall i = 1, \ldots, n$ and $v > 2\kappa - r \geq 0$. Let Assumptions 5.3, 5.4 hold, and Assumption 5.5 hold with $\phi(t) = \xi(t)$, $c < -1 - 2\kappa + r$, $d < -2\kappa$. Then, there exists $\omega^* > 0$ such that for all $\omega > \omega^*$, the following holds

- *$\theta(t) \to \theta^*(t)$ semi-globally with respect to ω and asymptotically at the rate of $1/\xi(t)$, and there exist a class $\mathscr{KL}$ function $\mathscr{B}$, a class $\mathscr{K}$ function $\mathscr{Y}$, and a nonnegative constant $D(\theta(t_0), \theta^*(t_0), \eta(t_0))$ such that*

$$\begin{aligned} |\theta(t) - \theta^*(t)| \leq \xi^{-1}(t) \Big(& D + \mathscr{B}(|\theta(t_0) - \theta^*(t_0)|, t - t_0) \\ & + \sup_{t_0 \leq s \leq t} \mathscr{B}\left(\mathscr{Y}\left(\xi^{-1}(s)\right), t - s\right) \Big). \end{aligned} \tag{5.18}$$

- $\eta(t), y(t) \to J(\theta^*(t))$ *semi-globally with respect to* ω *and asymptotically at the rate of* $1/\xi^{2\kappa}(t)$.

Proof Let us proceed through the proof step by step.

Step 1: State transformation. Let us consider the following transformations

$$\theta_f = \xi(t)(\theta - \theta^*(t)), \tag{5.19}$$

$$\eta_f = \xi^{2\kappa}(t)(\eta - J(\theta^*(t))), \tag{5.20}$$

which transform (5.16) to

$$\begin{cases} \dot{\theta}_f = -\xi(t)\dot{\theta}^*(t) + \dfrac{\beta}{v}\xi^{-v}(t)\theta_f + \displaystyle\sum_{i=1}^{n}\sqrt{\alpha_i\omega_i}e_i\cos(\omega_i t + k_i\xi^r(t)\left(J_f(\theta_f,t) - \xi^{-2\kappa}(t)\eta_f\right)), \\ \dot{\eta}_f = \left(\dfrac{2\beta\kappa}{v}\xi^{-v}(t) - \omega_h\right)\eta_f + \omega_h\xi^{2\kappa}(t)J_f(\theta_f,t) - \xi^{2\kappa}(t)\dot{J}(\theta^*(t)), \end{cases} \tag{5.21}$$

with

$$J_f(\theta_f,t) = J(\theta_f/\xi(t) + \theta^*(t)) - J(\theta^*(t)). \tag{5.22}$$

The initial and most critical step in our analysis relies on transformations (5.19), (5.20). These establish a precondition: once we demonstrate the stability of the transformed system (5.21), the asymptotic convergence of θ to $\theta^*(t)$ and η to $J(\theta^*(t))$ naturally follows. To analyze the stability of (5.21), we employ the Lie bracket averaging technique. As a first step, we rewrite the θ_f-system in (5.21) by expanding the cosine term, as shown below

$$\begin{aligned} \dot{\theta}_f = &-\xi(t)\dot{\theta}^*(t) + \frac{\beta}{v}\xi^{-v}(t)\theta_f + \sum_{i=1}^{n}\sqrt{\alpha_i\omega_i}e_i\cos(\omega_i t)\cos\left(k_i\xi^r(t)\left(J_f(\theta_f,t) - \xi^{-2\kappa}(t)\eta_f\right)\right) \\ &- \sum_{i=1}^{n}\sqrt{\alpha_i\omega_i}e_i\sin(\omega_i t)\sin\left(k_i\xi^r(t)\left(J_f(\theta_f,t) - \xi^{-2\kappa}(t)\eta_f\right)\right). \end{aligned} \tag{5.23}$$

Next, we integrate the η_f-system from (5.21) with the transformed θ_f-system (5.23) to construct

the following system

$$\begin{bmatrix} \dot{\theta}_f \\ \dot{\eta}_f \end{bmatrix} = b_0(\theta_f, \eta_f, t) + \sum_{i=1}^{n} b_{c,i}(\theta_f, \eta_f, t)\sqrt{\omega_i}\cos(\omega_i t) - b_{s,i}(\theta_f, \eta_f, t)\sqrt{\omega_i}\sin(\omega_i t), \quad (5.24)$$

where

$$b_0(\theta_f, \eta_f, t) = \begin{bmatrix} -\xi(t)\dot{\theta}^*(t) + \frac{\beta}{v\xi^v(t)}\theta_f \\ \left(\frac{2\beta\kappa}{v\xi^v(t)} - \omega_h\right)\eta_f + \xi^{2\kappa}(t)\left(\omega_h J_f(\theta_f, t) - \dot{J}(\theta^*(t))\right) \end{bmatrix}, \quad (5.25)$$

$$b_{c,i}(\theta_f, \eta_f, t) = \begin{bmatrix} \sqrt{\alpha_i}e_i\cos\left(k_i\xi^r(t)\left(J_f(\theta_f, t) - \xi^{-2\kappa}(t)\eta_f\right)\right) \\ 0 \end{bmatrix}, \quad (5.26)$$

$$b_{s,i}(\theta_f, \eta_f, t) = \begin{bmatrix} \sqrt{\alpha_i}e_i\sin\left(k_i\xi^r(t)\left(J_f(\theta_f, t) - \xi^{-2\kappa}(t)\eta_f\right)\right) \\ 0 \end{bmatrix}. \quad (5.27)$$

Step 2: Feasibility analysis of (5.24) **for averaging.** To ensure the applicability of Lie bracket averaging, we need to verify that (5.24) satisfies the boundedness assumption outlined in Theorem 5.1. Towards this end, let $\mathscr{M} \subset \mathbb{R}^n$ and $\mathscr{Z} \subset \mathbb{R}$ be compact sets, and consider the bounds (5.9), (5.12), and (5.13). Then, we derive

$$\xi^{2\kappa}(t)|J_f(\theta_f, t)| \leq \rho_2|\theta_f|^{2\kappa}, \quad (5.28)$$

$$\xi^{2\kappa}(t)\left(|\dot{J}(\theta^*(t))| + |\ddot{J}(\theta^*(t))|\right) \leq M_J\xi^{d+2\kappa}(t), \quad (5.29)$$

$$\xi(t)\left(|\dot{\theta}^*(t)| + |\ddot{\theta}^*(t)|\right) \leq M_\theta\xi^{c+1}(t). \quad (5.30)$$

Note that $c+1<0$ due to $c<-1-2\kappa+r$ and $r\leq 2\kappa$, and also that $d+2\kappa<0$. Based the bounds (5.28)–(5.30), we establish the boundedness of $|b_0(\theta_f, \eta_f, t)|$, $|b_{c,i}(\theta_f, \eta_f, t)|$, and $|b_{s,i}(\theta_f, \eta_f, t)|$ for $(t, \theta_f, \eta_f) \in [t_0, \infty) \times \mathscr{M} \times \mathscr{Z}$. Noting from (5.19) that

$$\frac{d\theta}{d\theta_f} = \frac{1}{\xi(t)}, \quad (5.31)$$

and recalling the bounds in Assumption 5.4, we derive the following inequalities

$$\xi^{2\kappa}(t)\left|\frac{\partial J_f(\theta_f,t)}{\partial \theta_f}\right| = \xi^{2\kappa-1}(t)\left|\frac{\partial J(\theta)}{\partial \theta}\right| \leq \rho_3|\theta_f|^{2\kappa-1}, \tag{5.32}$$

$$\xi^{2\kappa}(t)\left|\frac{\partial^2 J_f(\theta_f,t)}{\partial \theta_f^2}\right| = \xi^{2\kappa-2}(t)\left|\frac{\partial^2 J(\theta)}{\partial \theta^2}\right| \leq \rho_4|\theta_f|^{2\kappa-2}, \tag{5.33}$$

$$\begin{aligned}\xi^{2\kappa}(t)\left|\frac{\partial J_f(\theta_f,t)}{\partial t}\right| &\leq \xi^{2\kappa}(t)\left(|\dot{J}(\theta^*(t))| + \left|\frac{\partial J(\theta)}{\partial \theta}\right|\left(|\theta_f|\frac{\dot{\xi}(t)}{\xi^2(t)} + |\dot{\theta}^*(t)|\right)\right),\\ &\leq M_J\xi^{d+2\kappa}(t) + \rho_3|\theta_f|^{2\kappa-1}(\beta\xi^{-v}(t)|\bar{\theta}_f|/v + M_\theta\xi^{1+c}(t)),\end{aligned} \tag{5.34}$$

$$\begin{aligned}\xi^{2\kappa}(t)\left|\frac{\partial^2 J_f(\theta_f,t)}{\partial \theta_f \partial t}\right| &= \xi^{2\kappa}(t)\left|\frac{\partial}{\partial t}\left(\frac{\partial J(\theta)}{\partial \theta}\frac{1}{\xi(t)}\right)\right|,\\ &\leq \xi^{2\kappa-1}(t)\left|\frac{\partial^2 J(\theta)}{\partial \theta^2}\right|\left(|\theta_f|\frac{\dot{\xi}(t)}{\xi^2(t)} + |\dot{\theta}^*(t)|\right) + \xi^{2\kappa}(t)\left|\frac{\partial J(\theta)}{\partial \theta}\right|\frac{\dot{\xi}(t)}{\xi^2(t)}\\ &\leq (\beta\rho_3/v)\xi^{-v}(t)|\theta_f|^{2\kappa-1} + \rho_4|\theta_f|^{2\kappa-2}(\beta\xi^{-v}(t)|\theta_f|/v + M_\theta\xi^{c+1}(t)),\end{aligned} \tag{5.35}$$

which are bounded for $(t,\theta_f,\eta_f) \in [t_0,\infty)\times\mathscr{M}\times\mathscr{Z}$. Considering the bounds (5.28)–(5.30), (5.32)–(5.35) and conditions in Table 5.1, we establish the boundedness of $\left|\frac{\partial b_0(\theta_f,\eta_f,t)}{\partial \theta_f}\right|$, $\left|\frac{\partial b_0(\theta_f,\eta_f,t)}{\partial \eta_f}\right|$, $\left|\frac{\partial b_0(\theta_f,\eta_f,t)}{\partial t}\right|$, $\left|\frac{\partial b_{c,i}(\theta_f,\eta_f,t)}{\partial \theta_f}\right|$, $\left|\frac{\partial b_{s,i}(\theta_f,\eta_f,t)}{\partial \theta_f}\right|$, $\left|\frac{\partial b_{c,i}(\theta_f,\eta_f,t)}{\partial \eta_f}\right|$, $\left|\frac{\partial b_{s,i}(\theta_f,\eta_f,t)}{\partial \eta_f}\right|$, $\left|\frac{\partial b_{c,i}(\theta_f,\eta_f,t)}{\partial t}\right|$, $\left|\frac{\partial b_{s,i}(\theta_f,\eta_f,t)}{\partial t}\right|$, $\left|\frac{\partial^2 b_{s,i}(\theta_f,\eta_f,t)}{\partial \theta_f \partial t}\right|$, $\left|\frac{\partial^2 b_{c,i}(\theta_f,\eta_f,t)}{\partial \theta_f \partial t}\right|$, $\left|\frac{\partial^2 b_{s,i}(\theta_f,\eta_f,t)}{\partial \eta_f \partial t}\right|$, and $\left|\frac{\partial^2 b_{c,i}(\theta_f,\eta_f,t)}{\partial \eta_f \partial t}\right|$ within the domain $(t,\theta_f,\eta_f) \in [t_0,\infty)\times\mathscr{M}\times\mathscr{Z}$. Next, we compute the following Lie bracket

$$\begin{aligned}\begin{bmatrix} b_{c,i}(\theta_f,\eta_f,t) & b_{s,i}(\theta_f,\eta_f,t)\end{bmatrix} &= k_i\sqrt{\alpha_i}\xi^r(t)\begin{bmatrix} e_i\frac{\partial J_f(\theta_f,t)}{\partial \theta_f}\cos(\rho) & -e_i\xi^{-2\kappa}(t)\cos(\rho)\\ 0 & 0\end{bmatrix}\\ &\quad\times b_{c,i}(\theta_f,\eta_f,t) + k_i\sqrt{\alpha_i}\xi^r(t)\\ &\quad\times\begin{bmatrix} e_i\frac{\partial J_f(\theta_f,t)}{\partial \theta_f}\sin(\rho) & -e_i\xi^{-2\kappa}(t)\sin(\rho)\\ 0 & 0\end{bmatrix} b_{s,i}(\theta_f,\eta_f,t),\\ &= k_i\alpha_i\xi^r(t)\begin{bmatrix} e_i\frac{\partial J_f(\theta_f,t)}{\partial \theta_{f,i}}\\ 0\end{bmatrix},\end{aligned} \tag{5.36}$$

where

$$\rho = k_i \xi^r(t) \left(J_f(\theta_f, t) - \xi^{-2\kappa}(t) \eta_f \right). \tag{5.37}$$

The boundedness of $\left| \frac{\partial [b_{c,i}(\theta_f, \eta_f, t), b_{s,i}(\theta_f, \eta_f, t)]}{\partial \theta_f} \right|$ and $\left| \frac{\partial [b_{c,i}(\theta_f, \eta_f, t), b_{s,i}(\theta, \eta_f, t)]}{\partial t} \right|$ for $r \leq 2\kappa$ in $(t, \theta_f, \eta_f) \in [t_0, \infty) \times \mathscr{M} \times \mathscr{Z}$ is established by recalling the bounds (5.32)–(5.35). Additionally, it should be noted that $\left| \frac{\partial [b_{c,i}(\theta_f, \eta_f, t), b_{s,i}(\theta_f, \eta_f, t)]}{\partial \eta_f} \right| = 0$. As a result, we fulfill the boundedness requirement for Lie bracket averaging.

Step 3: Lie bracket averaging. We derive the Lie bracket system for (5.24) as follows

$$\begin{bmatrix} \dot{\bar{\theta}}_f \\ \dot{\bar{\eta}}_f \end{bmatrix} = b_0(\bar{\theta}_f, \bar{\eta}_f, t) - \frac{1}{2} \sum_{i=1}^{n} \begin{bmatrix} b_{c,i}(\bar{\theta}_f, \bar{\eta}_f, t) & b_{s,i}(\bar{\theta}_f, \bar{\eta}_f, t) \end{bmatrix}. \tag{5.38}$$

Considering (5.25) and (5.36), we can express (5.38) as

$$\begin{cases} \dot{\bar{\theta}}_f = -\xi(t)\dot{\theta}^*(t) + \dfrac{\beta}{v} \xi^{-v}(t) \bar{\theta}_f - \displaystyle\sum_{i=1}^{n} \frac{k_i \alpha_i}{2} \xi^r(t) e_i \frac{\partial J_f(\bar{\theta}_f, t)}{\partial \bar{\theta}_{f,i}}, \\ \dot{\bar{\eta}}_f = \left(\dfrac{2\beta\kappa}{v} \xi^{-v}(t) - \omega_h \right) \bar{\eta}_f + \omega_h \xi^{2\kappa}(t) J_f(\bar{\theta}_f, t) - \xi^{2\kappa}(t) \dot{J}(\theta^*(t)). \end{cases} \tag{5.39}$$

Step 4: Stability of average system. Let us consider the following Lyapunov function

$$V(\bar{\theta}_f) = \frac{1}{2} |\bar{\theta}_f|^2. \tag{5.40}$$

Considering Assumption 5.4 and (5.14), we compute the time derivative of (5.40) along with (5.39) as

$$\begin{aligned} \dot{V} &\leq \xi(t) |\bar{\theta}_f| |\dot{\theta}^*(t)| + \frac{\beta}{v} \xi^{-v}(t) |\bar{\theta}_f|^2 - \sum_{i=1}^{n} \frac{k_i \alpha_i}{2} \xi^r(t) \bar{\theta}_{f,i} \frac{\partial J_f(\bar{\theta}_f, t)}{\partial \bar{\theta}_{f,i}}, \\ &\leq M_\theta \xi^{1+c}(t) |\bar{\theta}_f| + \frac{\beta}{v} \xi^{-v}(t) |\bar{\theta}_f|^2 - \frac{(k\alpha)_{\min} \rho_1}{2} \xi^{-2\kappa+r}(t) |\bar{\theta}_f|^{2\kappa}, \end{aligned} \tag{5.41}$$

where $(k\alpha)_{\min} = \min\{k_i\alpha_i\}$ for $i = 1,\dots,n$. However, (5.41) is not suitable for input-to-state stability (ISS) analysis presented in [49, Chapter 4.9] due to the asymptotically decaying signal in the third term. Nevertheless, the analysis can be performed in a different time domain. Let us define a new time domain as follows

$$\begin{aligned}\tau &= t_0 + \gamma\left(\xi^{-2\kappa+r+v}(t) - 1\right), \qquad \tau \in [t_0, \infty),\\ &= t_0 + \gamma\left(\left(1+\beta(t-t_0)\right)^{\frac{-2\kappa+r+v}{v}} - 1\right),\end{aligned} \tag{5.42}$$

where $\gamma = \frac{v}{\beta(-2\kappa+r+v)} > 0$. Then, we get

$$\frac{d\tau}{dt} = \left(1+\beta(t-t_0)\right)^{\frac{-2\kappa+r}{v}} = \xi^{-2\kappa+r}(t). \tag{5.43}$$

We rewrite (5.41) in the contracted time domain τ as follows

$$\frac{dV}{d\tau} \le \xi_\tau^{2\kappa-r}(\tau)|\bar{\theta}_f|\left(M_\theta \xi_\tau^{1+c}(\tau) + \frac{\beta}{v}\xi_\tau^{-v}(\tau)|\bar{\theta}_f|\right) - \frac{(k\alpha)_{\min}}{2}\rho_1|\bar{\theta}_f|^{2\kappa}, \tag{5.44}$$

where

$$\xi_\tau(\tau) = \left(1+(\tau-t_0)/\gamma\right)^{\frac{1}{-2\kappa+r+v}}. \tag{5.45}$$

For $\kappa = 1$, (5.44) results in

$$\frac{dV}{d\tau} \le -\left(\frac{(k\alpha)_{\min}\rho_1}{2} - \xi_\tau^{2-r-v}(\tau)\frac{2\beta}{v}\right)V, \quad \forall|\bar{\theta}_f| \ge \frac{2M_\theta\xi_\tau^{2-r+1+c}(\tau)}{(k\alpha)_{\min}\rho_1} =: \mathscr{Y}_1\left(\xi_\tau^{-1}(\tau)\right), \tag{5.46}$$

from which, by comparison principle, we derive

$$V(\tau) \le \xi_\tau^{\frac{2\beta\gamma}{v}}(\tau)e^{-\frac{(k\alpha)_{\min}\rho_1}{2}(\tau-t_0)}V(t_0), \qquad \forall|\bar{\theta}_f| \ge \mathscr{Y}_1\left(\xi_\tau^{-1}(\tau)\right). \tag{5.47}$$

Here, $\mathscr{Y}_1$ is a class $\mathscr{K}$ function. For $\kappa > 1$, we first apply Young's inequality to get

$$\frac{\beta}{v}|\bar{\theta}_f| \leq \frac{\varsigma^{2\kappa-1}}{2\kappa-1}|\bar{\theta}_f|^{2\kappa-1} + M_\varsigma, \tag{5.48}$$

where

$$M_\varsigma = \frac{2\kappa-2}{2\kappa-1}\left(\frac{\beta}{\varsigma v}\right)^{\frac{2\kappa-1}{2\kappa-2}} \tag{5.49}$$

with

$$\varsigma = \left((2\kappa-1)\frac{(k\alpha)_{\min}}{8}\rho_1\right)^{\frac{1}{2\kappa-1}}, \tag{5.50}$$

and rewrite (5.44) as

$$\begin{aligned}\frac{dV}{d\tau} &\leq -\frac{(k\alpha)_{\min}}{4}\rho_1|\bar{\theta}_f|^{2\kappa} - |\bar{\theta}_f|\left(\frac{(k\alpha)_{\min}}{8}\rho_1|\bar{\theta}_f|^{2\kappa-1} - \xi_\tau^{2\kappa-r+1+c}(\tau)M_\theta - \xi_\tau^{2\kappa-r-v}(\tau)M_\varsigma\right), \\ &\leq -\frac{(k\alpha)_{\min}}{4}\rho_1|\bar{\theta}_f|^{2\kappa},\end{aligned} \tag{5.51}$$

for all

$$\begin{aligned}|\bar{\theta}_f| &\geq \left(\frac{8\xi_\tau^{2\kappa-r}(\tau)}{(k\alpha)_{\min}\rho_1}\left(\xi_\tau^{1+c}(\tau)M_\theta + \xi_\tau^{-v}(\tau)M_\varsigma\right)\right)^{\frac{1}{2\kappa-1}} \\ &=: \mathscr{Y}_2\left(\xi_\tau^{-1}(\tau)\right).\end{aligned} \tag{5.52}$$

Note that $\mathscr{Y}_2$ is a class $\mathscr{K}$ function. Then, from (5.47) and (5.51), we establish the ISS of the $\bar{\theta}_f$-system for $\kappa \geq 1$ in τ-domain. Since $\xi_\tau^{2\kappa-r+1+c}(\tau)$ and $\xi_\tau^{2\kappa-r-v}(\tau)$ decay to zero due to the conditions $c+1+2\kappa-r<0$ and $2\kappa-r-v<0$, we prove the asymptotic convergence of $\bar{\theta}_f$ to zero in τ domain, and consequently, in t-domain. By exploiting the decaying nature of the inputs of the functions $\mathscr{Y}_1$ and $\mathscr{Y}_2$, we can characterize the "fading memory" ISS bound of $\bar{\theta}_f$ (see [30]

and [47]). Considering (5.46) and (5.51), the bound in the t-domain is given by

$$|\bar{\theta}_f(t)| \leq \mathscr{B}\left(|\bar{\theta}_f(t_0)|, t-t_0\right) + \sup_{t_0 \leq s \leq t} \mathscr{B}\left(\mathscr{Y}\left(\xi^{-1}(s)\right), t-s\right), \tag{5.53}$$

where $\mathscr{B}$ and $\mathscr{Y}$ are class $\mathscr{KL}$ and $\mathscr{K}$ functions, respectively, defined by

$$\mathscr{B}\left(|\bar{\theta}_f(t_0)|, t-t_0\right) = \begin{cases} p_0 e^{-p_1(\xi^{-2\kappa+r+\nu}(t)-1)}|\bar{\theta}_f(t_0)|, & \text{if } \kappa = 1, \\ \sqrt{2}(p_2 + p_3(\xi^{-2\kappa+r+\nu}(t)-1))^{\frac{1}{2-2\kappa}}, & \text{if } \kappa > 1, \end{cases} \tag{5.54}$$

and

$$\mathscr{Y}(s) = \begin{cases} \mathscr{Y}_1(s), & \text{if } \kappa = 1, \\ \mathscr{Y}_2(s), & \text{if } \kappa > 1, \end{cases} \tag{5.55}$$

with some $p_0 > 0$, $p_1 < (k\alpha)_{\min}\rho_1\gamma/4$, $p_2 = \left(|\bar{\theta}_f(t_0)|/2\right)^{1-\kappa}$, $p_3 = (k\alpha)_{\min}\rho_1\gamma(\kappa-1)/4$.

In addition to establishing the asymptotic stability of the $\bar{\theta}_f$-system, we also need to confirm the asymptotic stability of the $\bar{\eta}_f$-system in (5.39). We first examine the unforced system $\dot{\bar{\eta}}_f = \left(\frac{2\beta\kappa}{\nu\xi^{\nu}(t)} - \omega_h\right)\bar{\eta}_f$, which yields the following solution

$$\bar{\eta}_f(t) = \xi^{2\kappa}(t) e^{-\omega_h(t-t_0)}\bar{\eta}_f(t_0). \tag{5.56}$$

Therefore, the unforced system is exponentially stable at the origin. Furthermore, by revisiting the bound (5.28), we characterize an upper bound for the input of the $\bar{\eta}_f$-system in (5.39) as

$$|\omega_h\xi^{2\kappa}(t)J_f(\bar{\theta}_f, \xi(t)) - \xi^{2\kappa}(t)\dot{J}(\theta^*(t))| \leq \omega_h\rho_2|\theta_f|^{2\kappa} + M_J\xi^{d+2\kappa}(t). \tag{5.57}$$

Since $d < -2\kappa$ and $|\bar{\theta}_f| \to 0$, the $\bar{\eta}_f$-system is input-to-state stable and uniformly asymptotically stable at the origin.

Step 5: Lie bracket averaging theorem. Given the uniform asymptotic stability established for the averaged system in (5.39) in Step 4, we conclude from Theorem 5.1 that the origin of the transformed system (5.21) is practically uniformly asymptotically stable. The existence of ω^* and the role of ω are as defined in Definition C.1.

Step 6: Convergence to extremum. Considering the result in Step 5 and recalling from (5.17), (5.19) that

$$\theta = \theta^*(t) + \frac{1}{(1+\beta(t-t_0))^{\frac{1}{v}}}\theta_f, \tag{5.58}$$

we conclude the asymptotic convergence of $\theta(t)$ to $\theta^*(t)$ at the rate of $1/\xi(t)$. Considering the fading memory ISS bound (5.53), we can provide bound on the convergence error as follows

$$|\theta(t)-\theta^*(t)| \leq \xi^{-1}(t)\left(|\theta_f(t)-\bar{\theta}_f(t)|+|\bar{\theta}_f(t)|\right), \tag{5.59}$$

from which we conclude (5.18). The convergence of $\theta(t)$ to $\theta^*(t)$ implies the asymptotic convergence of the output $y(t)$ and the filtered state $\eta(t)$ to $J(\theta^*(t))$ at the rate of $1/\xi^{2\kappa}(t)$, based on (5.9), (5.19), (5.20), and thereby concludes the proof of Theorem 5.3. ■

5.3.2 Asymptotic uES with linearly-chirped probing

The following theorem presents an asymptotic ES design that employs a chirped probing signal, which grows asymptotically, in contrast to the constant probing in (5.16).

Theorem 5.4 *Consider the following asymptotic uES design*

$$\begin{cases} \dot{\theta} = \xi^{q-v-1}(t)\sum_{i=1}^{n}\sqrt{\alpha_i\omega_i}e_i\cos\Big(\omega_i(t_0+\gamma(\xi^q(t)-1))+k_i\xi^r(t)(J(\theta)-\eta)\Big), \\ \dot{\eta} = \left(-\omega_h\eta+\omega_h J(\theta)\right)\xi^{q-v}(t), \end{cases} \tag{5.60}$$

with the asymptotically growing function $\xi(t)$ defined by (5.17)*. Let $\omega_i = \omega\hat{\omega}_i$ such that $\hat{\omega}_i \neq \hat{\omega}_j$ $\forall i \neq j$, $t_0 \geq 0$, $\alpha_i, k_i, \beta, \omega_h > 0$ $\forall i = 1,\ldots,n$, $\gamma = v/(\beta q)$, and $q > 2\kappa - r \geq 0$. Let Assumptions*

5.3, 5.4 hold, and Assumption 5.5 hold with $\phi(t) = \xi(t)$, $c < q - v - 1 - 2\kappa + r$, $d < q - v - 2\kappa$. *Then, there exists* $\omega^* > 0$ *such that for all* $\omega > \omega^*$, *the input* $\theta(t) \to \theta^*(t)$ *semi-globally with respect to* ω *and asymptotically at the rate of* $1/\xi(t)$, *and there exist a class* $\mathscr{KL}$ *function* $\mathscr{B}$, *a class* $\mathscr{K}$ *function* $\mathscr{Y}$, *and a nonnegative constant* $D(\theta(t_0), \theta^*(t_0), \eta(t_0))$ *such that*

$$|\theta(t) - \theta^*(t)| \leq \xi^{-1}(t)\Big(D + \mathscr{B}\left(|\theta(t_0) - \theta^*(t_0)|, t - t_0\right) + \sup_{t_0 \leq s \leq t} \mathscr{B}\left(\mathscr{Y}\left(\xi^{-1}(s)\right), t - s\right)\Big). \tag{5.61}$$

Proof Refer to the proof of Theorem C.1 by choosing the parameters and satisfying conditions as in Table 5.2. ■

5.3.3 Numerical simulation

This subsection presents numerical results to illustrate the capabilities of the developed designs under two scenarios: a constant optimum and a diverging optimum.

Seeking constant θ^*

We consider the optimization problem (5.8) with the following nonlinear map

$$J(\theta) = 1 + (\theta - 2)^4. \tag{5.62}$$

Note that the function (5.62) has a unique minimum at $\theta^* = 2$ and satisfies Assumption 5.4 with $\kappa = 2$. To provide a basis for comparison, we use the classical ES introduced in [96]. Setting $\beta = 0$ in the asymptotic uES (5.16), our design simplifies to the classical approach. In all simulations, initial conditions are set to zero, and the oscillation frequency and high-pass filter frequency are set to $\omega = 5$ and $\omega_h = 3$, respectively.

In Figure 5.3a, we depict the trajectories of the classical ES with two distinct parameter sets. We observe that the classical ES with $k = 0.3$ and $\alpha = 1$ converges to a large neighborhood of the optimum due to the high α. To reduce the size of the steady-state oscillation, one might

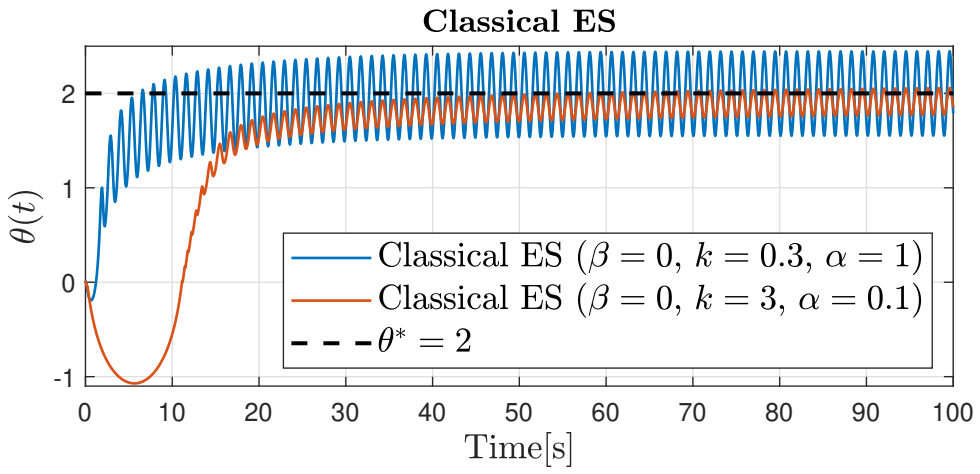

(a)

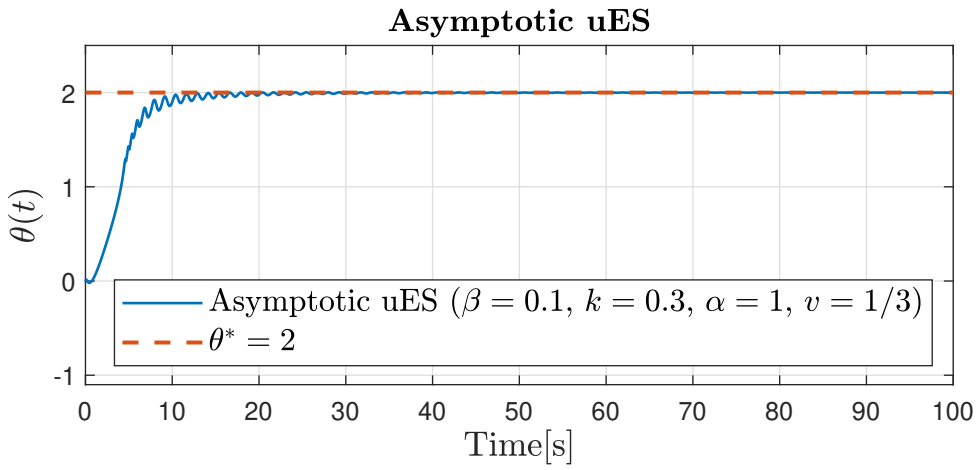

(b)

Figure 5.3. (a) The trajectories of the classical ES [96] with two distinct parameter sets. (b) The trajectory of the asymptotic uES (5.16) using constant frequency probing and achieving a convergence rate of $1/(1+0.1t)^3$.

consider decreasing α from 1 to 0.1, while simultaneously increasing the gain k from 0.3 to 3 to maintain the same convergence rate. However, as observed in Figure 5.3a, such adjustment leads to poorer transient performance, with an initial deviation in the opposite direction, despite the reduced oscillations at the steady state compared to one with higher amplitude. Our design, illustrated in Figure 5.3b, addresses this issue. We employ the asymptotic uES (5.16) with $\beta = 0.1$, $k = 0.3$, $\alpha = 1$, $v = 1/3$, $r = 4$. It starts with a high $\alpha = 1$ and low $k = 0.3$, and as $\xi(t)$ increases over time, the input settles to its optimum value with good transient performance. The

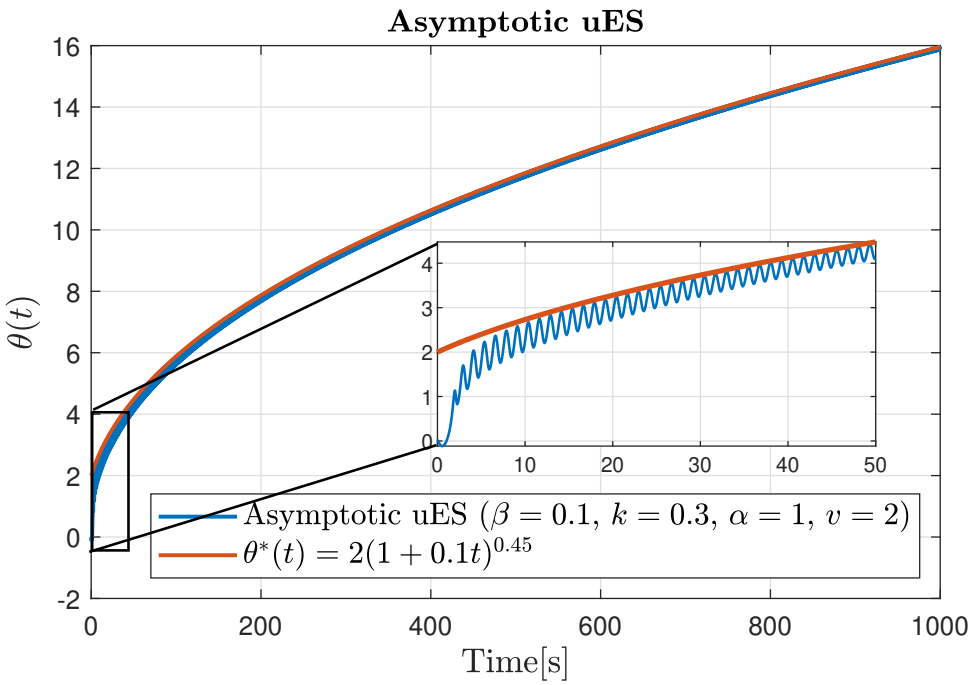

Figure 5.4. Perfect tracking of an asymptotically shifting optimum by asymptotic uES with constant-frequency probing (5.16). The convergence rate is $1/(1+0.1t)^{0.5}$.

chosen parameters ensure a convergence rate of $1/(1+0.1t)^3$.

Tracking divergent $\theta^*(t)$

We consider the following map where the optimum input $\theta^*(t)$ shifts from 2 to infinity

$$J(\theta) = 1 + \left(\theta - 2(1+0.1t)^{0.45}\right)^4. \tag{5.63}$$

The initial conditions and the parameters are same as in Fig. 5.3, except that the parameter v is increased from $1/3$ to $v = 2$ to make our design (5.16) capable of tracking a slowly shifting optimum. This adjustment slows the convergence rate to $1/(1+0.1t)^{0.5}$. Note that $\theta^*(t) = 2(1+0.1t)^{0.45} = 2\xi^{\frac{0.9}{2}}(t)$ satisfies (5.12) with $c = -1.1 < -1$. Fig. 5.4 illustrates the the performance of the design in terms of tracking a varying optimum.

5.4 Exponential uES

5.4.1 Exponential uES with constant-frequency probing

An ES design with unbiased and exponential convergence is presented in the following theorem.

Theorem 5.5 *Consider the following exponential uES design*

$$\begin{cases} \dot{\theta} = \zeta^{-1}(t)\sum_{i=1}^{n}\sqrt{\alpha_i\omega_i}e_i\cos\left(\omega_i t + k_i\zeta^2(t)(J(\theta)-\eta)\right), \\ \dot{\eta} = -\omega_h\eta + \omega_h J(\theta), \end{cases} \tag{5.64}$$

with the exponentially growing function

$$\zeta(t) = e^{\lambda(t-t_0)}, \quad \lambda > 0, \quad t \in [t_0,\infty). \tag{5.65}$$

Let $\omega_i = \omega\hat{\omega}_i$ such that $\hat{\omega}_i \neq \hat{\omega}_j$ $\forall i \neq j$, $t_0 \geq 0$, and $k_i\alpha_i > 2\lambda/\rho_1$, and $\omega_h > 2\lambda$ for all $i = 1,\ldots,n$. Let Assumptions 5.3, 5.4 hold with $\kappa = 1$, and Assumption 5.5 hold with $\phi(t) = \zeta(t)$, $c < -1, d < -2$. Then, there exists $\omega^* > 0$ such that for all $\omega > \omega^*$, the following holds

- *$\theta(t) \to \theta^*(t)$ semi-globally with respect to ω and exponentially at the rate of λ, and there exist a nonnegative constant $D(\theta(t_0),\theta^*(t_0),\eta(t_0))$ such that*

$$|\theta(t)-\theta^*(t)| \leq e^{-\lambda(t-t_0)}\left[e^{-\ell_0\ell_1(t-t_0)}|\theta(t_0)-\theta^*(t_0)| + \frac{M_\theta}{(1-\ell_0)\ell_1}e^{-\min\{\ell_0\ell_1,\ell_2\}(t-t_0)} + D\right] \tag{5.66}$$

for any $0 < \ell_0 < 1$ with

$$\ell_1 = (k\alpha)_{min}\rho_1/2 - \lambda > 0, \tag{5.67}$$

$$\ell_2 = -\lambda(c+1) > 0. \tag{5.68}$$

- $\eta(t), y(t) \to J(\theta^*(t))$ *semi-globally with respect to* ω *and exponentially at the rate of* 2λ.

Remark 5.5 *The design parameters* λ *and* $(k\alpha)_{min}$*, as well as the system parameters* M_θ*,* ρ_1*, and c, determine the size and decay rate of the bound* (5.66)*. Increasing* λ *accelerates the decay of the update gain and the growth of the controller gain in* (5.64)*, leading to a faster convergence rate for the bound* (5.66)*. The convergence rate* λ *can be made arbitrarily fast, provided that* $\lambda < (k\alpha)_{min}\rho_1/2$*. A large gain* $(k\alpha)_{min}$ *further contributes to a faster decay of the initial conditions and to the rate of expiration of the time-dependent term parameterized by* M_θ *if* $\ell_0\ell_1 < \ell_2$*, where* ℓ_2 *is an increasing function of c. The effect of the residual term D, which arises from the difference between the average and original state, diminishes exponentially at the rate of* λ*, independent of other parameters.*

Proof Let us proceed through the proof step by step.

Step 1: State transformation. Let us consider the following transformations

$$\theta_f = \zeta(t)(\theta - \theta^*(t)), \tag{5.69}$$

$$\eta_f = \zeta^2(t)(\eta - J(\theta^*(t))). \tag{5.70}$$

Using (5.69) and (5.70), we transform (5.64) to

$$\begin{cases} \dot{\theta}_f = -\zeta(t)\dot{\theta}^*(t) + \lambda\theta_f + \sum_{i=1}^{n}\sqrt{\alpha_i\omega_i}e_i\cos\Big(\omega_i t + k_i\zeta^2(t)\left(J_f(\theta_f,t) - \zeta^{-2}(t)\eta_f\right)\Big), \\ \dot{\eta}_f = (2\lambda - \omega_h)\eta_f + \omega_h\zeta^2(t)J_f(\theta_f,t) - \zeta^2(t)\dot{J}(\theta^*(t)), \end{cases} \tag{5.71}$$

with

$$J_f(\theta_f,t) = J(\theta_f/\zeta(t) + \theta^*(t)) - J(\theta^*(t)). \tag{5.72}$$

Step 2: Lie bracket averaging and stability analysis. The feasibility of the error system (5.71) for Lie bracket averaging can be verified analogously to Step 2 in the proof of Theorem

5.3. In contrast to (5.39), the average of (5.71) results in

$$\begin{cases} \dot{\bar{\theta}}_f = -\zeta(t)\dot{\theta}^*(t) + \lambda\bar{\theta}_f - \sum_{i=1}^{n} \dfrac{k_i\alpha_i}{2} e_i\zeta^2(t)\dfrac{\partial J_f(\bar{\theta}_f,t)}{\partial\bar{\theta}_{f,i}}, \\ \dot{\bar{\eta}}_f = (2\lambda-\omega_h)\bar{\eta}_f + \omega_h\zeta^2(t)J_f(\bar{\theta}_f,t) - \zeta^2(t)\dot{J}(\theta^*(t)). \end{cases} \tag{5.73}$$

Consider the following Lyapunov function

$$V = \frac{1}{2}|\bar{\theta}_f|^2. \tag{5.74}$$

Taking Assumption 5.4 into consideration and using (5.73), we compute the time derivative of (5.74) as

$$\begin{aligned} \dot{V} &\leq \zeta(t)|\bar{\theta}_f||\dot{\theta}^*(t)| + \lambda|\bar{\theta}_f|^2 - \sum_{i=1}^{n}\frac{k_i\alpha_i}{2}\zeta^2(t)\bar{\theta}_{f,i}\frac{\partial J_f(\bar{\theta}_f,t)}{\partial\bar{\theta}_{f,i}}, \\ &\leq M_\theta\zeta^{c+1}(t)|\bar{\theta}_f| - \left(\frac{(k\alpha)_{\min}\rho_1}{2} - \lambda\right)|\bar{\theta}_f|^2, \\ &\leq -\ell_0\ell_1|\bar{\theta}_f|^2, \qquad \forall|\bar{\theta}_f| \geq \frac{M_\theta\zeta^{c+1}(t)}{(1-\ell_0)\ell_1} =: \mathscr{Y}\left(\zeta^{-1}(t)\right), \end{aligned} \tag{5.75}$$

which establishes ISS of the $\bar{\theta}_f$-system for $k_i\alpha_i > 2\lambda/\rho_1$. In (5.75), $0 < \ell_0 < 1$, ℓ_1 is defined in (5.67), and $\mathscr{Y}$ is a class $\mathscr{K}$ function. Recalling $c < -1$, we prove the asymptotic convergence of $\bar{\theta}_f$ to zero. The corresponding fading memory ISS bound can be written as

$$|\bar{\theta}_f(t)| \leq \mathscr{B}\left(|\bar{\theta}_f(t_0)|, t-t_0\right) + \sup_{t_0\leq s\leq t}\mathscr{B}\left(\mathscr{Y}\left(\zeta^{-1}(s)\right), t-s\right) \tag{5.76}$$

with

$$\mathscr{B}\left(|\bar{\theta}_f(t_0)|, t-t_0\right) = e^{-\ell_0\ell_1(t-t_0)}|\bar{\theta}_f(t_0)|. \tag{5.77}$$

We can characterize the decay rate of the sup term in (5.76) using (5.65), (5.75) and (5.77) as

follows

$$\sup_{t_0\le s\le t}\mathscr{B}\left(\mathscr{Y}\left(\zeta^{-1}(s)\right),t-s\right)=\sup_{t_0\le s\le t}\frac{M_\theta e^{-\ell_0\ell_1(t-s)-\ell_2(s-t_0)}}{(1-\ell_0)\ell_1}$$
$$\le\frac{M_\theta e^{-\min\{\ell_0\ell_1,\ell_2\}(t-t_0)}}{(1-\ell_0)\ell_1} \tag{5.78}$$

with ℓ_2 as defined in (5.68), respectively. We note that $-\ell_0\ell_1(t-s)-\ell_2(s-t_0)<-\ell_0\ell_1(t-t_0)$ for $\ell_0\ell_1\le\ell_2$ and $-\ell_0\ell_1(t-s)-\ell_2(s-t_0)<-\ell_2(t-t_0)$ for $\ell_2\le\ell_0\ell_1$.

To establish the asymptotic stability of the $\bar{\eta}_f$-system, we analyze its unforced dynamics, governed by $\dot{\bar{\eta}}_f=(2\lambda-\omega_h)\bar{\eta}_f$. This system is exponentially stable at the origin for $\omega_h>2\lambda$. The input-to-state stability of the $\bar{\eta}_f$-system is established by noting from (5.9) that

$$\zeta^2(t)|\omega_h J_f(\bar{\theta}_f,\zeta(t))-\dot{J}(\theta^*(t))|\le\omega_h\rho_2|\bar{\theta}_f|^2+M_\theta\zeta^{d+2}(t). \tag{5.79}$$

Since $d<-2$, the asymptotic convergence of $\bar{\theta}_f$ results in the asymptotic convergence of $\bar{\eta}_f$ as well.

Step 3: Lie bracket averaging theorem. Given the uniform asymptotic stability established for the averaged system in (5.73) in Step 2, we conclude from Theorem 5.1 that the origin of the transformed system (5.71) is practically uniformly asymptotically stable. The existence of ω^* and the role of ω are as defined in Definition C.1.

Step 4: Convergence to extremum. Considering the result in Step 3 and recalling from (5.65), (5.69) that

$$\theta=\theta^*(t)+e^{-\lambda(t-t_0)}\theta_f, \tag{5.80}$$

we conclude the exponential convergence of $\theta(t)$ to $\theta^*(t)$ at the rate of λ. Recalling the ISS

bound (5.76), the bound on the convergence error is provided below

$$|\theta(t)-\theta^*(t)| \leq \zeta^{-1}(t)\left(|\theta_f(t)-\bar{\theta}_f(t)|+|\bar{\theta}_f(t)|\right), \tag{5.81}$$

from which we conclude (5.66). The convergence of $\theta(t)$ to $\theta^*(t)$ implies the exponential convergence of the output $y(t)$ and the filtered state $\eta(t)$ to $J(\theta^*(t))$ at the rate of 2λ, as evident from (5.9), (5.69), (5.70), and completes the proof of Theorem 5.5. ■

5.4.2 Exponential uES with exponentially-chirped probing

The following theorem presents an alternative design to (5.64) using an exponentially chirped probing signal.

Theorem 5.6 *Consider the following asymptotic uES design*

$$\begin{cases} \dot{\theta} = \zeta^{q-1}(t)\sum_{i=1}^{n}\sqrt{\alpha_i\omega_i}e_i\cos\Big(\omega_i(t_0+\gamma(\zeta^q(t)-1))+k_i\zeta^r(t)(J(\theta)-\eta)\Big), \\ \dot{\eta} = \left(-\omega_h\eta+\omega_h J(\theta)\right)\zeta^q(t), \end{cases} \tag{5.82}$$

with the exponentially growing function $\zeta(t)$ defined by (5.65)*. Let $\omega_i=\omega\hat{\omega}_i$ such that $\hat{\omega}_i\neq\hat{\omega}_j$ $\forall i\neq j$, $t_0\geq 0$, $\alpha_i,k_i,\beta,\omega_h>0$ $\forall i=1,\ldots,n$, $\gamma=1/(\lambda q)$, and $q>2\kappa-r\geq 0$. Let Assumptions 5.3, 5.4 hold, and Assumption 5.5 hold with $\phi(t)=\zeta(t)$, $c<q-1-2\kappa+r$, $d<q-2\kappa$. Then, there exists $\omega^*>0$ such that for all $\omega>\omega^*$, the input $\theta(t)\to\theta^*(t)$ semi-globally with respect to ω and exponentially at the rate of λ, and there exist a class $\mathscr{KL}$ function $\mathscr{B}$, a class $\mathscr{K}$ function $\mathscr{Y}$, and a nonnegative constant $D(\theta(t_0),\theta^*(t_0),\eta(t_0))$ such that*

$$|\theta(t)-\theta^*(t)| \leq \zeta^{-1}(t)\Big(D+\mathscr{B}\left(|\theta(t_0)-\theta^*(t_0)|,t-t_0\right)+\sup_{t_0\leq s\leq t}\mathscr{B}\left(\mathscr{Y}\left(\zeta^{-1}(s)\right),t-s\right)\Big). \tag{5.83}$$

Proof Refer to the proof of Theorem C.1 by choosing the parameters and satisfying conditions as in Table 5.2. ■

5.4.3 Numerical simulation

We consider a quadratic map of the form

$$J(\theta) = 1 + \left(\theta - 2e^{0.01t}\right)^2, \tag{5.84}$$

in which the optimum input $\theta^*(t) = 2e^{0.01t}$ diverges exponentially. We apply the exponential uES with chirped probing (5.82) by setting the parameters $\lambda = 0.1$, $k = 0.3$, $\omega = 1$, $\omega_h = 3$, $\alpha = 1$, $q = 1.2$, and $r = 2$. Note that $\theta^*(t) = 2\zeta^{0.1}(t)$ and $\kappa = 1$. Thus, the parameters c and q satisfy the conditions $q = 1.2 > 2\kappa - r = 0$ and $c = 0.1 < q - 1 - 2\kappa + r = 0.2$. We present the results in Fig. 5.5. As discussed in Remark 5.4, we terminate the growth of the signal $\zeta(t)$ and the instantaneous frequency, $\omega\gamma d\zeta^q/dt$, at $t = 40$ seconds, which is sufficient to track the optimum closely.

5.5 Prescribed-Time uES

We present the prescribed-time uES design in the following theorem, which offers the strongest result in terms of convergence speed and convergence error compared to the asymptotic and exponential designs.

Theorem 5.7 *Consider the following prescribed-time uES design*

$$\begin{cases} \dot{\theta} = \mu^{q+\rho-1}(t) \sum_{i=1}^{n} \sqrt{\alpha_i \omega_i} e_i \cos\Big(\omega_i(t_0 + \gamma(\mu^q(t) - 1)) + k_i \zeta^r(t)(J(\theta) - \eta)\Big), \\ \dot{\eta} = \left(-\omega_h \eta + \omega_h J(\theta)\right) \mu^{q+\rho}(t), \end{cases} \tag{5.85}$$

with the blow-up function

$$\mu(t) = \left(\frac{T}{T + t_0 - t}\right)^{\frac{1}{\rho}}, \qquad t \in [t_0, t_0 + T), \tag{5.86}$$

Let $\omega_i = \omega\hat{\omega}_i$ such that $\hat{\omega}_i \neq \hat{\omega}_j$ $\forall i \neq j$, $t_0 \geq 0$, $\alpha_i, k_i, \beta, \omega_h > 0$ $\forall i = 1, \ldots, n$, $\gamma = \rho T/q$, and

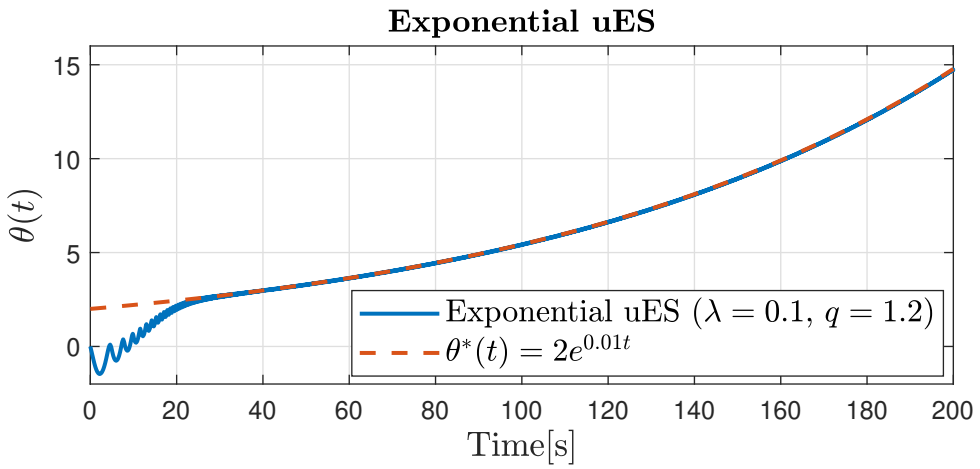

(a)

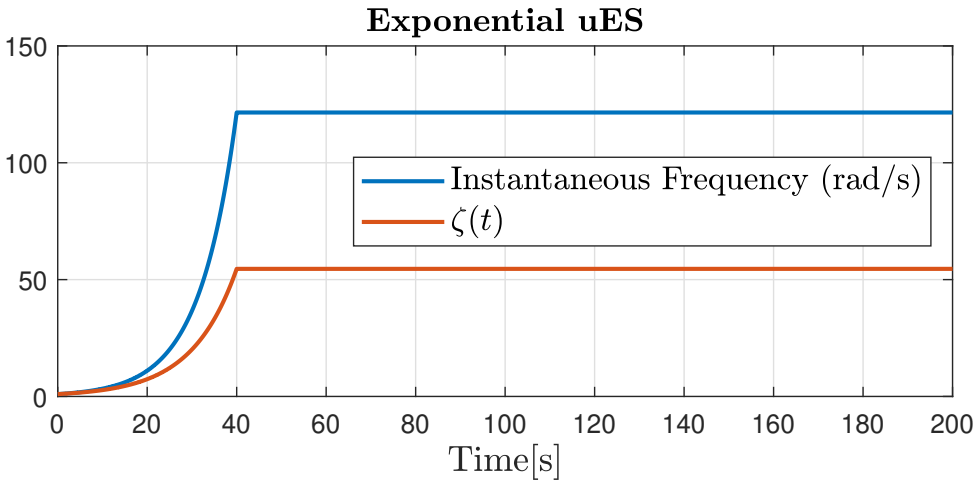

(b)

Figure 5.5. (a) Tracking of an exponentially shifting optimum by exponential uES with chirped probing (5.82). (b) Evolution of $\zeta(t)$ and the instantaneous frequency $\omega\gamma d\zeta^q/dt$, with their growth terminated at $t = 40$ seconds.

$q > 2\kappa - r \geq 0$. *Let Assumptions 5.3, 5.4 hold, and Assumption 5.5 hold with* $\phi(t) = \mu(t)$, $c < q + \rho - 1 - 2\kappa + r$, $d < q + \rho - 2\kappa$. *Then, there exists* $\omega^* > 0$ *such that for all* $\omega > \omega^*$, *the input* $\theta(t) \to \theta^*(t)$ *semi-globally with respect to* ω *and in prescribed-time* $t_0 + T$, *and there exist a class* $\mathscr{KL}$ *function* $\mathscr{B}$, *a class* $\mathscr{K}$ *function* $\mathscr{Y}$, *and a nonnegative constant*

$D(\theta(t_0), \theta^*(t_0), \eta(t_0))$ *such that*

$$|\theta(t) - \theta^*(t)| \leq \mu^{-1}(t)\Big(D + \mathscr{B}\left(|\theta(t_0) - \theta^*(t_0)|, t - t_0\right) + \sup_{t_0 \leq s \leq t} \mathscr{B}\left(\mathscr{Y}\left(\mu^{-1}(s)\right), t - s\right)\Big). \tag{5.87}$$

Proof Refer to the proof of Theorem C.1 by choosing the parameters and satisfying conditions as in Table 5.2. ■

Remark 5.6 *For strongly convex maps with* $\kappa = 1$ *and fixed optima, two alternative PT-uES designs are developed in Chapter 3. One design has a frequency that grows at a power-of-*μ *rate and an update rate that decays at an exp-of-power-of-*μ *rate. The other design has a frequency that grows at a log-of-*μ *rate and an update rate that decays at a power-of-*μ *rate. However, convex maps with* $\kappa \geq 1$ *and time-varying optima require a different design approach, as presented in* (5.85).

5.5.1 Numerical simulation

In this section, we return to the cost function (5.62), now aiming for convergence to θ^* within the time period of $T = 5$ seconds. We apply the prescribed-time uES (5.85) with two different parameter sets:

- In the first configuration, we use parameters $q = 0.01$, $\rho = 0.6$ $\alpha_1 = 1$, $\omega_1 = 10$, $\omega_h = 3$, and $k_1 = 0.1$. The motivation here is to demonstrate that the update law, $\dot{\theta}$, can be guaranteed to remain bounded by choosing $r = 2\kappa = 4$ and making $p = q + \rho - 1$ negative through small values of q and ρ.

- In the second configuration, we use parameters $q = 2.1$, $\rho = 2$, and the parameters $\alpha_1, \omega_1, \omega_h$, and k_1 are the same as in the first configuration. Opting for a "safe" $r = 2$ (as discussed in Remark 5.2) leads to a compromise on the boundedness of the update law. This is because the condition $q > 2\kappa - r = 2$ must be met, which forces $p = q + \rho - 1$

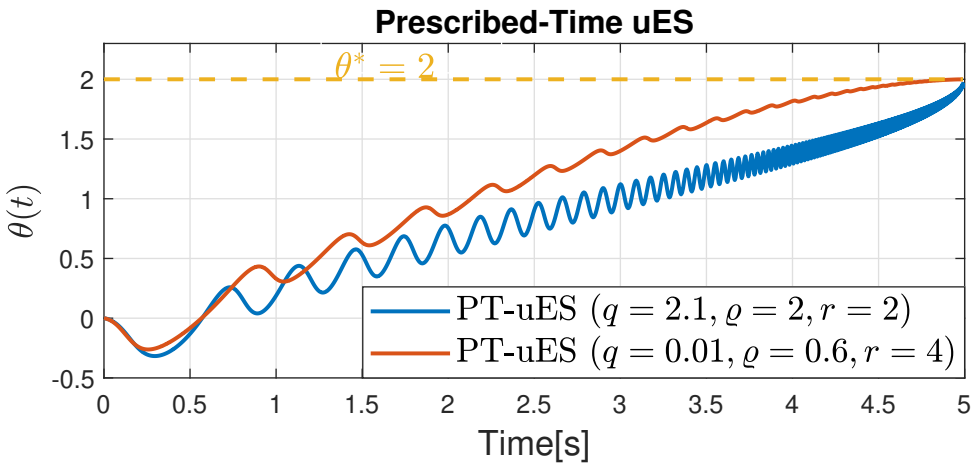

(a)

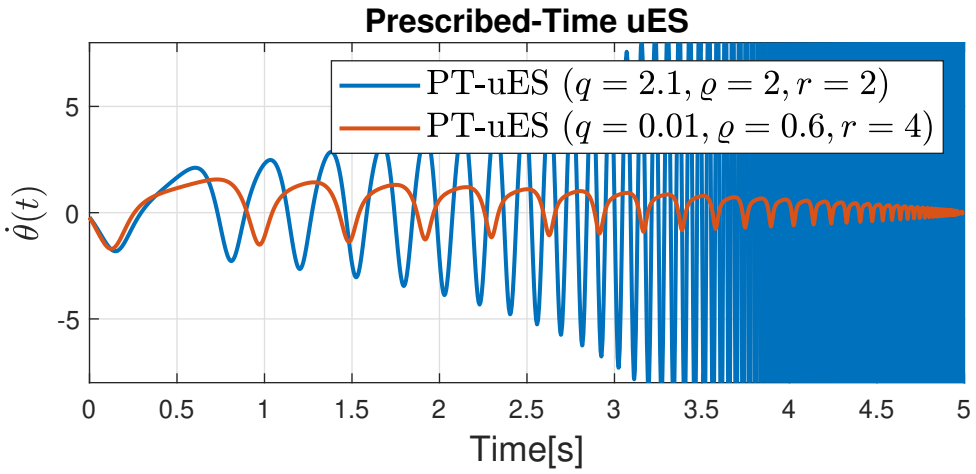

(b)

Figure 5.6. (a) Unbiased convergence to $\theta^* = 2$ in user-prescribed $T = 5$ seconds with two different parameter sets. (b) Evolution of their corresponding update laws.

to be positive. To mitigate the aggressive increase in frequency during the transient, a relatively high value of ρ is used compared to the first configuration.

We present the simulation results in Fig. 5.6, which illustrate the trade-off between the parameter sets. Both designs achieve prescribed-time convergence, but they differ in the growth rate of adaptation and frequency.

5.6 Unbiased Source Seeking by Unicycle

In this section, we investigate the problem of source localization by a unicycle in a two-dimensional plane modeled by

$$\dot{x} = u_1 \begin{bmatrix} \cos(\theta) \\ \sin(\theta) \end{bmatrix}, \tag{5.88}$$

$$\dot{\theta} = u_2, \tag{5.89}$$

where $x = \begin{bmatrix} x_1, & x_2 \end{bmatrix}^T \in \mathbb{R}^2$ denotes the coordinates of the vehicle's center with $x(0) = x_0$, $\theta \in \mathbb{R}$ is the orientation of the unicycle with $\theta(0) = \theta_0$, $u_1(t) \in \mathbb{R}$ and $u_2(t) \in \mathbb{R}$ are the forward and angular velocity inputs, respectively. For simplicity, but without loss of generality, we assume that $J(\cdot)$ is quadratic with diagonal Hessian matrix, i.e.,

$$J(x) = J^* - \frac{\rho_{x_1}}{2}(x_1 - x_1^*)^2 - \frac{\rho_{x_2}}{2}(x_2 - x_2^*)^2, \tag{5.90}$$

where $x^* = \begin{bmatrix} x_1^*, & x_2^* \end{bmatrix}^T \in \mathbb{R}^2$ is the unknown maximizer, $J^* = J(x^*) \in \mathbb{R}$ is the unknown maximum, and ρ_{x_1}, ρ_{x_2} are some unknown positive constants. Our aim is to design an unbiased source seeker that drives the vehicle to the exact position of the source, i.e. $x \to x^*$, exponentially at a user-defined rate of $\lambda > 0$.

The source seeker design follows similar steps to those of exponential uES with constant-frequency probing in Section 5.4.1, but a challenge arises because the angle θ is not directly controlled; instead, the angular velocity $\dot{\theta}$ is manipulated. This makes the system (5.88) and (5.89) compatible with (5.3) and (5.4) instead of (5.1), requiring singular perturbation analysis as another layer of the design.

5.6.1 Design and analysis

We design the inputs u_1 and u_2 in (5.88) and (5.89) such that

$$\dot{x} = e^{-\lambda t}\sqrt{\alpha\omega}\begin{bmatrix}\cos(\theta)\\ \sin(\theta)\end{bmatrix}, \tag{5.91}$$

$$\dot{\theta} = \omega - ke^{2\lambda t}(\eta + J(x)) \tag{5.92}$$

with a low-pass filter

$$\dot{\eta} = -\omega_h\eta - \omega_h J(x). \tag{5.93}$$

The parameters satisfy

$$k\alpha > \frac{2\lambda}{\rho_{x_i}}(\omega_h - 2\lambda), \quad \lambda < \frac{\omega_h}{2}, \quad i = 1,2. \tag{5.94}$$

We present the exponential convergence result for this source seeking problem as follows.

Theorem 5.8 *Consider the closed-loop system* (5.91)–(5.92) *with the parameters that satisfy* (5.94) *and with the cost function of the form* (5.90)*. Then, there exists* ω^* *such that for all* $\omega > \omega^*$ *there exists* $\omega_h^* > 0$ *such that for all* $\omega_h > \omega_h^* + 2\lambda$*,* $x(t)$ *semi-globally exponentially converges to* x^* *at the rate of* λ*.*

Proof Let us proceed through the proof step by step.

Step 1: State transformation. Let us consider the following transformations

$$x_f = e^{\lambda t}(x - x^*), \tag{5.95}$$

$$\eta_f = e^{2\lambda t}(\eta + J^*) \tag{5.96}$$

with

$$x_f = \begin{bmatrix} x_{1,f} & x_{2,f} \end{bmatrix}^T. \tag{5.97}$$

We write the transformed system using (5.91) and (5.93) as

$$\dot{x}_f = \begin{bmatrix} \lambda x_{1,f} + \sqrt{\alpha\omega}\cos(\theta) \\ \lambda x_{2,f} + \sqrt{\alpha\omega}\sin(\theta) \end{bmatrix}, \tag{5.98}$$

$$\dot{\theta} = \omega - k(\eta_f + J_f(x_f)), \tag{5.99}$$

$$\dot{\eta}_f = -(\omega_h - 2\lambda)\eta_f - \omega_h J_f(x_f), \tag{5.100}$$

where

$$J_f(x_f) = -\frac{\rho_{x_1}}{2}x_{1,f}^2 - \frac{\rho_{x_2}}{2}x_{2,f}^2. \tag{5.101}$$

In view of (5.100), θ-dynamics in (5.99) can be expressed as

$$\dot{\theta} = \omega + \frac{k}{\omega_h}\dot{\eta}_f - \frac{2k\lambda}{\omega_h}\eta_f. \tag{5.102}$$

Considering (5.102), let us perform the change of variables

$$\theta_e = \theta - \omega t - \frac{k}{\omega_h}\eta_f, \tag{5.103}$$

and rewrite (5.98) as

$$\dot{x}_f = \begin{bmatrix} \lambda x_{1,f} + \sqrt{\alpha\omega}\cos(\omega t + \check{k}\eta_f + \theta_e) \\ \lambda x_{2,f} + \sqrt{\alpha\omega}\sin(\omega t + \check{k}\eta_f + \theta_e) \end{bmatrix}, \tag{5.104}$$

$$\dot{\theta}_e = -2\check{k}\lambda\,\eta_f, \tag{5.105}$$

$$\dot{\eta}_f = -(\omega_h - 2\lambda)\eta_f - (\omega_h - 2\lambda)\check{J}_f(x_f), \tag{5.106}$$

where

$$\check{k} = k/\omega_h, \tag{5.107}$$

$$\check{J}_f(x_f) = -\frac{\check{\rho}_{x_1}}{2}x_{1,f}^2 - \frac{\check{\rho}_{x_2}}{2}x_{2,f}^2, \tag{5.108}$$

with

$$\check{\rho}_{x_i} = \rho_{x_i}\frac{\omega_h}{\omega_h - 2\lambda}, \quad i = 1,2. \tag{5.109}$$

Step 2: Singular perturbation analysis. In order to use the singular perturbation analysis outlined in Section 5.1.2, we consider a new time scale $t = \varepsilon\tau$, where $\varepsilon = 1/(\omega_h - 2\lambda)$. Then, using trigonometric identities, we rewrite (5.104)–(5.106) in τ-domain as

$$\frac{d}{d\tau}\begin{bmatrix} x_{1,f} \\ x_{2,f} \\ \theta_e \end{bmatrix} = \varepsilon\begin{bmatrix} \lambda x_{1,f} \\ \lambda x_{2,f} \\ -2\check{k}\lambda\eta_f \end{bmatrix} + \varepsilon\begin{bmatrix} \sqrt{\alpha\omega}\cos(\check{k}\eta_f + \theta_e) \\ \sqrt{\alpha\omega}\sin(\check{k}\eta_f + \theta_e) \\ 0 \end{bmatrix}\cos(\omega\varepsilon\tau) + \varepsilon\begin{bmatrix} -\sqrt{\alpha\omega}\sin(\check{k}\eta_f + \theta_e) \\ \sqrt{\alpha\omega}\cos(\check{k}\eta_f + \theta_e) \\ 0 \end{bmatrix} \times \sin(\omega\varepsilon\tau), \tag{5.110}$$

$$\frac{d\eta_f}{d\tau} = \underbrace{-\eta_f - \check{J}_f(x_f)}_{=g(x_f,\eta_f)}. \tag{5.111}$$

The quasi-steady-state is $\eta_f = -\check{J}_f(x_f)$. Defining $\eta_{f,b} = \eta_f - (-\check{J}_f(x_f))$, the boundary layer model for (5.111) is obtained es

$$\begin{aligned} \frac{d\eta_{f,b}}{d\tau} &= g(x_f, \eta_{f,b} - \check{J}_f(x_f)) \\ &= -\eta_{f,b}, \end{aligned} \tag{5.112}$$

which is globally exponentially stable. By substituting the quasi-steady state into (5.110), we obtain the reduced model as

$$\frac{d}{d\tau}\begin{bmatrix} x_{1,f,r} \\ x_{2,f,r} \\ \theta_{e,r} \end{bmatrix} = \varepsilon \begin{bmatrix} \lambda x_{1,f,r} \\ \lambda x_{2,f,r} \\ 2\check{k}\lambda \check{J}_f(x_{f,r}) \end{bmatrix} + \varepsilon \begin{bmatrix} \sqrt{\alpha}\cos(-\check{k}\check{J}_f(x_{f,r}) + \theta_{e,r}) \\ \sqrt{\alpha}\sin(-\check{k}\check{J}_f(x_{f,r}) + \theta_{e,r}) \\ 0 \end{bmatrix} \sqrt{\omega}\cos(\omega\varepsilon\tau)$$
$$+ \varepsilon \begin{bmatrix} -\sqrt{\alpha}\sin(-\check{k}\check{J}_f(x_{f,r}) + \theta_{e,r}) \\ \sqrt{\alpha}\cos(-\check{k}\check{J}_f(x_{f,r}) + \theta_{e,r}) \\ 0 \end{bmatrix} \sqrt{\omega}\sin(\omega\varepsilon\tau) \tag{5.113}$$

with $x_{f,r} = \begin{bmatrix} x_{1,f,r} & x_{2,f,r} \end{bmatrix}^T$.

Step 3: Lie bracket averaging and stability analysis. The Lie bracket average of the reduced system (5.113) is given by

$$\frac{d}{d\tau}\begin{bmatrix} \bar{x}_{1,f,r} \\ \bar{x}_{2,f,r} \\ \bar{\theta}_{e,r} \end{bmatrix} = \begin{bmatrix} (\lambda - \check{k}\alpha\check{\rho}_{x_1}/2)\bar{x}_{1,f,r} \\ (\lambda - \check{k}\alpha\check{\rho}_{x_2}/2)\bar{x}_{2,f,r} \\ 2\check{k}\lambda\check{J}_f(\bar{x}_{f,r}) \end{bmatrix}, \tag{5.114}$$

with $\bar{x}_{f,r} = \begin{bmatrix} \bar{x}_{1,f,r} & \bar{x}_{2,f,r} \end{bmatrix}^T$. We compute from (5.114) that

$$\bar{x}_{i,f,r}(\tau) = \bar{x}_{i,f,r}(0)e^{(\lambda - \check{k}\alpha\check{\rho}_{x_i}/2)\tau}, \quad i = 1,2, \tag{5.115}$$

$$\bar{\theta}_{e,r}(\tau) = \bar{\theta}_{e,r}(0) - \sum_{i=1}^{2} \frac{\check{k}\lambda\check{\rho}_{x_i}\bar{x}_{i,f,r}^2(0)}{2(\lambda - \check{k}\alpha\check{\rho}_{x_i}/2)}\left(e^{2(\lambda - \check{k}\alpha\check{\rho}_{x_i}/2)\tau} - 1\right). \tag{5.116}$$

Then, we conclude that $(\bar{x}_{1,f,r}, \bar{x}_{2,f,r}, \bar{\theta}_{e,r}) = (0,0,p_\theta) =: \Upsilon$, where $p_\theta = \bar{\theta}_{e,r}(0) + \sum_{i=1}^{2} \frac{\check{k}\lambda\check{\rho}_{x_i}\bar{x}_{i,f,r}^2(0)}{2(\lambda - \check{k}\alpha\check{\rho}_{x_i}/2)}$, of (5.114) is globally uniformly exponentially stable for $\check{k}\alpha > \frac{2\lambda}{\check{\rho}_{x_i}}$ for $i = 1,2$. This condition implies from (5.107) and (5.109) that (5.94) needs to be satisfied.

Step 4: Singularly perturbed Lie bracket averaging theorem. Combining the global

uniform exponential stability of (5.114) at Υ with the global exponential stability of the boundary layer system (5.112) at the origin, by Theorem 5.2, we prove the semi-global practical uniform asymptotic stability of (5.110) at Υ. The result holds for $\varepsilon < \varepsilon^*$ with some $\varepsilon^* > 0$, which implies $1/\varepsilon = \omega_h - 2\lambda > 1/\varepsilon^* =: \omega_h^*$. This simplifies to $\omega_h > \omega_h^* + 2\lambda$. The existence of ω^* and the role of ω are as defined in Definition C.2.

Step 5: Convergence to extremum. Considering the result in Step 4 and

$$x = e^{-\lambda t} x_f + x^*, \tag{5.117}$$

we conclude the semi-global exponential convergence of $x(t)$ to x^* at the rate of λ. This implies, from (5.90) and (5.96), the semi-global exponential convergence of the cost function $J(x(t))$ and the filtered state $-\eta(t)$ to $J(x^*)$ at the rate of 2λ. ■

5.6.2 Experimental results

We demonstrate the effectiveness of the exponential uES designed in (5.91)–(5.92) through a light-seeking experiment for proof-of-concept. Fig. 5.7a depicts the experimental setup, which includes a 750-lumen lamp positioned approximately 80 cm above the surface, and a TurtleBot3 unicycle robot starting about 112 cm from the center of maximum light intensity on the surface. The robot is equipped with a light sensor (Adafruit VEML7700) mounted on top. We placed the camera above, parallel to the surface, to capture a top-down view of the robot's motion and used Python's Open Computer Vision (OpenCV) library to visualize the robot's trajectory from the recorded videos.

The parameters in (5.91)–(5.93) are set to $\omega = 0.5, \omega_h = 7, k = 0.01, \alpha = 0.002, \lambda = 0.005$, resulting in an initial forward velocity of $u_1(0) = 0.1$ m/s and an angular velocity of $u_2(0) = 0.5$ rad/s, with $\eta(0) = -J(0)$. The initial position is approximately $x(0) = \begin{bmatrix} 1.5 & 1.5 \end{bmatrix}^T$ in meters. For a comparison, we implement classical ES with the same parameters except for $\lambda = 0$. The vehicle trajectories for both designs are shown in Fig. 5.7a, where the light intensity shifts from blue to red as it increases. We can see the enhancement of the convergence error

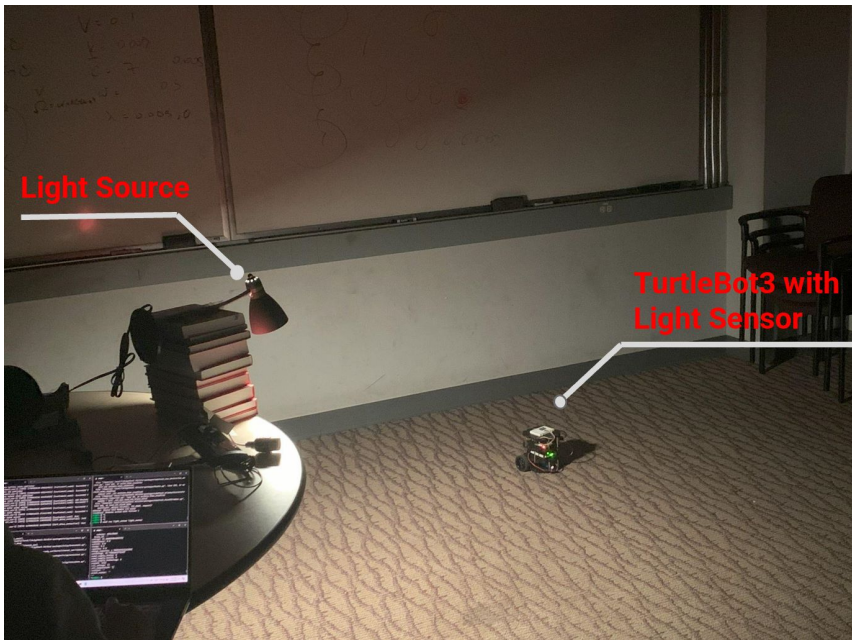

(a)

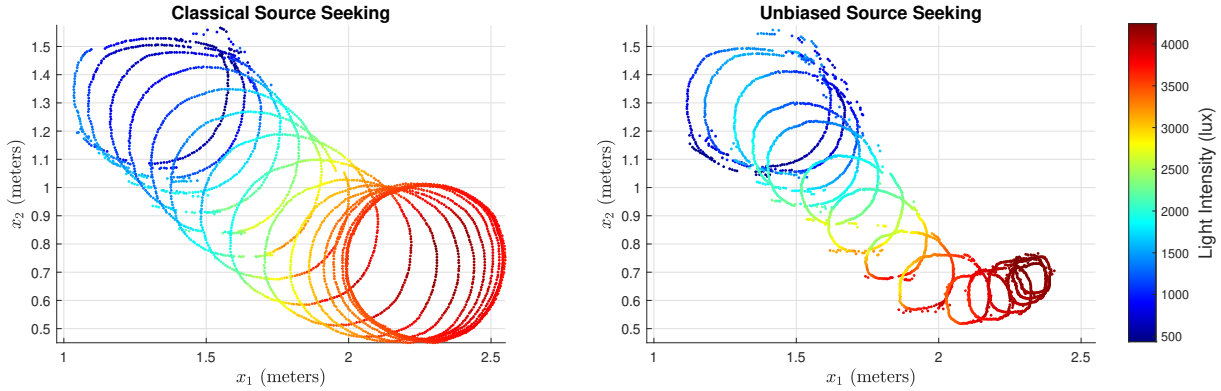

(b)

Figure 5.7. (a) Experimental setup consisting of a light source and a unicycle robot equipped with a light sensor on top. (b) The vehicle trajectory for two ES designs on a 2D plane, with color-coded light intensity in lux representing the intensity at each position.

with the developed design. The classical ES reaches an average light intensity of 3627 lux at steady state, while uES increases this value to 4179 lux, exceeding the classical ES by more than 15 percent. However, several practical limitations and challenges were encountered in this implementation. First, sensor noise significantly affects the light intensity readings, along with the limited resolution of the light sensor. Second, the spatial distribution of light intensity includes a relatively large region near the center of maximum intensity. These limitations constrain the

further reduction of the convergence error. Furthermore, the real-time implementation required careful fine-tuning of the design parameters, considering the robot's motion constraints.

For the classical ES design, reducing the size of the neighborhood around the optimum at steady state is possible by decreasing α in (5.91) and increasing k in (5.92) for the same convergence rate. However, a large k in (5.92) can result in a high initial angular velocity, exceeding the robot's speed limits and causing a large deviation from the current path. Our design addresses this issue with smooth transient behavior. A similar discussion is provided in Section 5.3.3 for Fig. 5.3.

5.7 Conclusion

There has been a long-standing interest in designing ES that can seek and track optima as closely and quickly as possible. We provide various ES designs that achieve unbiased seeking of fixed optima and perfect tracking of time-varying optima at any user-defined rate, including asymptotic, exponential, and in prescribed time. The optima can be static, decaying, or growing unbounded at any rate, including in finite time. These designs leverage methods known as state scaling and time scaling. In essence, these methods use the boundedness of the state-scaled state in a dilated time domain to guarantee convergence of the original system in the original time domain, resulting in accelerated and unbiased optimization. Numerical results are accompanied by experimental results on the problem of source seeking by a unicycle. Future work involves extending these results to achieve unbiased Nash equilibrium seeking.

5.8 Acknowledgment

We would like to thank Wenhan Tang, Max Lee, Eric Foss, and Sankalp Kaushik for their tremendous effort in conducting the experiments. Chapter 5 is a reprint of the material as it appears in:

- C. T. Yilmaz, M. Diagne, and M. Krstic, "Asymptotic, Exponential, and Prescribed-Time

Unbiasing in Seeking of Time-Varying Extrema", *IEEE Transactions on Automatic Control*, under review, 2024.

The dissertation author was the primary investigator and author of this paper.

Chapter 6

Adaptive Model-Free Disturbance Rejection for Continuum Robots

This chapter presents two model-free control strategies for the rejection of unknown disturbances in continuum robots. The strategies utilize a neural network-based approximation technique to estimate the uncertain Jacobian matrix using position measurements. The first strategy is designed for periodic disturbances and employs an adaptive model-free controller in conjunction with an adaptive disturbance observer. The second strategy is designed for robustness against arbitrary disturbances and employs time-varying input and update law gains that grow monotonically, resulting in the achievement of asymptotic, exponential, and prescribed-time reference trajectory tracking. The notion of fixed-time stabilization in prescribed time is particularly noteworthy, as it allows for the predefinition of a terminal time, independent of initial conditions and system parameters. A formal stability analysis is presented for each strategy, and the strategies are both tested experimentally with a concentric tube robot subject to unknown disturbances.

This chapter is organized as follows: Section 6.1 defines the problem. Section 6.2 introduces a neural network-based Jacobian estimation technique. Adaptive model-free control designs, both without and with a disturbance estimator, are presented in Sections 6.3 and 6.4, respectively. Accelerated robust adaptive model-free algorithms are detailed in Section 6.5. The effectiveness of the two control strategies is evaluated experimentally on a concentric tube robot

in Section 6.6, and the chapter concludes in Section 6.7.

Notation. Throughout the paper, we use the following notation: state/parameter estimation and estimation errors are denoted with the symbols " ˆ " and " ˜ ", respectively. As an example, estimation error of x state is $\tilde{x} = x - \hat{x}$ where $\hat{x}$ is the estimation of x. We denote the Euclidean norm by $\|\cdot\|$. trace$(\cdot)$ denotes the trace of a matrix. $\hat{J}^{\dagger}(u)$ denotes the pseudo inverse of the matrix $\hat{J}(u)$. The exponential function is denoted by exp.

6.1 Problem Statement

The kinematic equation of a continuum robot can be written as

$$x = f(u), \tag{6.1}$$

where $x \in \mathbb{R}^n$ denotes the position and orientation of the robot tip, $u \in \mathbb{R}^m$ denotes the input vector, and $m \geq n$. The time derivative of (6.1) is given by

$$\dot{x} = J(u)\dot{u}, \tag{6.2}$$

where $J(u) = \begin{bmatrix} J_1(u)^T & \dots & J_n(u)^T \end{bmatrix}^T \in \mathbb{R}^{n\times m}$ is the Jacobian matrix that defines the relationship between $\dot{x}$ and $\dot{u}$. Due to the physiological disturbances described in Section 1.2, continuum robots can experience unwanted fluctuations in tip position. Thus, robot tip position measurement, denoted as $y \in \mathbb{R}^n$, is expressed as a combination of the actual robot tip position x and the unknown disturbance $\delta = \begin{bmatrix} \delta_1 & \cdots & \delta_n \end{bmatrix}^T \in \mathbb{R}^n$, i.e.,

$$y(t) = x(t) + \delta(t). \tag{6.3}$$

Let us define the following error state

$$e(t) = y(t) - y^r(t), \tag{6.4}$$

where $y^r \in \mathbb{R}^n$ is the desired trajectory. Our objective is to design a neural-network-based estimator for the Jacobian of the uncertain forward kinematic function f, and to develop an adaptive model-free controller $\dot{u}$ that uses error feedback e. In order to reject the disturbance δ in the measurement, we develop two algorithms. The first algorithm is capable of estimating and rejecting harmonic disturbances with unknown periodicity, while the second algorithm is capable of rejecting any type of disturbance by achieving asymptotic, exponential, and prescribed-time convergence of the error state e to zero through the use of monotonically increasing gain functions. We make the following assumptions regarding the disturbance and reference trajectory.

Assumption 6.1 *Each element of the disturbance δ and their first derivative are bounded*

$$|\delta_i(t)| \leq \delta_i^{max}, \qquad |\dot{\delta}_i(t)| \leq \bar{\delta}_i^{max}, \qquad \forall t \in [0, \infty), \tag{6.5}$$

where the bounds are unknown.

Assumption 6.2 *The reference signal y^r and its first derivative are known and bounded.*

Assumption 6.1, asserting that $\delta(t)$ and $\dot{\delta}(t)$ exhibit finite energy, with unknown upper bounds, aligns with common practices in disturbance rejection strategies for continuum robots, as discussed in [27, 83].

6.2 Neural Network Based Jacobian Estimation

As suggested in [66], [76], by preserving the structure of (6.2), each element of the state derivative $\dot{x}$ can be approximated by a single-layer feedforward neural network over a compact

set $\mathbb{U}$ as

$$\dot{x}_i = (\Psi_i(u)^T W_i^*)\dot{u} + \varepsilon_i(\bar{u}), \qquad \forall \bar{u} \in \mathbb{U} \subset \mathbb{R}^{2m} \tag{6.6}$$

with $\bar{u} = \begin{bmatrix} u & \dot{u} \end{bmatrix}^T$ for $i = 1, \ldots, n$, where $\Psi_i(u) \in \mathbb{R}^{q \times 1}$ is the basis function vector, $\varepsilon_i(\bar{u}) \in \mathbb{R}$ is the approximation error, $q \in \mathbb{N}$ is the number of neurons, and $W_i^* \in \mathbb{R}^{q \times m}$ is the ideal constant weight matrix defined by

$$W_i^* = \arg \min_{W_i \in \mathbb{R}^{q \times m}} \left\{ \sup_{\bar{u} \in \mathbb{U}} \left| J_i(u)\dot{u} - (\Psi_i(u)^T W_i)\dot{u} \right| \right\}. \tag{6.7}$$

By the high-order Weierstrass approximation theorem [42], we define an upper bound for the approximation error ε_i over the defined compact region

$$|\varepsilon_i(\bar{u})| \leq \bar{\varepsilon}_i, \quad \forall i = 1, \ldots, n, \quad \forall \bar{u} \in \mathbb{U} \subset \mathbb{R}^{2m}, \tag{6.8}$$

where the bound $\bar{\varepsilon}_i \in \mathbb{R}^+$ is unknown. In addition, the approximation error ε_i for $i = 1, \ldots, n$ converges to zero as the number of basis functions n increases, i.e., $\varepsilon_i \to 0$ for $i = 1, \ldots, n$ as $n \to \infty$. The neural network structure is illustrated in Fig. 6.1.

Remark 6.1 *The neural network approximation technique requires the input space of the uncertain function to be a compact set, which makes the stability results semi-global [42]. In other words, the results are valid as long as $\bar{u}$ stays within $\mathbb{U}$. We can choose the set $\mathbb{U}$ to be arbitrarily large at the expense of a larger approximation error ε_i. Global results are obtained for the case in which* (6.8) *holds for all $\bar{u} \in \mathbb{R}^{2m}$.*

Remark 6.2 *It is important to note that approximating the state derivative in* (6.6) *by maintaining the structure of* (6.2) *is crucial for controller design and stability analysis. A naive approach that approximates the function $f(\cdot)$ in* (6.1) *and takes the time derivative of the approximation would cause the term $\nabla \varepsilon_i(u)\dot{u}$ to appear in* (6.6) *instead of $\varepsilon_i(\bar{u})$, which makes it difficult to*

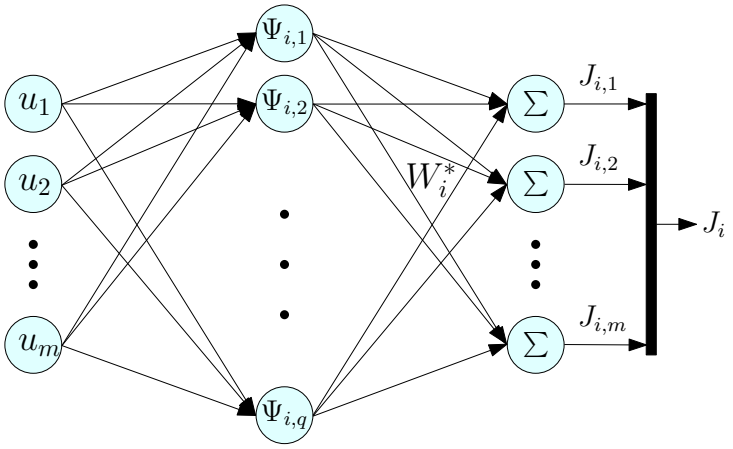

Figure 6.1. The structure of the neural network. The first layer consists of the input vector u, which is fed into basis functions Ψ_i at the middle layer. The output of this layer is multiplied by weights W_i^* and summed up at the third layer, which gives us an approximation of elements in each row of Jacobian matrix J_i for $i = 1, \ldots, n$.

design a controller and guarantee stability.

We therefore write the time derivative of (6.4) in view of (6.3) and (6.6) as follows

$$\dot{e} = \begin{bmatrix} \Psi_1(u)^T W_1^* \\ \vdots \\ \Psi_n(u)^T W_n^* \end{bmatrix} \dot{u} + \dot{\delta} - \dot{y}^r + \varepsilon, \tag{6.9}$$

where $\varepsilon = [\varepsilon_1 \quad \cdots \quad \varepsilon_n]^T$.

6.3 Adaptive Model-Free Control Design without Disturbance Estimator

In this section, we introduce a model-free adaptive controller that ignores the effect of the disturbance in (6.9) but still guarantees the boundedness of the closed-loop system. We state the following theorem that presents the designed controller with the update law and provide an ultimate bound for the closed-loop system.

Theorem 6.1 *Consider the closed-loop system consisting of* (6.9)*, the following controller*

$$\dot{u} = \hat{J}^{\dagger}(u)\left(-Ke + \dot{y}^{r}\right) \tag{6.10}$$

with the Jacobian estimate

$$\hat{J}(u) = \begin{bmatrix} \Psi_1(u)^T \hat{W}_1 \\ \vdots \\ \Psi_n(u)^T \hat{W}_n \end{bmatrix} \tag{6.11}$$

and the parameter update law

$$\dot{\hat{W}}_i = \Gamma_{w_i}\Psi_i(u)\dot{u}^T e_i - \Gamma_{w_i}\gamma_{w_i}\hat{W}_i, \qquad \forall i = 1,\ldots,n, \tag{6.12}$$

where $K = diag(k_1,\ldots,k_n)$, Γ_{w_i} are positive definite gain matrices, γ_{w_i} is a positive scalar gain. Under Assumptions 6.1-6.2, the signals $e_i, \tilde{W}_i$ for $i = 1,\ldots,n$ are uniformly ultimately bounded and each error state e_i converges to a compact set provided that the estimated Jacobian matrix (6.11) *is nonsingular. Moreover,*

$$|e_i(t)| \leq \exp^{-c_i t/2}\left(|e_i(0)| + \text{trace}\left(\tilde{W}_i(0)\Gamma_{w_i}^{-1}\tilde{W}_i^T(0)\right)^{\frac{1}{2}}\right) + \sqrt{2\frac{D_i}{c_i}} \tag{6.13}$$

for $i = 1,\ldots,n$, where

$$c_i = \min\left\{k_i, \frac{\gamma_{w_i}}{\lambda_{max}(\Gamma_{w_i}^{-1})}\right\}, \tag{6.14}$$

$$D_i = \frac{1}{k_i}\bar{\varepsilon}_i^2 + \frac{1}{k_i}(\bar{\delta}_i^{max})^2 + \frac{\gamma_{w_i}}{2}\text{trace}\left(W_i^*(W_i^*)^T\right). \tag{6.15}$$

The proof of this result is given in Appendix D.2.

Remark 6.3 *The stability result presented in Theorem 6.1 and other results presented throughout*

this chapter are based on the assumption that the neural network Jacobian estimation $\hat{J}(u)$ with the updated weights is nonsingular. This assumption is common in many papers (see [111, 108, 66, 76, 13, 121]) that develop algorithms that require the existence of the Jacobian estimation during the implementation of the controller. While some suitable parameter projection algorithms that prevent this singularity condition have been introduced in [11, 14], it remains an open problem.

Remark 6.4 *It is well known that online update laws help the system adapt to changing environments and achieve the desired control objectives. However, poor initial values for the estimated weight matrices $\hat{W}_i \in \mathbb{R}^{q\times m}$ can degrade the transient performance of the closed-loop system. To mitigate this issue, the weights can be trained offline using the following state observer in an environment without external disturbances before implementing the controller online,*

$$\dot{\hat{x}} = \begin{bmatrix} \Psi_1(u)^T \hat{W}_1 \\ \vdots \\ \Psi_n(u)^T \hat{W}_n \end{bmatrix} \dot{u} + F_x(x-\hat{x}) \tag{6.16}$$

with the learning law

$$\dot{\hat{W}}_i = \Gamma_{w_i}\Psi_i(u)\dot{u}^T(x-\hat{x}) - \Gamma_{w_i}\gamma_{w_i}\hat{W}_i, \quad \forall i = 1,\ldots,n, \tag{6.17}$$

where $\hat{x}$ is the estimate of x, $F_x \in \mathbb{R}^{n\times n}$ is a positive definite matrix. As highlighted in the Introduction, the adaptation of weight matrices W_i and the estimation of the Jacobian matrix $J(u)$ rely on state feedback x. Note that the leakage term $-\Gamma_{w_i}\gamma_{w_i}\hat{W}_i$ is integrated into our update laws (6.12) *and* (6.17) *to avoid the parameter drift arising from model inaccuracies and unmodeled disturbances [45]. This technique is widely adopted in the adaptation of weight matrices of neural networks [20]. Note also that the minimal $\tilde{W}_i$ at the initial time enhances the transient performance of the closed-loop system, as indicated in* (6.13)*. To further minimize the ultimate*

bound of the error signal, it is crucial to simultaneously reject disturbances and learn the weight matrices online.

6.4 Adaptive Model-Free Control Design with Disturbance Estimator

In this section, we consider the case in which each element of the unknown disturbance vector $\delta(t) \in \mathbb{R}^n$ is a continuous periodic signal. We develop a control strategy that estimates the fundamental frequency using a cascade of low-pass and high-pass filters, along with a parameter update law in an offline setting. The disturbance is then compensated for by adding a reduplicated model of an exosystem consisting of a finite number of estimated harmonics to the feedback loop. We make the following assumption regarding the structure of the disturbance vector $\delta(t)$.

Assumption 6.3 *Each element of the unknown disturbance vector $\delta(t) \in \mathbb{R}^n$ is a continuous periodic signal. For simplicity, but without loss of generality, we assume that each element of the disturbance vector $\delta(t) \in \mathbb{R}^n$ is identical (i.e., $\delta_1(t) = \cdots = \delta_n(t)$ for all $t \geq 0$) and can be represented by its Fourier series expansion*

$$\delta_1(t) = a_0 + \sum_{k=1}^{\infty} \left[a_k \cos(k\omega t) + b_k \sin(k\omega t)\right] \tag{6.18}$$

in which the fundamental frequency $\omega \in \mathbb{R}$, the bias $a_0 \in \mathbb{R}$ and the amplitudes $a_k, b_k \in \mathbb{R}$, $k \in \mathbb{N}$ are unknown. The amplitude of the first harmonics is nonzero, i.e., $\sqrt{a_1^2 + b_1^2} > 0$.

6.4.1 Offline frequency estimation

In offline mode, where the controller is deactivated, the output measurement is written as follows

$$\begin{aligned} y_j(t) &= x_j + \delta_1(t), \qquad j = 1, \ldots, n, \\ &= x_j + a_0 + \bar{a}_1 \sin(\omega t + \bar{\varphi}) + \delta_{1,h}(t), \end{aligned} \tag{6.19}$$

where $\bar{a}_1 = \sqrt{a_1^2 + b_1^2}$, $\bar{\varphi} = \arctan(a_1/b_1)$ and $\delta_{1,h}(t)$ contains the high frequency components as follows

$$\delta_{1,h}(t) = \sum_{k=2}^{\infty} \left[a_k \cos(k\omega t) + b_k \sin(k\omega t) \right]. \tag{6.20}$$

In order to attenuate the higher order harmonics (6.20) and detect the fundamental frequency, we design the following filters, which are inspired by [78]:

$$y_f = y_\eta + B_y y_j, \qquad j = 1, \ldots, n, \tag{6.21}$$

$$\dot{y}_\eta = A_y (y_\eta + B_y y_j), \tag{6.22}$$

with the matrices $A_y \in \mathbb{R}^{p \times p}, B_y \in \mathbb{R}^p$, $p \geq 3$, defined by

$$A_y = \begin{bmatrix} -\lambda_f & \lambda_f & 0 & \cdots & 0 \\ 0 & -\lambda_f & \lambda_f & \ddots & 0 \\ \vdots & \ddots & \ddots & \ddots & \vdots \\ \vdots & \ddots & \ddots & -\lambda_f & \lambda_f \\ 0 & \cdots & \cdots & 0 & -\lambda_f \end{bmatrix}, B_y = \begin{bmatrix} 0 \\ 0 \\ \vdots \\ 0 \\ \lambda_f \end{bmatrix}. \tag{6.23}$$

Note that taking the derivative of (6.21) yields a cascade of low-pass filters of order $p-1$ and a first-order high-pass filter of the washout filter type, expressed as $\dot{y}_f = A_y y_f + B_y \dot{\delta}_1$. Additionally, Lemma D.1 in Appendix D shows that the second filter state y_{f_2} can be expressed in terms of the first and third filter states, and this relationship includes information about the unknown fundamental frequency ω. Considering this lemma and defining the following constant

$$\Omega = \omega^2, \tag{6.24}$$

a least-squares frequency estimator is designed as follows

$$\dot{\hat{\Omega}} = 2\rho_y \lambda_f^2 y_{f_1} \left[y_{f_2} - \left(\frac{\hat{\Omega} + \lambda_f^2}{2\lambda_f^2} y_{f_1} + \frac{1}{2} y_{f_3} \right) \right], \tag{6.25}$$

$$\dot{\rho}_y = \rho_y \beta_y - \rho_y^2 y_{f_1}^2, \qquad \rho_y(0) > 0, \tag{6.26}$$

$$\begin{aligned} \hat{\omega} &= \sqrt{\hat{\Omega}}, \qquad \forall \hat{\Omega} > 0 \\ &= 0, \qquad \text{otherwise} \end{aligned} \tag{6.27}$$

with positive gain β_y. Based on the solution of the filter states obtained through (D.2)–(D.4), we ensure the persistent excitation of the regressor of y_{f_1}. As stated in the proof of Corollary 4.3.2 of [45], as long as this persistent excitation is satisfied, then the following holds

$$0 < \rho_{y_l} \leq \rho_y(t) \leq \rho_{y_u}, \qquad \forall t \geq 0, \tag{6.28}$$

for some positive lower and upper bounds ρ_{y_l}, ρ_{y_u}.

Lemma 6.1 *The frequency estimator* (6.25)–(6.27) *with the output signal* (6.19) *and the low-pass filters* (6.21)–(6.23) *ensure that*

$$|\omega^2 - \hat{\omega}^2| \leq \sqrt{2\rho_{y_u} V_0} \exp^{-\frac{c_v}{2}t} + \sqrt{\frac{2\rho_{y_u}}{c_v} \varepsilon_\omega}, \tag{6.29}$$

for all $t \geq 0$ with some positive constants $V_0, c_v, \varepsilon_\omega$.

The proof of this result is given in Appendix D.3.

6.4.2 Frequency estimator comparison

We present a comparison of our frequency estimator, as described in (6.25)–(6.27), with the frequency estimators introduced in [69, 12]. The primary difference between our approach and the previously mentioned estimators lies in the fact that their overall dynamics have a state dimension of $l_f + 9$ and $l_f + 5$, respectively, where l_f is the number of prefilters, a positive integer

and the prefilters used are essentially a cascade of low-pass filters. In contrast, our estimator has a reduced number of filters used and a dimension of $l_f + 2$, where $l_f \geq 3$. The minimum dynamic-order of the estimators in [69, 12] and (6.25)–(6.27) are $10, 8$ and 5, respectively.

To facilitate comparison, we replicate the example presented in [69, 12], which involves the estimation of the fundamental frequency of a noisy square wave given by

$$\delta_1(t) = 1 + \text{sign}(\sin(3t) - 0.5) + n_r(t), \tag{6.30}$$

where $n_r(t)$ denotes uniformly distributed random noise over the interval $[-0.25, 0.25]$. We use the same parameters as in [69, 12] to implement their estimators, while for our estimator we select the filter parameter $\lambda = 2.75$, the number of filters $p = 5$, the gain $\beta_y = 0.1$, and the initial gain $\rho_y(0) = 70$ to achieve a similar response time. The initial estimate $\hat{\Omega}(0)$ is set to 0.1 for all three estimators. It is worth noting that the dynamics of our estimator has a dimension of 7, whereas the dynamics of the estimators proposed in [69, 12] have dimensions of 10 and 8, respectively. Our estimator provides a smoother transition and more accurate estimation of the fundamental frequency of $\omega = 3$ rad/s at steady state, as shown in Figure 6.2. This is achieved using a smaller number of filters as compared to the estimators in [69, 12].

6.4.3 Disturbance observer-based control design

The first derivative of the disturbance $\delta_1(t)$ appears in the derivative of the error state (6.9) and needs to be rejected by the controller $\dot{u}$. To achieve this, we first represent the first derivative of (6.18) as the output of a linear exosystem, as follows

$$\dot{\mathscr{W}} = \mathscr{S}\mathscr{W}, \tag{6.31}$$

$$\dot{\delta}_1 = h^T \mathscr{W} + \dot{\delta}_{1,h_q}, \tag{6.32}$$

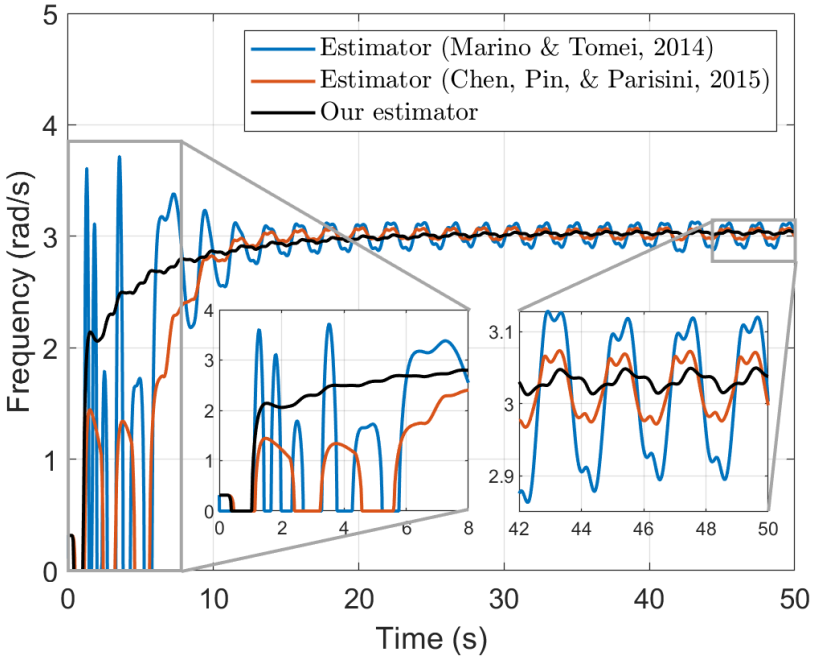

Figure 6.2. The evolution of the frequency estimates with the first and last 8 seconds zoomed in. The convergence of our estimate is compared with that of [69, 12].

where $\dot{\delta}_{1,h_q}$ defines the harmonics higher than a user defined number $q \in \mathbb{N}\backslash\{1,2\}$ and

$$\mathscr{W} = \begin{bmatrix} \bar{a}_1 \omega \sin(\omega t + \varphi_1) \\ \bar{a}_1 \omega \cos(\omega t + \varphi_1) \\ \vdots \\ \bar{a}_q q\omega \sin(q\omega t + \varphi_q) \\ \bar{a}_q q\omega \cos(q\omega t + \varphi_q) \end{bmatrix}, \quad h = \begin{bmatrix} 1 \\ 0 \\ \vdots \\ 1 \\ 0 \end{bmatrix}$$
$$\mathscr{S} = \text{block diag} \begin{bmatrix} S_1 & \cdots & S_q \end{bmatrix},$$
$$S_i = \begin{bmatrix} 0 & i\omega \\ -i\omega & 0 \end{bmatrix}, \qquad i = 1, \ldots, q \tag{6.33}$$

with $\bar{a}_i = \sqrt{a_i^2 + b_i^2}$, $\varphi_i = \arctan(a_i/b_i)$ for $i = 1, \ldots, q$. In the next theorem, we design a disturbance observer for the unknown exosystem (6.31)–(6.32) using the offline learned frequency $\hat{\omega}$

and its q number of harmonics as well as design an adaptive disturbance rejection algorithm.

Theorem 6.2 *Consider the closed-loop system consisting of* (6.9)*, the following controller*

$$\dot{u} = \hat{J}^{\dagger}(u)\left(-K\hat{e} - \begin{bmatrix} h^T \hat{\mathscr{W}} \\ \vdots \\ h^T \hat{\mathscr{W}} \end{bmatrix} + \dot{y}^r + \begin{bmatrix} c_1 \tilde{e}_1 \\ \vdots \\ c_n \tilde{e}_n \end{bmatrix}\right) \tag{6.34}$$

with the Jacobian estimate

$$\hat{J}(u) = \begin{bmatrix} \Psi_1(u)^T \hat{W}_1 \\ \vdots \\ \Psi_n(u)^T \hat{W}_n \end{bmatrix}, \tag{6.35}$$

the parameter update law

$$\dot{\hat{W}}_i = \Gamma_{w_i} \Psi_i(u) \dot{u}^T (e_i - \hat{e}_i) - \Gamma_{w_i} \gamma_{w_i} \hat{W}_i, \tag{6.36}$$

the state and disturbance observers

$$\dot{\hat{e}}_i = (\Psi_i(u)^T \hat{W}_i)\dot{u} + h^T \hat{\mathscr{W}} - c_i(e_i - \hat{e}_i) - \dot{y}_r, \tag{6.37}$$

$$\dot{\hat{\mathscr{W}}} = \hat{\mathscr{S}} \hat{\mathscr{W}} + \hat{\mathscr{L}}(e_i - \hat{e}_i), \tag{6.38}$$

where the structure of $\hat{\mathscr{S}}$ *is equivalent to that of* (6.33)*, with the exception that the offline-learned* $\hat{\omega}$ *is utilized in place of the unknown* ω*, and the observer gain* $\hat{\mathscr{L}}$ *is selected such that the desired poles are assigned to the following matrix*

$$\mathscr{A} = \begin{bmatrix} -c_i & h^T \\ \hat{\mathscr{L}} & \hat{\mathscr{S}} \end{bmatrix}. \tag{6.39}$$

Under Assumptions 6.1–6.3, the signals $e_i, \tilde{W}_i, \tilde{\mathscr{W}}$ *for* $i = 1, \ldots, n$ *are uniformly ultimately bounded and each error state* e_i *converges to a compact set provided that the estimated Jacobian matrix* (6.11) *is nonsingular. Moreover,*

$$|e_i(t)| \leq \exp^{-c_i t/2} \left(|\tilde{e}_i(0)| + \text{trace}\left(\tilde{W}_i(0)\Gamma_{w_i}^{-1}\tilde{W}_i^T(0)\right)^{1/2} + ||\tilde{\mathscr{W}}(0)|| \right) + \exp^{-k_i t} |\hat{e}_i(0)| + \sqrt{2\frac{D_i}{c_i}} \tag{6.40}$$

where

$$c_i = \min\left\{ \frac{\kappa_\lambda}{2}, \frac{\gamma_{w_i}}{\lambda_{max}(\Gamma_{w_i}^{-1})} \right\}, \tag{6.41}$$

$$D_i = \frac{\bar{\varepsilon}_i^2}{\kappa_\lambda} + \frac{(\bar{\delta}_{h_q}^{max})^2}{\kappa_\lambda} + \frac{(q\tilde{\omega})^2}{2\kappa_\lambda} \sum_{j=1}^{q} (\bar{a}_j j\omega)^2 + \frac{\gamma_{w_i}}{2} \times \text{trace}\left(W_i^*(W_i^*)^T\right), \tag{6.42}$$

$$\kappa_\lambda = \lambda_{\min}(\mathscr{A}), \tag{6.43}$$

with $\dot{\delta}_{1,h_q} \leq \bar{\delta}_{h_q}^{max}$ *for some positive constant* $\bar{\delta}_{h_q}^{max}$ *for all* $t \in [0, \infty)$.

The proof of this result is given in Appendix D.4.

Remark 6.5 *While certain neural networks, such as Recurrent Neural Networks, can handle both spatial and periodic temporal features, our control strategy requires separate estimations of the unknown Jacobian matrix and the unknown periodic disturbance. This is due to the use of the Jacobian matrix's pseudo-inverse in our control formulation* (6.34)*, which would be incompatible with a joint neural network estimate of both elements.*

6.5 Accelerated Robust Adaptive Model-Free Algorithms

In this section, we introduce accelerated robust adaptive model-free algorithms. The idea is motivated by the fact that the second term on the right hand side of (6.13) can be eliminated by using high controller and parameter update gains. We define three different time-varying gains

that grow linearly, grow exponentially, and grow and blow up at a final time in order to achieve asymptotic, exponential and prescribed-time convergence of the error state e to zero, respectively, despite any arbitrary unknown disturbances, that do not necessarily need to be periodic as in Section 6.4, as well as neural network approximation error.

6.5.1 Adaptive robust design for asymptotic regulation

Let us define the following linearly growing signal

$$\mu_a(t) = 1 + \beta t, \qquad \beta > 0, \qquad t \in [0, \infty). \tag{6.44}$$

Then apply the following scaling transformation

$$z = \mu_a e, \tag{6.45}$$

which obeys the following dynamics

$$\begin{aligned} \dot{z} &= \mu_a \dot{e} + \dot{\mu}_a e, \\ &= \mu_a \left(\begin{bmatrix} \Psi_1(u)^T W_1^* \\ \vdots \\ \Psi_n(u)^T W_n^* \end{bmatrix} \dot{u} + \dot{\delta} - \dot{y}^r + \varepsilon + \frac{\beta}{\mu_a} e \right). \end{aligned} \tag{6.46}$$

The aim is to design a controller which stabilizes the state z as well as the error state e. We state the following theorem that summarizes our results in this subsection.

Theorem 6.3 *Consider the closed-loop system consisting of* (6.9)*, the following controller*

$$\dot{u} = \hat{f}(u)^{\dagger} \left(-K \mu_a e + \dot{y}^r - \frac{\beta}{1 + \beta t} e \right) \tag{6.47}$$

with the Jacobian estimate

$$\hat{J}(u) = \begin{bmatrix} \Psi_1(u)^T \hat{W}_1 \\ \vdots \\ \Psi_n(u)^T \hat{W}_n \end{bmatrix} \tag{6.48}$$

and the parameter update law

$$\dot{\hat{W}}_i = \Gamma_{w_i} \mu_a^2 \Psi_i(u) \dot{u}^T e_i - \Gamma_{w_i} \gamma_{w_i} \mu_a \hat{W}_i, \quad \forall i = 1, \ldots, n, \tag{6.49}$$

where $K = diag(k_1, \ldots, k_n)$, Γ_{w_i} are positive definite gain matrices, γ_{w_i} is a positive scalar gain. Under Assumptions 6.1-6.2, the signals $e_i, \tilde{W}_i$ for $i = 1, \ldots, n$ are uniformly ultimately bounded and each error state e_i converges to zero asymptotically, provided that the estimated Jacobian matrix (6.48) *is nonsingular. Furthermore,*

$$|e_i(t)| \leq \frac{1}{1+\beta t} \left[\exp^{-c_i(t/2+\beta t^2/4)} \left(|e_i(0)| + \text{trace}\left(\tilde{W}_i(0) \Gamma_{w_i}^{-1} \tilde{W}_i^T(0) \right)^{\frac{1}{2}} \right) + \sqrt{2 \frac{D_i}{c_i}} \right], \tag{6.50}$$

where

$$c_i = \min \left\{ k_i, \frac{\gamma_{w_i}}{\lambda_{max}(\Gamma_{w_i}^{-1})} \right\}, \tag{6.51}$$

$$D_i = \frac{1}{k_i} \bar{\varepsilon}_i^2 + \frac{1}{k_i} (\bar{\delta}_i^{max})^2 + \frac{\gamma_{w_i}}{2} \text{trace}\left(W_i^* (W_i^*)^T \right). \tag{6.52}$$

In addition, the controller $\dot{u}$ is bounded for all $t \in [0, \infty)$.

The proof of this result is given in Appendix D.5.

6.5.2 Adaptive robust design for exponential regulation

Let us define the following exponentially growing signal

$$\mu_e(t) = \exp^{\lambda t}, \qquad \lambda > 0, \qquad t \in [0, \infty). \tag{6.53}$$

We state the following theorem.

Theorem 6.4 *Consider the closed-loop system consisting of* (6.9)*, the following controller*

$$\dot{u} = \hat{J}(u)^{\dagger} \left(-K\mu_e e + \dot{y}^r - \lambda e \right) \tag{6.54}$$

with the Jacobian estimate

$$\hat{J}(u) = \begin{bmatrix} \Psi_1(u)^T \hat{W}_1 \\ \vdots \\ \Psi_n(u)^T \hat{W}_n \end{bmatrix} \tag{6.55}$$

and the parameter update law

$$\dot{\hat{W}}_i = \Gamma_{w_i} \mu_e^2 \Psi_i(u) \dot{u}^T e_i - \Gamma_{w_i} \gamma_{w_i} \mu_e \hat{W}_i, \quad \forall i = 1, \ldots, n, \tag{6.56}$$

where $K = diag(k_1, \ldots, k_n)$, Γ_{w_i} are positive definite gain matrices, γ_{w_i} is a positive scalar gain. Under Assumptions 6.1-6.2, the signals $e_i, \tilde{W}_i$ for $i = 1, \ldots, n$ are uniformly ultimately bounded and each error state e_i converges to zero exponentially, provided that the estimated Jacobian matrix (6.55) *is nonsingular. Furthermore,*

$$|e_i(t)| \leq \exp^{-\lambda t} \left[\exp^{-\frac{c_i}{2\lambda}(\exp^{\lambda t} - 1)} \left(|e_i(0)| + \text{trace}\left(\tilde{W}_i(0) \Gamma_{w_i}^{-1} \tilde{W}_i^T(0) \right)^{\frac{1}{2}} \right) + \sqrt{2 \frac{D_i}{c_i}} \right], \tag{6.57}$$

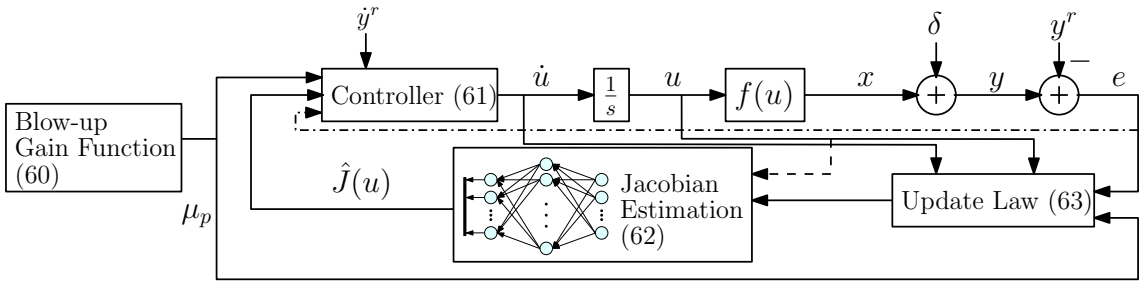

Figure 6.3. Prescribed-time model-free adaptive controller design scheme.

where

$$c_i = \min\left\{k_i, \frac{\gamma_{w_i}}{\lambda_{max}(\Gamma_{w_i}^{-1})}\right\}, \tag{6.58}$$

$$D_i = \frac{1}{k_i}\bar{\varepsilon}_i^2 + \frac{1}{k_i}(\bar{\delta}_i^{max})^2 + \frac{\gamma_{w_i}}{2}\text{trace}\left(W_i^*(W_i^*)^T\right). \tag{6.59}$$

In addition, the controller $\dot{u}$ is bounded for all $t \in [0,\infty)$.

The proof of this result is analogous to that of Theorem 6.3 and is omitted for brevity.

6.5.3 Adaptive robust design for prescribed-time regulation

Let us define the following blow-up function

$$\mu_p(t) = \frac{T^2}{(T-t)^2}, \qquad t \in [0,T), \tag{6.60}$$

where T is a final time that can be prescribed arbitrarily by user. We state the following theorem and give the closed-loop system schematically in Fig. 6.3.

Theorem 6.5 *Consider the closed-loop system consisting of* (6.9)*, the following controller*

$$\dot{u} = \hat{J}(u)^{\dagger}\left(-K\mu_p e + \dot{y}^r - \frac{2}{T-t}e\right) \tag{6.61}$$

with the Jacobian estimate

$$\hat{J}(u) = \begin{bmatrix} \Psi_1(u)^T \hat{W}_1 \\ \vdots \\ \Psi_n(u)^T \hat{W}_n \end{bmatrix} \tag{6.62}$$

and the parameter update law

$$\dot{\hat{W}}_i = \Gamma_{w_i} \mu_p^2 \Psi_i(u) \dot{u}^T e_i - \Gamma_{w_i} \gamma_{w_i} \mu_p \hat{W}_i, \quad \forall i = 1, \ldots, n, \tag{6.63}$$

where $K = diag(k_1, \ldots, k_n)$, Γ_{w_i} are positive definite gain matrices, γ_{w_i} is a positive scalar gain. Under Assumptions 6.1-6.2, the signals $e_i, \tilde{W}_i$ for $i = 1, \ldots, n$ are uniformly ultimately bounded and each error state e_i converges to zero in prescribed time, i.e.,

$$\lim_{t \to T} |e_i(t)| = 0, \quad \forall i = 1, \ldots, n, \tag{6.64}$$

provided that the estimated Jacobian matrix (6.62) *is nonsingular. Furthermore,*

$$|e_i(t)| \leq \frac{(T-t)^2}{T^2} \left[\exp^{-\frac{c_i T}{2}\left(\frac{T}{T-t}-1\right)} \left(|e_i(0)| + \text{trace}\left(\tilde{W}_i(0) \Gamma_{w_i}^{-1} \tilde{W}_i^T(0) \right)^{\frac{1}{2}} \right) + \sqrt{2 \frac{D_i}{c_i}} \right], \tag{6.65}$$

where

$$c_i = \min \left\{ k_i, \frac{\gamma_{w_i}}{\lambda_{max}(\Gamma_{w_i}^{-1})} \right\}, \tag{6.66}$$

$$D_i = \frac{1}{k_i} \bar{\varepsilon}_i^2 + \frac{1}{k_i} (\bar{\delta}_i^{max})^2 + \frac{\gamma_{w_i}}{2} \text{trace}\left(W_i^* (W_i^*)^T \right). \tag{6.67}$$

In addition, the controller $\dot{u}$ is bounded for all $t \in [0, T)$.

The proof of this result is analogous to that of Theorem 6.3 and is omitted for brevity.

Remark 6.6 *In practice, measurement noise prevents perfect error convergence and can lead to*

unbounded input signals and parameter estimates. To address this challenge, the time-varying gains can be constrained to a specific value, as discussed in [103, 54], at the cost of sacrificing ideal convergence.

6.6 Results and Discussions

We evaluate our proposed algorithms for disturbance rejection through an experiment involving a concentric tube robot (CTR). CTRs are a particular type of continuum robot made up of flexible, precurved tubes arranged in a telescoping fashion. The tubes can be inserted and rotated relative to one another, using an actuation unit (such as the one in Fig. 6.4), causing them to interact in bending and torsion. The ultimate shape of the continuum robot is dictated by the mechanical equilibrium of the tubes [99, 117].

We compare our proposed algorithms on a setpoint regulation task using a CTR subject to an applied periodic disturbance that perturbs the robot's tip position. By using a hardware system for comparison, we can better evaluate the performance of these algorithms in the presence real-world constraints such as joint velocity limits and sensor noise. While our accelerated algorithms are capable of rejecting any arbitrary bounded disturbance, for a fair comparison, we opt for a periodic disturbance that both approaches can handle.

6.6.1 Experimental setup

The particular CTR used in this experiment is the one from [29] (Fig. 6.4). The robot is tracked using an Aurora electromagnetic (EM) system (NDI), which measures the 3-D position of the robot's tip. Note that this measurement device has a reported accuracy of < 1 mm though this can increase due to noise present in the environment [100]. The CTR joint positions, which are the rotational and translational positions of each of its tubes, are measured by magnetic encoders attached to each of the motors housed in the robot's actuation unit.

In order to apply a periodic disturbance to the robot tip position, the robot is mounted to a lead screw that is driven by a stepper motor. The stepper motor, in turn, is controlled by an

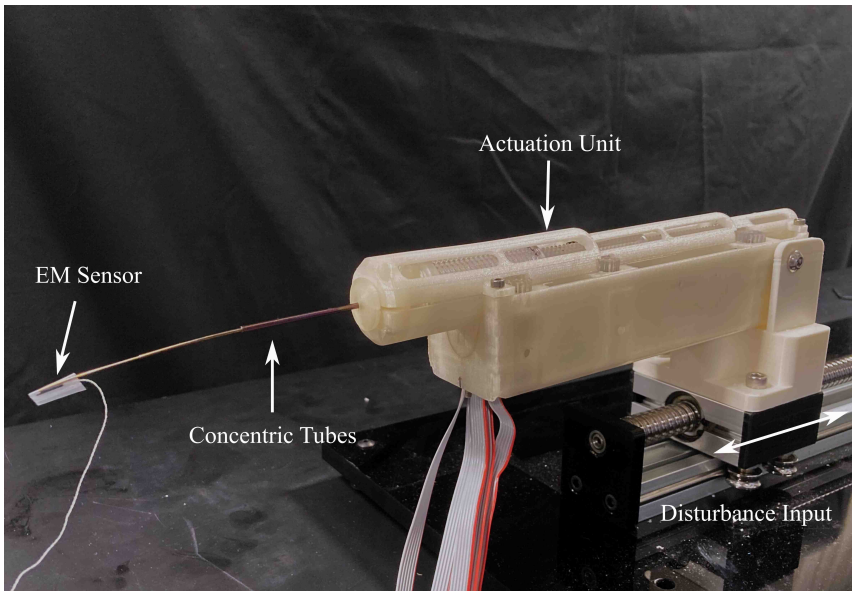

(a) Hardware setup for experimental evaluation of the proposed algorithms.

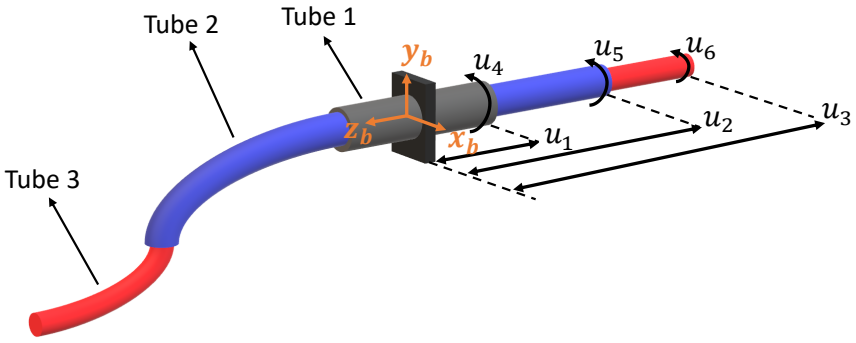

(b) An illustration of the concentric tube robot with three nested precurved tubes that are translated by the inputs u_i for $i = 1,2,3$ and rotated by the inputs u_i for $i = 4,5,6$.

Figure 6.4. Experimental setup with the illustrated control inputs in the actuation unit. The tip position used for feedback control is measured by an electromagnetic sensor taped to the robot. The harmonic disturbance affects the robot only in the z_b direction.

Arduino and can be programmed to produce a repeatable disturbance signal for testing. Though this disturbance input is unidirectional, its rejection requires coordinated motion of *all* of the CTR tubes due to the highly nonlinear nature of the robot's kinematics. The disturbance signal used in our experiment is a sum of two sine waves, one with high amplitude and low frequency,

and the other with low amplitude and high frequency, defined as

$$\delta_3(t) = a_1 \sin(\omega_1 t) + a_2 \sin(\omega_2 t), \tag{6.68}$$

which perturbs the robot only in z_b-direction. In other words, $\delta(t) = \begin{bmatrix} 0 & 0 & \delta_3(t) \end{bmatrix}^T$. The values of a_1, a_2, ω_1, and ω_2 are set to -3.75 mm, -1.25 mm, 0.41 rad/sec, and 1.36 rad/sec, respectively. It should be noted that although the timescales of this disturbance are slower than what would be typical for physiological signals, this is primarily a limitation of the linear actuator used to apply the disturbance and not the algorithms considered.

For our evaluation, we conduct three trials to assess three different control strategies for regulating the robot tip to a desired set point in the presence of a disturbance. These control strategies include: (a) the nominal adaptive controller with constant gain and without disturbance observer (6.10) presented in Section 6.3, (b) the accelerated adaptive controller with linearly growing gain (6.47) presented in Section 6.5, and (c) the adaptive controller with disturbance observer (6.34) presented in Section 6.4. The desired position y_r is $\begin{bmatrix} 22.34 & -12.89 & 100.00 \end{bmatrix}^T$ in mm. In all cases, the initial robot joint positions are set to 105 mm, 79 mm, and 40 mm in translation, and 0° in rotation, resulting in a initial tip error of $\begin{bmatrix} -22.00 & -14.00 & 0.00 \end{bmatrix}^T$ in mm. To illustrate this initial tip error as well as the effect of the disturbance, the controller is turned off for at the beginning of each trial and then switched on after 30 seconds. For all control algorithms, we use a gain of $K = \sigma I$, where $\sigma = 0.25$. For the accelerated method, we employ a linearly growing signal (6.44) with $\beta = 0.06$ chosen to highlight the ability of the method to gradually decrease error over time. For the disturbance observer based algorithm, we choose the observer gain $\mathscr{L}$ such that the closed loop poles are placed at $[-0.1, -0.125, -0.15, -0.175, -0.2, -0.25, -0.225]$. During parameter selection, we conducted trials to evaluate their impact on system response. The use of high gains, while offering faster reactions, resulted in amplified noise sensitivity, instability in disturbance estimation, and high initial control effort, due to the large initial error, exceeding actuator limits. To achieve good control performance without these drawbacks, we

opted for moderate gains, as described earlier. Notably, our accelerated controller initiates with a low gain K and linearly increases it over time. This approach eliminates the need for high initial control effort, enhances the rejection of disturbances, and ensures that actuator efforts remain within their limits.

The process of selecting parameters makes clear that non-idealities in the experimental hardware can pose challenges for the implementation of our control strategies. Phenomena such as sensor noise, a low sampling rate, physical limits of the actuators, and friction/hysteresis in the flexible tubes all constrain how aggressively the disturbance can be rejected in practice. The impact of these limitations may be reduced by using more performant hardware.

6.6.2 Results

Prior to conducting the experiment, we train the neural network weights offline using a set of input and output data consisting of random robot configurations and their corresponding tip positions over a limited workspace in a disturbance-free environment. The experimental results are presented in Fig. 6.5 through Fig. 6.7. Fig. 6.5 illustrates the evolution of the robot tip, as well as the translations and rotations of each tube over time for each algorithm. It is evident from Fig. 6.5 that all control strategies are able to substantially reduce the large, initial error in the robot tip position. However, it is also evident that the nominal controller is not as effective at suppressing the periodic disturbance as the other two algorithms. The presence of disturbance estimate in the observer-based controller manifests as additional oscillations, absent in the nominal controller's behavior. The rapid oscillation observed in the tube rotations around the 40th second is likely due to the slippage of gears in our prototype robot.

To quantitatively assess the efficacy of algorithms in rejecting the disturbances, we analyze the mean absolute error in the robot tip position along the z_b-direction after the controllers are activated. Specifically, we compute this statistic for times $t > 30$ s. For the nominal controller, this mean tip error is 1.26 mm. The adaptive controller employing estimated disturbance rejection however, achieves a much lower error of 0.65 mm. This result shows a clear gain

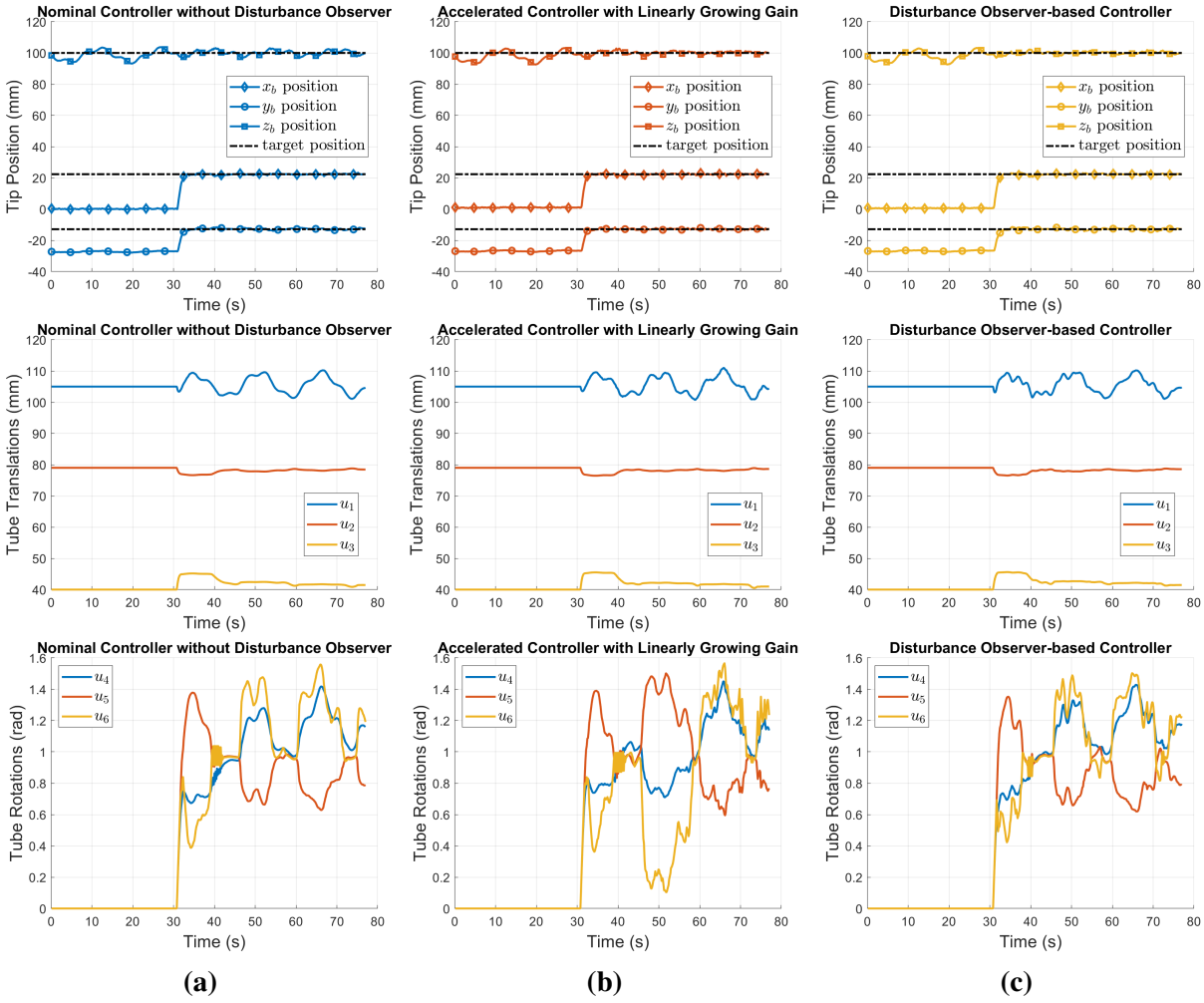

Figure 6.5. A comparative analysis of three distinct control strategies for driving the robot tip to a target position. The strategies are: (a) nominal adaptive controller with constant gain and without disturbance observer (6.10), (b) accelerated adaptive controller with linearly growing gain (6.47), (c) adaptive controller with disturbance observer (6.34). The plots depict the robot tip position in the x_b, y_b, and z_b directions, as well as the translational and rotational movement of tubes u_1 through u_6. The algorithms are activated at $t = 30$ seconds. The robot tip position in the z_b axis is disturbed harmonically by an unknown disturbance $\delta_3(t)$.

in performance over the nominal controller, even in the presence of some sensor noise. As expected, the accelerated adaptive algorithm similarly shows improvement, 0.77 mm mean error, although slightly larger than for the case where the disturbance is explicitly estimated and then rejected. This is likely due in large part to the design of the growth signal μ_a. Here we have chosen this signal to grow linearly over time with a rate that highlights the method's capability

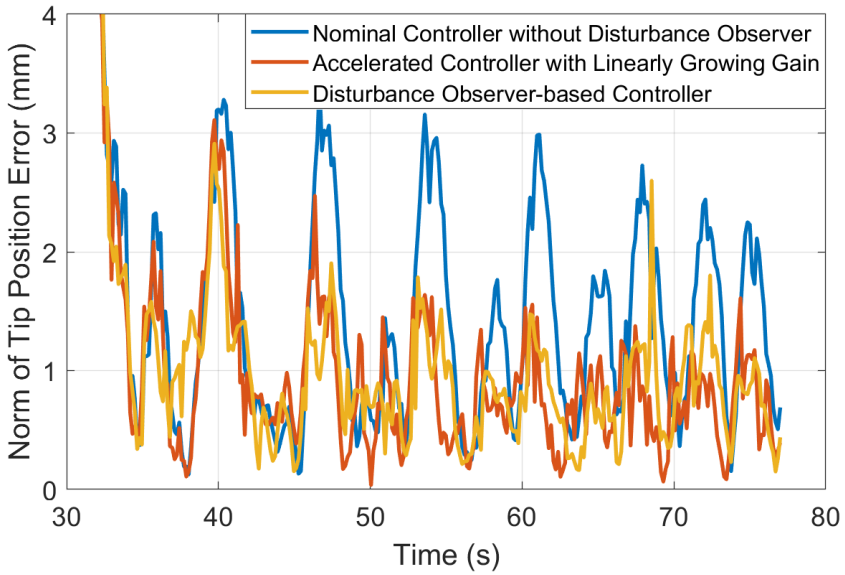

Figure 6.6. The norm of the tip position error resulting from the application of each algorithm, which is activated at $t = 30$ seconds.

to gradually decrease error over time. This is illustrated in the zoomed portion of Fig. 6.6 where the Euclidean norm of the tip position error of the accelerated algorithm is initially similar to the error of the nominal controller, but then slowly decreases for the rest of the experiment. It is possible to choose this signal to be more aggressive, as described in Sections 6.5.2 and 6.5.3, but with the trade-off that error due to sensor noise will be amplified as well. Furthermore, the continuous decrease in the norm of the error associated with the nominal design is a result of its convergence to an ultimate bound, as characterized in (6.13).

Prior to implementing the disturbance observer based algorithm (6.34), we estimate the low frequency ω_1 in the harmonically disturbed robot tip position in an offline mode. To filter the output, we employ the filters designed in (6.21) and (6.22), with $\lambda_f = 1$ and $p = 16$. Then, utilizing the frequency estimator in (6.25)–(6.27) with $\rho_y(0) = 30$, $\hat{\Omega}(0) = 0.8$, $\beta_y = 0.75$, we obtain a very accurate estimate of ω_1, as shown in Fig. 6.7. The obtained disturbance estimate is then integrated into the controller (6.34) to effectively reject the disturbances. For disturbances with varying periodicity, such as changes in the breathing frequency over time, a potential solution could involve continuous monitoring of the frequency using external sensing,

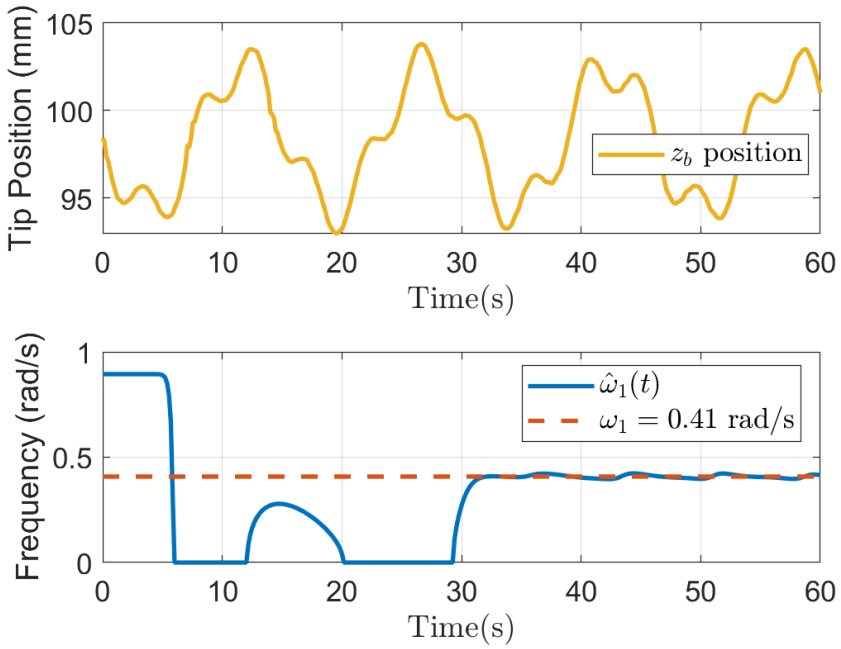

Figure 6.7. The upper subplot displays the robot tip position in the z_b axis that is disturbed by harmonics $\delta_3(t)$ with two distinct frequencies, namely ω_1 and ω_2. The lower subplot illustrates the offline estimation of the low frequency ω_1 using the estimator (6.25)–(6.27).

as discussed in [65], and updating the frequency estimate online within the observer (6.38).

6.7 Conclusion

In this chapter, we have presented two distinct adaptive model-free control strategies for continuum robots subjected to unknown disturbances: (i) disturbance observer-based adaptive controller (6.34), and (ii) accelerated adaptive controllers with asymptotic, exponential and prescribed-time convergence (6.47), (6.54), (6.61), respectively. The designs differ in their approach to disturbance rejection and their ability to drive the robot tip to a desired position. The disturbance observer-based design estimates periodic disturbances explicitly and drives the error state to an ultimate bound due to the residual term at the right hand side of (6.40). Although this residual term can be minimized by improving the neural-network model and disturbance estimate, it does not vanish. On the other hand, the accelerated designs suppress any type of

disturbances through monotonically increasing gains and ensure that the error state converges to zero. The error states vanish at the same rate that the gains grow over time, as shown in (6.50), (6.57) and (6.65).

We have conducted hardware experiments with a concentric tube robot to compare the performance of these strategies on a setpoint regulation task, serving as a proof-of-concept. Contrary to the theoretical results, the experimental findings demonstrate that the disturbance observer-based design (6.34) has slightly outperformed the accelerated design (6.47) in terms of the mean absolute error in the robot tip position over a finite time. This is primarily due to the physical limitation of the actuators and sensor noise, which limit the feasibility of accelerated designs. Consequently, we believe that the thorough theoretical and experimental validation presented in this chapter highlights the usefulness of these methods.

6.8 Acknowledgments

Chapter 6 is a reprint of the material as it appears in:

- C. T. Yilmaz, C. Watson, T. K. Morimoto, and M. Krstic, “Adaptive model-free disturbance rejection for continuum robots”, *Automatica*, vol. 171, p. 111949, 2025.

The dissertation author was the primary investigator and author of this paper.

Appendix A

Solutions of the Kernels in Chapter 2

A.1 Solutions of $\gamma_c(x,t)$, $q_c(x,y,t)$, and $q_r(x,y,t)$

Proposition A.1 *The time-varying kernel equations* (2.146)–(2.148)*,* (2.149)–(2.151)*, and* (2.152)–(2.154) *have unique solutions. The growth-in-time bounds of these time-varying kernels are given as follows*

$$|\gamma_c(\cdot,t)| \leq C_1 e^{C_2 \mu(t)}, \tag{A.1}$$

$$|q_c(\cdot,\cdot,t)| \leq C_4 e^{C_5 \mu(t)}, \tag{A.2}$$

$$|q_r(\cdot,\cdot,t)| \leq e^{\mu(t)\left(\frac{D^2}{4T}+C_6\sqrt{\mu_0}\right)}, \tag{A.3}$$

where $C_1 := \frac{|k|}{\mu_0 D}$, $C_2 := \frac{D^2}{T} + D\sqrt{5\mu_0}$, $C_3 := C_2 + \mu_0 T$, $C_4 := 2C_1$, $C_5 := \sqrt{5C_3D^2/(4T)} + C_2 + D^2/(4T)$*, and some positive* C_6 *independent of* μ_0 *and* $\mu(t)$.

Proof

The Kernel $\gamma_c(x,t)$: Let us integrate (2.152) twice with respect to x in view of the boundary conditions (2.153) and (2.154). Then, we obtain the following implicit solution

$$\gamma_c(x,t) = \int_0^x \int_0^\tau \left(\partial_t \gamma_c(s,t) + \mu_0 \mu^2(t) \gamma_c(s,t)\right) ds d\tau - k\mu^2(t)x. \tag{A.4}$$

We can show that the solution of (A.4) exists by using the method of successive approximations

$$\gamma_c(x,t) = \sum_{n=0}^{\infty} \gamma_c^n(x,t), \tag{A.5}$$

where

$$\gamma_c^0(x,t) = -k\mu^2(t)x, \tag{A.6}$$

$$\gamma_c^{n+1}(x,t) = \int_0^x \int_0^\tau \left(\partial_t \gamma_c^n(s,t) + \mu_0 \mu^2(t)\gamma_c^n(s,t)\right) ds d\tau, \tag{A.7}$$

for $n \in \mathbb{N}_0$. Let us compute the iteration formula (A.7) for a few steps to obtain a recursive formula

$$\begin{aligned}
\gamma_c^1(x,t) &= -k\frac{x^3}{3!}\frac{1}{T}\mu^3(t)(2+T\mu_0\mu(t)),\\
\gamma_c^2(x,t) &= -k\frac{x^5}{5!}\frac{1}{T^2}\mu^4(t)\Big(6+6(T\mu_0)\mu(t)+(T\mu_0)^2\mu^2(t)\Big),\\
\gamma_c^3(x,t) &= -k\frac{x^7}{7!}\frac{1}{T^3}\mu^5(t)\Big(24+36(T\mu_0)\mu(t)+12(T\mu_0)^2\mu^2(t)+(T\mu_0)^3\mu^3(t)\Big).
\end{aligned}$$

Continuing the iterations, we observe the following pattern

$$\gamma_c^n(x,t) = -k\frac{x^{2n+1}}{(2n+1)!}\frac{n!}{T^n}\mu^{n+2}(t)L_n^{(1)}(-(T\mu_0)\mu(t)), \tag{A.8}$$

which is written in terms of the generalized Laguerre polynomial $L_n^{(1)}$. We prove by induction that the expression (A.8) holds for all $n > 0$. Before giving the proof, recall the properties of generalized Laguerre polynomials:

$$L_{n+1}^{(\alpha)}(\check{p}) = \frac{1}{n+1}\Big((2n+\alpha+1-\check{p}))L_n^{(\alpha)}(\check{p}) - (n+\alpha)L_{n-1}^{(\alpha)}(\check{p})\Big), \tag{A.9}$$

$$\frac{d}{dp}L_n^{(\alpha)}(\check{p}) = \check{p}^{-1}\left(nL_n^{(\alpha)}(\check{p}) - (n+\alpha)L_{n-1}^{(\alpha)}(\check{p})\right), \tag{A.10}$$

for any $\alpha > -1$. Let us define $\check{p} = -T\mu_0\mu(t)$ and assume that the formula (A.8) is valid for an arbitrary n. Then, substituting (A.8) into (A.7) yields

$$\gamma_c^{n+1}(x,t) = -k\frac{x^{2n+3}}{(2n+3)!}\frac{n!}{T^n}\left(\frac{(n+2)}{T}\mu^{n+3}(t)L_n^{(1)}(\check{p}) + \mu^{n+2}\frac{1}{\check{p}}\left(nL_n^{(1)}(\check{p}) - (n+1)L_{n-1}^{(1)}(\check{p})\right)\right.$$
$$\left.\times\frac{d\check{p}}{dt} + \mu_0\mu^2(t)\mu^{n+2}(t)L_n^{(1)}(\check{p})\right), \tag{A.11}$$

where we use the property (A.10). By noting that $d\check{p}/dt = -\mu_0\mu^2(t)$, we get

$$\gamma_c^{n+1}(x,t) = -k\frac{x^{2n+3}}{(2n+3)!}\frac{n!}{T^{n+1}}\mu^{n+3}(t)\Big((2n+2+T\mu_0\mu(t))L_n^{(1)}(\check{p}) - (n+1)L_{n-1}^{(1)}(\check{p})\Big). \tag{A.12}$$

In the light of the fact (A.9), we rewrite (A.12) as follows

$$\gamma_c^{n+1}(x,t) = -\frac{kx^{2n+3}}{(2n+3)!}\frac{(n+1)!}{T^{n+1}}\mu^{n+3}(t)L_{n+1}^{(1)}(-(T\mu_0)\mu(t)),$$

which proves that (A.8) is valid for $n+1$ as well. In other words, it is proved by induction that (A.8) holds for all $n > 0$. Then, we finally obtain the unique C^∞ solution of the kernel from (A.5) and (A.8) as follows

$$\gamma_c(x,t) = -k\mu^2(t)\sum_{n=0}^{\infty}\frac{x^{2n+1}}{(2n+1)!}\frac{n!}{T^n}\mu^n(t)L_n^{(1)}(-(T\mu_0)\mu(t)).$$

The estimation of the growth-in-time of $\gamma_c(x,t)$ is given by

$$|\gamma_c(x,t)| \leq |k|\mu^2(t)x\sum_{n=0}^{\infty}\frac{(\mu(t)x^2)^n}{T^n(n+1)!}L_n^{(1)}(-(T\mu_0)\mu(t)),$$
$$\leq |k|\mu^2(t)De^{\frac{D^2}{T}\mu(t)}\frac{I_1(2\sqrt{D^2\mu_0\mu^2(t)})}{\sqrt{D^2\mu_0\mu^2(t)}}, \tag{A.13}$$

where we use the relation given in [107, Theorem 5.1], and where I_1 is the modified Bessel

function of the first kind. Let us consider the bound of the following term

$$\begin{aligned}\mu^2(t)D\frac{I_1(2\sqrt{D^2\mu_0\mu^2(t)})}{\sqrt{D^2\mu_0\mu^2(t)}} &= \mu^2(t)D\sum_{m=0}^{\infty}\frac{\left(\sqrt{D^2\mu_0\mu^2(t)}\right)^{2m}}{m!(m+1)!}\\ &= \frac{1}{\mu_0 D}\sum_{m=1}^{\infty}\frac{\left(\sqrt{D^2\mu_0\mu^2(t)}\right)^{2m}}{(m-1)!m!}\\ &\leq \frac{1}{\mu_0 D}\sum_{m=0}^{\infty}\frac{\left(\sqrt{5D^2\mu_0\mu^2(t)}\right)^{2m}}{(2m)!}\\ &\leq \frac{1}{\mu_0 D}e^{D\sqrt{5\mu_0}\mu(t)}, \end{aligned} \tag{A.14}$$

by using the inequality $\frac{1}{(n-1)!n!} \leq \frac{5^n}{(2n)!}$ for any $n \in \mathbb{N}$ and the property $\sum_{k=0}^{\infty}\frac{z^{2k}}{(2k)!} = \cosh(z)$ for any $z \in \mathbb{R}$. In view of the bound (A.14), we can rewrite (A.13) as (A.1).

The Kernel $q_c(x,y,t)$: The kernel $q_c(x,y,t)$ defined in (2.146)-(2.148) can be recursively computed by a successive approximation. Let $\xi = \frac{1}{2}(x+y)$ and $\eta = \frac{1}{2}(x-y)$, and perform the change of variables

$$Q_c(\xi,\eta,t) = q_c(\xi+\eta,\xi-\eta,t). \tag{A.15}$$

Then, (2.146)-(2.148) become

$$\partial_{\xi\eta}Q_c(\xi,\eta,t) = \partial_t Q_c(\xi,\eta,t) + \mu_0\mu^2(t)Q_c(\xi,\eta,t), \tag{A.16}$$

$$Q_c(\xi,\xi,t) = \gamma_c(2\xi,t), \tag{A.17}$$

$$Q_c(\xi,0,t) = 0. \tag{A.18}$$

This PDE needs to be solved on the domain $(\xi,\eta,t) \in \Omega = [\eta, D-\eta]\times[0,D/2]\times[t_0,t_0+T)$. Let us integrate (A.16) with respect to ξ and η in view of (A.17), (A.18) as follows

$$Q_c(\xi,\eta,t) = \gamma_c(2\eta,t) + \int_{\eta}^{\xi}\int_0^{\eta}\left(\partial_t Q_c(\sigma,\beta,t) + \mu_0\mu^2(t)Q_c(\sigma,\beta,t)\right)d\beta d\sigma, \tag{A.19}$$

which yields an implicit solution. Similarly, we look for a solution of (A.19) in terms of the infinite series

$$Q_c(\xi,\eta,t) = \sum_{n=0}^{\infty} Q_c^n(\xi,\eta,t), \tag{A.20}$$

where

$$Q_c^0(\xi,\eta,t) = \gamma_c(2\eta,t), \tag{A.21}$$

$$Q_c^n(\xi,\eta,t) = \int_\eta^\xi \int_0^\eta \Big(\partial_t Q_c^{n-1}(\sigma,\beta,t) + \mu_0\mu^2(t) Q_c^{n-1}(\sigma,\beta,t)\Big) d\beta d\sigma. \tag{A.22}$$

Let us compute the following estimates from (A.1), (A.21), (A.22)

$$\begin{aligned}
|Q_c^0(\xi,\eta,t)| &\le C_1 e^{C_2\mu(t)},\\
|Q_c^1(\xi,\eta,t)| &\le C_1 \frac{1}{T} C_3\mu^2(t) e^{C_2\mu(t)} \eta\xi,\\
|Q_c^2(\xi,\eta,t)| &\le C_1 \frac{1}{T^2} C_3\mu^3(t)(2 + C_3\mu(t)) e^{C_2\mu(t)} \frac{(\xi\eta)^2}{2!2!},\\
|Q_c^3(\xi,\eta,t)| &\le C_1 \frac{1}{T^3} C_3\mu^4(t)\Big(6 + 6C_3\mu(t) + C_3^2\mu^2(t)\Big) e^{C_2\mu(t)} \frac{(\xi\eta)^3}{3!3!}.
\end{aligned} \tag{A.23}$$

The iterative computations yield the following pattern

$$|Q_c^n(\xi,\eta,t)| \le C_1 \frac{1}{T^n} C_3\mu^{n+1}(t)(n-1)! e^{C_2\mu(t)} \frac{(\xi\eta)^n}{n!n!} L_{n-1}^{(1)}(-C_3\mu(t)), \tag{A.24}$$

for $n \in \mathbb{N}$, which can be proved by induction following the similar procedure done for (A.8). Then, it follows from (A.24) that the series (A.20) converges uniformly and absolutely on the domain Ω. We obtain the growth-in-time of the kernel by substituting (A.24) into (A.20) and inverting the change of variables as follows

$$|q_c(x,y,t)| \le C_1 e^{C_2\mu(t)} + \sum_{n=0}^{\infty} C_1 C_3 \left(\frac{(x^2-y^2)}{4T}\right)^{n+1} \frac{n!}{((n+1)!)^2} \mu^{n+2}(t) L_n^{(1)}(-C_3\mu(t)) e^{C_2\mu(t)},$$

$$\leq C_1 e^{C_2\mu(t)} + C_1 C_3 \frac{D^2}{4T}\mu^2(t) e^{\left(C_2+\frac{D^2}{4T}\right)\mu(t)} \frac{I_1(2\sqrt{C_3\mu^2(t)D^2/(4T)})}{\sqrt{C_3\mu^2(t)D^2/(4T)}}, \tag{A.25}$$

where we use the relation given in [107, Theorem 5.1]. Let us consider the bound of the following term

$$\begin{aligned} C_3\mu^2(t)\frac{D^2}{4T}\frac{I_1(2\sqrt{C_3\mu^2(t)D^2/(4T)})}{\sqrt{C_3\mu^2(t)D^2/(4T)}} &= \sum_{m=1}^{\infty} \frac{\left(\sqrt{C_3\mu^2(t)D^2/(4T)}\right)^{2m}}{(m-1)!m!}, \\ &\leq \sum_{m=0}^{\infty} \frac{\left(\sqrt{5C_3\mu^2(t)D^2/(4T)}\right)^{2m}}{(2m)!}, \\ &\leq e^{\sqrt{5C_3D^2/(4T)}\mu(t)}, \end{aligned} \tag{A.26}$$

by noting the fact that $\frac{1}{(m-1)!m!} \leq \frac{5^m}{(2m)!}$ for all $m \in \mathbb{N}$. In view of the bound (A.26), we can rewrite (A.25) as (A.2). The next step is to prove the uniqueness of the solution of the integral equation (A.19). Let us assume that $q_c'(x,y,t)$ and $q_c''(x,y,t)$ are two different solutions of (A.19). Then, let us define $\Delta q_c(x,y,t) = q_c'(x,y,t) - q_c''(x,y,t)$. Considering the boundedness result (A.2), we get $|\Delta q_c(x,y,t)| \leq 2C_4 e^{C_5\mu(t)}$. We use this inequality and follow the same estimates as in (A.24) to get

$$|\Delta Q_c(\xi,\eta,t)| \leq 2C_3C_4\left(\frac{(x^2-y^2)}{4T}\right)^n \frac{(n-1)!}{n!n!}\mu^{n+1}(t)L_{n-1}^{(1)}(-C_3\mu(t))e^{C_5\mu(t)} \to \quad 0$$

as $n \to \infty$ from which we conclude that the integral equation (A.19) has a unique solution for $t \in [t_0, t_0+T)$, $(x,y) \in \mathscr{T}$.

The Kernel $q_r(x,y,t)$: The analytical solution of this kernel is given in [21] as follows

$$q_r(x,y,t) = -y\mu_0\mu^2(t)e^{\frac{\mu(t)(x^2-y^2)}{4T}} \frac{I_1\left(\sqrt{\mu_0\mu^2(t)(x^2-y^2)}\right)}{\sqrt{\mu_0\mu^2(t)(x^2-y^2)}}$$

which is unique and C^∞ for $t \in [t_0, t_0+T)$, $(x,y) \in \mathscr{T}$. Additionally, it is shown in [21] that (A.3) holds. ■

A.2 Solutions of $\Gamma(x,t)$, $p(x,y,t)$

Proposition A.2 *The time-varying kernel equations* (2.160)–(2.162) *and* (2.163)–(2.165) *have unique solutions. The growth-in-time bounds of these time-varying kernels and their spatial derivatives are given as follows*

$$|\Gamma(x,t)| \leq C_7 \mu^2(t) e^{\frac{D^2}{T}\mu(t)}, \tag{A.27}$$

$$|\partial_x \Gamma(\cdot,t)| \leq kH\mu^2(t) e^{\frac{D^2}{T}\mu(t)}, \tag{A.28}$$

$$|p(\cdot,\cdot,t)| \leq C_{12} \mu^2(t) e^{\frac{3D^2}{2T}\mu(t)}, \tag{A.29}$$

$$|\partial_x p(\cdot,\cdot,t)| \leq C_{13} \mu^3(t) e^{\frac{3D^2}{2T}\mu(t)}, \tag{A.30}$$

where $C_7 := kHD$, $C_{13} := kH + C_{12}$ *for some* $C_{12} > 0$.

Proof

The Kernel $\Gamma(x,t)$**:** We perform the similar procedure as in the derivation of the solution for $\gamma_c(x,t)$ to characterize the kernel defined in (2.163)–(2.165). The integration of (2.163) twice with respect to x in view of the boundary conditions (2.164) and (2.165) yields following implicit solution

$$\Gamma(x,t) = -kH\mu^2(t)x + \int_0^x \int_0^\tau \big(\partial_t \Gamma(s,t) - kH\mu^2(t)\Gamma(s,t)\big) ds d\tau. \tag{A.31}$$

The existence of the solution of (A.31) can be shown by using the method of successive approximations

$$\Gamma(x,t) = \sum_{n=0}^{\infty} \Gamma^n(x,t), \tag{A.32}$$

where

$$\Gamma^0(x,t) = -kH\mu^2(t)x, \tag{A.33}$$

$$\Gamma^{n+1}(x,t) = \int_0^x \int_0^\tau \left(\partial_t \Gamma^n(s,t) - kH\mu^2(t)\Gamma^n(s,t)\right) ds d\tau, \tag{A.34}$$

for $n \in \mathbb{N}_0$. Computing (A.32) using the recursive formula (A.34) with the initial value (A.33), we obtain the following unique C^∞ solution

$$\Gamma(x,t) = \sum_{n=0}^{\infty} -kH \frac{x^{2n+1}}{(2n+1)!} \frac{n!}{T^n} \mu^{n+2} L_n^{(1)}(TkH\mu(t)). \tag{A.35}$$

The growth-in-time bound of (A.35) is determined as follows

$$\begin{aligned} |\Gamma(x,t)| &\leq kHD\mu^2(t) \sum_{n=0}^{\infty} \frac{(D^2\mu(t))^n}{T^n(n+1)!} L_n^{(1)}((TkH)\mu(t)), \\ &= kHD\mu^2(t) e^{\frac{D^2}{T}\mu(t)} \frac{J_1(2\sqrt{kHD^2\mu^2(t)})}{\sqrt{kHD^2\mu^2(t)}}, \\ &\leq kHD\mu^2(t) e^{\frac{D^2}{T}\mu(t)}, \end{aligned} \tag{A.36}$$

where $J_1(\cdot)$ is the Bessel function of the first kind, as defined in the Notation paragraph of Chapter 2. In (A.36), we use the relation in [107, Theorem 5.1] and note from [116, p. 49] the fact that $\left|\frac{J_1(2\sigma)}{\sigma}\right| \leq 1$ for all $\sigma \in \mathbb{R}$. Then, we get (A.27). The growth-in-time bound of the spatial derivative of (A.35) is obtained in a similar fashion as (A.28).

The Kernel $p(x,y,t)$: Due to two independent boundary conditions of the kernel defined in (2.160)–(2.162), we can separate this kernel PDE into two sets of PDE systems as follows

$$p(x,y,t) = p_c(x,y,t) + p_r(x,y,t), \tag{A.37}$$

where

$$\partial_t p_c(x,y,t) = \partial_{xx} p_c(x,y,t) - \partial_{yy} p_c(x,y,t) + \mu_0 \mu^2(t) p_c(x,y,t), \tag{A.38}$$

$$p_c(x,0,t) = \Gamma(x,t), \tag{A.39}$$

$$p_c(x,x,t) = 0, \tag{A.40}$$

and

$$\partial_t p_r(x,y,t) = \partial_{xx} p_r(x,y,t) - \partial_{yy} p_r(x,y,t) + \mu_0 \mu^2(t) p_r(x,y,t), \tag{A.41}$$

$$p_r(x,0,t) = 0, \tag{A.42}$$

$$p_r(x,x,t) = -\frac{x}{2}\mu_0 \mu^2(t), \tag{A.43}$$

for $t \in [t_0, t_0+T)$, $(x,y) \in \mathscr{T}$. The solution of the kernel (A.38)–(A.40) is proved by the method of successive approximation. Let $\xi = \frac{1}{2}(x+y)$ and $\eta = \frac{1}{2}(x-y)$, and perform the change of variables

$$P_c(\xi,\eta,t) = p_c(\xi+\eta, \xi-\eta, t), \tag{A.44}$$

for $(\xi,\eta,t) \in \Omega$. Then, (A.38)-(A.40) become

$$\partial_{\xi\eta} P_c(\xi,\eta,t) = \partial_t P_c(\xi,\eta,t) - \mu_0 \mu^2(t) P_c(\xi,\eta,t) \tag{A.45}$$

$$P_c(\xi,\xi,t) = \Gamma(2\xi,t), \tag{A.46}$$

$$P_c(\xi,0,t) = 0. \tag{A.47}$$

The implicit solution of (A.45)–(A.47) follows from the integration of (A.45) with respect to ξ

and η in view of (A.46) and (A.47),

$$P_c(\xi,\eta,t) = \Gamma(2\eta,t) + \int_\eta^\xi \int_0^\eta \Big(\partial_t P_c(\sigma,\beta,t) - \mu_0\mu^2(t) P_c(\sigma,\beta,t)\Big) d\beta d\sigma. \tag{A.48}$$

The solution of the integral equation (A.48) is obtained by the method of successive approximation

$$P_c(\xi,\eta,t) = \sum_{n=0}^{\infty} P_c^n(\xi,\eta,t), \tag{A.49}$$

where

$$P_c^0(\xi,\eta,t) = \Gamma(2\eta,t), \tag{A.50}$$

$$P_c^n(\xi,\eta,t) = \int_\eta^\xi \int_0^\eta \Big(\partial_t P_c^{n-1}(\sigma,\beta,t) - \mu_0\mu^2(t) P_c^{n-1}(\sigma,\beta,t)\Big) d\beta d\sigma. \tag{A.51}$$

The recursion formula (A.51) with (A.50) results in the following upper bound

$$|P_c^n(\xi,\eta,t)| \le C_7 \frac{1}{T^n} \mu^{n+2}(t) n! e^{C_8\mu(t)} \frac{(\xi\eta)^n}{n!n!} L_n^{(1)}(-C_9\mu(t)), \tag{A.52}$$

where $C_8 := D^2/T$, $C_9 := C_8 - \mu_0 T < 0$ provided that $\mu_0 > C_8/T = D^2/T^2$. The bound (A.52) holds for $n \in \mathbb{N}_0$ and its proof is obtained by induction following the similar procedure done for (A.8). It follows from (A.52) that the series (A.49) converges uniformly and absolutely on the domain Ω. Let us invert the change of variables in (A.52) from (ξ,η,t) to (x,y,t) and substitute it into (A.49) as follows

$$\begin{aligned}
|p_c(x,y,t)| &\le \sum_{n=0}^{\infty} C_7 \left(\frac{x^2-y^2}{4T}\right)^n \frac{1}{n!} \mu^{n+2}(t) e^{C_8\mu(t)} L_n^{(1)}(-C_9\mu(t)), \\
&\le C_7 \mu^2(t) e^{\frac{D^2}{2T}\mu(t) + C_8\mu(t)} \frac{J_1\left(2\sqrt{D^2 C_9 \mu^2(t)/(2T)}\right)}{\sqrt{D^2 C_9 \mu^2(t)/(2T)}}, \\
&\le C_7 \mu^2(t) e^{\frac{3D^2}{2T}\mu(t)},
\end{aligned} \tag{A.53}$$

by using the relation [107, Theorem 5.1], noting from [116, p. 49] the fact that $\left|\frac{J_1(2\sigma)}{\sigma}\right| \leq 1$ for all $\sigma \in \mathbb{R}$ and considering the property $\frac{1}{n!} \leq \frac{2^n}{(n+1)!}$ for all $n \in \mathbb{N}_0$. We can prove the uniqueness of the inverse kernel $|p_c(x,y,t)|$ as we proved for the direct kernel $|q_c(x,y,t)|$. Moreover, replacing the boundary condition (A.39) by $\partial_x \Gamma(x,t)$ and following the same procedure in view of (A.28), we obtain the following bound

$$|\partial_x p_c(\cdot,\cdot,t)| \leq kH\mu^2(t)e^{\frac{3D^2}{2T}\mu(t)}. \tag{A.54}$$

The unique C^∞ solution of (A.41)–(A.43) can be found in [21] and it is as follows

$$p_r(x,y,t) = -y\mu_0\mu^2(t)e^{\frac{\mu(t)(x^2-y^2)}{4T}} \frac{J_1\left(\sqrt{\mu_0\mu^2(t)(x^2-y^2)}\right)}{\sqrt{\mu_0\mu^2(t)(x^2-y^2)}}$$

for $t \in [t_0, t_0+T)$, $(x,y) \in \mathscr{T}$. The estimation of the growth-in-time bound is obtained as follows

$$|p_r(\cdot,\cdot,t)| \leq C_{10}\mu^2(t)e^{\frac{D^2}{4T}\mu(t)}, \tag{A.55}$$

where $C_{10} = D\mu_0/2$, by noting $\left|\frac{J_1(\sigma)}{\sigma}\right| \leq 0.5$ for all $\sigma \in \mathbb{R}$. Taking the spatial derivative of $p_r(x,y,t)$ and following the similar procedure, we obtain the following bound

$$|\partial_x p_r(\cdot,\cdot,t)| \leq C_{11}\mu^3(t)e^{\frac{D^2}{4T}\mu(t)}, \tag{A.56}$$

where $C_{11} = \mu_0(1+D^2/(2T))$. The solution of the kernel (2.160)–(2.162) is obtained from the solutions of (A.38)–(A.40) and (A.41)–(A.43). Hence, its growth-in time is calculated as follows

$$\begin{aligned} |p(\cdot,\cdot,t)| &\leq |p_c(\cdot,\cdot,t)| + |p_r(\cdot,\cdot,t)|, \\ &= C_7\mu^2(t)e^{\frac{3D^2}{2T}\mu(t)} + C_{10}\mu^2(t)e^{\frac{D^2}{4T}\mu(t)}. \end{aligned} \tag{A.57}$$

Then, we obtain (A.29). Furthermore, we get the bound (A.30) from (A.37), (A.54), (A.56). ■

Appendix B

Proof of Theorem 3.4

Proof Let us proceed through the proof step by step.

Step 1: State transformation. Consider the following transformations

$$\tilde{\theta}_f = \frac{1}{\alpha}\tilde{\theta}, \qquad \hat{G}_f = \frac{1}{\alpha}\hat{G}, \qquad \tilde{\eta}_f = \frac{1}{\alpha^2}\tilde{\eta}, \tag{B.1}$$

which transform (3.81) to the following system

$$\frac{d}{dt}\begin{bmatrix} \tilde{\theta}_f \\ \hat{G}_f \\ \tilde{\eta}_f \\ \alpha \end{bmatrix} = \begin{bmatrix} \lambda\tilde{\theta}_f - \lambda\frac{\beta}{\alpha}\tilde{\theta}_f + K\hat{G}_f \\ (\lambda - \omega_l - \lambda\frac{\beta}{\alpha})\hat{G}_f + \omega_l\left[\nu(\tilde{\theta}_f\alpha + S(t)\alpha) - \tilde{\eta}_f\alpha^2\right]\frac{M(t)}{\alpha^2} \\ (2\lambda - \omega_h - 2\lambda\frac{\beta}{\alpha})\tilde{\eta}_f + \omega_h\frac{1}{\alpha^2}\nu(\tilde{\theta}_f\alpha + S(t)\alpha) \\ -\lambda\alpha + \lambda\beta \end{bmatrix}, \tag{B.2}$$

where ν is as defined in (3.19) and satisfies (3.20).

Step 2: Averaging operation. We rewrite the system (B.2) in the time scale $\tau = \omega t$ as follows

$$\frac{d}{d\tau}\begin{bmatrix} \tilde{\theta}_f \\ \hat{G}_f \\ \tilde{\eta}_f \\ \alpha \end{bmatrix} = \frac{1}{\omega}\begin{bmatrix} \lambda\tilde{\theta}_f - \lambda\frac{\beta}{\alpha}\tilde{\theta}_f + K\hat{G}_f \\ (\lambda - \omega_l - \lambda\frac{\beta}{\alpha})\hat{G}_f + \omega_l\left[\nu(\tilde{\theta}_f\alpha + \bar{S}(\tau)\alpha) - \tilde{\eta}_f\alpha^2\right]\frac{\bar{M}(\tau)}{\alpha^2} \\ (2\lambda - \omega_h - 2\lambda\frac{\beta}{\alpha})\tilde{\eta}_f + \omega_h\frac{1}{\alpha^2}\nu(\tilde{\theta}_f\alpha + \bar{S}(\tau)\alpha) \\ -\lambda\alpha + \lambda\beta \end{bmatrix}. \tag{B.3}$$

where $\bar{S}(\tau) = S(\tau/\omega), \bar{M}(\tau) = M(\tau/\omega)$. The average of the system (B.3) over the period Π defined in (3.26) is given by

$$\frac{d}{d\tau}\begin{bmatrix}\tilde{\theta}_f^a\\ \hat{G}_f^a\\ \tilde{\eta}_f^a\\ \alpha^a\end{bmatrix} = \frac{1}{\omega}\begin{bmatrix}(\lambda-\lambda\frac{\beta}{\alpha^a})\tilde{\theta}_f^a + K\hat{G}_f^a\\ (\lambda-\omega_l-\lambda\frac{\beta}{\alpha^a})\hat{G}_f^a\\ (2\lambda-\omega_h-2\lambda\frac{\beta}{\alpha^a})\tilde{\eta}_f^a\\ -\lambda\alpha^a+\lambda\beta\end{bmatrix} + \frac{1}{\omega}\begin{bmatrix}0\\ \omega_l\frac{1}{\Pi}\int_0^\Pi \nu(\tilde{\theta}_f^a\alpha^a+\bar{S}(\sigma)\alpha^a)\frac{\bar{M}(\sigma)}{(\alpha^a)^2}d\sigma\\ \omega_h\frac{1}{\Pi}\int_0^\Pi \nu(\tilde{\theta}_f^a\alpha^a+\bar{S}(\sigma)\alpha^a)\frac{1}{(\alpha^a)^2}d\sigma\\ 0\end{bmatrix}. \quad \text{(B.4)}$$

It follows from (B.4) that the average equilibrium denoted as $\begin{bmatrix}\tilde{\theta}_f^{a,e} & \hat{G}_f^{a,e} & \tilde{\eta}_f^{a,e} & \alpha^{a,e}\end{bmatrix}^T$ satisfies

$$\alpha^{a,e} = \beta, \quad \text{(B.5)}$$

$$\hat{G}_f^{a,e} = 0, \quad \text{(B.6)}$$

$$\frac{\omega_l}{\Pi}\int_0^\Pi \nu(\tilde{\theta}_f^{a,e}\beta+\bar{S}(\sigma)\beta)\frac{\bar{M}(\sigma)}{\beta^2}d\sigma = 0, \quad \text{(B.7)}$$

$$\frac{1}{\Pi}\int_0^\Pi \nu(\tilde{\theta}_f^{a,e}\beta+\bar{S}(\sigma)\beta)\frac{1}{\beta^2}d\sigma = \tilde{\eta}_f^{a,e}. \quad \text{(B.8)}$$

Let us postulate the ith element $\tilde{\theta}_{f_i}^{a,e}$ of $\tilde{\theta}_f^{a,e}$ in the following form

$$\tilde{\theta}_{f_i}^{a,e} = \sum_{j=1}^n b_j^i a_j + \beta\sum_{j=1}^n\sum_{k\geq j}^n c_{j,k}^i a_j a_k + \mathscr{O}(\beta^2|a^3|), \quad \text{(B.9)}$$

where b_j^i and $c_{j,k}^i$ are real numbers, substitute (B.9) into (B.7), perform a Taylor series expansion of ν as in (3.29) and equate the like powers of a_j. Then, we obtain $b_j^i = 0\ \forall i,j \in \{1,2\ldots,n\}$,

$c^i_{j,k} = 0\ \forall i,j,k \in \{1,2,\ldots,n\}$ such that $j \neq k$ as well as

$$\begin{bmatrix} c^1_{j,j} \\ \vdots \\ c^{i-1}_{j,j} \\ c^i_{j,j} \\ c^{i+1}_{j,j} \\ \vdots \\ c^n_{j,j} \end{bmatrix} = -H^{-1} \begin{bmatrix} \frac{1}{4}\frac{\partial^3 \nu}{\partial z_1 \partial z_j^2}(0) \\ \vdots \\ \frac{1}{4}\frac{\partial^3 \nu}{\partial z_{j-1} \partial z_j^2}(0) \\ \frac{1}{8}\frac{\partial^3 \nu}{\partial z_j^3}(0) \\ \frac{1}{4}\frac{\partial^3 \nu}{\partial z_j^2 \partial z_{j+1}}(0) \\ \vdots \\ \frac{1}{4}\frac{\partial^3 \nu}{\partial z_j^2 \partial z_n}(0) \end{bmatrix}. \tag{B.10}$$

Following the same methodology, we compute $\tilde{\eta}^{a,e}_f$ in view (3.29), (B.8), (B.9). Then, we find the equilibrium of the average system (B.4) as follows

$$\tilde{\theta}^{a,e}_{f_i} = \beta \sum_{j=1}^{n} c^i_{j,j} a_j^2 + \mathscr{O}(\beta^2 |a|^3), \tag{B.11}$$

$$\tilde{\eta}^{a,e}_f = \frac{1}{4} \sum_{i=1}^{n} H_{i,i} a_i^2 + \mathscr{O}(\beta^2 |a|^4) \tag{B.12}$$

together with (B.5) and (B.6).

Step 3: Stability analysis. The Jacobian of the average system (B.4) at equilibrium is given by

$$J^a_f = \frac{1}{\omega} \begin{bmatrix} 0_{n\times n} & K & 0_{n\times 1} & 0_{n\times 1} \\ \frac{\omega_l}{\Pi}\int_0^\Pi \frac{\partial\left(\frac{\nu \bar{M}}{(\alpha^a)^2}\right)}{\partial \tilde{\theta}_f} d\sigma & -\omega_l I_{n\times n} & 0_{n\times 1} & \frac{\omega_l}{\Pi}\int_0^\Pi \frac{\partial\left(\frac{\nu \bar{M}}{(\alpha^a)^2}\right)}{\partial \alpha^a} d\sigma \\ \frac{\omega_h}{\Pi}\int_0^\Pi \frac{\partial\left(\frac{\nu}{(\alpha^a)^2}\right)}{\partial \tilde{\theta}_f} d\sigma & 0_{1\times n} & -\omega_h & \frac{\omega_h}{\Pi}\int_0^\Pi \frac{\partial\left(\frac{\nu}{(\alpha^a)^2}\right)}{\partial \alpha^a} d\sigma \\ 0_{1\times n} & 0_{1\times n} & 0 & -\lambda \end{bmatrix}. \tag{B.13}$$

Considering the structure of (B.13), we get that it is Hurwitz if and only if the following inequality

is satisfied

$$\frac{\omega_l}{\Pi}\left(\int_0^{\Pi}\frac{\bar{M}(\sigma)}{(\alpha^{a,e})^2}\frac{\partial}{\partial\tilde{\theta}_f}\nu(\tilde{\theta}_f^{a,e}\alpha^{a,e}+\bar{S}(\sigma)\alpha^{a,e})d\sigma\right)<0. \tag{B.14}$$

By performing a Taylor expansion of ν as in (3.29), we get that (B.14) is equal to $\omega_l H + [\mathscr{O}(\beta|a|)]_{n\times n}$. Let us define

$$\mathscr{A}=\begin{bmatrix}0_{n\times n} & K\\ \omega_l H+[\mathscr{O}(\beta|a|)]_{n\times n} & -\omega_l I_{n\times n}\end{bmatrix}, \tag{B.15}$$

which corresponds to $2n\times 2n$ submatrix in the upper left corner of (B.13). Then, we compute

$$\begin{aligned}\det(\lambda_{\mathscr{A}} I_{2n\times 2n}-(1/\omega)\mathscr{A}) = \det\big((\lambda_{\mathscr{A}}^2+\omega_l(1/\omega)\lambda_{\mathscr{A}})I_{n\times n}-\omega_l(1/\omega^2)KH\\ +[\mathscr{O}(\beta(1/\omega^2)|a|)]_{n\times n}\big),\end{aligned} \tag{B.16}$$

which, in view of $H<0$, proves that J_f^a is Hurwitz for sufficiently small $\beta|a|$. Then, based on the averaging theorem [49], we show that there exist $\bar{\omega},\bar{a}>0$ such that for all $\omega>\bar{\omega}$ and $\beta|a|\in(0,\bar{a})$, the system has a unique exponentially stable periodic solution $(\tilde{\theta}_f^{\Pi}(\tau),\mu_f^{\Pi}(\tau),\tilde{\eta}_f^{\Pi}(\tau),\alpha^{\Pi}(\tau))$ of period Π and this solution satisfies

$$\left|\tilde{\theta}_{f_i}^{\Pi}(\tau)-\beta\sum_{j=1}^{n}c_{j,j}^{i}a_j^2\right|\leq\mathscr{O}(1/\omega+\beta^2|a|^3), \tag{B.17}$$

$$\left|\hat{G}_f^{\Pi}(\tau)\right|\leq\mathscr{O}(1/\omega), \tag{B.18}$$

$$\left|\tilde{\eta}_f^{\Pi}(\tau)-\frac{1}{4}\sum_{i=1}^{n}H_{i,i}a_i^2\right|\leq\mathscr{O}(1/\omega+\beta^2|a|^4), \tag{B.19}$$

$$\left|\alpha^{\Pi}(\tau)-\beta\right|\leq\mathscr{O}(1/\omega). \tag{B.20}$$

In other words, the signals $\tilde{\theta}_f(\tau)$, $\hat{G}_f(\tau)$, $\tilde{\eta}_f(\tau)$ converge to an $\mathscr{O}(1/\omega+\beta|a|^2)$-, $\mathscr{O}(1/\omega)$-, and $\mathscr{O}(1/\omega+|a|^2)$-neighborhood of the origin, respectively. The signal $\alpha(\tau)$ converges to β.

Step 4: Convergence to extremum. Considering the results in Step 3 and recalling from (B.1) and Fig. 3.1 with the modified α-dynamics (3.78) that

$$\theta(t) = \alpha(t)\tilde{\theta}_f(t) + \theta^* + \alpha(t)S(t), \tag{B.21}$$

we conclude the exponential convergence of $\theta(t)$ to an $\mathscr{O}(\beta/\omega + \beta|a|)$-neighborhood of θ^*. Hence, performing a Taylor series expansion of ν as in (3.29) and noting (B.21), we conclude the convergence of the output $y(t)$ to an $\mathscr{O}((\beta/\omega)^2 + \beta^2|a|^2)$-neighborhood of $h(\theta^*)$ and complete the proof of Theorem 3.4. ■

Appendix C

Additional Theorem and Useful Definitions for Chapter 5

C.1 Additional Theorem

Theorem C.1 *Consider the following uES design*

$$\begin{cases} \dot{\theta} = \phi^p(t) \sum_{i=1}^{n} \sqrt{\alpha_i \omega_i} e_i \cos\Big(\omega_i(t_0 + \gamma(\phi^q(t)-1)) + k_i \phi^r(t)(J(\theta)-\eta)\Big), \\ \dot{\eta} = \left(-\omega_h \eta + \omega_h J(\theta)\right) \phi^{p+1}(t), \end{cases} \tag{C.1}$$

where the function $\phi(t)$ is defined in Table 5.2 with the corresponding parameters p,q,r,γ. Let $\omega_i = \omega\hat{\omega}_i$ such that $\hat{\omega}_i \neq \hat{\omega}_j \ \forall i \neq j$, $t_0 \geq 0$, $\alpha_i, k_i, \omega_h > 0 \ \forall i = 1,\ldots,n$. Let Assumptions 5.3, 5.4 hold, and Assumption 5.5 hold with $c < p - 2\kappa + r$, $d < p - 2\kappa + 1$. Then, there exists $\omega^* > 0$ such that for all $\omega > \omega^*$, the input $\theta(t) \to \theta^*(t)$ semi-globally with respect to ω and at the same rate that $1/\phi(t) \to 0$, and there exist a class $\mathscr{KL}$ function $\mathscr{B}$, a class $\mathscr{K}$ function $\mathscr{Y}$, and a nonnegative constant $D(\theta(t_0), \theta^*(t_0), \eta(t_0))$ such that

$$|\theta(t) - \theta^*(t)| \leq \phi^{-1}(t)\Big(D + \mathscr{B}\left(|\theta(t_0) - \theta^*(t_0)|, t - t_0\right) + \sup_{t_0 \leq s \leq t} \mathscr{B}\left(\mathscr{Y}\left(\phi^{-1}(s)\right), t - s\right)\Big). \tag{C.2}$$

Proof Let us proceed through the proof step by step.

Step 1: State transformation. Let us consider the following transformations

$$\theta_f = \phi(t)(\theta - \theta^*(t)), \tag{C.3}$$

$$\eta_f = \phi^{2\kappa}(t)(\eta - J(\theta^*(t))), \tag{C.4}$$

which transform (5.16) to

$$\begin{cases} \dot{\theta}_f = -\phi(t)\dot{\theta}^*(t) + \dfrac{\dot{\phi}(t)}{\phi(t)}\theta_f + \phi^{p+1}(t)\displaystyle\sum_{i=1}^{n}\sqrt{\alpha_i\omega_i}e_i\cos\Big(\omega_i(t_0+\gamma(\phi^q(t)-1)) + k_i\phi^r(t) \\ \qquad \times \big(J_f(\theta_f,t) - \phi^{-2\kappa}(t)\eta_f\big)\Big), \\ \dot{\eta}_f = \left(\dfrac{2\kappa\dot{\phi}(t)}{\phi(t)} - \omega_h\phi^{p+1}(t)\right)\eta_f + \omega_h\phi^{2\kappa+p+1}(t)J_f(\theta_f,t) - \phi^{2\kappa}(t)\dot{J}(\theta^*(t)), \end{cases} \tag{C.5}$$

with

$$J_f(\theta_f,t) = J(\theta_f/\phi(t) + \theta^*(t)) - J(\theta^*(t)). \tag{C.6}$$

Step 2: Time transformation. We introduce the following time dilation and contraction transformations

$$\tau = t_0 + \gamma(\phi^q(t) - 1) \tag{C.7}$$

$$t = \phi^{-1}\Big((1 + (\tau - t_0)/\gamma)^{\frac{1}{q}}\Big), \tag{C.8}$$

where $\phi^{-1}(\cdot)$ denotes the inverse of the function $\phi(\cdot)$. Each $\phi(t)$ function in Table 5.2 with the corresponding the parameters p, q yields

$$\dot{\phi}(t) = \phi^{p-q+2}(t)/(\gamma q). \tag{C.9}$$

Using (C.7) and (C.9), we compute

$$\frac{d\tau}{dt} = \phi^{p+1}(t). \tag{C.10}$$

Then, we rewrite (C.5) in dilated τ-domain as

$$\begin{cases} \dfrac{d\theta_f}{d\tau} = -\phi_\tau(\tau)\dfrac{d\theta^*_\tau(\tau)}{d\tau} + \dfrac{1}{\gamma q \phi^q_\tau(\tau)}\theta_f + \displaystyle\sum_{i=1}^{n}\sqrt{\alpha_i\omega_i}e_i \\ \qquad\qquad \times \cos\Big(\omega_i\tau + k_i\phi^r_\tau(\tau)(J_{f,\tau}(\theta_f,\tau) - \phi^{-2\kappa}_\tau(\tau)\eta_f)\Big) \\ \dfrac{d\eta_f}{d\tau} = \left(\dfrac{2\kappa}{\gamma q\phi^q_\tau(\tau)} - \omega_h\right)\eta_f + \omega_h\phi^{2\kappa}_\tau(\tau)J_{f,\tau}(\theta_f,\tau) - \phi^{2\kappa}_\tau(\tau)\dfrac{\partial J(\theta^*_\tau(\tau))}{\partial\tau}, \end{cases} \tag{C.11}$$

where

$$\phi_\tau(\tau) = (1 + (\tau - t_0)/\gamma)^{\frac{1}{q}}, \tag{C.12}$$

$$\theta^*_\tau(\tau) = \theta^*\left(\phi^{-1}\left((1+(\tau-t_0)/\gamma)^{\frac{1}{q}}\right)\right) \tag{C.13}$$

with

$$J_{f,\tau}(\theta_f,\tau) = J(\theta_f/\phi_\tau(\tau) + \theta^*_\tau(\tau)) - J(\theta^*_\tau(\tau)). \tag{C.14}$$

Step 4: Stability analysis. Note that the system (C.11) is in similar form to (5.21) with $\gamma = \frac{1}{\beta}, q = v$, except that the bounds in Assumption 5.5 need to be satisfied in τ-domain for (C.11). The growth bounds in Assumption 5.5 is rewritten in τ-domain as

$$\left|\frac{d\theta^*_\tau(\tau)}{d\tau}\right| + \phi^{p+1}_\tau(\tau)\left|\frac{d^2\theta^*(t)}{d\tau^2}\right| \le M_\theta\phi^{c-p-1}_\tau(\tau), \tag{C.15}$$

$$\left|\frac{\partial J(\theta^*_\tau(\tau))}{\partial\tau}\right| + \phi^{p+1}_\tau(\tau)\left|\frac{\partial^2 J(\theta^*_\tau(\tau))}{\partial\tau^2}\right| \le M_J\phi^{d-p-1}_\tau(\tau), \tag{C.16}$$

for $\tau \in [t_0,\infty)$. Recall that the conditions on the powers c,d in Assumption 5.5, for the practical

stability of the system (5.21) is that $c < -1-2\kappa+r$ and $d < -2\kappa$, as provided in Table 5.1. Following this analogy, for the stability of (C.11), the powers of the function $\phi_\tau(\tau)$ should satisfy

$$c-p-1 < -1-2\kappa+r, \tag{C.17}$$

$$d-p-1 < -2\kappa, \tag{C.18}$$

which are simply

$$c < p-2\kappa+r, \tag{C.19}$$

$$d < p-2\kappa+1. \tag{C.20}$$

Following the Step 2 to 6 in the proof of Theorem 5.3, we prove that the origin of (C.11) is practically uniformly asymptotically stable. By the time contraction (C.8), we conclude the practical uniform stability of (C.5) with the existence of ω^* and the role of ω attributed as in Definition C.1.

Similar to (5.53), the fading memory ISS bound of the average state $\bar{\theta}_f$ in t-domain is obtained as

$$|\bar{\theta}_f(t)| \leq \mathscr{B}\left(|\bar{\theta}_f(t_0)|, t-t_0\right) + \sup_{t_0\leq s\leq t} \mathscr{B}\left(\mathscr{Y}\left(\phi^{-1}(s)\right), t-s\right), \tag{C.21}$$

where the functions $\mathscr{B}$ and $\mathscr{Y}$ are defined as in (5.54) and (5.55), except that $\xi(t), \beta$, and v in (5.54) and (5.55) are replaced by $\phi(t), \frac{1}{\gamma}$, and q, respectively.

Step 5: Convergence to extremum. Considering the result in Step 4 and recalling from (C.3) that

$$\theta = \theta^*(t) + \frac{1}{\phi(t)}\theta_f, \tag{C.22}$$

we conclude the convergence of $\theta(t)$ to $\theta^*(t)$ at the same rate that $1/\phi(t) \to 0$. The bound on

the convergence error is obtained as

$$|\theta(t)-\theta^*(t)| \leq \phi^{-1}(t)\left(|\bar{\theta}_f(t)|+|\theta_f(t)-\bar{\theta}_f(t)|\right), \tag{C.23}$$

from which we conclude (C.2). From (5.9), (C.3), and (C.4), we prove the convergence of the output $y(t)$ and the filtered state $\eta(t)$ to $J(\theta^*(t))$ at the rate of $1/\phi^{2\kappa}(t)$ and complete the proof of Theorem C.1. ■

C.2 Useful Definitions

Definition C.1 ([19]) *A compact set $\mathscr{S} \subset \mathbb{R}^n$ is said to be **locally practically uniformly asymptotically stable** for* (5.1) *if the following three conditions are satisfied:*

- *Practical Uniform Stability: For any $\varepsilon > 0$ there exist $\delta, \omega^* > 0$ such that for all $t_0 \in \mathbb{R}^+$ and $\omega > \omega^*$, if $x(t_0) \in U_\delta^{\mathscr{S}}$, then $x(t) \in U_\varepsilon^{\mathscr{S}}$ for $t \in [t_0, \infty)$.*
- *δ-Practical Uniform Attractivity: Let $\delta > 0$. For any $\varepsilon > 0$ there exist $t_1 \geq 0$ and $\omega^* > 0$ such that for all $t_0 \in \mathbb{R}^+$ and $\omega > \omega^*$, if $x(t_0) \in U_\delta^{\mathscr{S}}$, then $x(t) \in U_\varepsilon^{\mathscr{S}}$ for $t \in [t_0+t_1, \infty)$.*
- *Practical Uniform Boundedness: For any $\delta > 0$ there exist $\varepsilon > 0$ and $\omega^* > 0$ such that for all $t_0 \in \mathbb{R}^+$ and $\omega > \omega^*$, if $x(t_0) \in U_\delta^{\mathscr{S}}$, then $x(t) \in U_\varepsilon^{\mathscr{S}}$ for $t \in [t_0, \infty)$.*

*Furthermore, if δ-practical uniform attractivity holds for every $\delta > 0$, then the compact set $\mathscr{S}$ is said to be **semi-globally practically uniformly asymptotically stable** for* (5.1).

Definition C.2 ([18]) *A compact set $\mathscr{S} \subset \mathbb{R}^n$ is said to be **singularly semi-globally practically uniformly asymptotically stable** for* (5.3) *if the following three conditions are satisfied:*

- *Singular Practical Uniform Stability: For all $\varepsilon_x, \varepsilon_z \in (0, \infty)$ there exist $\delta_x, \delta_z \in (0, \infty)$ and $\omega^* \in (0, \infty)$ such that for all $\omega \in (\omega^*, \infty)$ there exists a $\varepsilon^* \in (0, \infty)$ such that for all $\varepsilon \in (0, \varepsilon^*)$ and for all $t_0 \in \mathbb{R}$ if $x_0 \in U_{\delta_x}^{\mathscr{S}}$ and $z_0 - l(x_0) \in U_{\delta_z}^0$, then $x(t; t_0, x_0) \in U_{\varepsilon_x}^S$ and $z(t; t_0, z_0) - l(x(t; t_0, x_0)) \in U_{\varepsilon_z}^0$ for $t \in [t_0, \infty)$.*

- *Singular Practical Uniform Attractivity: For all δ_x, δ_z, ε_x, $\varepsilon_z \in (0,\infty)$, there exist a $t_f \in [0,\infty)$ and $\omega^* \in (0,\infty)$ such that for all $\omega \in (\omega^*,\infty)$ there exists a $\varepsilon^* \in (0,\infty)$ such that for all $\varepsilon \in (0,\varepsilon^*)$ and for all $t_0 \in \mathbb{R}$, if $x_0 \in U^{\mathscr{I}}_{\delta_x}$ and $z_0 - l(x_0) \in U^0_{\delta_z}$, then $x(t;t_0,x_0) \in U^S_{\varepsilon_x}$, $t \in [t_0 + \frac{t_f}{\varepsilon},\infty)$ and $z(t;t_0,z_0) - l(x(t;t_0,x_0)) \in U^0_{\varepsilon_z}$ for $t \in [t_0 + t_f,\infty)$.*

- *Singular Practical Uniform Boundedness: For all δ_x, $\delta_z \in (0,\infty)$ there exist $\varepsilon_x, \varepsilon_z \in (0,\infty)$ and $\omega^* \in (0,\infty)$ such that for all $\omega \in (\omega^*,\infty)$ there exists a $\varepsilon^* \in (0,\infty)$ such that for all $\varepsilon \in (0,\varepsilon^*)$ and for all $t_0 \in \mathbb{R}$, if $x_0 \in U^{\mathscr{I}}_{\delta_x}$ and $z_0 - l(x_0) \in U^0_{\delta_z}$, then $x(t;t_0,x_0) \in U^S_{\varepsilon_x}$ and $z(t;t_0,z_0) - l(x(t;t_0,x_0)) \in U^0_{\varepsilon_z}$ for $t \in [t_0,\infty)$.*

Appendix D

Additional Lemma for Chapter 6 and Proofs of Lemma 6.1 and Theorems 6.1–6.3

D.1 Additional Lemma for Chapter 6

Lemma D.1 *The second element of the filter state y_f, y_{f_2}, can be expressed as follows*

$$y_{f_2} = \frac{1}{2\lambda_f^2}\begin{bmatrix}\lambda_f^2+\omega^2 & \lambda_f^2\end{bmatrix}\begin{bmatrix}y_{f_1}\\ y_{f_3}\end{bmatrix} - \frac{1}{2\lambda_f^2}\begin{bmatrix}\lambda_f^2+\omega^2 & \lambda_f^2\end{bmatrix}\begin{bmatrix}y_{f_1}^{ssh}+y_{f_1}^{in}\\ y_{f_3}^{ssh}+y_{f_3}^{in}\end{bmatrix} + y_{f_2}^{ssh} + y_{f_2}^{in}, \tag{D.1}$$

where the steady state response of the higher order terms $y_{f_j}^{ssh}$ and the transient response of the filter state $y_f^{in} = \begin{bmatrix} y_{f_1}^{in} & \dots & y_{f_p}^{in}\end{bmatrix}$ are defined by

$$y_{f_j}^{ssh} = \sum_{k=2}^{\infty}\left(\frac{\lambda_f}{\sqrt{(\lambda_f^2+k^2\omega^2)}}\right)^{p-j+1}(k\omega)\big[-a_k\sin(k\omega t+j\varphi_k)+b_k\cos(k\omega t+j\varphi_k)\big], \tag{D.2}$$

$$\dot{y}_f^{in} = A_\lambda y_f^{in} \tag{D.3}$$

for $j = 1,\dots,p$ with $\varphi_k = \arctan(k\omega/\lambda)$.

Proof The filter state $y_{f_j}(t)$ can be written as summation of the steady state $y_{f_j}^{ss}$ and transient

responses $y^{\text{in}}_{f_j}$,

$$y_{f_j}(t) = y^{\text{ss}}_{f_j} + y^{\text{in}}_{f_j}. \tag{D.4}$$

The transient response obeys the dynamics (D.3). The transfer function for the steady state response is obtained from the filter (6.21)–(6.22) as follows

$$Y^{\text{ss}}_{f_j}(s) = \frac{\lambda_f^j s}{(\lambda_f + s)^j}\Delta(s). \tag{D.5}$$

Let us write (D.5) in the time domain using (6.18) as follows

$$\begin{aligned} y^{\text{ss}}_{f_j}(t) &= \sum_{k=1}^{\infty}\left(\frac{\lambda_f}{\sqrt{(\lambda_f^2 + k^2\omega^2)}}\right)^{p-j+1} (k\omega)\big[-a_k\sin(k\omega t + j\varphi_k) + b_k\cos(k\omega t + j\varphi_k)\big], \\ &= y^{\text{ssf}}_{f_j}(t) + y^{\text{ssh}}_{f_j}(t), \end{aligned} \tag{D.6}$$

where $\varphi_k = \arctan(k\omega/\lambda)$ and $y^{\text{ssh}}_{f_j}$ is defined in (D.2) and

$$y^{\text{ssf}}_{f_j} = \left(\frac{\lambda_f}{\sqrt{(\lambda_f^2 + \omega^2)}}\right)^{p-j+1} \omega\bar{a}_1\cos(\omega t + \bar{\varphi} + j\varphi_1) \tag{D.7}$$

with $\bar{a}_1, \bar{\varphi}$ defined after (6.19). Our next step is to prove the following equality

$$y^{\text{ssf}}_{f_2} = \frac{\lambda_f^2 + \omega^2}{2\lambda_f^2} y^{\text{ssf}}_{f_1} + \frac{1}{2} y^{\text{ssf}}_{f_3}. \tag{D.8}$$

Let us write the third state of (D.2) as follows

$$y^{\text{ssf}}_{f_3} = \left(\frac{\lambda_f}{\sqrt{(\lambda_f^2 + \omega^2)}}\right)^{p-2} \omega\bar{a}_1\cos(\omega t + \bar{\varphi} + 3\varphi_1) \tag{D.9}$$

in which we can represent the sinusoidal term using the following trigonometric identity

$$\cos(\omega t+\bar{\varphi}+3\varphi_1)=\cos(\omega t+\bar{\varphi}+\varphi_1)\cos(2\varphi_1)-\sin(\omega t+\bar{\varphi}+\varphi_1)\sin(2\varphi_1). \tag{D.10}$$

By substituting (D.10) into (D.9) and considering (D.7) for $j=1$, the right hand side of (D.8) can be computed as follows

$$\begin{aligned}\frac{\lambda_f^2+\omega^2}{2\lambda_f^2}y_{f_1}^{\text{ssf}}+\frac{1}{2}y_{f_3}^{\text{ssf}} &= \left(\frac{\lambda_f}{\sqrt{(\lambda_f^2+\omega^2)}}\right)^{p-1}\omega\bar{a}_1\left[\cos(\omega t+\bar{\varphi}+\varphi_1)\frac{\sqrt{\lambda_f^2+\omega^2}}{2\lambda_f}(1+\cos(2\varphi_1))\right.\\ &\quad\left.-\sin(\omega t+\bar{\varphi}+\varphi_1)\sin(2\varphi_1)\frac{\sqrt{\lambda_f^2+\omega^2}}{2\lambda_f}\right]\\ &= y_{f_2}^{\text{ssf}}\end{aligned} \tag{D.11}$$

where we use the relations $\cos(\varphi_1)=\frac{\lambda_f}{\sqrt{\lambda_f^2+\omega^2}}$, $\sin(\varphi_1)=\frac{\omega}{\sqrt{\lambda_f^2+\omega^2}}$ and the following trigonometric identities: $2\cos^2(\varphi_1)=1+\cos(2\varphi_1), \sin(2\varphi_1)=2\sin(\varphi_1)\cos(\varphi_1)$. The expression (D.1) is obtained in view of (D.4), (D.6) and (D.8). ■

D.2 Proof of Theorem 6.1

Upon substituting the controller (6.10) to (6.9) in view of $W_i^*=\tilde{W}_i+\hat{W}_i$ for $i=1,\ldots,n$, we obtain

$$\dot{e}=-Ke+\begin{bmatrix}\Psi_1(u)^T\tilde{W}_1\\ \vdots\\ \Psi_n(u)^T\tilde{W}_n\end{bmatrix}\dot{u}+\dot{\delta}+\varepsilon. \tag{D.12}$$

Consider the following Lyapunov function

$$V_i=\frac{1}{2}e_i^2+\frac{1}{2}\text{trace}\left(\tilde{W}_i\Gamma_{w_i}^{-1}\tilde{W}_i^T\right). \tag{D.13}$$

Let us take the time derivative of (D.13) in view of (D.12) as follows

$$\begin{aligned}\dot{V}_i =& -k_i e_i^2 + \text{trace}\left(\tilde{W}_i \dot{u} \Psi_i(u)^T e_i\right) + e_i \dot{\delta}_i + \varepsilon_i e_i - \text{trace}\left(\tilde{W}_i \Gamma_{w_i}^{-1} \dot{\hat{W}}_i^T\right), \\ \leq& -\frac{1}{2} k_i e_i^2 - \frac{\gamma_{w_i}}{2} \text{trace}\left(\tilde{W}_i \tilde{W}_i^T\right) + \frac{1}{k_i} \bar{\varepsilon}_i^2 + \frac{1}{k_i} (\bar{\delta}_i^{\max})^2 + \frac{\gamma_{w_i}}{2} \text{trace}\left(W_i^* (W_i^*)^T\right), \\ \leq& -c_i V_i + \frac{1}{k_i} \bar{\varepsilon}_i^2 + \frac{1}{k_i} (\bar{\delta}_i^{\max})^2 + \frac{\gamma_{w_i}}{2} \text{trace}\left(W_i^* (W_i^*)^T\right), \end{aligned} \tag{D.14}$$

where we define c_i in (6.14), use the following trace identity

$$\Psi_i(u)^T \tilde{W}_i \dot{u} e_i = \text{trace}(\tilde{W}_i \dot{u} \Psi_i(u)^T e_i) \tag{D.15}$$

and the following Young's inequalities

$$\begin{aligned}\gamma_{w_i} \text{trace}\left(\tilde{W}_i \hat{W}_i^T\right) =& -\gamma_{w_i} \text{trace}\left(\tilde{W}_i \tilde{W}_i^T\right) + \gamma_{w_i} \text{trace}\left(\tilde{W}_i (W_i^*)^T\right), \\ \leq& -\frac{\gamma_{w_i}}{2} \text{trace}\left(\tilde{W}_i \tilde{W}_i^T\right) + \frac{\gamma_{w_i}}{2} \text{trace}\left(W_i^* (W_i^*)^T\right). \end{aligned} \tag{D.16}$$

The solution of the differential inequality (D.14) is given by

$$V_i(t) \leq V_i(0) \exp^{-c_i t} + \frac{D_i}{c_i}, \tag{D.17}$$

where D_i is defined in (6.15). We establish the uniform ultimate boundedness of $e_i, \tilde{W}_i$ for $i = 1, \ldots, n$ from (D.17). It also follows from (D.13) and (D.17) that

$$e_i(t)^2 \leq 2V_i(t) \leq 2\left(V_i(0) \exp^{-c_i t} + \frac{D_i}{c_i}\right), \tag{D.18}$$

from which we conclude (6.13). ■

D.3 Proof of Lemma 6.1

Substituting (D.1) into (6.25) and noting (6.24), we get the following error system

$$\dot{\tilde{\Omega}} = -\rho_y y_{f_1}^2 \tilde{\Omega} - \rho_y y_{f_1} \Omega_h, \tag{D.19}$$

where

$$\Omega_h = -(\lambda_f^2 + \Omega)(y_{f_1}^{\text{ssh}} + y_{f_1}^{\text{in}}) - \lambda_f^2 (y_{f_3}^{\text{ssh}} + y_{f_3}^{\text{in}}) + 2\lambda_f^2 (y_{f_2}^{\text{ssh}} + y_{f_2}^{\text{in}}). \tag{D.20}$$

Using some trigonometric identities, we can express the steady state response defined in (D.2) as follows

$$\begin{aligned} y_{f_j}^{\text{ssh}} = & \begin{bmatrix} \sin(\omega t + j\varphi_1 + \bar{\varphi}_1) & \sin(2\omega t + j\varphi_2 + \bar{\varphi}_2) & \cdots \end{bmatrix} \\ & \times \text{block diag} \begin{bmatrix} \frac{\lambda_f}{\sqrt{(\lambda_f^2+4\omega^2)}} & \frac{\lambda_f}{\sqrt{(\lambda_f^2+9\omega^2)}} & \cdots \end{bmatrix}^{p-j+1} \begin{bmatrix} \bar{a}_1 \omega & 2\bar{a}_2 \omega & \cdots \end{bmatrix}^T, \end{aligned} \tag{D.21}$$

where $\bar{a}_i = \sqrt{a_i^2 + b_i^2}$, $\bar{\varphi}_i = \arctan(a_i/b_i)$ for $i = 1, \ldots, q$. Considering the maximum eigenvalue of the block diagonal matrix in (D.21), we can compute the upper bound of $y_{f_j}^{\text{ssh}}$ as follows

$$\begin{aligned} |y_{f_j}^{\text{ssh}}| &\leq \left(\frac{\lambda_f}{\sqrt{(\lambda_f^2 + 4\omega^2)}} \right)^{p-j+1} |\dot{\delta}_{1,h}|, \\ &\leq \left(\frac{\lambda_f}{\sqrt{(\lambda_f^2 + 4\omega^2)}} \right)^{p-j+1} \bar{\delta}_h^{\max}, \\ &\triangleq \bar{y}_{f_j}^{\text{ssh}}, \end{aligned} \tag{D.22}$$

where $\dot{\delta}_{1,h}$ is the derivative of (6.20) and $|\dot{\delta}_{1,h}| \leq \bar{\delta}_h^{\max}$ for some $\bar{\delta}_h^{\max} > 0$ for all $t \in [0,\infty)$. Let us consider the Lyapunov function

$$V = \frac{1}{2\rho_y}\tilde{\Omega}^2 + \frac{1}{2}(y_f^{\text{in}})^T P_{y_f} y_f^{\text{in}}, \tag{D.23}$$

where

$$P_{y_f} A_\lambda + A_\lambda^T P_{y_f} = -((\lambda_f^2 + \Omega)^2 + 5\lambda_f^4 + \rho_\lambda)I, \tag{D.24}$$

for any $\rho_\lambda > 0$. The time derivative of (D.23) along with (6.26), (D.3) and (D.19) is given by

$$\begin{aligned}\dot{V} \leq & -\frac{\beta_y}{2\rho_y}\tilde{\Omega}^2 - \frac{1}{8}y_{f_1}^2\tilde{\Omega}^2 - \left(\lambda_{\min}(Q_y) - (\lambda_f^2+\Omega)^2 - 5\lambda_f^4\right)(y_f^{in})^T y_f^{in} + \varepsilon_\omega \\ \leq & -c_v V + \varepsilon_\omega \end{aligned} \tag{D.25}$$

with

$$c_v = \min\left\{\beta_y, \frac{2\rho_\lambda}{\lambda_{min}(P_{y_f})}\right\}, \tag{D.26}$$

$$\varepsilon_\omega = 6(\lambda_f^2+\Omega)^2(\bar{y}_{f_1}^{ssh})^2 + 6\lambda_f^4\Omega^2(\bar{y}_{f_2}^{ssh})^2 + 24\lambda_f^4(\bar{y}_{f_3}^{ssh})^2, \tag{D.27}$$

where we define $\bar{y}_{f_j}^{\text{ssh}}$ in (D.22), apply the Young's inequalities for cross terms and use the property of $(a+b+c)^2 \leq 3(a^2+b^2+c^2)$. The solution of (D.25) is given by

$$V(t) \leq V(0)\exp^{-c_v t} + \frac{\varepsilon_\omega}{c_v}. \tag{D.28}$$

Then, we get from (6.27), (6.28) and (D.25) that

$$\tilde{\Omega}(t)^2 \leq 2\rho_y(t)V(t) \leq 2\rho_{y_u}\left(V(0)\exp^{-c_v t} + \frac{\varepsilon_\omega}{c_v}\right), \tag{D.29}$$

which concludes (6.29). ■

D.4 Proof of Theorem 6.2

Recalling the error system (6.9), the exosystem (6.31), (6.32) and the observers (6.37)–(6.38), the observer error system can be written in the following cascade form

$$\begin{bmatrix} \dot{\tilde{e}}_i \\ \dot{\tilde{\mathscr{W}}} \end{bmatrix} = \begin{bmatrix} -c_i & h^T \\ \hat{\mathscr{L}} & \mathscr{S} \end{bmatrix} \begin{bmatrix} \tilde{e}_i \\ \tilde{\mathscr{W}} \end{bmatrix} + \begin{bmatrix} (\Psi_i(u)^T \tilde{W}_i)\dot{u} + \dot{\delta}_{1,h_q} + \varepsilon_i \\ \tilde{\mathscr{S}}\mathscr{W} - \tilde{\mathscr{S}}\tilde{\mathscr{W}} \end{bmatrix}. \tag{D.30}$$

Let us consider the following Lyapunov function

$$V = \frac{1}{2}\left\| \begin{bmatrix} \tilde{e}_i \\ \tilde{\mathscr{W}} \end{bmatrix} \right\|^2 + \frac{1}{2}\text{trace}(\tilde{W}_i \Gamma_{w_i}^{-1} \tilde{W}_i^T). \tag{D.31}$$

The time derivative of (D.31) yields

$$\begin{aligned} \dot{V} \leq & -\kappa_\lambda \left\| \begin{bmatrix} \tilde{e}_i \\ \tilde{\mathscr{W}} \end{bmatrix} \right\|^2 + \tilde{e}_i \dot{\delta}_{1,h_q} + \tilde{e}_i \varepsilon_i + \frac{\gamma_{w_i}}{2}\text{trace}\left(W_i^*(W_i^*)^T\right) - \frac{\gamma_{w_i}}{2}\text{trace}\left(\tilde{W}_i \tilde{W}_i^T\right) + \tilde{\mathscr{W}}^T \tilde{\mathscr{S}} \mathscr{W} \\ & - \tilde{\mathscr{W}}^T \tilde{\mathscr{S}} \tilde{\mathscr{W}}, \\ \leq & -\frac{\kappa_\lambda}{2} \left\| \begin{bmatrix} \tilde{e}_i \\ \tilde{\mathscr{W}} \end{bmatrix} \right\|^2 - \frac{\gamma_{w_i}}{2}\text{trace}\left(\tilde{W}_i \tilde{W}_i^T\right) + \frac{(\bar{\delta}_{h_q}^{\max})^2}{\kappa_\lambda} + \frac{\bar{\varepsilon}_i^2}{\kappa_\lambda} + \frac{\gamma_{w_i}}{2}\text{trace}\left(W_i^*(W_i^*)^T\right) \\ & + \frac{1}{2\kappa_\lambda}(q\tilde{\omega})^2 \sum_{j=1}^{q} (\bar{a}_j j\omega)^2, \\ \leq & -c_i V_i + D_i, \end{aligned} \tag{D.32}$$

where c_i, D_i, κ_λ are defined in (6.41), (6.42), (6.43), respectively, by noting that

$$\begin{aligned} \tilde{\mathscr{W}}^T \tilde{\mathscr{S}} \mathscr{W} &\leq \frac{\kappa_\lambda}{2}||\tilde{\mathscr{W}}||^2 + \frac{1}{2\kappa_\lambda}\lambda_{\max}(\tilde{\mathscr{S}}^T \tilde{\mathscr{S}})||\mathscr{W}||^2, \\ &\leq \frac{\kappa_\lambda}{2}||\tilde{\mathscr{W}}||^2 + \frac{1}{2\kappa_\lambda}(q\tilde{\omega})^2 \sum_{j=1}^{q} (\bar{a}_j j\omega)^2, \end{aligned} \tag{D.33}$$

$$\tilde{\mathscr{W}}^T \tilde{\mathscr{S}} \tilde{\mathscr{W}} = 0 \tag{D.34}$$

as well as (D.16). The solution of the differential inequality (D.32) is given by

$$V_i(t) \leq V_i(0) \exp^{-c_i t} + \frac{D_i}{c_i}. \tag{D.35}$$

We establish the uniform ultimate boundedness of $e_i, \mathscr{W}, \tilde{W}_i$ for $i = 1, \ldots, n$ from (D.35). It also follows from (D.31) and (D.35) that

$$\tilde{e}_i(t)^2 \leq 2V_i(t) \leq 2\left(V_i(0) \exp^{-c_i t} + \frac{D_i}{c_i} \right). \tag{D.36}$$

Note that the closed-loop state observer system after substitution of the controller (6.34) to (6.37) is written as

$$\dot{\hat{e}}_i = -k_i \hat{e}_i. \tag{D.37}$$

Considering the solution of (D.37) as well as the bound (D.36), we conclude (6.40). ■

D.5 Proof of Theorem 6.3

By substituting (6.47) into (6.46) in view of $W_i^* = \tilde{W}_i + \hat{W}_i$ for $i = 1, \ldots, n$, we get

$$\dot{z} = -K\mu_a z + \mu_a \begin{bmatrix} \Psi_1(u)^T \tilde{W}_1 \\ \vdots \\ \Psi_n(u)^T \tilde{W}_n \end{bmatrix} \dot{u} + \mu_a \dot{\delta} + \mu_a \varepsilon. \tag{D.38}$$

Consider the following Lyapunov function

$$V_i = \frac{1}{2} z_i^2 + \frac{1}{2} \text{trace}\left(\tilde{W}_i \Gamma_{w_i}^{-1} \tilde{W}_i^T \right), \quad i = 1, \ldots, n. \tag{D.39}$$

By taking the time derivative of (D.39) along with (D.38), we get

$$\begin{aligned}\dot{V}_i =& -k_i\mu_a z_i^2 + \mu_a \text{trace}\left(\tilde{W}_i \dot{u}\Psi_i(u)^T z_i\right) + \mu_a z_i \dot{\delta}_i + \mu_a z_i \varepsilon_i - \text{trace}\left(\tilde{W}_i \Gamma_{w_i}^{-1} \dot{\hat{W}}_i^T\right), \\ \leq& -\frac{1}{2}k_i\mu_a z_i^2 - \mu_a \frac{\gamma_{w_i}}{2}\text{trace}\left(\tilde{W}_i\tilde{W}_i^T\right) + \mu_a \frac{\bar{\varepsilon}_i^2}{k_i} + \mu_a \frac{(\bar{\delta}_i^{\max})^2}{k_i} + \mu_a \frac{\gamma_{w_i}}{2}\text{trace}\left(W_i^*(W_i^*)^T\right), \\ \leq& -c_i\mu_a V_i + \mu_a \frac{\bar{\varepsilon}_i^2}{k_i} + \mu_a \frac{(\bar{\delta}_i^{\max})^2}{k_i} + \mu_a \frac{\gamma_{w_i}}{2}\text{trace}\left(W_i^*(W_i^*)^T\right), \end{aligned} \tag{D.40}$$

where c_i is defined in (6.51) and we perform Young's inequalities for the following term

$$\begin{aligned}\mu_a\gamma_{w_i}\text{trace}\left(\tilde{W}_i\hat{W}_i^T\right) =& -\mu_a\gamma_{w_i}\text{trace}\left(\tilde{W}_i\tilde{W}_i^T\right) + \mu_a\gamma_{w_i}\text{trace}\left(\tilde{W}_i(W_i^*)^T\right), \\ \leq& -\mu_a\frac{\gamma_{w_i}}{2}\text{trace}\left(\tilde{W}_i\tilde{W}_i^T\right) + \mu_a\frac{\gamma_{w_i}}{2}\text{trace}\left(W_i^*(W_i^*)^T\right). \end{aligned} \tag{D.41}$$

Let us multiply the both sides of (D.40) by $\exp^{\int_0^t c_i\mu_a(\tau)d\tau}$, then we get

$$\frac{d}{dt}(V_i(t)\exp^{\int_0^t c_i\mu_a(\tau)d\tau}) \leq \exp^{\int_0^t c_i\mu_a(\tau)d\tau}\mu_a(t)\left[\frac{\bar{\varepsilon}_i^2}{k_i} + \frac{(\bar{\delta}_i^{\max})^2}{k_i} + \frac{\gamma_{w_i}}{2}\text{trace}\left(W_i^*(W_i^*)^T\right)\right]. \tag{D.42}$$

Integrating (D.42) from 0 to t and multiplying the both sides of the resulting expression by $\exp^{-\int_0^t c_i\mu_a(\tau)d\tau}$, we obtain

$$V_i(t) \leq \exp^{-c_i(t+\beta t^2/2)}V_i(0) + \frac{D_i}{c_i}, \tag{D.43}$$

where D_i is defined in (6.52). Then, we conclude the uniform ultimate boundedness of $z_i, \tilde{W}_i$. Hence, considering the transformation (6.45), we write

$$\begin{aligned} e_i^2(t) = \frac{1}{\mu_a^2}z_i^2(t) \leq& \frac{1}{\mu_a^2}2V_i(t), \\ \leq& \frac{2}{\mu_a^2}\left(\exp^{-c_i(t+\beta t^2/2)}V_i(0) + \frac{D_i}{c_i}\right), \end{aligned} \tag{D.44}$$

from which we conclude (6.50). Considering the boundedness of $z, e, \dot{y}^r$ and noting the transformation $z = \mu_a e$, we prove, from (6.47), the boundedness of the controller $\dot{u}$. ■

Bibliography

[1] U. J. F. Aarsnes, O. M. Aamo, and M. Krstic. Extremum seeking for real-time optimal drilling control. In *2019 American Control Conference (ACC)*, pages 5222–5227. IEEE, 2019.

[2] M. Abdelgalil and H. Taha. Lie bracket approximation-based extremum seeking with vanishing input oscillations. *Automatica*, 133:109735, 2021.

[3] D. Acharya, S. K. Pradhan, and D. K. Das. Explicit model predictive control design for artificial respiratory ventilation system. *International Journal of Dynamics and Control*, pages 1–9, 2023.

[4] A. Alessandri, P. Bagnerini, R. Cianci, S. Donnarumma, and A. Taddeo. Stabilization of diffusive systems using backstepping and the circle criterion. *International Journal of Heat and Mass Transfer*, 149:119132, 2020.

[5] H. Alfalahi, F. Renda, and C. Stefanini. Concentric tube robots for minimally invasive surgery: Current applications and future opportunities. *IEEE Transactions on Medical Robotics and Bionics*, 2(3):410–424, 2020.

[6] H. Arenbeck, L. Wittschier, D. Kügler, and D. Abel. Control methods for robot-based predictive compensation of respiratory motion. *Biomedical Signal Processing and Control*, 34:16–24, 2017.

[7] K. T. Atta and M. Guay. Comment on "on stability and application of extremum seeking control without steady-state oscillation"[automatica 68 (2016) 18–26]. *Automatica*, 103:580–581, 2019.

[8] D. Bhattacharjee and K. Subbarao. Extremum seeking control with attenuated steady-state oscillations. *Automatica*, 125:109432, 2021.

[9] D. M. Bošković and M. Krstić. Backstepping control of chemical tubular reactors. *Computers & chemical engineering*, 26(7-8):1077–1085, 2002.

[10] S. P. Boyd and L. Vandenberghe. *Convex optimization*. Cambridge university press, 2004.

[11] C.-C. Cheah, C. Liu, and J.-J. E. Slotine. Adaptive tracking control for robots with unknown kinematic and dynamic properties. *The International Journal of Robotics Research*, 25(3):283–296, 2006.

[12] B. Chen, G. Pin, and T. Parisini. Frequency estimation of periodic signals: An adaptive observer approach. In *2015 American Control Conference (ACC)*, pages 2505–2510. IEEE, 2015.

[13] D. Chen, Y. Zhang, and S. Li. Tracking control of robot manipulators with unknown models: A jacobian-matrix-adaption method. *IEEE Transactions on Industrial Informatics*, 14(7):3044–3053, 2017.

[14] W. E. Dixon. Adaptive regulation of amplitude limited robot manipulators with uncertain kinematics and dynamics. *IEEE Transactions on Automatic Control*, 52(3):488–493, 2007.

[15] C. S. Draper and Y. T. Li. Principles of optimalizing control systems and an application to the internal combusion engine. *American Society Mechanical Engineers*, 1951.

[16] J. Duan and W. Wei. *Effective dynamics of stochastic partial differential equations*. Elsevier, 2014.

[17] P. E. Dupont, N. Simaan, H. Choset, and C. Rucker. Continuum robots for medical interventions. *Proceedings of the IEEE*, 110(7):847–870, 2022.

[18] H.-B. Dürr, M. Krstić, A. Scheinker, and C. Ebenbauer. Extremum seeking for dynamic maps using lie brackets and singular perturbations. *Automatica*, 83:91–99, 2017.

[19] H.-B. Dürr, M. S. Stanković, C. Ebenbauer, and K. H. Johansson. Lie bracket approximation of extremum seeking systems. *Automatica*, 49(6):1538–1552, 2013.

[20] S. A. Emami, P. Castaldi, and A. Banazadeh. Neural network-based flight control systems: Present and future. *Annual Reviews in Control*, 53:97–137, 2022.

[21] N. Espitia, A. Polyakov, D. Efimov, and W. Perruquetti. Boundary time-varying feedbacks for fixed-time stabilization of constant-parameter reaction–diffusion systems. *Automatica*, 103:398–407, 2019.

[22] J. Feiling, S. Koga, M. Krstić, and T. R. Oliveira. Gradient extremum seeking for static maps with actuation dynamics governed by diffusion pdes. *Automatica*, 95:197–206, 2018.

[23] M. L. Galvão, T. R. Oliveira, and M. Krstić. Extremum seeking for stefan pde with moving boundary and delays. *IFAC-PapersOnLine*, 55(36):222–227, 2022.

[24] T. George Thuruthel, Y. Ansari, E. Falotico, and C. Laschi. Control strategies for soft robotic manipulators: A survey. *Soft robotics*, 5(2):149–163, 2018.

[25] A. Ghaffari, M. Krstić, and D. Nešić. Multivariable newton-based extremum seeking. *Automatica*, 48(8):1759–1767, 2012.

[26] A. Ghaffari, M. Krstić, and S. Seshagiri. Power optimization and control in wind energy conversion systems using extremum seeking. *IEEE transactions on control systems technology*, 22(5):1684–1695, 2014.

[27] R. Ginhoux, J. Gangloff, M. de Mathelin, L. Soler, M. M. A. Sanchez, and J. Marescaux. Active filtering of physiological motion in robotized surgery using predictive control. *IEEE Transactions on Robotics*, 21(1):67–79, 2005.

[28] M. Giorelli, F. Renda, M. Calisti, A. Arienti, G. Ferri, and C. Laschi. Learning the inverse kinetics of an octopus-like manipulator in three-dimensional space. *Bioinspiration & biomimetics*, 10(3):035006, 2015.

[29] C. Girerd and T. K. Morimoto. Design and control of a hand-held concentric tube robot for minimally invasive surgery. *IEEE Trans. Robot.*, 37(4):1022–1038, 2021.

[30] L. Grune. Input-to-state dynamical stability and its lyapunov function characterization. *IEEE Transactions on Automatic Control*, 47(9):1499–1504, 2002.

[31] V. Grushkovskaya, H.-B. Dürr, C. Ebenbauer, and A. Zuyev. Extremum seeking for time-varying functions using lie bracket approximations. *IFAC-PapersOnLine*, 50(1):5522–5528, 2017.

[32] V. Grushkovskaya, A. Zuyev, and C. Ebenbauer. On a class of generating vector fields for the extremum seeking problem: Lie bracket approximation and stability properties. *Automatica*, 94:151–160, 2018.

[33] M. Guay. Uncertainty estimation in extremum seeking control of unknown static maps. *IEEE Control Systems Letters*, 5(4):1115–1120, 2020.

[34] M. Guay and M. Benosman. Finite-time extremum seeking control for a class of unknown static maps. *International Journal of Adaptive Control and Signal Processing*, 35(7):1188–1201, 2021.

[35] M. Guay, D. Dochain, M. Perrier, and N. Hudon. Flatness-based extremum-seeking control over periodic orbits. *IEEE Transactions on Automatic Control*, 52(10):2005–2012, 2007.

[36] N. Gupta, P. Simmen, D. Trachsel, A. Haeberlin, K. Jost, and T. Niederhauser. Respiratory rate estimation from multi-channel signals using auto-regulated adaptive extended kalman filter. *Biomedical Signal Processing and Control*, 84:104977, 2023.

[37] J. K. Hale and S. M. V. Lunel. Averaging in infinite dimensions. *The Journal of Integral Equations and Applications*, pages 463–494, 1990.

[38] M. Haring and T. A. Johansen. Asymptotic stability of perturbation-based extremum-seeking control for nonlinear plants. *IEEE Transactions on Automatic Control*, 62(5):2302–2317, 2016.

[39] M. Haring, N. Van De Wouw, and D. Nešić. Extremum-seeking control for nonlinear systems with periodic steady-state outputs. *Automatica*, 49(6):1883–1891, 2013.

[40] L. Hazeleger, M. Haring, and N. van de Wouw. Extremum-seeking control for optimization of time-varying steady-state responses of nonlinear systems. *Automatica*, 119:109068, 2020.

[41] Y. Ho, A. Bryson, and S. Baron. Differential games and optimal pursuit-evasion strategies. *IEEE Transactions on Automatic Control*, 10(4):385–389, 1965.

[42] K. Hornik, M. Stinchcombe, and H. White. Universal approximation of an unknown mapping and its derivatives using multilayer feedforward networks. *Neural networks*, 3(5):551–560, 1990.

[43] B. Hu, Y. Li, F. Cao, and Z. Xing. Extremum seeking control of cop optimization for air-source transcritical co2 heat pump water heater system. *Applied Energy*, 147:361–372, 2015.

[44] N. Hudon, M. Guay, M. Perrier, and D. Dochain. Adaptive extremum-seeking control of convection-reaction distributed reactor with limited actuation. *Computers & Chemical Engineering*, 32(12):2994–3001, 2008.

[45] P. A. Ioannou and J. Sun. *Robust adaptive control*. Courier Corporation, 2012.

[46] M. Jabeen, Q. H. Meng, T. Jing, and H. R. Hou. Robot odor source localization in indoor environments based on gradient adaptive extremum seeking search. *Building and Environment*, 229:109983, 2023.

[47] I. Karafyllis and M. Krstic. Input-to-state stability for pdes. *Encyclopedia of Systems and Control*, pages 1030–1033, 2021.

[48] M. Khadem, J. O'Neill, Z. Mitros, L. Da Cruz, and C. Bergeles. Autonomous steering of concentric tube robots via nonlinear model predictive control. *IEEE Transactions on Robotics*, 36(5):1595–1602, 2020.

[49] H. K. Khalil. *Nonlinear Systems*. Prentice Hall, 2002.

[50] N. J. Killingsworth, S. M. Aceves, D. L. Flowers, F. Espinosa-Loza, and M. Krstic. Hcci engine combustion-timing control: Optimizing gains and fuel consumption via extremum seeking. *IEEE Transactions on Control Systems Technology*, 17(6):1350–1361, 2009.

[51] N. J. Killingsworth and M. Krstic. Pid tuning using extremum seeking: online, model-free performance optimization. *IEEE control systems magazine*, 26(1):70–79, 2006.

[52] S. Koga, M. Krstic, and J. Beaman. Laser sintering control for metal additive manufacturing by pde backstepping. *IEEE Transactions on Control Systems Technology*, 28(5):1928–1939, 2020.

[53] P. Krishnamurthy, F. Khorrami, and M. Krstic. A dynamic high-gain design for prescribed-time regulation of nonlinear systems. *Automatica*, 115:108860, 2020.

[54] P. Krishnamurthy, F. Khorrami, and M. Krstic. Adaptive output-feedback stabilization in prescribed time for nonlinear systems with unknown parameters coupled with unmeasured states. *International Journal of Adaptive Control and Signal Processing*, 35(2):184–202, 2021.

[55] M. Krstić. Performance improvement and limitations in extremum seeking control. *Systems & Control Letters*, 39(5):313–326, 2000.

[56] M. Krstic. *Delay Compensation for Nonlinear, Adaptive, and PDE Systems*. Springer, 2009.

[57] M. Krstic, A. Ghaffari, and S. Seshagiri. Extremum seeking for wind and solar energy applications. In *Proceeding of the 11th World Congress on Intelligent Control and Automation*, pages 6184–6193. IEEE, 2014.

[58] M. Krstic and A. Smyshlyaev. *Boundary control of PDEs: A course on backstepping designs*. SIAM, 2008.

[59] M. Krstic and H.-H. Wang. Stability of extremum seeking feedback for general nonlinear dynamic systems. *Automatica*, 36(4):595–602, 2000.

[60] C. Labar, C. Ebenbauer, and L. Marconi. Iss-like properties in lie-bracket approximations and application to extremum seeking. *Automatica*, 136:110041, 2022.

[61] B. Laroche, P. Martin, and P. Rouchon. Motion planning for the heat equation. *International Journal of Robust and Nonlinear Control: IFAC-Affiliated Journal*, 10(8):629–643, 2000.

[62] C. K. Lauand and S. Meyn. Quasi-stochastic approximation: Design principles with applications to extremum seeking control. *IEEE Control Systems Magazine*, 43(5):111–136, 2023.

[63] M. Leblanc. Sur l'electrification des chemins de fer au moyen de courants alternatifs de frequence elevee. *Revue générale de l'électricité*, 12(8):275–277, 1922.

[64] M. Li, R. Kang, D. T. Branson, and J. S. Dai. Model-free control for continuum robots based on an adaptive kalman filter. *IEEE/ASME Transactions on Mechatronics*, 23(1):286–297, 2017.

[65] P. M. Loschak, A. Degirmenci, C. M. Tschabrunn, E. Anter, and R. D. Howe. Automatically steering cardiac catheters in vivo with respiratory motion compensation. *The International journal of robotics research*, 39(5):586–597, 2020.

[66] S. Lyu and C. C. Cheah. Data-driven learning for robot control with unknown jacobian. *Automatica*, 120:109120, 2020.

[67] W. M. Ruess. Linearized stability for nonlinear evolution equations. *Journal of Evolution Equations*, 3(2):361–373, 2003.

[68] T. Mahl, A. Hildebrandt, and O. Sawodny. A variable curvature continuum kinematics for kinematic control of the bionic handling assistant. *IEEE transactions on robotics*, 30(4):935–949, 2014.

[69] R. Marino and P. Tomei. Frequency estimation of periodic signals. In *2014 European Control Conference (ECC)*, pages 7–12. IEEE, 2014.

[70] T. Meurer and A. Kugi. Tracking control for boundary controlled parabolic pdes with varying parameters: Combining backstepping and differential flatness. *Automatica*, 45(5):1182–1194, 2009.

[71] E. Michael, C. Manzie, T. A. Wood, D. Zelazo, and I. Shames. Gradient free cooperative seeking of a moving source. *Automatica*, 152:110948, 2023.

[72] I. S. Morosanov. Method of extremum control. *Automatic and Remote Control*, 18:1077–1092, 1957.

[73] E. Moshksar, S. Dougherty, and M. Guay. Model-based extremum-seeking control for unstable systems with time-varying extremum. In *2015 54th IEEE Conference on Decision and Control (CDC)*, pages 6960–6965. IEEE, 2015.

[74] S. J. Moura and Y. A. Chang. Lyapunov-based switched extremum seeking for photovoltaic power maximization. *Control Engineering Practice*, 21(7):971–980, 2013.

[75] S. J. Moura, N. A. Chaturvedi, and M. Krstic. Pde estimation techniques for advanced battery management systems—part i: Soc estimation. In *2012 American Control Conference (ACC)*, pages 559–565. IEEE, 2012.

[76] H.-T. Nguyen and C. C. Cheah. Analytic deep neural network-based robot control. *IEEE/ASME Transactions on Mechatronics*, 2022.

[77] M. T. Nihtilä. On exponential convergence and robustness of least-squares identification. *Systems & control letters*, 8(4):327–331, 1987.

[78] V. O. Nikiforov. Observers of external deterministic disturbances. ii. objects with unknown parameters. *Automation and Remote Control*, 65(11):1724–1732, 2004.

[79] T. R. Oliveira and M. Krstic. Extremum seeking boundary control for pde–pde cascades. *Systems & Control Letters*, 155:105004, 2021.

[80] T. R. Oliveira and M. Krstic. Extremum seeking feedback with wave partial differential equation compensation. *Journal of Dynamic Systems, Measurement, and Control*, 143(4):041002, 2021.

[81] T. R. Oliveira and M. Krstic. *Extremum Seeking Through Delays and PDEs*. SIAM, 2022.

[82] T. R. Oliveira, M. Krstić, and D. Tsubakino. Extremum seeking for static maps with delays. *IEEE Transactions on Automatic Control*, 62(4):1911–1926, 2016.

[83] L. Ott, F. Nageotte, P. Zanne, and M. de Mathelin. Robotic assistance to flexible endoscopy by physiological-motion tracking. *IEEE Transactions on Robotics*, 27(2):346–359, 2011.

[84] A. A. Pervozvanskii. Continuous extremum control system in the presence of random noise. *Automatic and Remote Control*, 21:673–677, 1960.

[85] S. Pokhrel and S. A. Eisa. Control-affine extremum seeking control with attenuating oscillations: A lie bracket estimation approach. In *2023 Proceedings of the Conference on Control and its Applications (CT)*, pages 133–140. SIAM, 2023.

[86] J. I. Poveda and M. Krstić. Fixed-time seeking and tracking of time-varying extrema. In *2021 60th IEEE Conference on Decision and Control (CDC)*, pages 108–113. IEEE, 2021.

[87] J. I. Poveda and M. Krstić. Nonsmooth extremum seeking control with user-prescribed fixed-time convergence. *IEEE Transactions on Automatic Control*, 66(12):6156–6163, 2021.

[88] J. Reinders, M. Giaccagli, B. Hunnekens, D. Astolfi, T. Oomen, and N. van De Wouw. Repetitive control for lur'e-type systems: application to mechanical ventilation. *IEEE Transactions on Control Systems Technology*, 2023.

[89] D. C. Rucker and R. J. Webster III. Statics and dynamics of continuum robots with general tendon routing and external loading. *IEEE Transactions on Robotics*, 27(6):1033–1044, 2011.

[90] F. D. Sahneh, G. Hu, and L. Xie. Extremum seeking control for systems with time-varying extremum. In *Proceedings of the 31st chinese control conference*, pages 225–231. IEEE, 2012.

[91] I. W. Sandberg. Some results on the theory of physical systems governed nonlinear functional equations. *Bell System Technical Journal*, 44(5):871–898, 1965.

[92] A. Scheinker. 100 years of extremum seeking: A survey. *Automatica*, 161:111481, 2024.

[93] A. Scheinker, E.-C. Huang, and C. Taylor. Extremum seeking-based control system for particle accelerator beam loss minimization. *IEEE Transactions on Control Systems Technology*, 30(5):2261–2268, 2021.

[94] A. Scheinker, X. Huang, and J. Wu. Minimization of betatron oscillations of electron beam injected into a time-varying lattice via extremum seeking. *IEEE Transactions on Control Systems Technology*, 26(1):336–343, 2017.

[95] A. Scheinker and M. Krstic. Extremum seeking-based tracking for unknown systems with unknown control directions. In *2012 IEEE 51st IEEE Conference on Decision and Control (CDC)*, pages 6065–6070. IEEE, 2012.

[96] A. Scheinker and M. Krstić. Extremum seeking with bounded update rates. *Systems & Control Letters*, 63:25–31, 2014.

[97] A. Scheinker and M. Krstić. Non-c2 lie bracket averaging for nonsmooth extremum seekers. *Journal of Dynamic Systems, Measurement, and Control*, 136(1), 2014.

[98] A. Scheinker and M. Krstić. *Model-free stabilization by extremum seeking*. Springer, 2017.

[99] P. Sears and P. Dupont. A steerable needle technology using curved concentric tubes. In *2006 IEEE/RSJ Int. Conf. Intell. Robots Syst.*, pages 2850–2856. IEEE, 2006.

[100] R. Seeberger, G. Kane, J. Hoffmann, and G. Eggers. Accuracy assessment for navigated maxillo-facial surgery using an electromagnetic tracking device. *Journal of Cranio-Maxillofacial Surgery*, 40(2):156–161, 2012.

[101] A. Smyshlyaev and M. Krstic. Backstepping observers for a class of parabolic pdes. *Systems & Control Letters*, 54(7):613–625, 2005.

[102] A. Smyshlyaev and M. Krstic. On control design for pdes with space-dependent diffusivity or time-dependent reactivity. *Automatica*, 41(9):1601–1608, 2005.

[103] Y. Song, Y. Wang, J. Holloway, and M. Krstic. Time-varying feedback for regulation of normal-form nonlinear systems in prescribed finite time. *Automatica*, 83:243–251, 2017.

[104] Y. Song, H. Ye, and F. L. Lewis. Prescribed-time control and its latest developments. *IEEE Transactions on Systems, Man, and Cybernetics: Systems*, 2023.

[105] Y. Song, K. Zhao, and M. Krstic. Adaptive control with exponential regulation in the absence of persistent excitation. *IEEE Transactions on Automatic Control*, 62(5):2589–2596, 2016.

[106] R. Suttner. Extremum seeking control with an adaptive dither signal. *Automatica*, 101:214–222, 2019.

[107] G. Szegö. Orthogonal polynomials, vol. 23. In *American Mathematical Society Colloquium Publications*, 1975.

[108] N. Tan, P. Yu, X. Zhang, and T. Wang. Model-free motion control of continuum robots based on a zeroing neurodynamic approach. *Neural Networks*, 133:21–31, 2021.

[109] Y. Tan, D. Nešić, I. M. Y. Mareels, and A. Astolfi. On global extremum seeking in the presence of local extrema. *Automatica*, 45(1):245–251, 2009.

[110] V. Todorovski and M. Krstic. Practical prescribed-time seeking of a repulsive source by unicycle angular velocity tuning. *Automatica*, 154:111069, 2023.

[111] M. Verghese, F. Richter, A. Gunn, P. Weissbrod, and M. Yip. Model-free visual control for continuum robot manipulators via orientation adaptation. In *The International Symposium of Robotics Research*, pages 959–970. Springer, 2019.

[112] H.-H. Wang and M. Krstic. Extremum seeking for limit cycle minimization. *IEEE Transactions on Automatic control*, 45(12):2432–2436, 2000.

[113] L. Wang, S. Chen, and K. Ma. On stability and application of extremum seeking control without steady-state oscillation. *Automatica*, 68:18–26, 2016.

[114] T. Wang, U. Halder, H. S. Chang, M. Gazzola, and P. G. Mehta. Optimal control of a soft cyberoctopus arm. In *2021 American Control Conference (ACC)*, pages 4757–4764. IEEE, 2021.

[115] X. Wang, Y. Li, and K. Kwok. A survey for machine learning-based control of continuum robots. *Frontiers in Robotics and AI*, page 280, 2021.

[116] G. N. Watson. *A treatise on the theory of Bessel functions*, volume 2. The University Press, 1922.

[117] R. J. Webster, A. M. Okamura, and N. J. Cowan. Toward active cannulas: Miniature snake-like surgical robots. In *2006 IEEE/RSJ Int. Conf. Intell. Robots Syst.*, pages 2857–2863. IEEE, 2006.

[118] R. J. Webster III and B. A. Jones. Design and kinematic modeling of constant curvature continuum robots: A review. *The International Journal of Robotics Research*, 29(13): 1661–1683, 2010.

[119] D. A. Wepener, J. D. le Roux, and I. K. Craig. Extremum seeking control to optimize mineral recovery of a flotation circuit using peak air recovery. *Journal of Process Control*, 129:103033, 2023.

[120] M. Ye and G. Hu. Extremum seeking under input constraint for systems with a time-varying extremum. In *52nd IEEE Conference on Decision and Control*, pages 1708–1713. IEEE, 2013.

[121] M. C. Yip and D. B. Camarillo. Model-less feedback control of continuum manipulators in constrained environments. *IEEE Transactions on Robotics*, 30(4):880–889, 2014.

[122] M. C. Yip, J. A. Sganga, and D. B. Camarillo. Autonomous control of continuum robot manipulators for complex cardiac ablation tasks. *Journal of Medical Robotics Research*, 2(01):1750002, 2017.

[123] H. Yu, S. Koga, T. R. Oliveira, and M. Krstic. Extremum seeking for traffic congestion control with a downstream bottleneck. *Journal of Dynamic Systems, Measurement, and Control*, 143(3):031007, 2021.

[124] S. G. Yuen, D. T. Kettler, P. M. Novotny, R. D. Plowes, and R. D. Howe. Robotic motion compensation for beating heart intracardiac surgery. *The International journal of robotics research*, 28(10):1355–1372, 2009.

[125] G. Zames. Nonlinear time varying feedback systems—conditions for l_∞-boundedness derived using conic operators on exponentially weighted spaces. In *Proc. 3rd. Allerton Conf*, 1965.

[126] C. Zhang, A. Siranosian, and M. Krstić. Extremum seeking for moderately unstable systems and for autonomous vehicle target tracking without position measurements. *Automatica*, 43(10):1832–1839, 2007.